



MONASH University

**COMPLEX PATHWAYS IN
MYCOBACTERIAL CELL WALL
BIOSYNTHESIS**

BY

TAMARYN JANE CASHMORE (BMedSc; MScMed)

A thesis submitted for the degree of Doctor of Philosophy at Monash
University in 2015

Department of Microbiology

Faculty of Medicine, Nursing and Health Sciences

Monash University

Melbourne, Australia

Table of Contents

Table of Contents	2
List of Figures	8
General Declaration	13
Copyright notice	13
Abstract	14
Acknowledgements	16
Acronyms and Abbreviations	18
<u>Chapter 1</u>	23
<u>Cell Wall Biosynthesis in Mycobacteria and Corynebacteria</u>	
1.1 Corynebacterineae	23
1.2 Mycobacteria and Corynebacteria	24
1.2.1 Mycobacteria	24
1.2.2 Corynebacteria	29
1.3 Structure and Biosynthesis of the Mycobacterial Cell Envelope	30

1.3.1	Plasma membrane	34
1.3.2	Peptidoglycan	34
1.3.3	Arabinogalactan	35
1.3.3.1	Biosynthesis of arabinogalactan	37
1.3.4	Mycolic acids	38
1.3.4.1	Biosynthesis of mycolic acids	42
	1.Fatty Acid Synthase Cycles-1 and -II	42
	2. Condensation of fatty acids	44
1.3.5	Mannosylated phospholipids	47
1.3.5.1	Phosphatidylinositol mannosides (PIMs)	47
	Biosynthesis of PIMs	50
1.3.5.2	Lipomannan and Lipoarabinomannan	50
	Biosynthesis of lipoglycans	55
1.3.6	Phthiocerol dimycocerosate and phiocerol	58
1.4	The Role of Mycobacterial Components in Pathogenesis	59
1.5	Mycobacterial Cell Wall Biosynthesis Processes as Drug Targets	64
1.6	<i>Corynebacterium glutamicum</i> as a Laboratory Model for Pathogenic Mycobacteria	68
1.7	Rationale of this Study	69
1.8	Aims of this Study	72

<u>Chapter 2</u>	73
-------------------------	----

Materials and Methods

2.1	Bioinformatics Analysis	73
2.2	Chemicals and Reagents	73
2.3	Bacteriological Strains and Culture Conditions	74
2.3.1	Preparation of competent <i>Escherichia coli</i> cells	74

2.3.2	Preparation of competent <i>Corynebacterium glutamicum</i> cells	75
2.4	DNA Amplification and Sequencing	75
2.4.1	Polymerase Chain Reaction (PCR)	75
2.4.2	Sequencing	76
2.5	DNA Manipulation	77
2.5.1	Restriction endonuclease digestion and resolution by agarose gel electrophoresis	77
2.5.2	Isolation and quantitation of DNA restriction fragments	77
2.5.3	Cloning of DNA fragments	78
2.5.4	Transformation of DNA into <i>Escherichia coli</i> and isolation of plasmid DNA	78
2.5.5	Transformation of plasmid DNA into <i>Corynebacterium glutamicum</i> cells	79
2.5.6	Genomic DNA extraction from <i>Corynebacterium glutamicum</i> using a Nucleon® Kit	79
2.6	DNA Southern Hybridization	81
2.7	RNA Extraction and cDNA Analysis	83
2.8	Extraction of Cell Wall Components	86
2.8.1	Culture preparation	86
2.8.2	Extraction of non-covalently bound lipids and glycolipids	86
	2.8.2.1 Butanol partitioning	87
	2.8.2.2 Lipoglycan extraction	87
2.9	Differential Butanol Extraction of Labelled Lipids	89
2.10	High Performance Thin Layer Chromatography (HPTLC)	90
2.11	SDS-PAGE and Silver Stain Analysis of LM/LAM	91
2.12	Methanolysis of Extracted LM/LAM samples for GC-MS analysis	93
	2.12.1 GC-MS analysis of extracted LM/LAM samples	93
2.13	High pH Anion Exchange Chromatography (HPAEC)	94

2.13.1	Base hydrolysis to determine sugar head from the glycolipid	94
2.13.2	Aqueous hydro-fluoride dephosphorylation of glycoconjugates	95
2.14	ESI-QTOF Analysis of Wild Type <i>Corynebacterium glutamicum</i> and Mutant Mannose Residues	96

	<u>Chapter 3</u>	97
	<u>Characterisation of a New Mycolic Acid Biosynthesis Protein in</u> <u><i>Corynebacterium glutamicum</i></u>	
3.1	Rationale and Objectives	97
3.1.1	Introduction	97
3.1.2	Aims and general approach	98
3.2	Results	98
3.2.1	Protter prediction of protein topology	98
3.2.2	Bioinformatics analysis	101
3.2.3	Evidence of co-transcription of <i>NCgl2760/NCgl2761</i> and <i>MSMEG_0317/MSMEG_0315</i>	104
3.2.4	Generation of an <i>NCgl2761</i> mutant	110
3.2.5	Identification of potential <i>NCgl2761</i> deletion mutants by PCR	114
3.2.6	Confirmation of an <i>NCgl2761</i> mutant by Southern Blot hybridization	117
3.2.7	Complementation of the <i>Corynebacterium glutamicum</i> Δ <i>NCgl2761</i> mutant	123
3.2.8	<i>Corynebacterium glutamicum</i> Δ <i>NCgl2761</i> mutant has a growth phenotype	124
3.2.9	Glycolipid analysis of a <i>Corynebacterium glutamicum</i> Δ <i>NCgl2761</i> mutant	126
3.2.10	Lack of <i>NCgl2761</i> affects transport of TCMs across the cell membrane	131

3.2.11	Analysis of lipomannans/ lipoarabinomannans from an $\Delta NCgl2761$ mutant	136
3.3	Discussion	138

<u>Chapter 4</u>		144
-------------------------	--	-----

Characterisation of a New Lipoarabinomannan Biosynthesis Protein in

Corynebacterium glutamicum

4.1	Rationale and Objectives	144
4.1.1	Introduction	144
4.1.2	Aims	145
4.2	Results	146
4.2.1	Protter prediction of protein topology	146
4.2.2	Bioinformatics analysis	149
4.2.3	Generation of a <i>NCgl2760</i> mutant	151
4.2.4	Southern blot hybridization confirms deletion of <i>NCgl2760</i>	157
4.2.5	Complementation of the $\Delta NCgl2760$ mutant	162
4.2.6	Deletion of the <i>NCgl2760</i> gene does not affect growth of <i>Corynebacterium glutamicum</i>	162
4.2.7	HPTLC analysis of glycolipids reveals no phenotype for a $\Delta NCgl2760$ mutant	164
4.2.8	Characterization of lipoglycans from an $\Delta NCgl2760$ mutant	168
4.2.9	Complementation of the $\Delta NCgl2760$ mutant with <i>Rv0227</i>	172

4.2.10	LM/LAM profile when complementing <i>ΔNCgl2760</i> with <i>Rv0227</i>	174
4.2.11	Complementation of <i>ΔNCgl2760</i> with <i>Rv0227</i> fused to the <i>NCgl2760</i> upstream sequence	176
4.2.12	DIONEX high pH anion-exchange chromatography reveals characteristic oligosaccharides	181
4.2.13	GC-MS analysis of extracted LM/LAM samples	183
4.3	Discussion	189
<hr/>		
	<u>Chapter 5</u>	197
<u>Final Discussion</u>		
<hr/>		
	References	204
<hr/>		
Appendix 1	Bacterial Strains	227
Appendix 2	Bacteriological Media Formulations	228
Appendix 3	Oligonucleotide Primers	231

List of Figures

Chapter 1

Cell Wall Biosynthesis in Mycobacteria and Corynebacteria

Figure 1.1	Countries in which national population-based surveys of the prevalence of TB disease have been implemented (WHO, 2015)	25
Figure 1.2	Estimated Global Incidence Rate of 2013 (WHO, 2014)	25
Figure 1.3	Cryo-electron micrographs of vitreous cross-sections from Mycobacteria	31
Figure 1.4	Schematic cross-section of the mycobacterial cell wall	32
Figure 1.5	Mycobacterial arabinogalactan	36
Figure 1.6	General mycolic acid structure	40
Figure 1.7	Fatty acid biosynthesis pathways in mycobacteria	43
Figure 1.8	Proposed reactions of mycolic acid biosynthesis pathway at the corynebacterial plasma membrane	45
Figure 1.9	Structure of 1-phosphatidyl-L- <i>myo</i> -inositol 2,6-di-O- α -D-mannopyranoside (PIM2)	49

Figure 1.10	Schematic of the proposed structural relationship between mycobacterial PIM2, LM and LAM	52
Figure 1.11	Proposed divergent metabolic pathways of LM-A/LAM and LM-B	54
Figure 1.12	Proposed lipoglycan biosynthesis in <i>Corynebacterineae</i>	57
Figure 1.13	Structures of mycobacterial lipoglycans	62
Figure 1.14	Current trends in discovery of new drugs for TB treatment	67
Figure 1.15	A new cell wall biosynthesis locus highly conserved in <i>Corynebacterineae</i>	71

Chapter 3

The Characterisation of a New Mycolic Acid Biosynthesis Protein in

Corynebacterium glutamicum

Figure 3.1	Outer cell membrane topology according to the Protter prediction	100
Figure 3.2	Protein sequence alignment of <i>M. tuberculosis</i> (Rv0226c) and putative orthologues in <i>M. smegmatis</i> (MSMEG_0315), <i>M. leprae</i> (ML2582) and <i>C. glutamicum</i> (NCgl2761)	102
Figure 3.3	Evidence of co-transcription of <i>NCgl2761</i> and <i>NCgl2760</i>	106
Figure 3.4	Evidence of co-transcription of <i>MSMEG_0315</i> and <i>MSMEG_0317</i>	108
Figure 3.5	Cloning and recombination strategy to create a <i>C. glutamicum</i> Δ <i>NCgl2761</i> mutant	112
Figure 3.6	Identification of potential <i>NCgl2761</i> mutants via PCR followed by visualization on 1% agarose gel	115

Figure 3.7	Confirmed disruption of <i>NCgl2761</i> by Southern Blot hybridization using <i>Pst</i> I	119
Figure 3.8	Confirmed disruption of <i>NCgl2761</i> by Southern Blot hybridization using <i>Xho</i> I	121
Figure 3.9	Deletion of the <i>NCgl2761</i> gene causes a lag in growth compared to wild type <i>C. glutamicum</i> which is abolished by genetic complementation	125
Figure 3.10	Glycolipid analysis of a Δ <i>NCgl2761</i> mutant	128
Figure 3.11	Sequential extraction of cell wall components	133
Figure 3.12	SDS-PAGE analysis of lipomannans and lipoarabinomannans from a <i>NCgl2761</i> mutant	137
Figure 3.13	Proposed mycolic acid transport pathway in Corynebacteria	141

Chapter 4

Characterisation of a New Lipoarabinomannan Biosynthesis Protein

in *Corynebacterium glutamicum*

Figure 4.1	Outer cell membrane topology according to the Protter prediction	147
Figure 4.2	Protein sequence alignment of <i>M. tuberculosis</i> (Rv0227c) and putative orthologues in <i>C. glutamicum</i> (NCgl2760), <i>M. smegmatis</i> (MSMEG_0317) and <i>M. leprae</i> (ML2581)	150

Figure 4.3	Cloning and recombination strategy to create a <i>C. glutamicum</i> $\Delta NCgl2760$ mutant	153
Figure 4.4	PCR profiles of seven putative $\Delta NCgl2760$ mutants compared to that of wild type	156
Figure 4.5	Confirmed disruption of <i>NCgl2760</i> by Southern blot hybridization	159
Figure 4.6	Growth characteristics of the wild type <i>C. glutamicum</i> , $\Delta NCgl2760$ mutant, $\Delta NCgl2760 + pSM22$ and $\Delta NCgl2760 + pSM22:NCgl2760$	163
Figure 4.7	Glycolipid analysis of a $\Delta NCgl2760$ mutant	166
Figure 4.8	Lipoglycan profiles of wild type <i>C. glutamicum</i> , $\Delta NCgl2760$, $\Delta NCgl2760 + pSM22$ and $\Delta NCgl2760 + pSM22:NCgl2760$	170
Figure 4.9	Growth characteristics of wild type <i>C. glutamicum</i> , $\Delta NCgl2760$, $\Delta NCgl2760 + pSM22$, and $\Delta NCgl2760 + pSM22:NCgl2760$ strains	173
Figure 4.10	LM/LAM profiles when complementing $\Delta NCgl2760$ with both <i>NCgl2760</i> and <i>Rv0227</i>	175
Figure 4.11	Fusion of <i>Rv0227</i> to the upstream sequence from <i>NCgl2760</i> using SOE PCR	177
Figure 4.12	PCR profiles of individual components of SOE reaction	178
Figure 4.13	SDS-PAGE analysis of LM/LAM from the $\Delta NCgl2760$ mutant containing plasmid $pSM223:*Rv0227$	180
Figure 4.14	HPAEC of HF-treated LM/LAM fraction	182

Figure 4.15	Ratio of mannose:arabinose in LM/LAM fractions isolated in LM/LAM fractions isolated from wild type <i>C. glutamicum</i> , $\Delta NCgl2760$ mutant, $\Delta NCgl2760$ +pSM22 and $\Delta NCgl2760$ +pSM22:NCgl2760	183
Figure 4.16	Ratio of arabinose between LM/LAM fractions of wild type <i>C. glutamicum</i> and $\Delta NCgl2760$ mutant strains	185
Figure 4.17	Size, distribution and number of mannose residues of different LM/LAM molecules of wild type <i>C. glutamicum</i> (red) and mutant $\Delta NCgl2760$ (blue)	187
Figure 4.18	Proposed site of action of NCgl2760 in the <i>C. glutamicum</i> LM/LAM biosynthetic pathway	195

Copyright notice

© Tamaryn Cashmore (2015). Except as provided in the Copyright Act 1968, this thesis may not be reproduced in any form without the written permission of the author.

I certify that I have made all reasonable efforts to secure copyright permissions for third-party content included in this thesis and have not knowingly added copyright content to my work without the owner's permission.

General Declaration

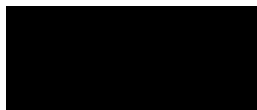
Monash University

Monash Research Graduate School

This thesis contains no material which has been accepted for the award of any other degree or diploma at any university or equivalent institution and that, to the best of my knowledge and belief, this thesis contains no material previously published or written by another person, except where due reference is made in the text of the thesis.

I, Tamaryn Jane Cashmore, hereby declare that the work presented for examination in this thesis has been conducted by myself except where acknowledgement has been given either in the figure legends or text.

Signed:



Date: 21st January 2016

Tamaryn Jane Cashmore, BScMed; MMedSc

The undersigned hereby certify that the above declaration correctly reflects the nature and extent of the student and co-authors' contributions to this work.

Signed:



Date: 21st January 2016

Professor Ross Coppel, Main Supervisor

Abstract

Mycobacterium tuberculosis is a significant human pathogen, responsible for approximately 1.3 million deaths annually. The increase of multi-drug resistant (MDR) and extensively drug resistant (XDR) tuberculosis is of particular concern as current first and even second line medications are less or no longer effective. Current antibacterial drugs, such as isoniazid and ethambutol, target various biosynthetic pathways within the complex cell wall of these bacteria, which is a key virulence factor. Its successful defence against the host immune system is due to a largely impermeable cell wall consisting of a multi-laminate mycolyl-arabinogalactan-peptidoglycan complex (mAGP) and a glycolipid layer embedded into the cell wall. Phosphatidylinositol mannosides (PIMs), lipomannan (LM) and lipoarabinomannan (LAM), all virulence factors, are included in this glycolipid layer.

Previous studies in our group identified a highly conserved genetic locus involved in mycobacterial cell wall synthesis. Gene knockout studies in *Corynebacterium glutamicum*, a related model species tolerant of cell wall defects that kill mycobacteria, identified three proteins involved in the transport of mycolic acid intermediates across the cell wall. We have shown that the orthologs *NCgl2764*, *NCgl2762* and *NCgl2759* are involved in mycolic acid synthesis. The aim of this study was to determine the roles of *NCgl2760* and *NCgl2761*, the two remaining genes within the putative complex.

NCgl2761 was disrupted in *C. glutamicum* by homologous recombination and next the mutant was studied for cell wall defects. Total lipids, PIMs LM, LAM and mycolic acids were investigated by high performance thin layer chromatography (HPTLC), sodium dodecyl sulphate-polyacrylamide gel

electrophoresis (SDS-PAGE) and gas chromatography-mass spectrometry (GC-MS). Delayed growth and a block in the path from acetyl trehalose monocorynomylate (AcTMCM) to trehalose dicorynomylate (TDCM) indicate their involvement in mycolate metabolism. These conclusions were congruent with those of the other three genes in the putative complex. RNA extraction and co-transcription with *NCgl2760* were additionally investigated. The results do indeed show co-transcription of *C. glutamicum NCgl2761* and *C. glutamicum NCgl2760*. This co-transcription was replicated in *Mycobacterium smegmatis*, between genes *MSMEG_0315* and *MSMEG_0317*, the orthologs of *NCgl2761* and *NCgl2760*.

Deletion mutants of *NCgl2760* using the same principles were completed. Initial growth experimentation showed no delayed growth, unlike the other four genes, so the following procedures were performed in triplicate. Complementation of Δ *NCgl2760* was unsuccessful, consequently slice overlap extension (SOE) was attempted. This too failed. Nevertheless, experimental procedures continued and next showed absence of a block in the mycolic acid biosynthetic pathway. But, a Pierce™ silver stain showed a truncated, faster migrating LAM of a size measuring approximately 10kDa on a 15% SDS-PAGE gel.

Both these findings are novel and suggest that a complex of at least four proteins mediates mycolic acid transport, and RNA studies raise the possibility of a link between the mycolic acid and LM/LAM biosynthesis pathways in mycobacteria and corynebacteria. All these studies contribute to our understanding of mycobacterial cell wall pathways which may offer attractive drug targets.

Acknowledgements

I would like to sincerely thank my supervisors, Prof Ross Coppel and Dr Paul Crellin for their guidance, encouragement and patience throughout the course of my PhD. It has been a long road of “falls and stumbles”, but you both continued to believe in me and motivated me. Thank you for never allowing me to give up! Ross you are amazing to somehow manage to send a message of care somewhere in your hectic schedule. What a special person! Paul - thank you for all those long hours you ploughed into my thesis and presentations; compliments I received should always have been directed at you too.

My thanks also to the members of my PhD review panel who helped keep my supervisors and I focussed and target-driven. John Davies and Julian Rood had the task of panel chairmen and always somehow managed to keep me relaxed enough to speak. To Marina Harper I truly want to say what a blessing you were on my panel. Thank you for lifting the atmosphere, stating the facts as they should be and for helping me realize that life wasn't all that bad after all! I still look forward to every Monday's delivery from the Happiness Institute...

Thank you to our biochemistry collaborators, Malcolm McConville, Julie Ralton, Yoshiki Yamaryo-Botte, Stephan Klatt and Fleur Sernee for your work and assistance in the Metabolomics, Bio21 unit, University of Melbourne. Mal - your insight was always incredible. And a huge congratulations to you, Stephan, for mastering so many new proteomics techniques. Thank you for your additional biochemical input which all keeps leading our team in the right direction.

My utmost thanks to Rajini Brammananth without whose laboratory skills and guidance this degree would certainly not have been possible. Never doubt your talent and expertise Raj! Thank you for becoming my most special friend as we braved the “battlefields of *glutamicum*” together!

To our budding gold-star photographer - Arek Rainczuk, “Well done”! Thank you so very much for sharing so many of your patient computer hours with me, especially at Bio21. But, not only were you so bright and helpful, you were brave and made a big career decision. I’ll miss you.

And to the other special members of the Coppel/Cook lab, you have been great for a chat, a laugh or maybe even a tear. Thanks to Donna Buckingham, Ika Setyabudi, Ghizhal Siddiqui, Siti Shahpudin, Teresa Carvalho, Mitchell Batty, Megan Rees and Megan Bird, Charles Ma, Nick Proellocks, Belinda Morahan, Suzie Herrmann and Sejal Gohil. You have all helped create a supportive and dynamic working atmosphere; one in which I have been truly blessed.

In addition to my Monash family, I am honoured to have had the financial support of Monash University scholarships. I can’t thank you enough - without these my entire PhD experience would have been impossible.

But most especially, I would like to thank my long-distance family back in South Africa. Even though you were all on the other side of the world, Skype brought you into my arms when I needed you most - and you were always available. “Vasbyt!” I’ll never be able to thank you enough for your hours of listening, encouraging and moreover for sponsoring Qantas with my homeward-bound flights! We won the final race together, and I’ll always love you all for loving me.

Acronyms and Abbreviations

°C	degrees Celsius
%	percent
μCi	microcurie
μl	microlitre
μM	micromolar
AcPIM2	dimannosyl-PIM
AcPIM6	hexamannosyl-PIM
Ac ₃ PIM ₂	triacylated phosphatidylinositol dimannoside
Ac ₃ PIM ₄	triacylated phosphatidylinositol tetramannoside
Ac ₃ PIM ₆	triacylated phosphatidylinositol hexamannoside
Ac ₄ PIM ₂	tetraacylated phosphatidylinositol dimannoside
Ac ₄ PIM ₆	tetraacylated phosphatidylinositol hexamannoside
AcTMCM	acetyltrehalose monocorynomycolate
ADM	adenine monophosphate
AftA	arabinofuranosyltransferase A
AG	arabinogalactan
AIDS	acquired immune deficiency syndrome
APS	ammonium persulphate
Ara	D-arabinofuranose
<i>araf</i>	arabinofuranose
AraT	arabinofuranosyltransferase
ATP	adenine triphosphate
BCG	Bacille Calmette-Guérin
BHI	brain heart infusion
BLAST	Basic Local Alignment Search Tool

bp	base pairs
BSA	bovine serum albumin
BSTFA	bis(trimethylsilyl) trifluoroacetamide
CL	cardiolipin
Cmp	corynebacterial membrane proteins large
CMR	Comprehensive Microbial Resource
CO ₂	carbon dioxide (dry ice)
DAG	diacylglycerol
DCO	double cross-over
DC-SIGN	dendritic cell-specific intracellular-adhesion molecule-grabbing non-integrin
DIG	digoxigenin
DMSO	dimethyl sulfoxide
DNA	deoxyribonucleic acid
dNTP	deoxynucleotide triphosphate
DTT	dithiothreitol
EEA1	early endosomal antigen-1
EI	electron ionization
DPA	decaprenylphosphoryl-β-D-arabinofuranose
DTT	dithiothreitol
EDTA	ethylene diamine tetraacetic acid
EMB	ethambutol
ESI-TOF	electrospray ionization-time of flight
ESI-QTOF	electrospray ionization quadrupole time-of-flight
FAS-1	fatty acid synthase cycle-1
FAS-2	fatty acid synthase cycle-2
galf	D-galactofuranose

Fbp	fibronectin binding protein
galf	galactofuranose
GC-MS	gas chromatography - mass spectrometry
HF	hydrofluoric acid
HMM	Hidden Markov Model
HPAEC	high performance anion exchange chromatography
HPTLC	high performance thin layer chromatography
IFN γ	interferon gamma
IGRA	interferon-gamma release assay
IN	inner membrane
kb	kilobase pairs
LAM	lipoarabinomannan
LB	Luria-Bertani media
LiF	lithium fluoride
LiOH	lithium hydroxide
LM	lipomannan
LPS	lipopolysaccharide
LTBI	latent tuberculosis infection
M	molar
MAC	<i>Mycobacterium avium</i> complex
mAGP	mycolyl-arabinogalactan-peptidoglycan
MALDI-TOF	matrix assisted laser desorption/ionization time of flight
manp	D-mannopyranose
man ρ	mannospyranosyl
manT	mannosyl transferase
MDR-TB	multi-drug resistant tuberculosis

mg/ml	milligrams per millilitre
min	minute
ml	millilitre
mM	millimolar
mm	millimetre
MmpL	mycobacterial membrane protein large
NaCl	sodium chloride
NaOAc	sodium acetate
NaOH	sodium hydroxide
NH ₄	ammonium
nmole	nanomolar
PAGE	polyacrylamide gel electrophoresis
PBS	phosphate buffered saline
PCR	polymerase chain reaction
PE	phosphatidylethanolamine
PG	phosphodiacylglycerol
PI	phosphatidylinositol
PI3K	phosphatidylinositol-3-kinase
PIM	phosphatidylinositol mannoside
Pks13	polyketide synthase 13
PPM	polyprenolphosphomannose
rpm	revolutions per minute
RVC	rotational vacuum concentrator
SCO	single cross-over
SDS-PAGE	sodium dodecyl sulphate - polyacrylamide gel electrophoresis
SEM	standard error of the mean

SOE	splice overlap extension
TACO	tryptophan aspartate-containing coat protein
TAE	tris-actetate ethylene diamine tetraacetic acid
TB	tuberculosis
TDCM	trehalose dicorynomycolate
TDM	trehalose dimycolate
TDR-TB	totally-drug resistant tuberculosis
TFA	tri-fluoroacetic acid
t-LM	truncated lipomannan
TmaT	trehalose mycolyl acetyl transferase
TMCM	trehalose monocorynomycolate
TMCS	trimethylchlorosilane
TMM	trehalose monomycolate
TST	tuberculin skin test
v/v	volume per volume
w/v	weight per volume
WHO	Worldwide Health Organisation
WT	wild type
XDR-TB	extensively-drug resistant tuberculosis

Chapter 1

Cell Wall Biosynthesis in Mycobacteria and Corynebacteria

1.1 Corynebacterineae

The interaction of members of the bacterial kingdom with humans, particularly during the course of an infection has been and continues to be a subject of intense interest. The recognition of the beneficial effects of microbial flora on human physiology and immune surveillance has nuanced the view that bacteria are either harmful or irrelevant to human health. Nevertheless, bacterial pathogens still continue to play an important negative role in human health. Many species are involved in causing disease both in intact and immunocompromised hosts. A suborder of the Actinomycetales group, the Corynebacterineae (1) comprises *Mycobacterium*, *Corynebacterium*, *Rhodococcus* and *Nocardia*, amongst other genera. Members of this suborder are gram-positive bacteria and include pathogenic species such as *Mycobacterium tuberculosis*, *Corynebacterium diphtheriae* and *Mycobacterium leprae*. These are the causative agents of tuberculosis (TB), diphtheria and leprosy, respectively. Of increasing importance is multi-drug resistant (MDR) TB, which is believed to result from incomplete or partial antibiotic courses of therapy and is now posing a global threat to mankind.

The suborder Corynebacterineae also includes *Corynebacterium glutamicum* and *Mycobacterium smegmatis*. Both are considered non-pathogenic but are commonly used for laboratory research with *C. glutamicum* also serving as an industrial workhorse originally for large-scale glutamate production but also more recently amino acid and vitamin production (2).

1.2 Mycobacteria and Corynebacteria

1.2.1 Mycobacteria

Currently, the most significant bacterium causing human disease is *M. tuberculosis*, the causative agent of TB. Although *M. tuberculosis* is the most frequent cause of infection, other members of the “*Mycobacterium tuberculosis* complex”, a group of related species including *M. bovis*, *M. africanum* and *M. microti*, can also be responsible for TB infection.

Host and bacterial factors interplay to determine the outcome of infection with *M. tuberculosis*: cure, latency or active disease. Although much information regarding the pathophysiology is lacking, latent TB infection (LTBI) comprises a continuum of infection from asymptomatic to (re)activated disease. How far along the continuum one finds oneself is thought to depend upon the host immune system, size of the bacterial inoculum, intensity of exposure to the index case, and strain virulence (3). An estimated 30% of the global population is latently infected with TB from which active disease can be generated. Most recent surveys suggest a worldwide prevalence figure of 2.3 billion. However, surveys are difficult to conduct, standardise and maintain as demonstrated by figure 1.1. The worldwide incidence of TB continues to increase at an alarming rate, especially in southern Africa (Figure 1.2) where poverty and poor living conditions greatly influence pathogenesis.

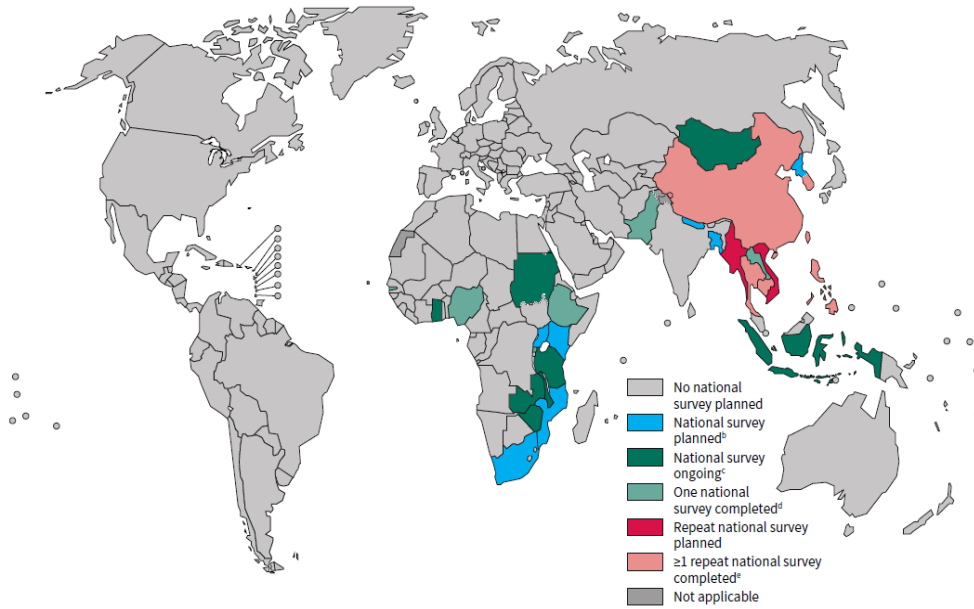


Figure 1.1 Countries in which national population-based surveys of the prevalence of TB disease have been implemented. Currently recommended screening and diagnostic methods have been in use since 1990 or are planned in the near future: status in July 2014 (WHO, 2015)

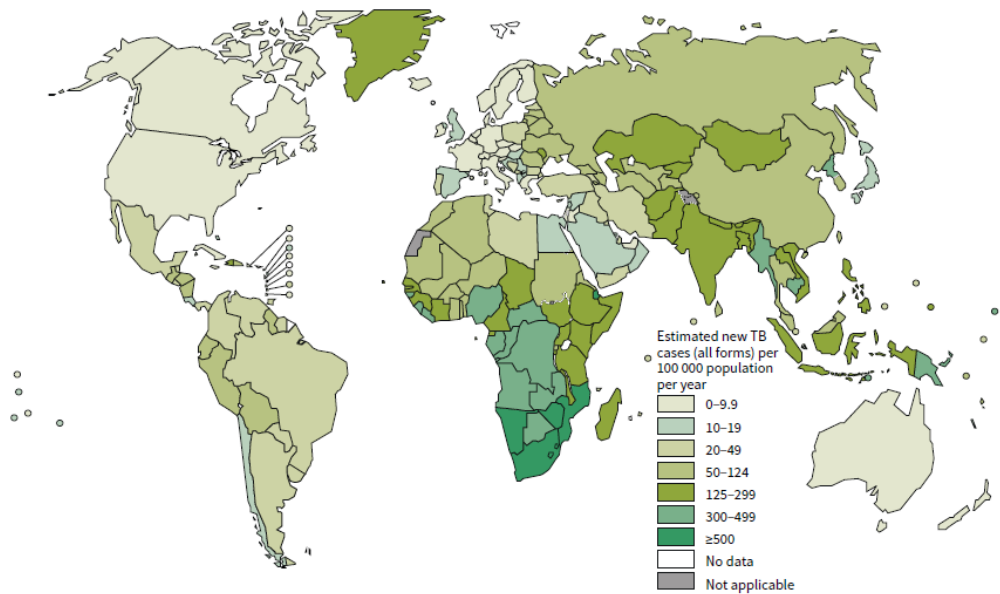


Figure 1.2 Estimated Global Incidence Rate of 2013 (from WHO, 2014).

The worldwide incidence of both reactivated latent and active TB is 4 485 000.

Clinical symptoms of TB include haemoptysis, weight loss, fatigue, fever and night sweats (4, 5). In addition, a consistent X-ray appearance is sought in diagnosis and in screening surveys. Early identification and a six month course of antibiotic treatment needs to be administered timeously. Diagnosis of tuberculosis is ideally shown by isolation and identification of the causative organism in a patient with a compatible clinical picture. However it is often difficult to recover bacteria from patients as the bacilli are typically deep within the lungs. In that case, evidence of an anti-mycobacterial immune response is sought either by a delayed type hypersensitivity response, the age-old tuberculin skin test (TST) or by cytokine release in response to antigen – the interferon-gamma release assay (IGRA), These immunological assays can also be used in patients who are asymptomatic (6).

The typical histological lesion in TB infection is a granuloma with core caseous necrosis (which has a cheese-like appearance), surrounded by a margin of infected alveolar macrophages, with an outer rim of polymorphonuclear lymphocytes. This caseous centre is composed of necrotic macrophages and cells without nuclei, as well as cell debris (7). However such lesions are not visualised directly except at post-mortem. These granulomas also offer the means whereby the bacilli can remain dormant permitting the TB infection to remain latent. Approximately 5% of individuals who are latently infected reactivate the loci to develop active TB. The granuloma is a microenvironment of dendritic cells, B-cells, T-cells, NK-cells and monocytes positioned around infected macrophages (8). As each macrophage undergoes apoptosis, its cell debris becomes part of the central caseous material and the bacillus infects a healthy macrophage, thereby increasing the granuloma size and possibility of penetration into a blood vessel or pulmonary airway. The granulomas occur predominantly in pulmonary disease following infection and replication in the alveolar macrophages (9). Upon penetration of a pulmonary blood vessel, the bacteria are disseminated throughout the

body followed by infection of multiple organs. Alternatively, the granuloma penetrates a pulmonary airway which irritates the airways, thereby causing further coughing and spread of the disease to other potential sufferers (10).

The spread of TB is facilitated by various factors: a) poverty, particularly in the developing world where living conditions are a significant contributory factor. Housing is limited, so overcrowding, squatting, and poor sanitation are problems; b) HIV co-infection. A study performed in 2004 suggested a chance of re-activation of TB in HIV-positive patients of 8-10% annually; and c) drug resistant strains of *M. tuberculosis*. MDR and XDR strains are becoming more prevalent, and may fail to respond to current drug regimes or require drugs with higher levels of toxicity and lower efficacy. Interestingly, it has been found that low vitamin D also predisposes towards TB infection (11).

Isoniazid, rifampicin, ethambutol and pyrazinamide comprise the four “first-line” TB drugs. MDR-TB is resistant to isoniazid and rifampicin, the two most commonly used TB treatments and requires a minimum of two years treatment. Worldwide, an estimated 3.5% of new cases and 20.5% of previously treated cases of TB recorded in 2013 were classified as MDR-TB. In the same year, 480 000 new cases and 210 000 deaths due to MDR-TB were reported. Of the 300 000 patients diagnosed with pulmonary TB in India, China, Russian Federation in 2013, more than half were infected by MDR-TB (WHO, 2014).

Yet, possibly even more concerning because of the high mortality rate, is extensively drug-resistant TB (XDR-TB) which has been reported in approximately 100 countries. XDR-TB is resistant to fluoroquinolone and any of the three injectable drugs: capreomycin, kanamycin and amikacin, in addition to rifampicin and isoniazid (12). In 2013, approximately 9% of patients with MDR-TB actually had XDR-TB (WHO, 2014).

Recently even totally-drug resistant (TDR) TB is emerging in some countries, such as India, Italy and Iran (13). It is resistant to all second-line drugs i.e. aminoglycosides, cyclic polypeptides, fluoroquinolones, thioamides, serine analogues, and salicylic acid derivatives in addition to the four first line drugs listed above (12)

Leprosy, caused by *M. leprae*, is a global problem, with especially high rates in Brazil, Bangladesh and India (WHO 2012). The prevalence of cases calculated across 103 registered countries at the end of 2014 was 180 464, and the number of new cases detected during 2013 was 215 557 (www.who.int/lep/en/). *M. leprae* causes damage to the skin and peripheral nerves resulting in life-long deformities and anaesthesia of the hands and feet. Nerve function is significantly impaired throughout the disease, which often rapidly deteriorates due to the immunologic reactions (14). The eyes can also be affected causing loss of sight and/or corneal and iris problems.

Mycobacterium ulcerans causes the third most common mycobacterial disease in humans. Being carried by aquatic insects, it causes disease predominantly in west and central Africa where it is associated with tropical wetlands. It causes painful Buruli ulcers, a devastating necrotic skin and subcutaneous disease which can progress to non-ulcerative disease and osteomyelitis (15). Mycolactone is the toxic macrolide through which it causes its cytotoxic and immunosuppressive effects (16). The incidence of *M. ulcerans* infection is increasing in tropical developing countries. This is most likely due to flooding and de-forestation, forcing people to live in overcrowded, poverty-stricken areas.

Mycobacterial species often cause infection in immunocompromised individuals. Consequently, their incidence is increasing due to the global emergence of Human Immuno-deficiency Virus (HIV).

Mycobacterium avium Complex (MAC) including *Mycobacterium avium* and *Mycobacterium intracellulare*, causes pneumonia but have little virulence in the normal host. They are more common in people with chronic lung diseases or HIV/AIDS (17, 18). *Mycobacterium kansasii* also causes pulmonary disease, whereas *Mycobacterium fortuitum* and *Mycobacterium chelonae* cause localized cutaneous infections after trauma such as surgery (19). *Mycobacterium chelonae* is a soil and water dwelling species which causes opportunistic infections such as abscesses, whereas *Mycobacterium marinum* usually infects aquatic creatures. One of the non-pathogenic species, *M. smegmatis*, is often used as a convenient laboratory model for *M. tuberculosis* research which would otherwise require BSL3 safety conditions. *M. smegmatis* takes approximately three days to culture on solid media, can be easily manipulated and genetically disrupted, and requires BSL2 conditions (20). As a member of the *Mycobacterium* genus, sequences with similarity to *M. tuberculosis* are likely to be true orthologs with a more predictable and understandable behaviour.

1.2.2 Corynebacteria

Diphtheria is an important human disease caused by *C. diphtheriae*. The disease typically manifests as an acute upper respiratory tract infection with a more systemic effect on the heart, kidneys, and peripheral nerves. Initially, diphtheria presents as severe pharyngitis with or without tough membranes which can later grow over the airways and cause suffocation and death. Alternatively, death can result from myocarditis (21). *Corynebacterium pseudotuberculosis* is an important veterinary organism. It primarily infects ungulates, most often sheep and goats, however horses, cows and camels can also be infected. A few isolated cases of human infection have been reported, but these are extremely rare (22, 23). This pathogen causes a chronic, caseating lymphadenitis with fever and wasting and histological features of infection show many similarities to TB. *C. glutamicum* is important in the industrial production of glutamate, amino acids and vitamins (24). It also serves

as a useful laboratory model for mycobacteria as it is non-pathogenic, fast-growing, amenable to genetic manipulation, and can tolerate cell wall defects that would render mycobacteria non-viable.

1.3. Structure and Biosynthesis of the Mycobacterial Cell Envelope

A unique, complex, waxy impermeable cell wall is characteristic of Mycobacteria. The cell wall continues to be an area of research interest due to its role in pathogenesis and as a target for anti-tubercular medications. The structure and biosynthesis of the mycobacterial cell wall is the focus of this PhD study, particularly the mycolic acid and glycolipid layers.

The cell wall of these bacteria is the target of most current antitubercular medications such as ethambutol and isoniazid. Unfortunately, frequent therapeutic use of these and other drugs is contributing to increases in acquired resistance. In general, where the mechanism of resistance is known, it arises via one of two mechanisms: either the gene encoding the target of the drug is mutated eg. *embB* for ethambutol, or the gene encoding an activator is disrupted eg. *katG* for isoniazid (25).

The cytoplasm and lipid bilayer limiting membrane of mycobacteria is surrounded by a hydrophobic, highly impermeable cell wall which is essential for bacterial survival within pulmonary alveolar macrophages (26). The cell wall is referred to as the mycolyl- arabinogalactan -peptidoglycan (mAGP) complex (27, 28). The individual components have been far better studied than the overall structure of the cell wall whose overall picture has been gleaned from electron microscopy sections (Figure 1.3). These have provided a theoretical model of the cell wall cross-section (Figure 1.4).

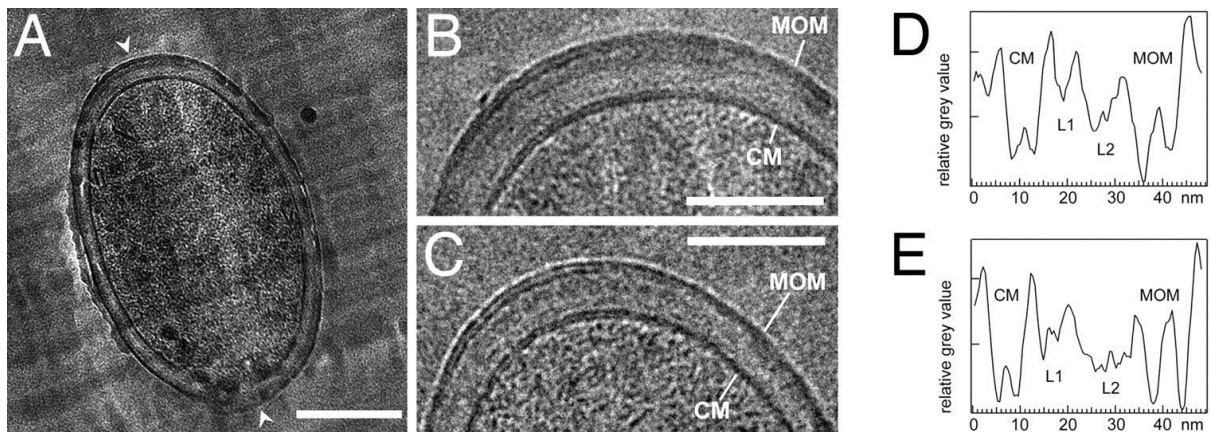


Figure 1.3 Cryo-electron micrographs of vitreous cross-sections from Mycobacteria. Sections have a nominal thickness of 35nm. The cross-section of an *M. smegmatis* cell deformed by the cutting process is shown in **A**. Regions perpendicular to the cutting direction (arrowheads) were used for further analyses (Scale bar = 200nm). **B** represents the cell envelope of an *M. smegmatis* cell (from **A**) while **C** shows the cell envelope of an *M. bovis* bacillus Calmette-Guerin (Scale bars = 100nm). The averaged profiles of **B** and **C** are shown in **D** and **E** respectively. CM = cytoplasmic membrane; MOM = mycobacterial outer membrane; L1, L2 = periplasmic layers. (From Hoffmann, C *et al.* (29))

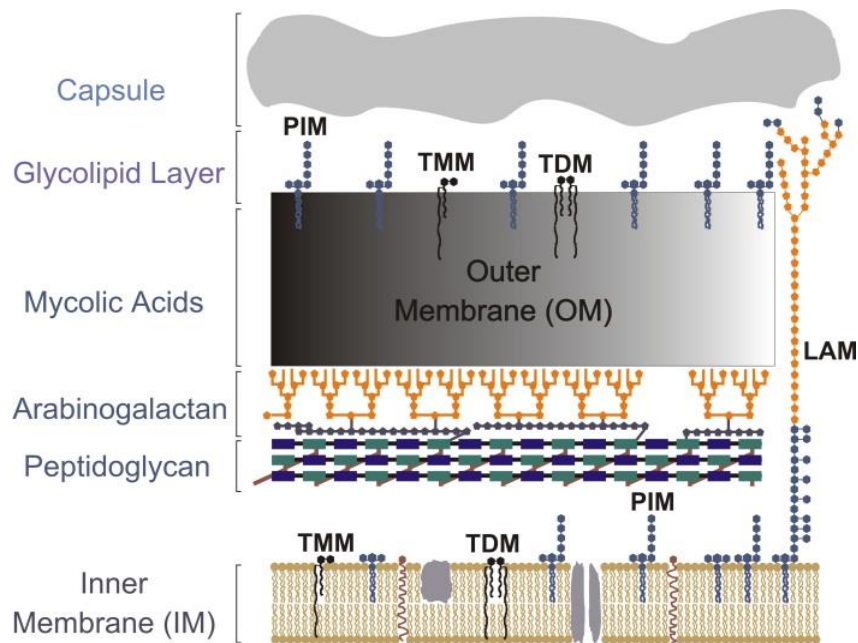


Figure 1.4 Schematic cross-section of the mycobacterial cell wall. The mycolyl-arabinogalactan-peptidoglycan (mAGP) complex is illustrated showing likely locations of trehalose monomycolate (TMM), trehalose dimycolate (TDM), phosphatidylinositol mannoside (PIM) and lipoarabinomannan (LAM).

The plasma membrane, or inner membrane (IM), is a typical lipid bilayer structure, i.e. two layers containing the polar headgroups of the membrane phospholipids separated by an electron-translucent layer comprising their acyl chains. Although the outer layer appears to be thinner than that of other bacteria, it is nevertheless thicker than the inner leaflet of the plasma membrane. This could be due to the presence of phosphatidylinositol (PI) moieties within phosphatidylinositol mannosides (PIMs), lipomannan (LM), and lipoarabinomannan (LAM) (30). These species are described in detail later in this chapter. The plasma membrane also contains phospholipids such as cardiolipin (CL) and phosphatidylethanolamine. Although the function of CL is currently uncertain, there is some evidence that it provides a platform for membrane-protein interactions (31).

Adjacent to the IM is a layer of insoluble peptidoglycan consisting of alternating units of N-acetylglucosamine and modified muramic acid residues. It is of the A1 γ type (32). The peptidoglycan is covalently attached to a layer of arabinogalactan, comprised of repeating arabinofuranose (*araf*) and galactofuranose (*galf*) residues. A specific linker unit, phosphoryl-N-acetylglucosaminosylrhamnosyl (32), joins the arabinan to the muramic acid of the peptidoglycan layer (33), and enzymes involved in its synthesis are considered to be very attractive drug targets.

The outer membrane consists of hydrophobic mycolic acids packed side-by-side and perpendicular to the plasma membrane and peptidoglycan (34). Mycolic acids are long chain 2-alkyl 3-hydroxy fatty acids which are either covalently linked to arabinogalactan or to the 6-hydroxy moiety of the disaccharide, trehalose, as trehalose TMM or TDM (35, 36). Additionally, in this outer membrane are porin proteins (37, 38), LM, the highly glycosylated LAM, and PIMs (39, 40). All have a PI anchor which attaches to the inner membrane. In mycobacteria, the most abundant PIMs are triacylated species termed dimannosyl-PIM (AcPIM2) and hexamannosyl-PIM (AcPIM6), carrying two and six mannoses, respectively. A much longer chain of α -1,6-linked mannoses is carried by LAM and LM,

while the α -1,6-mannan backbone is branched with multiple α -1,2-monomannoses (41). So the mycolic acids are interspersed by the acyl chains of the free glycolipids, LAM and proteins (42). The composition of each of these wall components, and the pathways used to synthesise them, are described in more detail below. My thesis will examine proteins involved in the synthesis of mycolic acids and LAM.

The capsule, electron-transparent in EM sections, is situated outside the bacterial wall and plasma membrane. It consists primarily of proteins and polysaccharides, with small amounts of lipid. Being at the interface of host-bacteria contact, the capsule is believed to play a role in bacterial pathogenicity, *eg.* some of the glycans have been shown to be involved in adhesion and penetration of the bacilli into the host macrophages. Inducible proteases and lipases have also been found. In addition, the capsule represents a physical barrier between the bacterium and the lytic enzymes of the host cell, offering an explanation for the bacterium's resistance of host defence mechanisms. (43)

1.3.1 Plasma membrane

The cytoplasmic membrane of this gram-positive organism consists of a characteristic bilayer of conventional glycerophospholipids, interrupted by apolar lipids. The lipids are mostly PGs derived from phosphatidic acid. In addition, there are PIs and the early intermediates of PIMs, including Ac/Ac₂PIM2 and the more mannosylated Ac/Ac₂PIM6 (44). The acyl components of the phospholipids consist of a mixture of fatty acids, the majority being palmitic (C₁₆), stearic (C₁₈) and tuberculostearic acids (C₁₉) (45). PIMs and LAM are anchored in the plasma membrane (Chatterjee *d*, 1992 pg6228). PG, CL, PE are also found (30) as well as trehalose monomycolate (TMM) which is situated on the inner membrane before acylation and transport to the outer cell surface (46).

1.3.2 Peptidoglycan

Peptidoglycan forms part of the mAGP complex outside of the plasma membrane and provides rigidity and strength to the bacterial cell. It is made up of alternating N-acetyl- β -D-glucosaminyl and N-glycolylmuramic acid units via repeating β (1-4) linkages (36, 47). Most bacterial peptidoglycan consists of the standard N-acetylmuramic acid residues (48). Additionally, tetrapeptide (L-alanyl-D-isoglutaminyl-meso-diaminopimelyl-D-alanine) side chains decorate the muramic acid residues (32, 49).

1.3.3 Arabinogalactan

The electron-dense layer around Corynebacterineae consists of arabinogalactan (AG), composed of *araf* and *galf* sugars (Figure 1.5). It is a linear galactan polymer of approximately 30-40 residues, to which arabinan chains are linked. The galactan core consists of a series of 5- and 6-linked units of β -D-*galf* residues. These reducing galactan domains are linked to peptidoglycan through phosphoryl-N-acetylglucosaminosyl-rhamnosyl specialised linker units (49), attaching to the linker unit via a 5-*galf* moiety (27). The model by Bhamidi *et al.* (50) suggests the galactan domain of 30 β -D-*galf* units in *M. tuberculosis* has additional branched arabinan chains each made up of 31 α -D-*araf* residues. The arabinan domain is arranged with different α (1 \rightarrow 5), α (1 \rightarrow 3) and β (1 \rightarrow 2) *araf* linkages (49) (Figure 1.5).

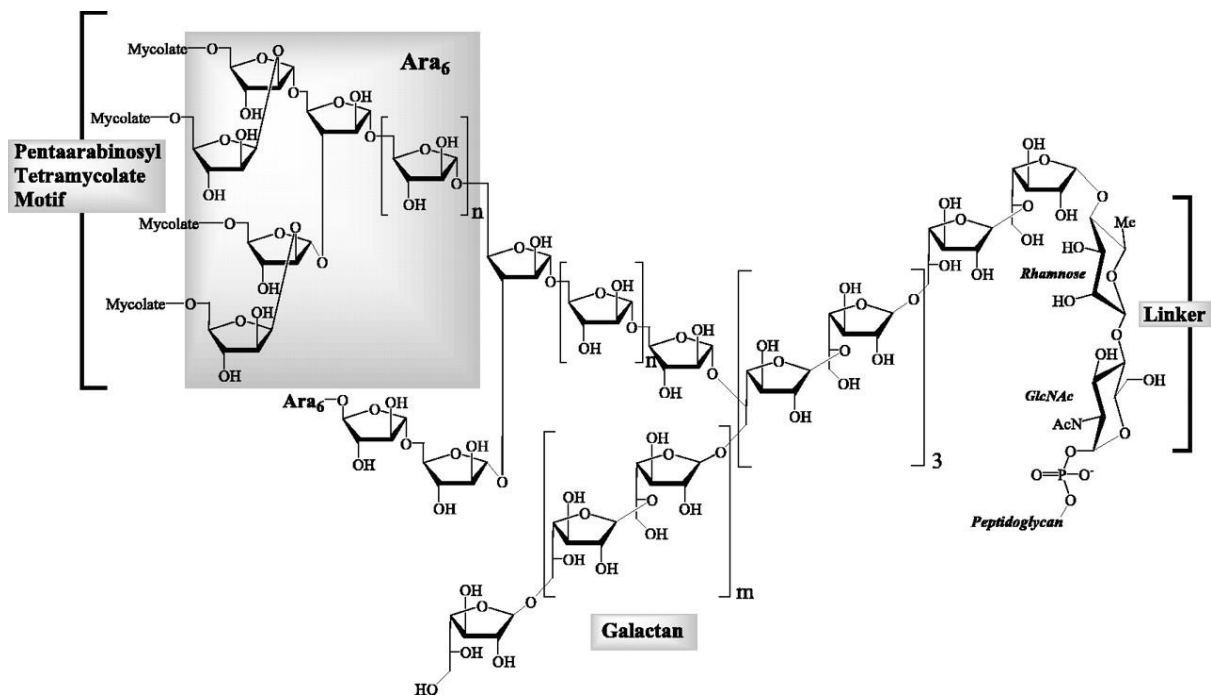


Figure 1.5 Mycobacterial arabinogalactan. Arabinogalactan is composed of alternating $\beta(1-5)$, $\beta(1-6)$ galactan chains with arabinan branches. Peptidoglycan is attached via a linker (rhamnose-GlcNAc). Arabinan consists of $\text{Ara}\alpha_1 \rightarrow [5\text{Ara}\alpha_1 \rightarrow]_n$ with branched Ara_6 termini. Mycolic acids are attached at the arabinose termini. (from Lee, RE *et al.* (51)).

At the distal nonreducing termini of two thirds of these *araf* polysaccharides, esterification links these chains to mycolic acids, thereby forming the outer layer of the mAGP complex (52). The mAGP complex is formed via a unique diglycosylphosphoryl bridge (53) which, together with AG and mycolic acids, contributes to the high impermeability of the outer membrane (54).

The arabinan domain is made up of $\alpha(1-5)$, $\alpha(1-3)$ and $\beta(1-2)$ *araf* linkages (52, 55). The terminal Ara₆ motif consists of *araf* β 1 - 2*araf* α 1 - 5(*araf* β 1 - 2*araf* α 1-3) *araf* α 1 - 5*araf* α 1 residues. The β -*araf* and penultimate 2 – α -*araf* are the mycolate binding sites. The inner core of the arabinan domain with importantly positioned α -2,5-branch sites is made up of α -1,5-linked *araf* residues (56). The arabinogalactan together with mycolic acids contribute to the high impermeability of the outer membrane (54). Enzymes involved in the polymerization of arabinose into AG and LAM are the target of ethambutol, a first-line TB treatment (57).

1.3.3.1 Biosynthesis of arabinogalactan

Although the structure of AG is reasonably well understood, its biosynthesis still requires much investigation. A study by Alderwick, LJ *et al.* (58) showed the importance of the gene for the arabinofuranosyltransferase, AftA, which is adjacent to the *emb* cluster, encoding a set of unique arabinofuranosyltransferases responsible for the synthesis of arabinan. It transfers the initial *araf* to the galactan backbone (58) using β -D-arabinofuranosyl-1-monophosphoryl-decaprenol (DPA) as the donor. It transfers singular *araf* residues to the 8th, 10th and 12th *gal*f residues on the linear galactan chain (54). These initial *araf* residues facilitate the subsequent binding of further α (1-5) - linked *araf* residues.

Next AftB caps the terminal β -1,2-arabinan. Either AftB, or an unknown GT-C arabinofuranosyltransferase, may be responsible for the binding of the second β (1-2)-linked araf residue. Either before or during completion of the formation of the terminal Ara₆ motif, mycolylation can occur (59). AftC functions in the internal branching of α -1,3- branching arabinan (60). EmbA and EmbB are necessary for the further extension of arabinogalactan through formation of the Ara₆ motif (55, 61, 62), while EmbC is vital in the elongation of the arabinan domain of LAM (63). The findings of Skovierova *et al.* suggest that AftD is an active arabinofuranosyltransferase on linear α -(1-5)-linked araf acceptors (56). In contrast to *M. tuberculosis*, *C. glutamicum* has only one form of *emb* which, when knocked out, results in a slow-growing mutant with only terminal araf residues characteristic of truncated arabinogalactan. This is due to the loss of the terminal Ara₆ motif (53).

1.3.4 Mycolic acids

Mycolic acids are unique to Corynebacterineae and very important in pathogenesis. They are involved in mycobacterial virulence and pathogenesis, cell envelope permeability, host immunomodulation, and persistence of *M. tuberculosis* within the human host (64). Mycolic acids are thought to form the inner leaflet of the outer membrane (36). These lipids are responsible for the characteristic waxy surface of mycobacterial cells which constitutes the primary defence against the antibacterial activities of host macrophages. Mycolic acids, being essential for bacterial growth and survival, are the major target of anti-tubercular drugs such as isoniazid which target specific enzymes involved in fatty acid synthesis (35).

Intrinsic drug-resistance and toxic properties of mycobacteria are largely a consequence of the α -alkyl- β -hydroxy fatty mycolic acids (36) which make up a large proportion of the cell wall (65). They are bound to the outer membrane by their attachment to the arabinogalactan layer or located in the

plasma membrane as TMM and TDM (66). While their structures vary considerably, they are found in all mycobacteria and related genera (45) (Figure 1.6). Mycobacterial TMM and TDM have similar structures to trehalose monocorynomylate (TMCM) and trehalose dicorynomylate (TDCM) in Corynebacteria, respectively, except that the latter have shorter fatty acyl chains and are termed corynomylates (67) (Figure 1.6).

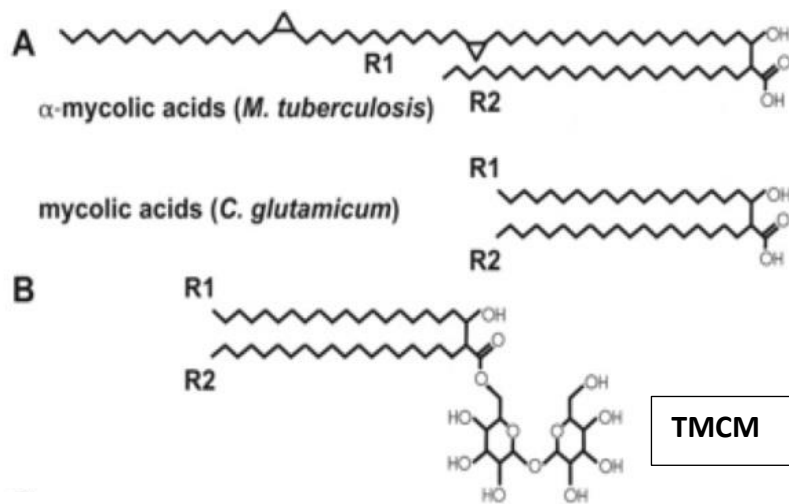


Figure 1.6 General mycolic acid structure. (A) The fatty acid chains in *C. glutamicum* are significantly shorter than those of *M. tuberculosis*; **(B)** linkage of the polysaccharide trehalose to a corynomycolic acid forms corynebacterial TMCM.

These molecules vary in length from 60-90 carbons in *M. tuberculosis* and 22-36 carbons in *Corynebacteria* (68). Mycolic acids consist of 2 main components: a) a shorter lipid α -branch constituting a saturated fatty acid of 20-26 carbons in length, and b) a longer meromycolate branch of approximately 60 carbons in length. Three classes of meromycolates exist: α -mycolate (2 *cis* cyclopropane rings on the meromycolate chain), methoxymycolate (a single, proximal *cis* or *trans* cyclopropane ring and a distal methoxy group), and ketomycolate (a single, proximal *cis* or *trans* cyclopropane ring and a distal ketone group) (69, 70). In addition to these *cis* and *trans* double bonds, cyclopropane structures, oxygen groups and methyl branches, the meromycolate contains a β -hydroxy motif.

Mycobacterial cell walls generally contain variable combinations of mycolic acids. A family of S-adenosyl methionine-dependent methyl transferases, namely cyclopropane mycolic acid synthases (64), synthesize the cyclopropane rings and methyl branches of these lipids (70). Glickman MS, *et al.* (71) showed that PcaA and MmaA2 are required for alpha mycolate cyclopropanation, and CmmaA2 for *trans* cyclopropanation of the oxygenated mycolates (72). MmaA3 and MmaA4 are required for functionality of the oxygenated mycolates (73, 74). Finally, MmaA1 is needed for branch formation preceding the cyclopropanation step by CmaA2.

Mycobacterial cells typically aggregate in microscopic cords, a characteristic feature initially attributed to TDM. These microscopic cords are associated with virulence of *M. tuberculosis* and have more recently been shown to be associated with persistence in macrophages (75). TDM is an especially antigenic, surface-exposed glycolipid contributing to the hydrophobicity of the cell wall. Because of its adjuvant properties, bacteria have evolved mechanisms to shield TDM from exposure to the immune system (76).

1.3.4.1 Biosynthesis of mycolic acids

1. Fatty acid synthase cycles-I and -II

The mycobacterial cell wall is unique and essential to the growth and survival of these bacteria, and an improved understanding of its complex biosynthetic pathways has the potential to reveal new drug targets. Being such a complex, multilayered structure, biosynthesis of this outer layer is also very complex. The pathways of mycolic acid synthesis and transport are of particular relevance to the projects described later in this thesis.

The two fatty acyl components of the mycolic acids are synthesized via separate reactions before being condensed to form the final mycolic acid. First they sequentially progress through the fatty acid synthase cycle-1 (FAS-I), the products of this cycle being processed in the fatty acid synthase cycle-2 (FAS-II). The *fas* gene encodes a protein which elongates acyl groups using malonyl-CoA and acetyl-CoA. (Figure 1.7). Mycobacteria use acetyl-CoA and malonyl-CoA as substrates primarily for the *de novo* synthesis of the fatty acid C-20 and C-26-Enz derivatives via the FAS-I system (35) (Figure 1.7). These fatty acids are released as the Co-A derivatives, with the C20 fatty acid being the starting point for the FAS-II cycle or to form membrane phospholipids. The FAS-I cycle also synthesizes hexacosanoyl (C26) acid and this develops into the short α -alkyl chain of the mycolic acid (35). The FAS-II system very likely takes over the production of the mero segment of the α -, methoxy-, and keto-mycolic acids. Meroacid is the long α -alkyl mycolic acid chain.

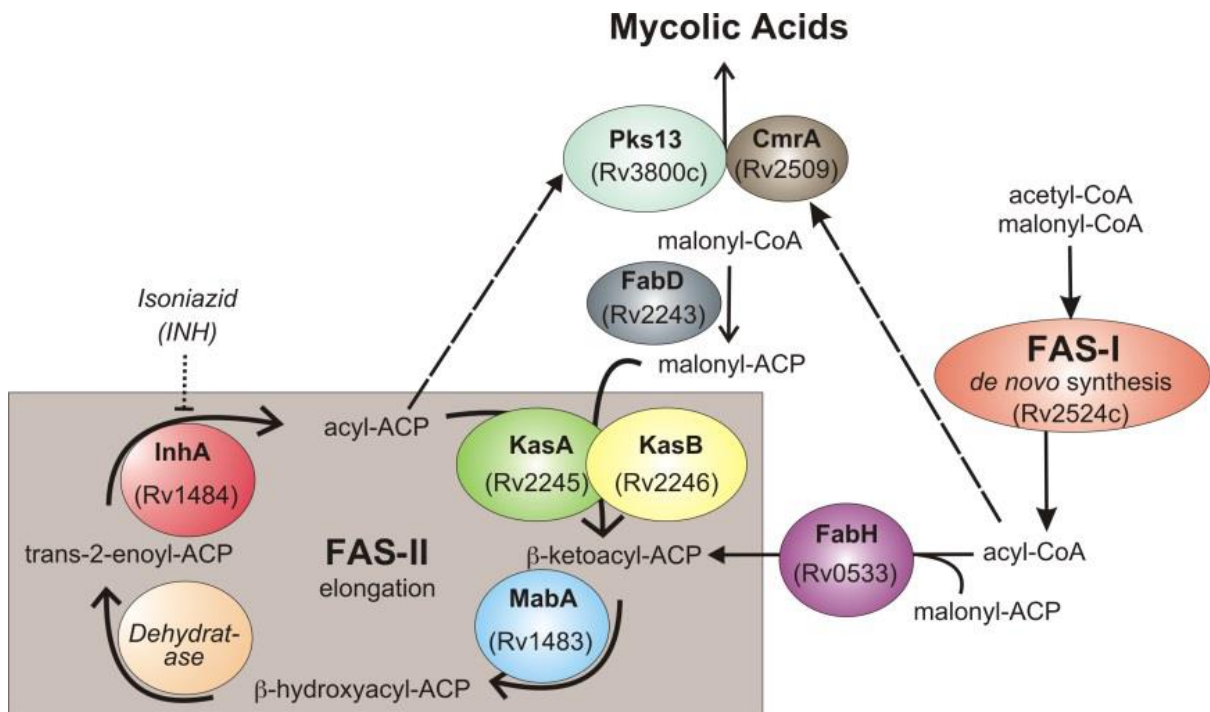


Figure 1.7 Fatty acid biosynthesis pathways in mycobacteria. Fatty acids are synthesized by two sequential cycles before being utilised for the production of mycolic acids. Dashed lines indicate the products which continue to be used for mycolic acid biosynthesis. The point of inhibition of the drug isoniazid (INH) is also indicated (from Crellin, PK *et al.* (77))

The FAS-II cycle is initiated by the enzyme FabH, catalysing the condensation of acetyl-CoA and malonyl-S-acyl carrier proteins (malonyl-S-ACP) (78). The FAS-II fatty acid cycle is similar to the FAS-I system except the latter synthesises long chain fatty acids and cannot produce new fatty acids from acetate. Also unlike FAS-I, which is a single large protein, the FAS-II system is comprised of a series of enzymes catalysing repeated condensation, reduction, and dehydration reactions (79). Five cycles of FAS-II are needed for synthesis of α -meroacids and 8 cycles for methoxy- and keto-meroacids (80).

2. Condensation of fatty acids

Next follows the condensation reaction in which the two fatty acids are linked. A large polyketide synthase, Pks13 (Rv3800c), catalyses this reaction. A study by Portevin *et al.* (81) reported that after synthesis of the C23-C27 α -branch by the FAS-II cycle, Pks13 is responsible for the condensation with the meromycolic acid to form alkyl-3-keto fatty acid (Figures 1.7 and 1.8). It is a Claisen-type reaction and essential for bacterial viability.

Prior to condensation, one fatty acid chain is activated by addition of adenine monophosphate (AMP) while the other is carboxylated (82). Studies done in *C. glutamicum* suggest that the two proteins, AccD2 and AccD3, and the putative carboxylase AccD4, form part of an acyl-CoA carboxylase complex allowing carboxylation of the fatty acids (83).

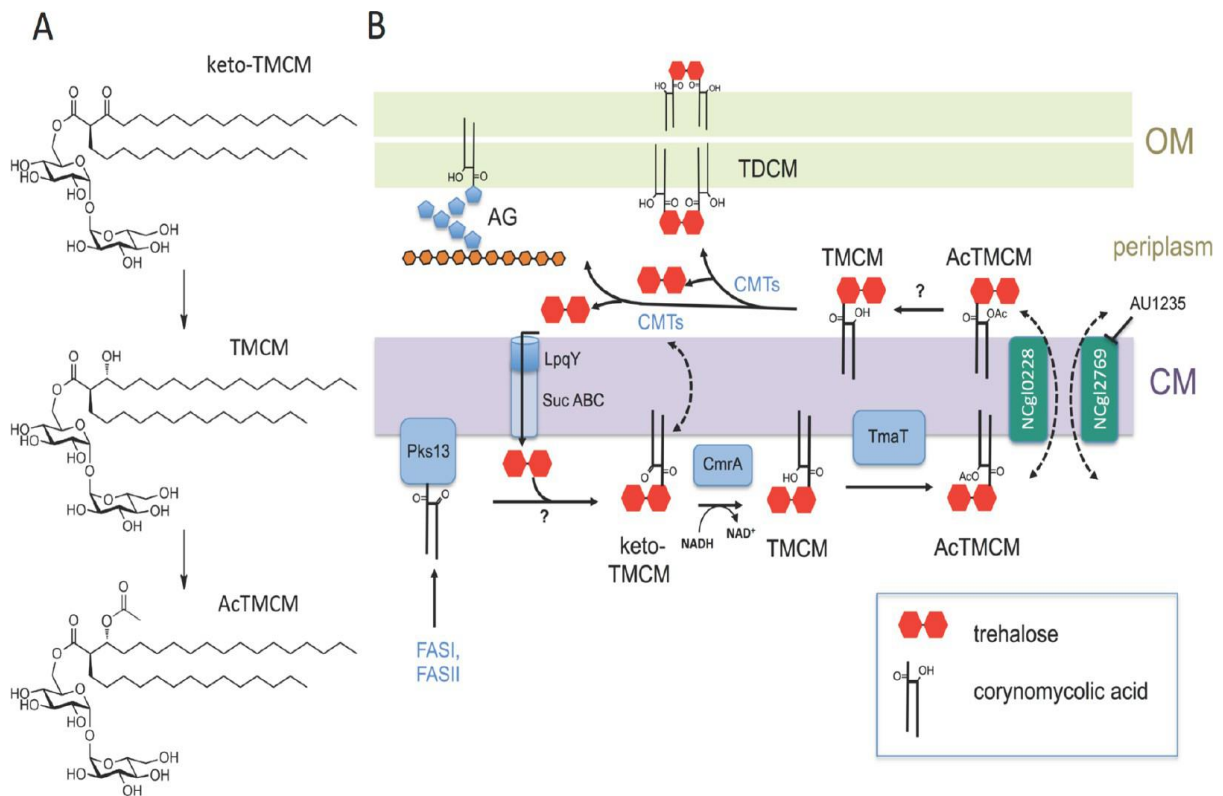


Figure 1.8 Proposed reactions of mycolic acid biosynthesis pathway at the corynebacterial plasma membrane. A) The biochemical structure of keto-TMCM, TMCM and AcTMCM as they proceed and develop through the mycobacterial metabolic pathway. **B)** Disruption of NCgl0228 and/or NCgl2769 lessens the amount of TMCM flipped across the cell membrane suggesting their possible function. AU1235 is a synthetic drug which blocks the function of NCgl2769, thereby mimicking a gene knock-out. TmaT is the homologue of NCgl2759 and functions as an acyltransferase (from Yarmayo-Botte, Y *et al.* (46)).

The mycolate is subsequently attached to the 6-hydroxyl group of the disaccharide, trehalose, by a mycolyltransferase to form keto-TMCM in *C. glutamicum* (81) (Figure 1.8). The product is then reduced by CmrA to form the mature mycolic acid on the cytoplasmic leaflet of the cell membrane. CmrA reduces the keto-group to form TMCM (84). Recent studies suggest that the majority of mycolic acids are transported across the membrane as TMCMs (85). After loss of the keto group, the mycolic acid is modified by addition of an acetyl group then flipped to the periplasm of the cell after conversion to AcTMCM (46). The addition of the acetyl group is mediated by an acetyltransferase, NCgl2759, in *C. glutamicum*, which is the likely orthologue of Rv0228 in *M. tuberculosis* (46). The precise role of this acetylation is still unclear. Either the acetyl group is a signal necessary for recognition by a polytopic membrane protein called Mmpl3, a member of the mycobacterial membrane protein large family (86, 87), or it reduces mycolyl polarity to facilitate transport across a pore formed by Mmpl-proteins (88).

Recent studies suggest that NCgl2769 and NCgl0228 are two functional orthologs of the Mmpl3 protein which are involved in TMCM transport (89). While *C. glutamicum* mutants lacking either *NCgl0228* or *NCgl2769* have no apparent phenotype, disruption of both genes simultaneously causes a complete loss of cell wall bound and trehalose-associated corynomycolates, suggesting at least one of these proteins must be present for Pks13 to function (89).

After deacetylation in the periplasm, TMCM either reacts with another TMCM to form TDCM (90) or is esterified to a terminal araf of arabinogalactan by one or a series of mycolyltransferases. In mycobacteria, these include members of the Antigen 85 complex, also referred to as fibronectin binding proteins (Fbps) (65, 91). This complex is made up of FbpA (Rv3804c), FbpB (Rv1886c) and FbpC (Rv0129c). All appear to have mycolyltransferase activity, inclusive of the carboxylesterase

domain in FbpC (91). FbpA and FbpB are situated on the outer leaflet of the cell membrane, and FbpC is in the cell wall fraction (92). In *C. glutamicum*, Cop1, Cmt1 and Cmt2, all corynomycolic acid transferases, are believed to be responsible for the formation of TDCM. Cmt4 is an essential enzyme and its substrate is unknown (93, 94). The free trehalose is recycled back into the cell cytoplasm via LpqY-SucABC, an ABC-transporter (95) (Figure 1.8).

While many of the genes and proteins involved in the mycolic acid biosynthetic pathways are understood and well described, reactions at the plasma membrane require further investigation and characterization. New studies on mycolic acid transport across the cell membrane are presented in Chapter 3 of this thesis.

1.3.5 Mannosylated phospholipids

In addition to the mycolic acids, the mycobacterial cell envelope has an abundance of mannosylated phospholipids, namely phosphatidylinositol mannosides (PIMs), lipomannan (LM) and its arabinosylated form, lipoarabinomannan (LAM). The structures of these lipids remain relatively constant among all mycobacterial species (30). They form an integral part of the mycobacterial and corynebacterial cell wall and have been shown to influence both the innate (96, 97) and adaptive immune responses of the host (98-100).

1.3.5.1. Phosphatidylinositol mannosides (PIMs)

PIMs are oligomannosylated forms of phosphatidyl-*myo*-inositol (PI) and may contain up to 6 mannose residues. They are formed by the addition of mannopyranosyl (*manp*) residues to the acetylated PI anchor (101). They consist of a glycerol backbone with two acyl chains attached at the C1 and C2 positions, which serve to anchor them in the plasma or outer membranes (102). Acylation

at C1 and C2 is normally with 10-methyl-octadecanoic acid (tuberculostearic acid, C19) and hexadecanoic fatty acid (palmitic acid, C16), respectively (103) (Figure 1.9).

Examples of C14 and mono-acetylated forms have also been noted with one of the two identified acids occurring at position C1 (104, 105). The C3 position of the glycerol is the site of attachment of the phosphate group, which is subsequently linked to the 1-position of *D-myo*-inositol (106). α -1-D mannopyranose groups are linked to the C2 and C6 of the *D-myo*-inositol at their 1-position to form PIM2. The nomenclature AcxPIMy is generally used where x refers to the number of additional acyl chains and y refers to the number of mannose residues (107). PIM2 is the precursor of the larger PIMs: PIM3, PIM4, PIM5 and PIM6 (Figure 1.9). Each one carries an additional mannose residue. For PIM2 to PIM3 and PIM4, the linkages are α (1 \rightarrow 6) and as both α (1 \rightarrow 6) and α (1 \rightarrow 2) for PIM5 and PIM6 (108, 109). AcPIM4 is a branch point of polar PIM and LM/LAM biosynthesis (40, 110). It can be further mannosylated with α 1(1 \rightarrow 2) linkages by the PimE mannosyltransferase (111), thereby forming AcPIM5 and AcPIM6. PIM6 is capped with 2 α (1-2) linked mannoses so cannot serve as a precursor for LM or LAM (112). Alternatively, AcPIM4 can be elongated with α (1 \rightarrow 6) linkages of mannoses and side chains of α (1 \rightarrow 2) ultimately forming LM. Next LM can be arabinosylated to form LAM (113).

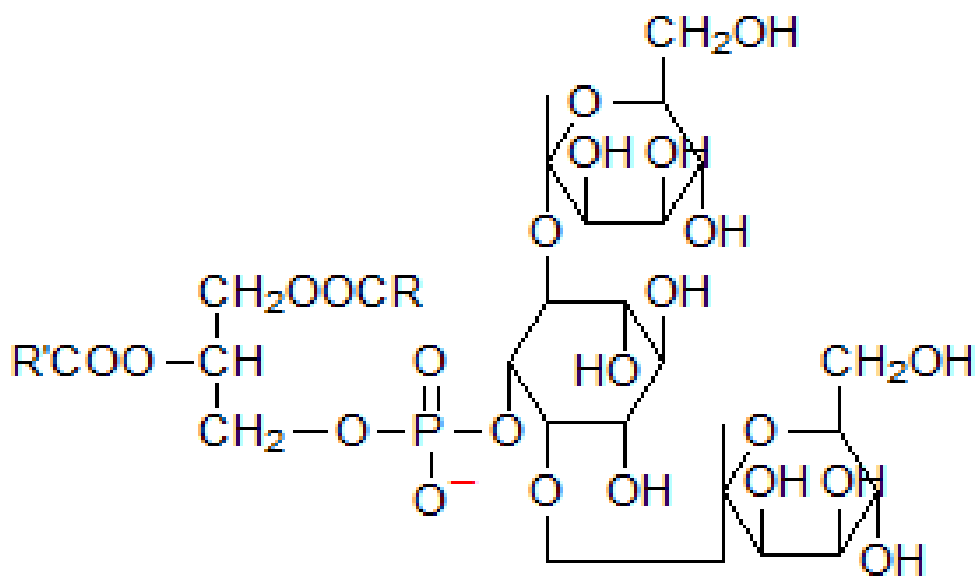


Figure 1.9 Structure of 1-phosphatidyl-L-myo-inositol 2,6-di-O- α -D-mannopyranoside (PIM2). PIM2 is the basic structure from which the more complex PIMs are constructed by the sequential addition of mannose molecules. The main fatty acids characteristic of PIMs are normally tuberculostearic acid (C_{19}) on R with palmitic (C_{16}) normally on R'. (Glycosylphosphatidylinositol anchors for proteins and phosphatidylinositolmannosides, AOCs Lipid Library 2014)

Biosynthesis of PIMs

Lipoglycan biosynthetic pathways are highly conserved within the Actinomycetales (101). Myo-inositol is condensed with CDP-diacylglycerol by the PI synthase PgsA (Rv2612c) to form PI. This is subsequently modified by the consecutive transfer of mannosyl units from GDP-mannose, in reactions catalysed by cytoplasmic mannosyltransferases (114) to form the early PIMs. Mannose is essential in a) the cytosol as the sugar donor GDP-mannose, and b) as an extra-cytosolic glycosyl donor molecule polyprenolphosphomannose (PPM) (115). It is either obtained from the growth medium or synthesised from cytosolic glucose via the glycolytic pathway. Initially, PIM1 is synthesized from glucose 6-P by the enzyme inositol-1-phosphate synthase (116). This reaction is followed by acylation of the 2-mannose (which is encoded by the acyltransferase Rv2611c) to yield monoacylated AcPIM1. PimB adds the second Man_p to the 6-position to synthesise AcPIM2 (117, 118). As well as having a structural role, AcPIM2 is highly immunogenic. It is able to both induce granuloma formation and recruit natural killer T-cells (104). PimC is also involved in the initial formation of LAM glycolipids, synthesising AcPIM3 (42). However, Bifani *et al.* (119) showed that not all *M. tuberculosis* isolates carry the *pimC*.

1.3.5.2. Lipomannan and Lipoarabinomannan

LM and LAM are long complex lipopolysaccharides responsible for cell wall integrity and virulence (120). The presence of large diffuse bands when analysed by SDS-PAGE suggests that they exist in heterogeneous forms. Their heterogeneity is explained by the varying degrees of acetylation and glycosylation (103, 121). A band which migrates faster on gels represents LM, the less complex lipoglycan (101).

Mycobacterial LAM, LM and PIMs are not only responsible for the structural integrity of the cell wall (111), they are potent regulators of macrophage function which may have an impact on mycobacterial disease (122). LAM may even be involved in macrophage phagocytosis (123). It has been suggested that LAM is one of the chemotactic factors released by *M. tuberculosis*-infected alveolar macrophages (124). Indeed, in *M. smegmatis*, loss of acid-fast staining, increased sensitivity to B-lactams, and faster macrophage killing resulted from structural defects in LM and LAM (125).

Endo- α 1-6-mannosidase digestion of LM results in a product similar to PIM2, suggesting that PIMs are precursors of LM (41). When mature, LM may be arabinosylated to form LAM (39, 53, 60) by further glycosylation with a branched D-arabinan side chain of approximately 70 Araf residues (Figure 1.10) (102).

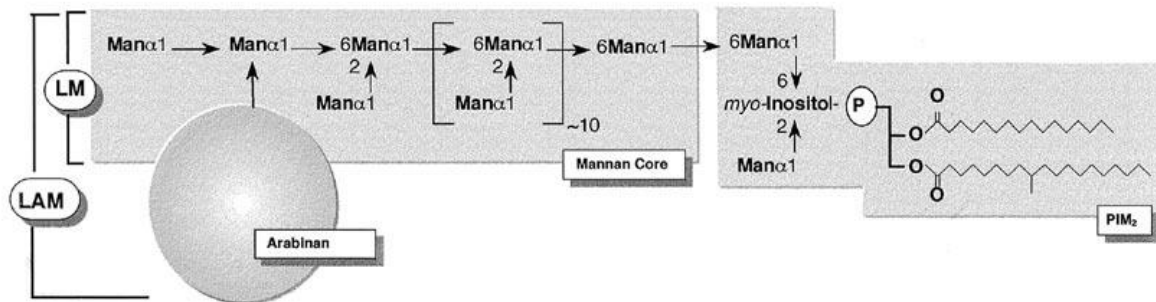


Figure 1.10 Schematic of the proposed structural relationship between mycobacterial PIM2, LM and LAM. The mannan core has an $\alpha 1 \rightarrow 6$ backbone, with single mannose branches in position 2. The backbone is directly attached to position 6 of the *myo*-inositol moiety of the PI anchor (from Chatterjee, D *et al.* (103)).

Following further investigations, GC-MS showed that LAM is most commonly made up of PIM2 and lipomannan-like products (41). This same study showed that LAM consists of a *myo*-inositol-1-P group and a glycerol group which is acetylated with palmitic and tuberculostearic acids. This region is clearly similar to PIMs. PIM4 is the largest PIM that can perform this function as PIM6 is capped with 2 $\alpha(1-2)$ linked mannoses so cannot serve as a precursor for LM or LAM (112).

The arabinan component of LAM is similar, although not identical, to that of arabinogalactan, since both share a common Ara₁₈ motif. The arabinan of LAM can be more variable in terms of length, consisting of a chain of $\alpha(1\rightarrow5)$ Araf residues with occasional $\alpha(1\rightarrow3)$ branching and a non-reducing terminus characterized by either an Ara₄ or Ara₆ motif (126). The LAM structure consists of 50 Manp and 60 Araf units (127-129). A detailed study of purified LAM from *M. tuberculosis* H37Ra by NMR and GC-MS of the hydrolysed LAM fragments confirmed the fragments are in the furanose conformation, similar to those of arabinogalactan (101, 130).

In *C. glutamicum*, the organism of study in this thesis, two types of LM can be found: LM-A and LM-B, as there are two pathways for LM synthesis, with the LM-A pool capable of being further processed to form LAMs. LM-A synthesis is therefore analogous to the mycobacterial LM/LAM pathway (called LM-A/LAM) whereas the second pathway (called LM-B) is so far only described in corynebacteria and is based upon a different anchor. The majority of LM in *C. glutamicum* is LM-B which is structurally similar to LM-A but based upon a glucuronic acid anchor molecule (Figure 1.11), instead of the phosphatidylinositol anchor (PI) found in LM-A.

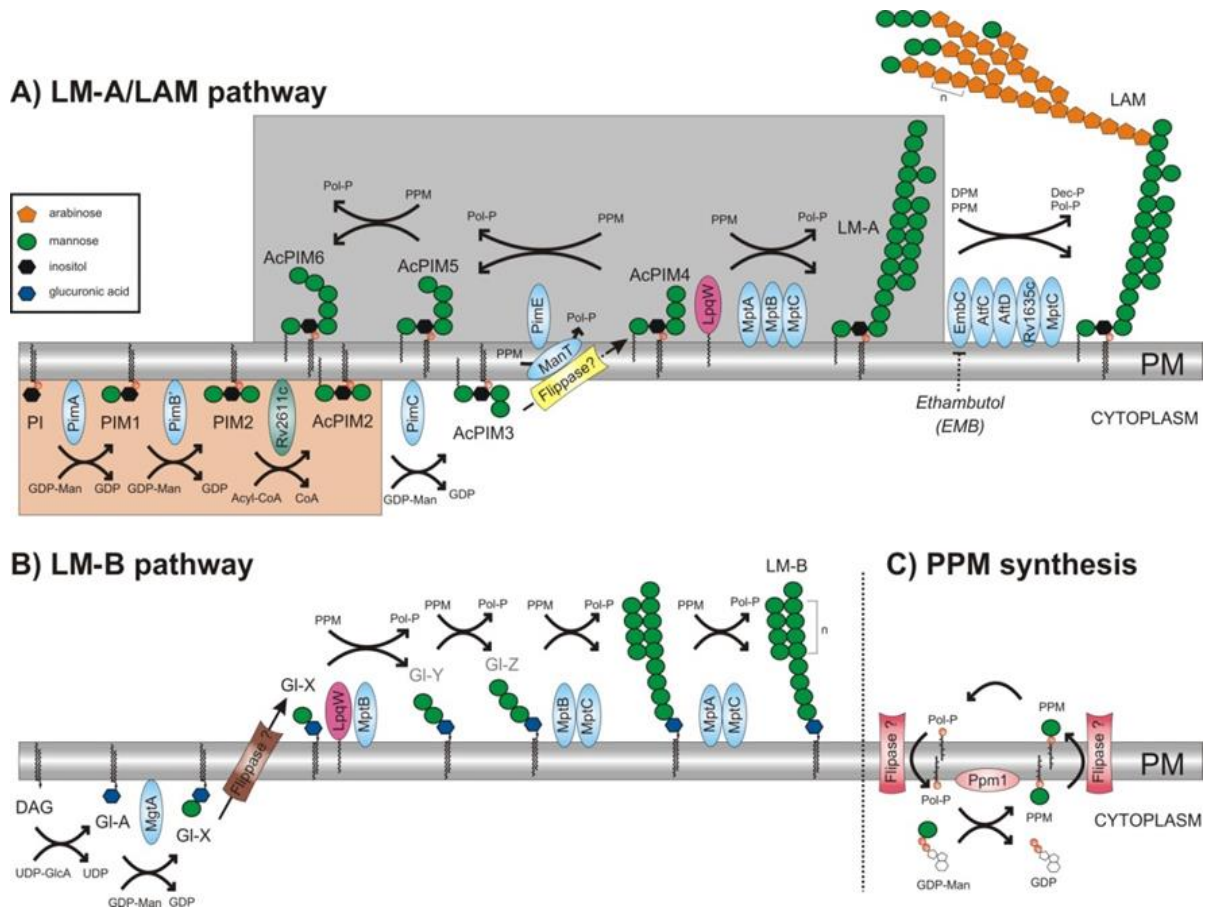


Figure 1.11. Proposed divergent metabolic pathways of LM-A/LAM and LM-B. **A)** The LM-A/ LAM pathway is based upon PI acylation and mannosylation. Man_p residues are sequentially added until AcPIM4 is formed, where the pathway diverges. PPM either donates another 2 mannoses to form AcPIM6 or LM-A. Arabinose residues can then be added to form LAM. **B)** Cg-LM-B is based upon a glucuronosyl diacylglycerol. Interestingly, no arabinosyltransferases participate in this pathway, in contrast to the LM-A/LAM pathway. **(C)** PPM is a periplasmic mannose donor. It is active in both the LM-A/LAM and LM-B pathways and formed from GDP-Man by the enzyme Ppm1 (from Crellin, PK (77)).

Three hypotheses exist concerning the position of LAM in the cell wall. Either its lipid moiety anchors it in the plasma membrane, allowing the terminal arabinose or mannose caps to protrude through the bulk of the cell wall (131). Alternatively, LAM is anchored by its PI-core in the outer leaflet of the cell's outer membrane, and makes up this membrane together with other wall-associated lipids (132). A third possibility is that LAM is constantly secreted so the surface-exposed arabinose/mannose-termini are exposed only while the lipoglycan is in transit from its place of synthesis to the cell surface (103). All of these hypothesised locations are consistent with exposure of LAM at the bacterial surface for activation of the host immune system.

Biosynthesis of lipoglycans

Lipoglycan biosynthetic pathways are highly conserved within Actinomycetales. LM and LAM synthesis appears to progress through two divergent biosynthetic cascades in *Corynebacteria*. (Figure 1.11). A family of glycosyltransferases performs sequential transfer of mannose at each biosynthetic step using the high-energy nucleotide GDP-mannose to a PI-based anchor, suggesting localization to the cytoplasm (60). Synthesis of PIMs, as described in Section 1.3.5.1A, takes place within the cytoplasm until AcPIM4, which is a branch point in the LM-A/LAM pathway. When the pathway reaches AcPIM4, it appears to diverge forming either AcPIM6 or LM-A/LAM (110). PimE is evidently vital in the branching to AcPIM6 (111, 125).

Synthesis of LM-A is based on PI acetylation and mannosylation (133). Larger PIMs are formed by the addition of consecutive Man_p residues to the mannose attached to the 6-position of the *myo*-inositol. Either one or two $\alpha(1\rightarrow2)$ -linked mannose residues may be added or alternatively, linkage of long (>20) mannose chains results in the mannan backbone of LM-A/LAM (111). The mannosyltransferases involved in all of these reactions utilize PPM, a lipid-linked mannose donor, in

reactions occurring in the outer leaflet of the plasma membrane (111) and/or cell wall compartment (134) suggesting that these reactions must be extracytoplasmic (39). PPM is continually recycled by transport of polyprenol phosphate (PP) across the membrane for mannosylation using GDP-Man in the cytoplasm, followed by transport back to the periplasm (Figure 1.13C). Thus, the biosynthetic pathway of polar PIMs and hypermannosylated LM and LAM must involve transport from the inner cytoplasm to the periplasmic side of the plasma membrane (114). How PIM intermediates, and the PPM donor, are flipped across the inner membrane remains unknown.

MptB and MptA synthesise both the proximal and distal $\alpha(1\rightarrow6)$ mannan backbones in LM-A and LAM (135). MptA, MptB, PimE and Rv2181 are the only known mannosyltransferases (ManTs) for which PPM is used (Figure 1.11) (60). LM-A species are further elongated to form LAM by the sequential addition of arabinose by EmbC (136), mannose and multiple arabinan side chains (133). EmbC and AftC are the other two identified arabinosyltransferases (AraTs) which, together with an unknown AraT, prime LM-A to form mature LAM before it is capped. They use decaprenyl-1-monophosphoarabinose (DPA) (60) as the arabinose donor. Yet, given the complexity of LAM branching, it is highly likely that there are more enzymes involved in its synthesis. Rv1635c has been shown to be involved in mannose-capping to form ManLAM (126, 137). While Rv2181 has been implicated in the formation of $(\alpha1-2)$ branching in LM (138), the backbone core is still largely unidentified. Mishra *et al.* (135) and Morita *et al.* (111) suggested that MptA, a PPM-dependent $\alpha(\rightarrow6)$ mannosyltransferase, could be involved in the initial steps of chain formation. This could then serve as a backbone for further $\alpha(1\rightarrow2)$ branching by other α -mannosyltransferases, such as Rv2181 (138). Thus, it appears that the biosynthesis of LM and LAM occurs in discrete steps with each enzyme recognizing appropriately “primed” steps to complete the lipoglycan (Figure 1.12). For example, MptA functions as an $\alpha(1\rightarrow6)$ mannosyltransferase in the construction of the backbone in the latter stages of LM-biosynthesis (135).

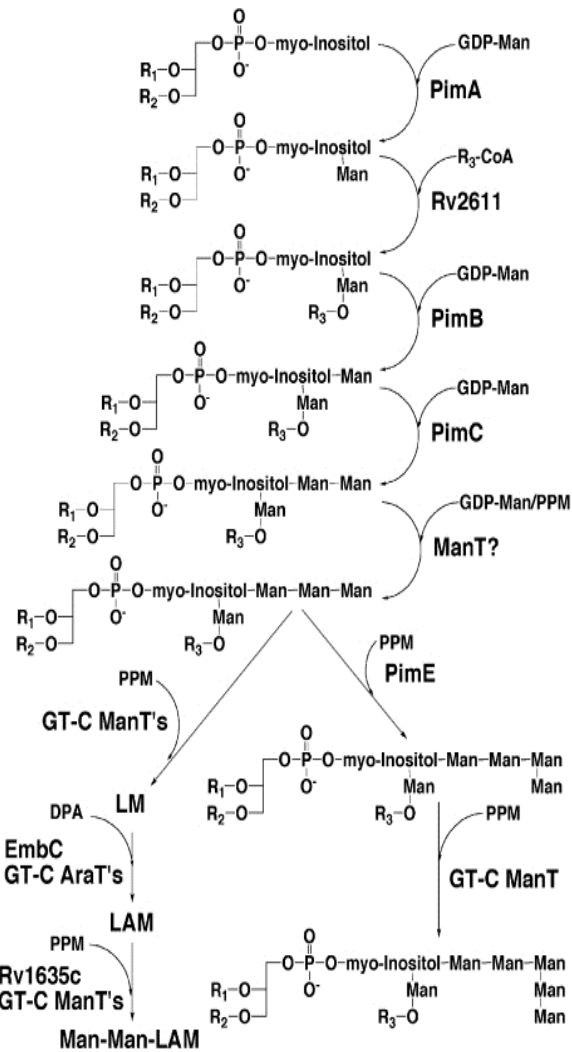


Figure 1.12 Proposed lipoglycan biosynthesis in *Corynebacterineae*. AcPIM₂ serves as the starting point leading to assembly of truncated LM, LM and LAM. N denotes residues of unknown numbers; x denotes residues of 0-2 (from Mishra, AK *et al.* (135))

While the LM-A/LAM pathway occurs in both mycobacteria and corynebacteria, Lea-Smith *et al.* (118) and Tatituri *et al.* (139) described a second lipoglycan pathway in Corynebacteria in which diacylglycerol (DAG) is glycosylated to synthesise a pool of LM designated LM-B. They re-assigned PimB (Rv0557) as α -mannosyl-glucopyranosyluronic acid transferase A (MgtA) involved in LM-B synthesis. It catalyses the production of 1,2-di-O-C16/C₁₈₋₁-(α -D-mannopyranosyl)-(1 \rightarrow 4)-(α -D-glucopyranosyluronic acid)-(1 \rightarrow 3)-glycerol [ManGlcAGroAc₂], designated GL-X, from the precursor, GlcAGroAc₂ or GL-A. A recently described lipoprotein, LpqW and its homologue NCgl1054, are required for synthesis of LM-A, LM-B and LAM (140). MptB, MptC and MptA are all involved in sequential mannose additions to produce LM-B (141) and LpqW has been proposed to activate MptB (140). Thus two forms of LM have been described in *C. glutamicum*: a minor pool of Cg-LM-A based on PI mannosylation and acetylation, and a more abundant Cg-LM-B based on a glycosylated diacylated glycerol (139). Whether LM-B exists in Mycobacteria remains to be determined. Only LM-A can be arabinosylated, possibly because LM-B is more heavily branched, thus removing potential arabinan binding sites (141). While some of the enzymes involved in these pathways have now been identified, other proteins remain to be discovered including those involved in transporting intermediates across the membrane and others that regulate the pathways. One such protein is described in Chapter 4 of this thesis.

1.3.6 Phthiocerol dimycocerosate and phiocerol

Surface exposed lipids such as phiocerol esters are found in pathogenic mycobacteria and play an important role in host-pathogen interactions. These lipids contain two components: phiocerol and phenolphthiocerol. They protect the bacilli from nitric oxide-dependent killing by the macrophages as well as modulating the production of key inflammatory cytokines such as TNF α (142). Blocking synthesis of these two lipids by new drugs may therefore affect the virulence of *M. tuberculosis*. Studies using ¹⁴C-labelled propionate and acetate indicate that these two intermediates are

incorporated into these two β -diols of 33 to 41 carbons (143). However nothing is known about their biosynthesis or the genes which encode these activities (144) .

Phthiocerol dimycocerosate (PDIM) is a wax containing two saturated fatty acids (mycocerosic acid) esterified to phthiocerol. Identification of their biosynthetic enzymes was aided by specifically-deficient strains. These included *fadD26*, encoding a putative acyl-CoA synthase, five genes encoding putative polyketide synthase genes (*ppsA-ppsE*), *mas*, encoding the mycocerosic synthesis enzyme, and two genes encoding proteins resembling transporters. (*ddrC* and *mmpL7*) (145).

1.4 The Role of Mycobacterial Components in Pathogenesis

M. tuberculosis is a facultative intracellular pathogen. It resides primarily within the early endosomes of macrophages resident in host alveoli in which it uses various mechanisms to prevent/decelerate phagosome maturation. Mycobacterial infectious capability is largely attributed to the impermeable, hydrophobic, acid-fast cell wall (36). This is responsible not only for the resistance to host and outside factors, but also has an important immunogenic role (146).

It has been suggested that TDM, or cord factor, plays a role in pathogenesis of tuberculous secondary and cavitary disease (147). The upregulated production of trehalose mycolates maintains a neutral pH in which the organism is protected and able to survive, replicate and continue to infect the host. Mycobacteria use lipids as their main energy source, as their environment is carbohydrate deficient. TDM is the most abundant lipid released by *M. tuberculosis*, and plays two main roles: a) it prevents phagocytosis by macrophages and, b) on lipid surfaces it is highly toxic and antigenic (147).

The interaction of TDM with lipids causes granulomas. This lipid pneumonia can progress to secondary disease causing caseating necrosis and cavities in the alveoli typical of TB (147).

Following entry into the macrophage, modulation of the immune response is of vital importance. Under normal circumstances, a pathogen is engulfed by a phagosome which then fuses with a lysosome, an acidic organelle. This forms a phagolysosome, an endosome responsible for digestion of foreign material. Mycobacteria are capable of delaying their digestion by preventing the formation of phagolysosomes (148) and providing an environment more conducive to survival and replication. An enzyme involved in phagosome maturation, phosphatidylinositol-3-kinase (PI3K) (120, 149) is recruited by ManLAM. Ferrari *et al.* (150) detected TACO (tryptophan aspartate containing coat protein) on vesicles containing only live bacteria, implying this protein could prevent phagolysosome maturation. Mycobacteria have also been noted to prevent the accumulation of Rab7, a GTPase, and early endosomal antigen 1 (EEA1), both reported to be essential for phagosome maturation (151, 152).

The immunomodulatory function of LM/ LAM is largely determined by its terminal moiety. (Fig 1.13) Mycobacterial LAM, LM and PIMs are not only responsible for the structural integrity of the cell wall (111), they are potent regulators of macrophage function which may have an impact on mycobacterial disease (122). It has been suggested that LAM is one of the chemotactic factors released by *M. tuberculosis*-infected alveolar macrophages (124) thereby involving it in macrophage phagocytosis (123). In addition, *M. smegmatis* loss of acid-fast staining, increased sensitivity to B-lactams, and faster macrophage killing resulted from structural defects in LM and LAM (125).

ManLAMs are mannose-capped LAMs, which may exist as mono-, di-, or even tri- saccharides with an $\alpha(1-2)$ linkage (41). They are characteristic of slow-growing pathogens including *M. tuberculosis*, *M. leprae* (153), *M. bovis* (154) and *M. avium* (127). They have been shown to bind to dendritic cells and macrophages, being responsible for host cell invasion (154-156). Another role of ManLAM is its ability to lower intracellular cytosolic calcium (157) (158) and therefore the recruitment of phosphatidylinositol-3-kinase (PI3K), another enzyme involved in phagosome maturation (120, 149).

The direct ManLAM receptor to explain its pleiotropic effects had not been clearly identified until Yonekawa *et al.* (159) reported that a C-type lectin receptor, Dectin-2, is a direct receptor for ManLAM. This demonstrates that Dectin-2 is able to recognize ManLAM, thereby contributing to host immunity to mycobacterial infection. Yet another C-type lectin has also been shown to be a receptor for TDM: macrophage inducible C-type lectin (Mincle) (160)

PIMs have been shown to encourage natural killer T cells encouraging the host granulomatous response (104, 161). Fast growing mycobacteria, such as *M. smegmatis*, have inositol phosphate (PI) capping (162) and *M. chelonae* has araLAM *i.e.* no capping (162).

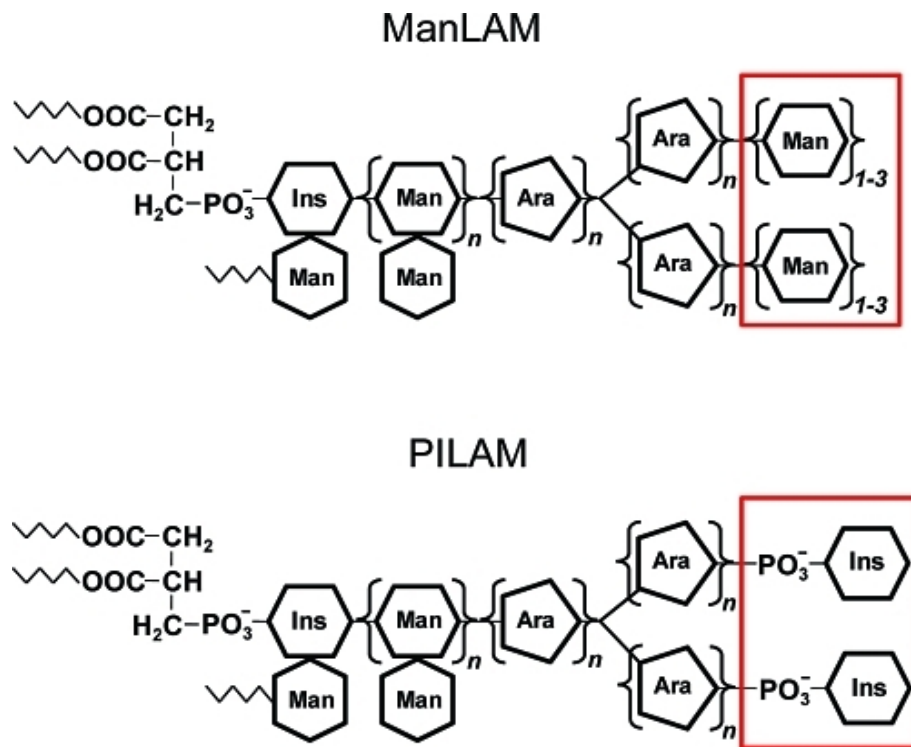


Figure 1.13 Structures of Mycobacterial lipoglycans. ManLAM and PILAM, which differ only in terms of their capping on the arabinan moiety. Ins = inositol, Man = mannose, Ara = arabinose, PO_3^- = phosphate (from Shui, W *et al.* (163))

ManLAMs have an immunosuppressive effect. Studies of this down-regulation at various stages have shown LAM functions at various stages: a) scavenging of potentially fatal oxygen free radicals, b) inhibition of protein kinase C activation, and c) blockage of transcription of IFN- γ inducible genes in human macrophage-like cell lines. These results suggest that LAM is able to prevent macrophage activation and cytotoxic activity and that it is a virulence factor explaining the persistence of mycobacteria in mononuclear phagocytes (164).

Through inhibition of the Th1-cellular immune system, ManLAM can inhibit factors such as IFN- γ signalling by macrophages (164) and IL-12 secretion by dendritic cells (103, 165). In addition, they decrease apoptosis and phagosome maturation. Thus, it appears that slow growing mycobacteria have mechanisms supporting their survival within the host. The further importance of ManLAM is its ability to prevent the activation of T-helper cells by blocking dendritic cell maturation. This is caused by ManLAM either on the bacterial surface or from infected macrophages binding to DC-SIGN (dendritic cell-specific intracellular-adhesion molecule-grabbing non-integrin) (155, 166). DC-SIGN normally targets endosomal/phagosomal processing of internalised foreign antigens for presentation of the antigen to T-cells (167). Binding to DC-SIGN inhibits Toll-like receptor signalling thereby reducing IL-10 stimulation. IL-10 is a pro-inflammatory agent which in turn stimulates the secretion of IL-12, tumour necrosis factor- α and major histocompatibility complex II, all necessary for antigen presentation (165).

Mycobacteria inhibit phagolysosome fusion by a variety of mechanisms. These include the lowering of cytosolic calcium (157) of which ManLAM has been noted to be a cause (158). Another enzyme involved in phagosome maturation, phosphatidylinositol-3-kinase (PI3K) (120, 149) is recruited by ManLAM.

In contrast to slow-growing species, fast growing mycobacteria characteristically have phospho-*myo*-inositol caps or lack caps, *i.e.* PILAM or AraLAM, respectively (121). PILAM has a more immunostimulatory effect. LAMs of these fast-growing, non-pathogenic species stimulate the immune response of macrophages via Th2, and secretion of TNF α , IL-8 and IL-12 (168).

Additional surface constituents have immunomodulatory functions, notably phthiocerol dimycocerosate (PDIM). It evidently plays a role during the acute stage of infection (145) by affecting cell membrane permeability (169). Rousseau *et al.* (170) showed that PDIM also down-regulates the production of IL-6 and TNF- α .

1.5 Mycobacterial Cell Wall Biosynthesis Processes as Drug Targets

The current WHO regime of TB treatment is a combination of isoniazid, EMB (ethambutol), pyrazinamide and rifampicin taken for 2 months, followed by rifampicin and isoniazid taken for 4 months (WHO Global TB report 2014). Nevertheless, both drugs used and the duration of treatment may vary due to several factors such as anti-retroviral treatment for HIV, deficient immune status due to malnourishment or diabetes, etc. Worryingly, these antimicrobials, and others, are proving far less effective with the rise in incidence of MDR- and XDR-TB (WHO 2014). The treatment of MDR-TB is prescribed for 20 months with second-line drugs (fluoroquinolones, amikacin, kanamycin and capreomycin). Cure rate ranges from only 60-75% (171). Described in this section are a few key examples of biosynthetic pathways which are targeted by various classes of antimycobacterial drugs and may offer potential candidate pathways for future anti-tubercular drug therapies.

EMB appears to target synthesis of arabinogalactan through the inhibition of AraTs (60, 172). It is known to target at least 3 AraTs (EmbA, EmbB and EmbC), but shows no inhibitory effects against the more recently discovered AraTs (AftA, AftB and AftC).

EmbA, EmbB, and EmbC encode AraTs which are targeted by EMB (173). EmbC is known to be involved in the biosynthesis of LAM as experimental evidence shows that deletion of *embC* disrupts LAM production (63, 69). It appears that LAM may induce the macrophage-derived cytokines which in turn are responsible for the clinical manifestations of tuberculosis such as weight loss, fever and tissue necrosis (174). On the other hand, EmbA and EmbB are essential for the formation of the terminal hexaarabinofuranosyl motif in arabinogalactan (175) and act as $\alpha(1\rightarrow3)$ arabinofuranosyltransferases (50). Alsteens, D *et al.* (176) have shown that isoniazid and EMB interfere with the synthesis of mycolic acids, arabinogalactans or proteins altering the cell surface roughness, thereby decreasing cell hydrophobicity. Removal of the outermost mycolic acid layer results in exposure of hydrophilic proteins, making the cells more vulnerable to desiccation.

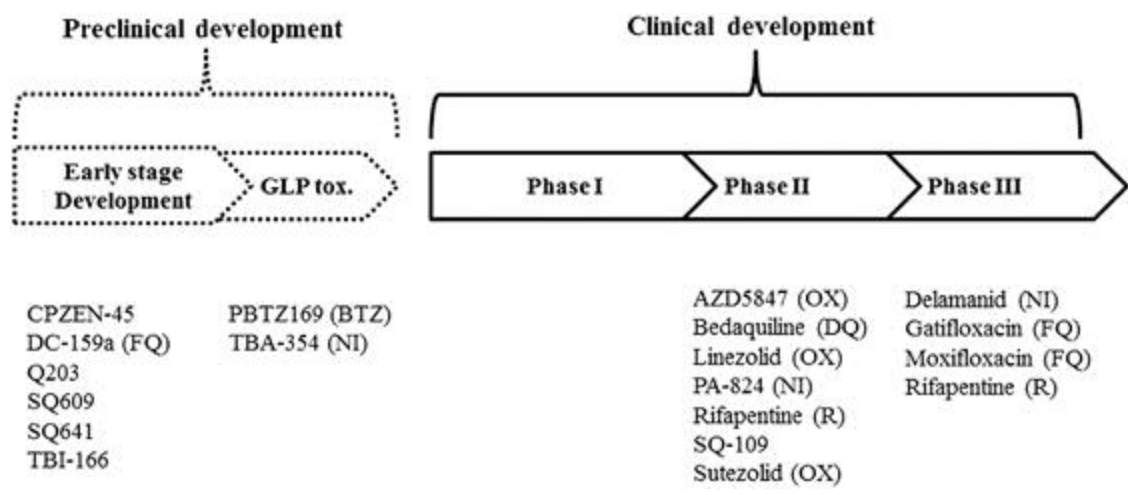
The majority of antitubercular medications inhibit cell metabolic cycles involved in cell wall biosynthesis, thus being bactericidal as well as being able to effectively target latent forms of the bacterium. Numerous metabolic pathways within mycobacteria are well characterized allowing us to understand the mechanism and design of antibacterials. Many examples follow illustrating how different drugs make use of a specific intracellular structure or growth stage. Age-old streptomycin targets the 30S subunit of ribosomes, an integral part of the cell wall structure (177). Fortunately new drugs have been designed and as more biosynthetic pathways of *M. tuberculosis* are understood, even newer drugs should be discovered in future. By inhibiting the multiple functions of mycolic acids, dioctylamine acts as a substrate mimic causing loss of intracellular cyclopropanation, and synergistic cell death by isoniazid and ciprofloxacin (178, 179).

EMB, while not a recently discovered drug, affects the same pathway blocked by the new class of drugs, benzothiazinones. eg. Triclosan which is modelled on the mode of action of ethambutol, yet is

not as potent. Tahlan *et al.* (86) has designed a drug known as SQ109, which is also structurally related to ethambutol (178) and proving successful. Pyrazinamide interferes with bacterial survival under stressful non-replicating conditions. It is an analogue of nicotinamide and targets RpsA thereby preventing binding to mRNA (163, 180, 181). Derivatives of rifampicin are yet another example. Rifapentine, rifabutin and rifalazil target the β -RNA subunit, thereby preventing cellular transcription (182).

Scientists today know that novel TB drugs (Figure 1.14) as well as novel drug targets are vital for many reasons including a reduction in the length of treatment time, which may in turn improve patient compliance, the ability to treat MDR-, XDR- and maybe even TDR-TB, as well as the ability to increase drug effectiveness against both active and latent TB. All novel drugs require the ability to work in an additive manner to current, existing anti-TB drugs. In addition, it should be kept in mind that TB treatment needs to be compatible with anti-HIV medication as among the 9 million people living with TB, 11-13% are HIV-positive (183).

Thus, it appears that one solution to sourcing new drugs may indeed lie within an improved understanding of the cell wall structure and/or metabolic processes.



FQ: fluoroquinolone
 BTZ: benzothiazinone
 NI: nitroimidazole

OX: oxazolidinone
 DQ: diarylquinolone
 R: rifamycin

Figure 1.14 Current trends in discovery of new drugs for TB treatment. New drugs are being designed and are in various stages of development.

1.6 *Corynebacterium glutamicum* as a Laboratory Model for Pathogenic Mycobacteria

M. tuberculosis is difficult to use experimentally due to its slow growth and necessity for extremely costly laboratory facilities. In addition, cell wall biosynthesis processes are usually essential for the growth of this organism so that deletion mutants that have lost synthetic genes may not be viable, precluding further studies. In the studies reported here, most experimental work was done in the related species, *C. glutamicum*. While the human pathogen takes approximately 6 weeks to grow, colonies of *C. glutamicum* form within 1 day under optimal conditions. Importantly, both organisms share a common cell wall structure since both belong to the same taxon. They share the same core mAGP-complex (184, 185), suggesting that a high proportion of cell wall genes are conserved. Also, the biosynthetically related glycolipids, PIMs, LM and LAM, are found in the cell walls of both Mycobacteria (30) and Corynebacteria (185). This permits experimental deductions from laboratory studies in non-pathogenic Corynebacteria to be extended to Mycobacteria, including *M. tuberculosis*. A further advantage of using *C. glutamicum* is that many cell wall biosynthesis genes are not essential for viability, allowing viable mutants to be made for study, despite being indispensable in *M. tuberculosis*. In addition, the *C. glutamicum* genome is only 3282 kb in size, containing 3002 genes, reducing the likelihood of redundancy (186). The two genes studied in this thesis are both essential for growth in *M. tuberculosis* and gene deletion mutants are not viable.

However *C. glutamicum* is not a perfect model as the cell wall components of Corynebacteria and their biosynthetic pathways, are generally simpler than those in Mycobacteria. For example, the fatty acyl chains of corynomycolic acids in *C. glutamicum* average a length of approximately 30 carbon atoms, whereas those of *M. tuberculosis* consist of approximately double this number. This greater simplicity of structures suggests that there may be particular enzymes in Mycobacteria that do not have a functional homologue in Corynebacteria and cannot be studied in that organism.

1.7 Rationale of this Study

Tuberculosis is a rampant disease, particularly in the 3rd world, lower socio-economic groups such as the poor or homeless. It is particularly prevalent in people who use drugs, are incarcerated, or who have compromised immune systems resulting in a greater risk of contracting disease e.g. those with diabetes, HIV, malnutrition or who are smokers or heavy drinkers. It is fast developing into a drug-resistant TB pandemic for which treatment is not only prolonged and costly, but may even sometimes be totally ineffective. The identification of new drug targets is an important first step in the development of new classes of drugs with novel mechanisms of action.

Beyond the intrinsic interest of identifying biosynthetic mechanisms for unusual glycolipids, a thorough knowledge of the mycobacterial cell wall and associated biosynthetic pathways is likely to be helpful in identifying new drug targets. Although there has been much investigation into the structure of cell wall components, less is known about the metabolic processes which form them. Previous work in this laboratory has led to the identification of three *M. tuberculosis* genes: *Rv0224*, *Rv0225* and *Rv0228*, which may form part of a new cell wall biosynthesis locus (Figure 1.14).

Deletion of the orthologs of these genes in *C. glutamicum*, *NCgl2764*, *NCgl2762* and *NCgl2759*, respectively, was found to disrupt transport of corynomycolic acids to the cell surface (46) and (group unpublished data). Consequently, *Rv0226* and *Rv0227* (*NCgl2761* and *NCgl2760* in *C. glutamicum*) were selected for further investigation in this project (Figure 1.14). As deletion mutants of these two genes are not apparently viable in Mycobacteria, we used *C. glutamicum* as a convenient model of study. Its capacity to tolerate cell wall lesions and retain viability is a particular advantage in context of the work described in this chapter.

Gene knockout mutants of *NCgl2764*, *NCgl2762*, *NCgl2759* have been studied in our laboratory (46) (and unpublished results). All three mutants appear to have the same defect i.e. a dramatically reduced rate of TMCM transport across the cell membrane. Bioinformatics predicts that *NCgl2764* (Rv0224) functions as a methyltransferase and *NCgl2762* (Rv0225) as a glycosyltransferase, whereas *NCgl2759* (Rv0228) has been identified as an acyltransferase (46). As remaining members of this biosynthetic gene cluster, the orthologs of Rv0227c and Rv0226c in *C. glutamicum*, *NCgl2760* and *NCgl2761*, were studied in projects described in this thesis.

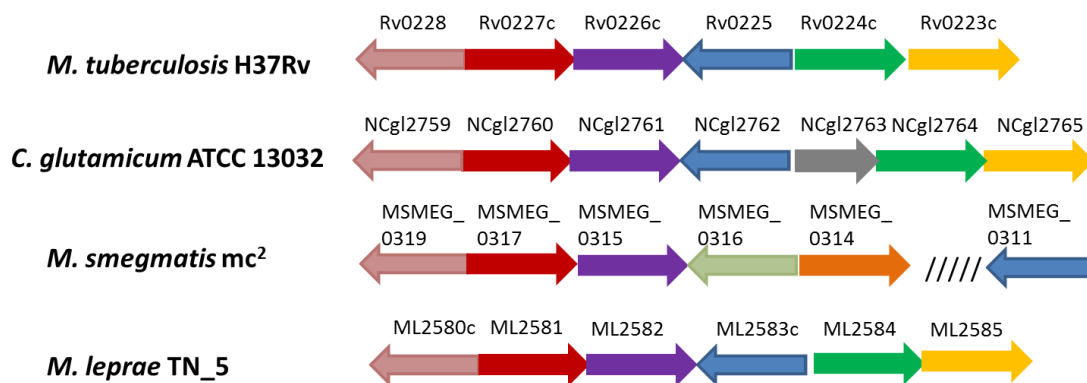


Figure 1.15 A new cell wall biosynthesis locus highly conserved in Corynebacterineae. *NCgl2760* and *NCgl2761* from *C. glutamicum* ATCC 13032 are located within a genetic region that is conserved in members of the Corynebacterineae. They have probable orthologs in the genomes of *M. tuberculosis* H37Rv (*Rv0227c*, *Rv0226*), *M. smegmatis* mc²155 (*MSMEG_0317*, *MSMEG_0315*) and *M. leprae* TN_5 (*ML2581*, *ML2582*).

1.8 Aims of this Study

The overall aim of this study was to determine whether NCgl2760 and NCgl2761 have roles in cell wall biosynthesis in *C. glutamicum*. These putative membrane proteins are hypothesised to cooperate with the proteins described above to transport corynomycolic acid intermediates across the membrane. The genes were deleted and the resultant mutants analysed to determine any role in corynomycolic acid transport. In addition, the possibility of involvement in the PIM/LM/LAM biosynthetic pathway was investigated. These studies have provided functional insights into the essential *M. tuberculosis* proteins Rv0226c and Rv0227c which are potential drug targets for this devastating human pathogen.

Chapter 2

Materials and Methods

2.1. Bioinformatics Analysis

The Tuberculist World-Wide Web server at the Institut Pasteur (<http://genolist.pasteur.fr/TubercuList/>) supplied the DNA sequences of *M. tuberculosis* strain H₃₇R_v. *C. glutamicum* ATCC 13032 Kitasato gene sequences were obtained from the Comprehensive Microbial Resource (CMR) tool at the J. Craig Venter Institute (<http://jcv.org/cms/home/>). Clustal Omega (www.ebi.ac.uk/tools/msa/clustalo/) and ClustalW were used to derive protein alignments. Vector NTI (company) was used as a tool for *in silico* DNA manipulation.

2.2. Chemicals and Reagents

All chemicals and reagents used in this study were supplied by BHD Laboratory Supplies, Bio-Rad Laboratories, Difco Laboratories, Sigma-Aldrich Co. and Univar Corporation. Media ingredients were supplied by Difco Laboratories and Oxoid Ltd. DNA restriction and modification enzymes were supplied by Qiagen, Roche Molecular Biochemicals, Promega Corporation, Pharmacia Biotech and New England Biolabs Inc.

2.3. Bacteriological Strains and Culture Conditions

E. coli DH5 α , XL1-Blue MRF' and *C. glutamicum* ATCC 13032 were used in this project. All strains used in this project are listed in Appendix 1. *E. coli* was cultured in Luria-Bertani (LB) media and incubated aerobically at 37°C. *C. glutamicum* was grown in brain heart infusion (BHI) media (Oxoid) at 30°C, cultured aerobically. Agar LB and BHI plates were made by the addition of 15g/L agar and were supplemented with 10% (w/v) sucrose when appropriate. Antibiotics were added as needed. Bacteriological media formulations are listed in Appendix 2.

2.3.1 Preparation of competent *Escherichia Coli* cells

Chemically competent DH5 α cells were prepared from bacteria grown overnight at 37°C on an LB plate. A single colony was inoculated into 10 ml of LB broth and grown at 37°C with shaking. At an OD (600 nm) = 1.5, 100 μ l of the culture was inoculated into 100 ml of autoclaved SOB medium (2% (w/v) tryptone, 0.5% (w/v) yeast extract, 10 mM NaCl, 2.5 mM KCl - one ml of sterile 25% (w/v) glucose, and 1 ml of 1M MgCl₂+MgSO₄ was added just before use). This culture was incubated overnight at room temperature with shaking. At an OD (600 nm) = 0.4-0.8 (ideally 0.6), the cells were transferred to 50 ml polypropylene tubes and incubated on ice for 10 minutes. After centrifugation at 500xg for 10 minutes at 4°C and discard of the supernatant, the cells were resuspended in 20 ml of transformation buffer containing 0.3% PIPES, 0.22% CaCl₂.H₂O, and 1.86% KCl. After adjustment to pH=6.7 with 5M KOH, the content was completely dissolved. Manganese Chloride (1.09% MnCl₂.4H₂O) was added to make up to 100 ml and filter sterilized. The transformation buffer was stored at 4°C until necessary. The previous step was repeated twice, the second time after resuspension in 10 ml of transformation buffer. DMSO was added and the cells incubated for 10 minutes on ice. Next, 100 μ l of cells was aliquoted into Eppendorf tubes before snap freezing in a dry ice/ ethanol bath. The competent cells were then stored at -80°C until needed.

2.3.2 Preparation of competent *Corynebacterium glutamicum* cells

Electrocompetent *C. glutamicum* cells were prepared by first selecting a single colony from a BHI plate to inoculate a “starter culture” of 10ml BHI. This was left to grow at 30°C overnight. The following day, 50 ml of transformation supplement was prepared (6.25 g glycine, 1 g isoniazid, 0.25 ml Tween 80 made up to 50 ml with mqH₂O and filter sterilized). Autoclaved EPO media (2 g tryptone, 1 g yeast extract, 2 g NaCl made up to 80 ml with mqH₂O) was prepared and 20 ml of transformation supplement added. Sufficient bacteria were added to 100 ml of EPO to an OD (600nm) = 0.3. The culture was then left at 18°C shaking at 120 rpm for 2-5 days until an OD(600nm) = 0.9 was reached. The culture was transferred to 50 ml polypropylene Falcon tubes and left on ice for 5 minutes before centrifuging at 4°C for 10 minutes at 2500xg. Two washes with 50 ml cold 10% (v/v) glycerol were performed before combining the pellets into one tube and doing one further glycerol wash. The pellet was then resuspended in approximately 500 µl cold glycerol and 100 µl aliquots transferred to Eppendorf tubes. These electrocompetent *C. glutamicum* cells were stored at -80°C until needed.

2.4. DNA Amplification and Sequencing

Oligonucleotide primers used for DNA amplification and sequencing were designed using Vector NTI Explorer computer program. The sequence of each oligonucleotide is listed in Appendix 3.

2.4.1 Polymerase chain reaction (PCR)

Two different enzymes were used for DNA amplification, depending upon accuracy of base read required: either Taq DNA polymerase (Roche), or HotStar HiFidelity DNA Polymerase (Qiagen). When using Taq, 1 µl was added to a solution of 1-5 µl plasmid or genomic DNA, 1 µl forward and reverse

primer, 2 μ l 10 μ M dNTPs, 5 μ l 10 x reaction buffer (100 mM Tris-HCl (pH 8.3), 500 mM KCl, 0.1% (w/v) gelatine and either 10, 15, 20 or 25 mM MgCl₂) and distilled H₂O to make up a final volume of 50 μ l. For HotStar reactions, solutions from a HotStar HiFidelity DNA Polymerase Kit (Qiagen) were used, namely 10 μ l Q solution, 10 μ l 5 x reaction buffer, 1 μ l Hotstar enzyme, 1 μ l MgCl₂, 1.6 μ l each of 20 μ M forward and 20 μ M reverse primer, 1-5 μ l plasmid or genomic DNA and distilled H₂O to make up a final reaction volume of 50 μ l. A PTC-200 Peltier Thermal Cycler was used for all PCR amplifications. A 2 μ l aliquot of each reaction was resolved by agarose gel electrophoresis and compared to 100bp marker (Invitrogen) and λ HindIII-digested DNA markers to estimate approximate product size.

2.4.2 Sequencing

Plasmid DNA sequencing reactions contained approximately 500 ng of template DNA, 1 μ l of each 20 mM primer, 1 μ l BigDye terminator pre-mix (Perkin Elmer) and were adjusted to a final reaction volume of 20 μ l with distilled H₂O. Purified PCR products were sequenced using 10-50 ng of template DNA. The reactions were run in a PTC-200 Peltier Thermal Cycler using the following reaction:

Program:	96°C	1 minute	
	96°C	10 seconds	30 cycles
	50°C	5 seconds	
	60°C	4 minutes	
	12°C	infinite	

Before performing the sequencing reaction, the reaction products were purified by adding 62.5 μ l 100% ethanol, 14 μ l distilled H₂O, and 3 μ l 3 M NaOAc. The mixture was vortexed then left at room temperature for 15 minutes before centrifuging at 15000xg for 30 minutes. After removing the

supernatant, 200 µl of 100% ethanol was added, the tube vortexed, then centrifuged at 18000xg for 4 minutes. Once again, the supernatant was removed and 200 µl of 70% ethanol was added, vortexed and centrifuged for 4 minutes. After removing the ethanol, the tube was heated at 75°C for 1 minute to evaporate the ethanol, then sent for sequencing (Monash University, Micromon Sequencing Facility). Sequencing results were compared to the expected nucleotide sequences of the genes of interest using the computer program VectorNTI® (Invitrogen). Any variations were analysed using various BLAST algorithms (Basic Local Alignment Search Tool) accessible through <http://www.ncbi.nlm.nih.gov/BLAST/>.

2.5. DNA Manipulation

2.5.1 Restriction endonuclease digestion and resolution by agarose gel electrophoresis

DNA digestion by restriction enzymes was performed according to the manufacturer's instructions. Enzymes used were all supplied by Roche and New England BioLabs. Fragments were separated according to size in 1% (w/v) agarose gels run in Tris-acetate-EDTA (TAE) buffer (0.1% (v/v) glacial acetic acid, 2 mM Na₂EDTA.2H₂O and 40 mM Tris-HCl, pH 8.5) and stained with GelRed Nucleic Acid Stain, diluted 20 000x in H₂O (Biotium). They were visualised on a Syngene BioImaging System using the GeneSnap image acquisition software (Syngene) or on a Bio-Rad Chemidoc™ XRS with Imagemag software.

2.5.2 Isolation and quantitation of DNA restriction fragments

Plasmids, restriction enzyme digested fragments and PCR products were excised from agarose gels and purified using the Mo Bio Ultra Clean 15 DNA purification Kit, according to the manufacturer's

instructions. DNA concentration was determined using a NanoDrop R1000 3.7.1 (ThermoFisher Scientific).

2.5.3 Cloning of DNA fragments

Ligations between vector and insert fragments were performed using one of two methods. For both ligation reactions, a ratio of 3:1 (insert:vector) was used. Either T4 ligase (Roche), 10x ligase buffer and mqH₂O were added to the reaction. This reaction was incubated at room temperature overnight. Ten µl of ligation solution was transformed into chemically competent *E. coli* DH5α cells. The alternative reaction utilized the Rapid DNA Ligation Kit (Thermo Scientific). The vector (10-100ng) and insert (3:1 molar excess over vector), 5x Rapid Ligation Buffer, T4 DNA Ligase and mqH₂O were combined. Incubation time was 1 hour at room temperature, and 5 µl of the reaction was used for subsequent transformation of chemically competent *E. coli* DH5α cells. (This latter method was favoured in our laboratory during the later duration of my PhD).

2.5.4 Transformation of DNA into *Escherichia coli* and isolation of plasmid DNA

Chemically competent *E. coli* DH5α cells were removed from -80°C storage and thawed on ice. Either 10 µl or 5 µl of ligation solution (depending upon ligation method utilized) was added, and left to rest on ice for 30 minutes. The mixture was then incubated at 37°C for 2 minutes followed by the addition of 400 µl LB media (Refer to Appendix 2). After a recovery period of 1 hour at 37°C, the bacteria were plated on LB agar (refer to Appendix 2) plates containing appropriate antibiotics and incubated overnight at 37°C.

To extract plasmid DNA from *E. coli*, a single colony was inoculated into 10 ml of LB media (refer to Appendix 2) and incubated overnight at 37°C with shaking. The bacteria were pelleted and plasmid DNA isolated using a High Pure Plasmid Isolation Kit (Roche). The concentration of DNA extracted was measured using a NanoDrop R1000 3.7.1 machine (ThermoFisher Scientific) at 260nm.

2.5.5 Transformation of plasmid DNA into *Corynebacterium glutamicum* cells

Five µl of plasmid DNA was added to a 100 µl aliquot of electrocompetent *C. glutamicum* cells which had been thawed on ice from -80°C storage. The cuvette was kept on ice while 1 ml of BHI media was pre-warmed in a waterbath at 46°C. The following settings were used for electroporation using an ECM 630 Electro Cell Manipulator (Genetronics Inc.): 2.5 kV, 200 Ω, 25 mA. A pulse duration of 5.6-5.9 was expected. Some pre-warmed media was added to the cuvette, before removing the entire contents to the Eppendorf tube and incubating in the waterbath at 46°C for 6 minutes. The contents in the tube were shaken for 1-2 hours at 30°C to allow the cells to recover, then plated on BHI agar containing appropriate antibiotics and incubated at 30°C. Colonies appeared after 2-5 days.

2.5.6 Genomic DNA extraction from *Corynebacterium glutamicum* using a Nucleon® kit

Approximately 2 ml of glass beads were added to approximately 8 screw cap Eppendorf tubes and 350 µl of Reagent B was added to each tube. A large loopful of bacteria from growth on solid media was added to each tube before adding 10 µl of RNase and 50 µl of Proteinase K. The tubes were beadbeaten for 45 seconds at 6.5 speed followed by brief centrifugation and followed by incubation for at least 30 minutes at 37°C.

After centrifugation for 2-3 minutes, the supernatant was transferred to fresh Eppendorf tubes where to 100 µl of sodium perchlorate was added. The solution was mixed gently approximately 7 times by hand followed by further hand mixing for a further approximate 7 times after addition of 600 µl of chloroform.

After vortexing Nucleon™ Resin to liquefy, 150 µl of the resin was added to the chloroform-sodium perchlorate, being careful not to mix, and followed by a brief 1 minute spin to separate the solutions into the specific layers. The upper phase was transferred to fresh Eppendorf tubes, while being careful not to contaminate with the resin. Cold 100% ethanol was added to each Eppendorf tube, totalling 1.5 ml in each, and was followed by vortexing. This should reveal tiny, fragile DNA fragments precipitates. If not visible, the tubes were left at -20°C for 20-30 minutes.

The Eppendorf tubes were centrifuged for 10 minutes at maximum speed to pellet the DNA, before removing the supernatant. If the pellet appeared discoloured with transferred resin or proteins, the pelleted DNA was resuspended in 200 µl of water. The tubes were centrifuged again for 5 minutes followed by removal of the supernatant. Cold 600 µl of 100% ethanol was added before vortexing then centrifuging for 8 minutes. Once again, a white DNA-containing pellet should be visible. Again the supernatant was removed and the pellet washed with 500 µl of 70% ethanol. Finally the genomic DNA was suspended in 50-100 µl water depending on the amount of DNA and concentration calculated on a Nanodrop reader.

2.6. DNA Southern Hybridization

Genomic DNA was digested with the appropriate enzyme then run on a 1% (w/v) agarose gel at 120V for approximately 3.5 hours until the blue dye front reaches the end of the gel. The digoxigenin-labelled marker (5 μ l) was run in a lane alongside the digested DNA.

The agarose gel was then submerged in denaturation solution (0.5M NaOH and 1.5M NaCl). It was gently agitated at room temperature for 15 minutes before being rocked for a further 15 minutes in fresh denaturation solution. After rinsing for 2-3 minutes in mqH₂O the gel was submerged for 15 minutes in neutralisation solution (0.5M Tris pH 7.5, 1.5M NaCl). Fresh neutralisation buffer was then added for a further 15 minutes with rocking, then rinsing the gel again with mqH₂O for 2-3 minutes.

The capillary transfer apparatus was set up for transfer of the DNA to the nitrocellulose membrane. The reservoirs of an agarose gel electrophoresis tank were filled with 20X SSC (3M NaCl, 0.3M pH 7.0). Two pieces of Whatman filter paper approximately 0.5 cm wider than the gel, and long enough to reach the bottom of the tank reservoirs were prepared and wet with 20X SSC, ensuring no air bubbles were trapped. The gel was inverted onto the Whatman papers and a piece of nitrocellulose membrane positioned onto the gel, being careful to only handle the membrane edges and once again ensuring no air bubbles were trapped. This was cut approximately 0.5 cm wider and 1 cm longer than the gel. Three pieces of Whatman filter paper, pre-wet in 20X SSC, were positioned over the membrane avoiding air bubbles. A layer of paper towels approximately 3-5 cm thick was placed over these filter papers to ensure even capillary transfer through the gel and membrane, followed by a weight balanced evenly over the transfer apparatus. The DNA was allowed to transfer to the nitrocellulose membrane overnight.

Next, the membrane was removed and placed on an ultraviolet transilluminator for 3 minutes on either side. It was removed into a glass hybridization bottle, DNA-side facing inwards, with approximately 25 ml pre-hybridization solution (5X SSC, 0.1% (w/v) sodium lauryl sarcosinate, 0.02% (w/v) SDS and 1% (w/v) skim milk powder and incubated at 65°C for 4 hours with gentle rotation.

Meanwhile, the DIG-labelled DNA probe was heat denatured for 10 minutes and immediately quenched on ice for 5 minutes. To make the probe, wild type genomic DNA was used to prepare 1.1 µg of DNA by PCR. This was boiled for 10 minutes then left on ice for 5 minutes. Thirteen microliters of DNA was added to 2 µl H₂O, 2 µl of hexanucleotide mix, 2 µl of digoxigenin dNTP labelling mix and 1 µl of Klenow enzyme. All products were from a digoxigenin hybridization kit (Roche Applied Science). After 12 hour incubation at 37°C, 2 µl of 0.2M EDTA was added. The probe was frozen at -20°C until needed.

The probe was added to approximately 25 ml of the pre-hybridization solution, pre-heated to 65°C. This constituted the hybridization solution. The pre-hybridization solution was discarded and replaced with the hybridization solution for overnight incubation at 65°C with gentle rotation.

The 0.5X wash solution was warmed. Meanwhile the membrane was rolled twice, 5 minutes per wash, with 2X wash solution (2X SSC and 0.1% (w/v) SDS) at room temperature in the hybridization bottle. After discard, the membrane was washed twice, 15 minutes per wash, with 0.5 X wash solution (0.5X SSC and 0.1% SDS) at 65°C in the oven.

Next followed detection for which the membrane was first equilibrated in washing buffer (1M maleic acid, 1.5M NaCl and 0.3% (v/v) Tween 20, pH 7.5) for 1 minute with gentle rocking. The buffer was replaced with blocking solution (1% skim milk powder) for 1 hour. The antibody solution (1:10 000 dilution of the anti-Digoxigenin-AP Fab Fragments (Roche) in blocking solution) was added after pouring off the blocking solution. The membrane was incubated for 30 minutes in antibody solution then washed twice in washing buffer, first for 15 minutes and the second time for 30 minutes. The membrane was then equilibrated in detection buffer (0.1M Tris and 0.1M NaCl dissolved in m_qH₂O for 2 minutes, pH 9.5) for 2 minutes. Finally, the CDP-*Star* (25mM; Roche) was diluted (1:100) in 1ml of detection buffer then dripped onto the membrane before sealing it in plastic for exposure, DNA-side up, to X-ray film.

2.7. RNA Extraction and cDNA Analysis

First, the bacteria were grown overnight: *C. glutamicum* was grown in BHI media and *MSMEG_0315* was grown in 7H9 media. After centrifugation, the pellets were resuspended in 600 µl 0.05% Tween80 followed by centrifugation for 1 minute. The pellets were then lysed by resuspension in a buffer containing 20 mM NaOAc, 0.05% SDS, 1 mM EDTA, and 100 µg proteinase K (pH=4.0). Approximately 18 µl lysis buffer was added per mg pellet weight, dividing the sample among 4 screw-capped Eppendorf tubes. The mixture was agitated twice for 30 seconds in a bead beater using sterilised, acid-washed glass beads. No cooling was needed between bursts as phenol and chloroform were used for further extraction. After centrifugation for 10 minutes, the clarified supernatant was then transferred to clean screw-capped Eppendorf tubes.

Next the clarified supernatant was extracted with phenol:chloroform:isoamyl alcohol (25:24:1 v/v), then re-extracted with chloroform:isoamyl alcohol (24:1 v/v). The clarified supernatant was

precipitated in an equal volume of ice-cold isopropanol before incubation at -70°C for 30 minutes. Centrifugation for 30 minutes at 4°C followed to precipitate the pellet which was washed with 70% ethanol then dried at room temperature under rotational vacuum. The pellet(s) were resuspended in mqH₂O, next quantitated. DNaseI treatment was performed by adding RNasin (Promega), 10xRQ1 DNaseI buffer (Promega) and RQ1 DNase1 (Promega) at 37°C for 20 minutes. The sample was then purified using RNeasy Purification columns (Qiagen). The extraction protocol as per the manufacturer was followed before final elution in 60 µl H₂O. This method produced a total of 3 µg RNA, which was stored at -80°C until needed.

To synthesize and amplify cDNA from RNA from *C. glutamicum*, the Transcriptor High Fidelity cDNA Synthesis Kit (Roche) was used according to the manufacturer's instructions. Next the cDNA was used as a template for the following PCR reaction:

10 x buffer	5 µl
dNTPs (10 µM)	2 µl
10µM forward primer	1 µl
10µM reverse primer	µl
<i>Taq</i> polymerase	1 µl
cDNA or gDNA	2 µl
H ₂ O	38 µl

Program:	94°C	8 minutes	
	94°C	15 seconds	} 35 cycles
	63°C	1 minute	
	72°C	2 minutes	
	72°C	7 minutes	

4°C infinite

For MSMEG_0315, an RT-PCR protocol was chosen using 10 μ M forward primer (MSMEG_0317_F) and 10 μ M reverse primer (MSMEG_0315_R), 10 mM dNTPs and 200 ng RNA. The mixture was heated at 65°C for 5 minutes and next incubated on ice for 5 minutes. 5x First-strand Buffer, 0.1 M DTT and Superscript RT (Invitrogen) were added before incubation at 55°C for 60 minutes. The reaction was terminated by heating to 70°C. The experiment was done multiple times adjusting for different amounts of RNA (100 ng and 250 ng) and controls. cDNA from the reaction was used as a template for the following PCR reaction:

10xbuffer	10 μ l
q-solution	10 μ l
20 μ M forward primer	1.6 μ l
20 μ M reverse primer	1.6 μ l
cDNA	5 μ l
H ₂ O	12 μ l
Hotstar® enzyme	1 μ l

Program:	95°C	2 minutes	
	94°C	15 seconds	} 30 cycles
	65°C	1 minute	
	72°C	2 minutes	
	72°C	4 minutes	
	12°C	infinite	

2.8. Extraction of Cell Wall Components

Covalently and non-covalently linked components of the *C. glutamicum* cell wall were sequentially extracted using organic solvents, mild base and acids.

2.8.1 Culture preparation

C. glutamicum strains were all grown on BHI agar plates with kanamycin added where necessary. A single colony was selected and inoculated into a BHI starter culture then incubated at 30°C overnight. Approximately 0.5 ml of starter culture was inoculated into 100 ml of BHI broth to OD(600nm) ≈ 0.3. The flasks were shaken and incubated at 30°C. In the mid-log phase of growth, a 30 ml sample of culture was collected in a pre-weighed 50 ml polypropylene tube, and at the stationary phase of growth, a 10 ml sample was collected. These were centrifuged at 2500xg for 10 minutes, supernatant discarded, and the pellet collected which was either stored at -20°C or analysed immediately.

2.8.2 Extraction of non-covalently bound lipids and glycolipids

Each cell pellet was resuspended in chloroform:methanol (2:1 v/v), in a volume equivalent to 20 times the original cell pellet weight and transferred to an acid-washed glass tube. After rocking for 2 hours at room temperature, the tube was centrifuged at 500xg for 10 minutes to remove insoluble material and the solvent supernatant was transferred to a new acid-washed glass tube, then dried under a stream of nitrogen gas. The remaining pellet was resuspended in an equal volume of chloroform:methanol (2:1 v/v), rocked for 2 hours and insoluble material harvested by centrifugation. This solvent supernatant was pooled with the previous solvent extract and similarly dried. The pellet was further extracted in chloroform:methanol:water (1:2:0.8 v/v/v), using the same

volume as that in the previous two extractions. The cells were then rocked and centrifuged as above. The solvent supernatant was decanted, pooled with the chloroform:methanol (2:1 v/v) extracts and dried. The extracts and pellets were stored at -20°C.

2.8.2.1 Butanol partitioning

Butanol partitioning removes salts from the solvent extracts. Water (100 µl) and 200 µl water-saturated butanol were added to the dried solvent extracts in the glass tube to create a bi-phasic system. The tube was sonicated in a sonic bath and vortexed to emulsify the lipids, then centrifuged for 1 minute at 15000xg to separate the phases. The upper 1-butanol phase was removed to a 1.5 ml screw-capped Eppendorf tube. One hundred µl of water-saturated butanol was added to the glass tube before vortexing and centrifugation as before. The upper 1-butanol layer was once again removed and pooled with the layer from before. One hundred µl of water was added to the pooled 1-butanol layers in the Eppendorf tube. The tube was vortexed then centrifuged for 1 minute at 15000xg. The upper 1-butanol phase was once again removed to a new Eppendorf tube to be concentrated by evaporation using a Savant Speed Vac Plus SC110A concentrator. The lipidic pellets were resuspended in water-saturated 1-butanol (10 µl water-saturated butanol per 0.1g weight pellet) before high performance thin layer chromatography (HPTLC) analysis (see Section 2.10.) Glycolipids and phospholipids (PIMs, glycopeptidolipids, trehaloses and membrane lipids) are expected to be found in the resultant butanol phase.

2.8.2.2 Lipoglycan extraction

The lipid-extracted pellet was refluxed in 50% ethanol to extract the non-covalently bound, highly glycosylated molecules (such as LAM and LM). The solution was then passed through octyl-sepharose columns which bind the lipid molecules (LM, LAM and highly glycosylated PIMs). Solvent

components such as mannans and arabinomannans would wash through in the eluent. Further analysis can be done by methanolysis and GC-MS.

An extraction method described by Nigou *et al.*(187) was used in this protocol. The de-lipidated pellet was resuspended in 5 ml of 50% (v/v) high grade ethanol by sonication followed by ethanol refluxing at 100°C for 2 hours. After centrifugation at 500xg for 10 minutes, the supernatant was decanted to a 15 ml polypropylene tube and a further 5 ml of 50% ethanol (v/v) added to the pellet. After sonication, the material was subjected to further reflux for 2 hours. The tube was again centrifuged and supernatant pooled and dried under a stream of nitrogen gas. Finally the extracted LM/LAM (in the supernatant) was frozen at -80°C, then freeze-dried overnight.

The freeze-dried pellets were dissolved in H₂O, 0.2% CaCl₂, proteinase K (20 mg/ml) and incubated at 37°C for 2-3 hours. Next, 50% propanol and 1M ammonium acetate were added. Purification of glycolipids using octyl-sepharose resin (octyl-sepharose in 0.1M ammonium acetate diluted in 5% propanol) packed in Econo-Pac^R Chromatography Columns (Amersham Pharmacia Biotech) followed. The resin was first prepared by packing a bed volume of 0.4-0.5 ml of octyl-sepharose in the column. Two ml of mqH₂O was flowed through, followed by 1 ml of a mixture of 0.1M ammonium acetate in 5% propanol, 1 ml of 60% propanol, and lastly 2 ml of the 0.1 M ammonium acetate in 5% propanol. The flow was then stopped with the tip cap.

The sample was loaded onto the octyl-sepharose bed and left for 10 minutes at room temperature allowing it to bind. The flow through was collected in a 2 ml Eppendorf tube. Next, a 2ml wash of 0.1 M ammonium acetate in 5% propanol was collected. The elutions then began, collecting each in a 1.5 ml Eppendorf tube for further analysis: 1 ml 30% (v/v) 1-propanol, 40% (v/v) 1-propanol, 50%

(v/v) 1-propanol, 60% (v/v) 1-propanol. The columns were then rinsed with the 0.1 M ammonium acetate in 5% propanol mixture.

The sugar content of each eluent was detected by dotting 1 μ l of sample onto an aluminium-backed Silica Gel-60 HPTLC, Merck sheet and staining with orcinol spray. The spots were visualized at 160°C. Concentrations of interest were pooled, dried under rotational vacuum, snap frozen at -80°C or in liquid nitrogen, then freeze-dried overnight. At this stage, only LM and LAM should be contained in the samples. For LM/LAM analysis by SDS-PAGE gel or GC-MS (see Sections 2.11 and 2.12), samples were dissolved in 100 μ l/0.1 g 30% (v/v) 1-propanol.

2.9. Differential Butanol Extraction of Labelled Lipids

A 50 ml BHI culture of wild type and Δ NCgl2761 *C. glutamicum* was grown to mid-log phase ie. Approximately OD(600nm)=3, then harvested into pre-weighed 50 ml Falcon tubes. After centrifugation at 1500xg for 5 minutes at room temperature, the cell pellets were washed with 5 ml of pre-warmed phosphate buffered saline (PBS) then weighed. The pellets were resuspended in pre-warmed PBS (1 ml/ 0.15g pellet (v/w)). Aliquots of 400 μ l each were transferred to 15 ml Falcon tubes then shaken, for 10 minutes at 30°C. One μ Ci of 14 C-acetate was added to each sample before a 5 minute pulse at 30°C. Pre-warmed BHI media of 2.6 ml volume was added to each sample followed by incubation, with shaking, for 2 hours at 30°C. The samples were quenched on ice, before centrifugation at 1500xg for 10 minutes at 4°C. The radioactive supernatant was discarded and the pellets resuspended in 2 ml cold PBS which was then divided into 2 fractions: butanol fraction (a), and butanol/chloroform/methanol fraction (b). These were centrifuged at 14 000xg for 30 seconds before discarding the supernatant. A sequential pellet extraction process was compared to a one step-extraction with chloroform/ methanol (2:1v/v). Pellet (a) was differentially extracted first in 600

µl of water-saturated butanol. It was rotated for 30 minutes at room temperature in water-saturated butanol before centrifugation and transfer of the supernatant to an Eppendorf tube. The pellet was resuspended in another 200 µl of water-saturated butanol then centrifuged. The butanol-supernatants were pooled and dried under rotational vacuum. Next, pellet (a) was extracted with 600 µl chloroform/methanol (2:1 v/v) overnight.

Pellet (b) was extracted directly with chloroform/methanol (2:1 v/v) overnight. Both pellets (a) and (b) were subjected to chloroform/ methanol (2:1 v/v) extraction by adding 200 µl of chloroform/ methanol (2:1 v/v) and incubating for 2 hours at room temperature. The pellets were centrifuged and supernatants removed to new tubes. They were then resuspended in another 600 µl of chloroform/ methanol/water (1:2:0.8 v/v/v) and extracted for 2 hours at room temperature. The supernatants were pooled in their respective Eppendorf tubes and dried under nitrogen stream. Pellet (b) was butanol-partitioned.

All samples were resuspended in butanol. HPTLC analysis was performed to analyse the localization of the total free mycolic and total lipids, e.g. TMCs and TDCMs.

2.10. High Performance Thin Layer Chromatography (HPTLC)

HPTLC and carbohydrate staining with orcinol/sulphuric acid to visualise resolved carbohydrates was used to examine glycolipids. Two µl of the 1-butanol solvent obtained after butanol partitioning (see Section 2.8.2.1) was loaded onto an aluminium backed Silica Gel-60 HPTLC sheet (Merck). The loading sites were 4 mm in length and 6 mm apart, allowing a margin of 1.5 cm along the plate edges and base.

After rinsing the TLC tank with methanol, a 10cm X 10-20cm (height X width) size Whatman blotting paper the size of the tank was cut and placed inside, and the solvent added. The solvent system was left to equilibrate. Two different solvent systems were used depending on the separation of individual species required. Solvent System A referred to a mixture of chloroform: methanol: 1 M ammonium acetate: 13 M ammonia: water (180: 140: 9: 9: 23, v/v/v/v/v). Solvent system B also referred to a mixture of chloroform: methanol: 1 M ammonium acetate: 13 M ammonia: water, but in a different ratio i.e. 180: 140: 9: 9: 2.3, (v/v/v/v/v) Solvent system B gave better migration of TMCM, GI-X, AcPIM2. The TLC tank was saturated with the solvent before placing the silica sheet against the Whatman sheet in the tank. The solvent was allowed to run until the front was approximately 0.5 cm from the top of the plate (approximately 40-50 minutes). The plate was then removed and air-dried.

To visualize the sugars, the HPTLC sheet was sprayed with orcinol stain (180 mg orcinol in 5 ml water, 75 ml ethanol and 10 ml sulphuric acid) then heated at 100°C for approximately 5 minutes until the lipid species appeared. In order to visualize phospholipids, the sheet was baked at 160°C for approximately 5 minutes.

2.11. SDS-PAGE and Silver Stain Analysis of LM/LAM

The sample to be used for LAM analysis was dissolved in 100 µl/0.1 g 30% (v/v) 1-propanol (as per the previous section). Twenty µl was aliquoted into a 1.5 µl Eppendorf Tube and evaporated under a nitrogen stream. Forty µl of 2X SDS sample buffer (2.5 g 1M Tris-HCl (pH 6.8), 0.5 ml ddH₂O, 1 g SDS, 0.8 ml 0.1% Bromophenol Blue, 4 ml 100% glycerol, 2 ml 14.3M β-mercaptoethanol, adjusted to a final volume of 10 ml) was added, before sonication and vortexing to thoroughly dissolve the sample which was then heated at 95°C for 5 minutes. After brief centrifugation, 5-7 µl of sample was loaded

onto a 15% SDS-PAGE gel (4% stacking gel) in a tank of 1 X running buffer. The resolving and stacking gels contained dH₂O, 40% (w/v) acrylamide, TEMED, a catalyst for the polymerization of polyacrylamide gels, and 10% ammonium persulphate (APS) which functions together with TEMED to catalyse the polymerization of the gel; the running buffer was made up of 10 X Tris glycine, a combination of Tris-chloride, glycine, 10% (w/v) sodium dodecyl sulphate (SDS), and dH₂O. Pre-stained Benchmark protein marker (Invitrogen; 1 µl) was also loaded. The SDS-PAGE gel was run at 100 volts for approximately 90 minutes, before silver staining.

A glass, acid washed container was used for silver staining of the SDS-PAGE gel. The gel was removed directly from the glass plates, then fixed in a 100 ml solution of 40% methanol, 10% acetic acid and incubated at room temperature for 45 minutes with gentle agitation. After incubating for 10 minutes in 0.7% periodic acid, the gel was washed for a further 10 minutes in a 5% methanol, 7% acetic acid solution. The solution was discarded and the gel rinsed thoroughly four times, for a minimum of 5 minutes each time. To the final dH₂O wash, 16.2 µl 1 M dithiothreitol (DTT) was added and incubated for 5 minutes. The DTT solution was discarded and the gel was incubated in the working solution of the Pierce Silver Stain Kit®. One gel can be incubated in 12.5 ml solution + 0.5 ml enhancer. The developing solution was made, again using 12.5 ml solution + 0.5 ml enhancer per gel, before discarding the working solution. The gel was quickly rinsed in 100 ml dH₂O, then developed with gentle agitation in the premixed solution until heterogenous bands just become visible. Further staining was stopped by the addition of 100 ml 5% (v/v) acetic acid, leaving the gel to incubate for 5 minutes. This wash was repeated, before a final wash with mqH₂O to rinse off the acid.

2.12. Methanolysis of Extracted LM/LAM Samples for GC-MS Analysis

The mannose and arabinose content/ ratio of all four strains of *C. glutamicum* was analysed by GC-MS. After following the cell wall extraction protocol (as described in section 2.8), approximately 40mM of the LM/LAM fraction was transferred to a heat sealed capillary tube (250 µl Drummond Microdispenser, Drummond Scientific Scientific Company). Next, 10 mM *scyllo*-inositol was added to each tube as an internal standard and mannose and arabinose were added to additional capillaries as external standards. All samples were then dried under rotational vacuum concentrator (RVC) (RVC 2-25, Christ) and resuspended three times in 50 µl 0.5M methanolic HCl (Supelco). Next, the glass tubes were flame-sealed under vacuum and subjected to solvolysis at 80°C for 12-18 hours. After cooling to room temperature, the capillary tubes were cut open leaving samples to be transferred to a 250 µl pulled point glass GC vial insert (Agilent Technologies). The addition of 10 µl of pyridine to neutralize the methanolysate followed. The vial was incubated for 10 minutes at room temperature, before another drying step under RVC (RVC 2-25, Christ). Dried samples were silylated by adding 30µl N₂O-bis(trimethylsilyl) trifluoroacetamide (BSTFA) + 1% trimethylchlorosilane (TMCS) (Thermo Scientific) and incubated at room temperature for one hour.

The samples were then ready for analysis by GC-MS (as follows)

2.12.1 GC-MS analysis of extracted LM/LAM samples

GC-MS analysis was performed on an Agilent HP 6890 GC system and an Agilent HP 5973 MSD (Agilent Technologies) in electron ionization (EI) mode, equipped with a DB5 capillary column (J&W Scientific) of 250 µm inner diameter, 0.25 µm film thickness and with a 10 m inert duraguard. The injector insert and GC-MS transfer line temperatures were 270°C and 250 °C, respectively. The oven temperature gradient was set to: 80 °C (2 min); 80 °C to 140 °C at 30.0 °C/min; 140 °C to 250 °C at 5 °C/min; and 250 °C to 265 °C at 15 °C/min; 265 °C for ten minutes. The total ion chromatogram (the

mannose and arabinose content as well as the mannose/arabinose ratio) of the analyzed samples were identified and compared based on the GC-retention time, relative abundance and mass spectra of the mannose and arabinose standards.

ChemStation software (Agilent Technologies) was used to integrate samples, and calculations were made using Microsoft Excel.

2.13 High pH Anion Exchange Chromatography (HPAEC)

HPAEC requires many reactions and much preparation before analysis with the DIONEX software can be performed: the sugar head first needs to be removed, followed by HF dephosphorylation then desalting of the neutral glycan.

2.13.1 Base hydrolysis to determine sugar head from the glycolipid

The samples used were lipids, preferably purified by HPTLC. After aliquoting into screw cap tubes, 50 μ l methanol was added. The sample was then dried under RVC. A further 50 μ l methanol was added before sonication to dissolve the lipid. After adding 50 μ l ammonium (NH_4) solution, the solution was incubated at 37°C for at least 16 hours. Next, the solution was dried under N_2 and 50-100 μ l methanol was added before drying under RVC. Addition of 100 μ l water-saturated 1-butanol and 50 μ l water, partitioned the solution into two layers with an upper layer of butanol and a lower phase containing the LAM. Repetition once was followed by drying under RVC of both layers and finally resuspension of the upper organic phase in 10 μ l butanol and 10 μ l 30% isopropanol for the bottom aqueous phase (which contains the LM/LAM).

2.13.2 Aqueous hydro-fluoride dephosphorylation of glycoconjugates

A sample of LM/LAM resuspended in 30% isopropanol was dried in screw-top microfuge tubes under RVC at approximately 45°C, then placed on an ice/water mixture in a large Dewar flask. Cold 48% aqueous hydrofluoric acid (HF) from the freezer was added with great care, before incubating the Dewar for 48-60 hours at 0°C allowing for hydrolysis. LiOH (lithium hydroxide) is then needed for neutralization of the HF. However, the reaction between HF and LiOH is extremely exothermic so the LiOH is first frozen in dry ice (CO₂). This reaction also results in digestion of glycosidic bonds. The HF was then transferred into the frozen LiOH and vortexed until completely thawed and mixed, without allowing the tube to warm up. Centrifugation was then followed by removal of the supernatant. The supernatant can cloud a little due to the formation of insoluble lithium fluoride (LiF) by the residual HF. So the supernatant is once again removed and the remaining pellet washed twice with 50 µl water. By removing the supernatant back to this tube, it will contain dephosphorylated glycans in 100mM LiF and a trace of HF.

The sample, a neutral glycan, was desalted by passage through a 0.2 ml AG50 (H⁺) over 0.3 ml AG3X4 (OH⁻) over 0.1 ml QAE-Sephadex A25 (OH⁻) and eluted with 2.5 ml H₂O. It was then filtered through a 0.2 µm membrane and concentrated by RVC. After snap freezing in dry ice, it was frozen at -80°C overnight then freeze-dried overnight. The neutral molecules were then ready for analysis by HPAEC. Before use on the DIONEX, the filtered glycan was resolubilized by the addition of 25 µl water.

The HPAEC system was equipped with a DIONEX GP-50 gradient pump, a Carbo PacPA-1 column (4X250mm), with a PA-1 guard column and an ED50 integrated pulsed amperometric detector. The system was controlled and data analysed by Chromeleon version 6.50 software (DIONEX). The

eluent used in the system were 75mM NaOH (E1) and E2; T₄₀=100% (v/v) E2, T₆₀=100% (v/v) E2, at a flow rate of 0.6 ml/minute.

Before use, buffers for use on the DIONEX needed to be made up fresh. They were 75mM NaOH (sodium hydroxide), 250mM NaOAc (sodium acetate), 1mM NaOH and 1M NaOAc.

2.14 ESI-QTOF Analysis of Wild Type *C. glutamicum* and Mutant Mannose Residues

C. glutamicum cultures were harvested in exponential phase, OD(600nm) =3.2

For compositional analysis of the LM/LAM fraction, the extract from the wild type *C. glutamicum* or the mutant was mixed 1:1 with 10mM ammonium carbonate buffer (pH 8.2). A 4 µl aliquot was used for direct infusion analysis on an Agilent 6220 Accurate Mass TOF LC/MS System (Agilent Technologies). The run was performed in a negative ion mode with a mass range between 100-3000 Da. The Ref Nebulizer was set to 20 psig with a detection window of 100 ppm, minimum height of 1000 counts, an acquisition rate of 0.63 spectra/s and an acquisition time of 1589.4ms/spectrum. The gas temperature was set to 325°C with a drying gas of 7 l/min, dual ESI 3500V, Fragmentor 150V, and Skimmer 65V. The flow rate was set to 0.25 ml/min and a mobile phase consisting of 50:50 water:acetonitrile with 10 mM formic acid was used to push out the sample and wash out the system. Technical triplicate performed.

Chapter 3

Characterisation of a New Mycolic Acid Biosynthesis Protein in

Corynebacterium glutamicum

3.1 Rationale and Objectives

3.1.1 Introduction

The virulence and survival of *M. tuberculosis* within the host are largely attributed to the “Mycolyl-arabinogalactan-peptidoglycan complex” framework of the outer cell wall, which includes mycolic acids. These are either covalently bound to the arabinogalactan layer (35) or exist as free lipids bound to trehalose, a disaccharide of glucose (36). The biosynthetic pathways that form mycolic acids have been studied intensively for many years, revealing a series of reactions occurring in the cytoplasm and transfer steps occurring outside the cell membrane (reviewed in Chapter 1 and recently in Nataraj *et al*, 2015 (188)). In contrast, the transport of nascent mycolic acids across the *Mycobacterial* membrane for incorporation into the cell wall is less well understood with the initial identification of a dedicated transporter, Mmpl3, occurring only recently (85) along with identification of equivalent transport proteins in Corynebacteria (89).

Three *C. glutamicum* genes located close to each other, suggesting a single locus, *NCgl2764*, *NCgl2762*, *NCgl2759*, all encode proteins with roles in corynomycolate transport. These genes have been studied in our laboratory (46) (and unpublished results). Since disruption of these three genes resulted in mutants with defects in corynomycolate transport across the membrane, it seemed reasonable to hypothesise that the two remaining genes in the locus may also be involved in this

process. An investigation of this hypothesis is described in Chapters 3 and 4 of this thesis with *NCgl2761*, the likely ortholog of *Rv0226c* from *M. tuberculosis*, being the focus of the current chapter.

3.1.2 Aims and general approach

The overall aim of this section was to determine whether *NCgl2761* has a role in cell wall biosynthesis. Based on previous findings on adjacent genes, it was hypothesised that this protein has a role in the corynomycolic acid biosynthesis pathway, specifically a role in membrane transport of corynomycolates. The first objective was to confirm that the most likely ortholog of *M. tuberculosis* *Rv0226* in *C. glutamicum* is *NCgl2761*, which occupies the same relative position with respect to the three previously studied genes. Next, the *NCgl2761* gene was disrupted in *C. glutamicum* by homologous recombination and the mutant studied for effects on growth and for cell wall defects. Total lipids, PIMs, LM, LAM and mycolic acids from the mutant strain were analysed by High Performance Thin Layer Chromatography (HPTLC), Sodium Dodecyl Sulphate - Polyacrylamide Gel Electrophoresis (SDS-PAGE) and Gas Chromatography - Mass Spectrometry (GC-MS).

3.2 Results

3.2.1 Protter prediction of protein topology

Rv0226c, encoded by an essential gene in *M. tuberculosis*, is a predicted polytopic membrane protein conserved across mycobacterial and corynebacterial strains. The gene in *M. tuberculosis* is 1731bp and is predicted to encode a protein of 576 residues that would be expected to be 59kDa in size. The Protter prediction (wlab.ethz.ch/protter) of *Rv0226* (Figure 3.1A) indicates the presence of 11 transmembrane helices and one significant periplasmic loop between residues G387 and H540

located before the C-terminal transmembrane domain. A second, smaller periplasmic domain is predicted between residues S214 and R264 and a single cytoplasmic loop after the N-terminal transmembrane domain (R29 to G69). Extensive database searching revealed no significant similarity to proteins of known function and no motifs suggesting function.

However, the protein structure of both Rv0226 (Figure 3.1A) and NCgl2761 (Figure 3.1B) was analysed to highlight not only similarities, but also interesting differences. Rv0226 has 11 helices whereas NCgl2761 has only 9 transmembrane helices. Yet, both orthologs have a prominent extracytoplasmic loop between their last two transmembrane helices. The transmembrane helices, if that is indeed what they are, do not have absolutely classical sequences. Thus although they are tagged as such by the Protter prediction, the Hidden Markov Model (HMM) prediction suggests that Rv0226 has 10 transmembrane helices and NCgl2761 has only 3 transmembrane helices.

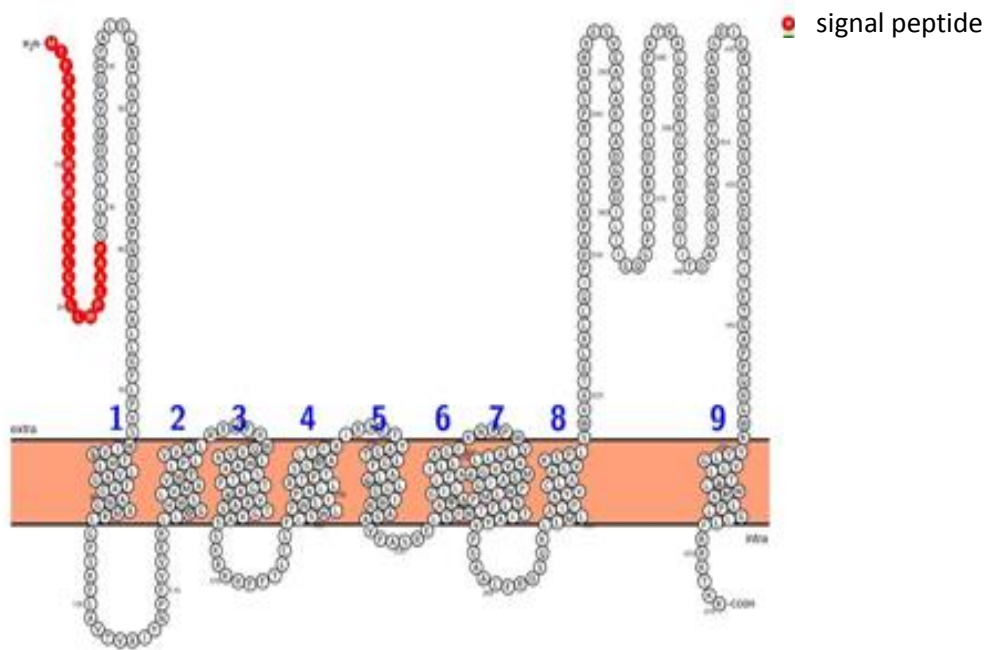
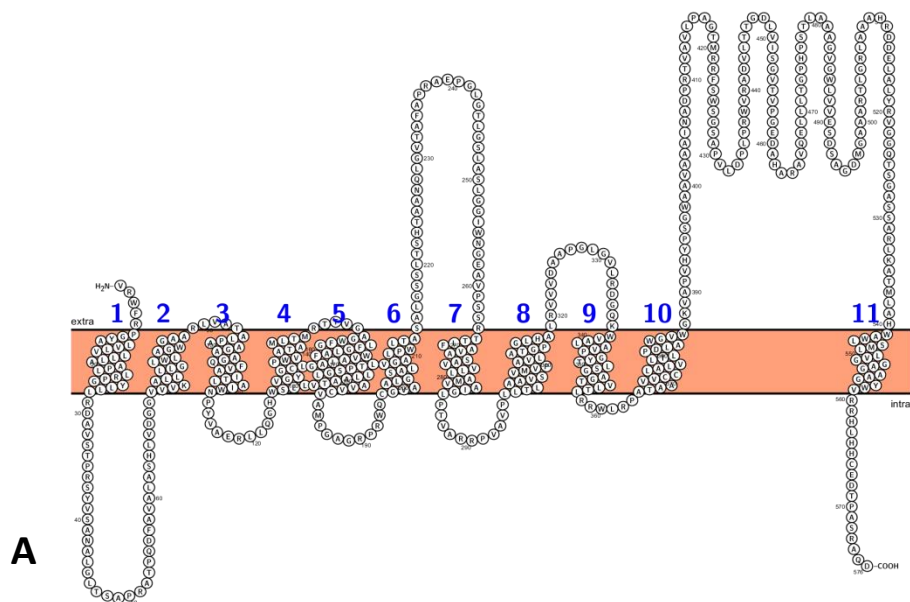


Figure 3.1

Figure 3.1 Outer cell membrane topology according to the Protter prediction. A) *M. tuberculosis* Rv0226; B) *C. glutamicum* NCgl2761. The prediction of a signal sequence within NCgl2761 seems to be the most prominent difference between the two putative orthologs, although prediction algorithms cannot always distinguish signal peptides from transmembrane helices. Both proteins have a significant periplasmic domain between the two C-terminal transmembrane domains that may be of functional relevance.

3.2.2 Bioinformatics analysis

To investigate the similarity between Rv0226c and its likely orthologs in other Mycobacteria and Corynebacteria, particularly *C. glutamicum*, the proteins were aligned using Clustal Omega. Alignment of the best matching proteins from *M. tuberculosis* H37Rv (Rv0226c); *M. leprae*, (ML2582); *M. smegmatis* mc²155 (MSMEG_0315) and *C. glutamicum* ATCC 13032 (NCgl2761) in the suborder Corynebacterineae, was performed (Figure 3.2). While the amino acid sequences of the mycobacterial proteins were at least ~60% identical to one another, the likely corynebacterial ortholog NCgl2761 was only ~30% identical to the mycobacterial proteins. However, NCgl2761 was the best match for Rv0226c in the *C. glutamicum* proteome and this, combined with the presence of its gene in the same position -between orthologs of *Rv0225* and *Rv0227c* (Figure 1.15, Chapter 1), suggested that it is indeed the ortholog of Rv0226c.

1

NCg12761 --MTPTRRILLWA---WTTVLLGSLWPLAAPGELLRLDMSVVDHPALSLNALGFGLDPS
M.SMEG_0315 -----MPAYALVLSVLVTAPLLAPGYLLLRDAVSTPRS YVTDAAALGLTEAAP
Rv0226 -----VRWFR**PGYALVLLVLLAAPLLRPGYLLLRDAVSTPRS**YVSANALGLTS-AP
ML2582 VSRELYHRSMSWSRPSYALGMALLVVGFLMRPGYLLLRDAVSTPRS YLSDAALGLTS-AP
: : : * * * * * . : : * * * .

2 3

NCg12761 RNAPQDGV LALLGFLPVSW-IVRTMLLVAGFAGAWGAMRLG-----PSKFLAVTVA
M.SMEG_0315 RALPQDFAVALASSVLDGGVVKALLLAGLAAAGWGAARLVGHVLF DAGLAGRFTAATLA
Rv0226 RATPQDFAVALASHLVDGG**VVKALLLGLWLAGWGAARLVATALPAAGAAGQFVAITLA**
ML2582 RSTPQDFAVAMASHLVDGGIVVKLSALVGLWLAGWGAARLVVTALPSAGVAGQFVASTLA
* * * * * . : : . : * * . . * * * * * . : * * * . *

4 5

NCg12761 IYNPFVVERLLQGHWSLVMAVWLLPLVV----ALRR-----HPRWQV---VAIW--AASL
M.SMEG_0315 IWNPYVAERLLQGHWSLLVGYGCLPWVAVSVLRRLRE-----RASWTPVAPLVFWMALAGL
Rv0226 **IWN**PYVAERLLQGHWS**LLVGYGCLPWVATAMLTMR**TV---GAGW**FLGLAFWVALAGL**
ML2582 VWNPYVAERLLQGHWSLLVGYGCLPWVAEAMLMRLSSDNASRPGLLGFALACWIALAGL
: * * * * * . * * * * * . : * * * * * . : * * * * *

6

NCg12761 TPTGAVVAAVTGVAS-----SKRKRFT-----TLCFSLSWLPWLI PALLATP-----
M.SMEG_0315 TPTGLVLAATVALVCAAPG----DGWRRARVAGLGLGVAVAAACPWLVAAFVSGAVSS-
Rv0226 **TPSGLLLAATVAVVCVAMP**----GAGRPRW**QCGVVALGSALVGPWLTA**SALGSSLTSH
ML2582 TPTGLMLAATVALICVAVPVEGPGEP RPRLCAAATLGSALGAALPWL TASAVGTSLTAH
* * * * * . : * * * * * . : * * * * * . : * * * * *

7

NCg12761 ---TSGGALTFAIRSETYAGTLGTALGLGGIWNAGAVPASRELGF AVAGIL-LFAILLAG
M.SMEG_0315 SPDPGAGVRAFAARAEPGLATLGS LAGLGGIWNDAVPASRTSLFAVVATV VLLGVVAAG
Rv0226 TAANQLGVTAFAPRAEPGLGT LGS LAGLGGIWNGEAVPSSR**TTLFAVASAVVLLAMVAIG**
ML2582 TVANTLGVTVFAPRAEPGLGT LGS LAGLGGIWNGEAVPTSR**TTLFAVLSATVLLGVVVAG**
* . * * * * . * * * * * . * * * * * . * * * * * . * * * * *

8

NCg12761 FKNC---PWVLALLA--VVGFM----GAIGPWLMPNLF TWTIAYVPGAALFRDSQKLLML
M.SMEG_0315 LPVVARRRAAVPLL VLAAGAVIMPALMASAPG--LVVVEALIDAVPGLGIVRDGQKVVVAL
Rv0226 **LPTVARRPVAVPLLTLAAVSVMPAVLATGPG--LHALRVVVDAAPGLGVLRDGQKVVVAL**
ML2582 LPVAARRPAVPLL VLAAGAVATPAALATGPG--IDMLKAVVNAV PGLGVLRDGQKVVVAL
: : * * . . . * * . : * * . : * * * * * : *

9 10

NCg12761 AIPAYVCLAAGVKSPLS-WVATGL-----ALLQIPDAPREVS-----VIRP
M.SMEG_0315 AMPGYALAAGAAPMLRRLRIPAA-----AAAAVCCAALIAVLPDLTWGVGNQMRVRYR
Rv0226 **AVPGYTLSGAGTVLTLRRLRPAT**-----**AAVCCCLALVLTLPDLAWGVW**KVAPVHYR
ML2582 AVPGYSLAGAGAVVTLGRWLRPSRPLSPVVTALACCLALILALPDLAWGVWGVVQPVHYR
* : * * . . . * . : : * * * * * * * *

11

NCg12761 -----VDGDTITETGAPPQHGWKYYLGVGLTVLWMALPLG-----LLFRRKTKK-
M.SMEG_0315 -----TAQRIGGE---APSSPHRGLL----IAAHLVWLAALAGGALGLVAGRVRVLSRR
Rv0226 RDDELALYRVGGQTS GASSARLKAT-----MLAHWAWLSMLLVGGAGAAGYWVRRHLHHC
ML2582 RDDAIGLYRIGGSNAKTAPSPYRGLL----IAAHLTVLVILVMAVVG---MQITRHTHER
* : : : * : * : *

NCg12761 -----
M.SMEG_0315 TWRHRPRPG---
Rv0226 EDTPASRAQD--
ML2582 DVSSVALLSRR*

Figure 3.2

Figure 3.2. Protein sequence alignment of *M. tuberculosis* (Rv0226c) and putative orthologs in *M. smegmatis* (MSMEG_0315), *M. leprae* (ML2582) and *C. glutamicum* (NCgl2761). Residues indicated by “*” are completely conserved among the sequences; those indicated by “.” or “:” are similar. M= *Mycobacterium tuberculosis* H37Rv, Rv0226c; *Mycobacterium leprae*- ML 2582; *Mycobacterium smegmatis* mc² 155- MSMEG 0315; *Corynebacterium glutamicum* ATCC 13032- NCgl2761. The eleven predicted transmembrane domains of Rv0226 presented in Figure 3.1A are indicated in bold and numbered.

3.2.3 Evidence of co-transcription of *NCgl2760/NCgl2761* and *MSMEG_0317/MSMEG_0315*

This thesis describes the functional characterisation of two adjacent *C. glutamicum* genes: the analysis of *NCgl2761* is described in this chapter and *NCgl2760* is discussed in Chapter 4. Before analysing the genes individually via the production of knockout mutants, we wished to investigate whether the genes were transcriptionally linked. Such linkage might indicate that they have related functions, already suggested by the fact that they are adjacent to each other in all available mycobacterial and corynebacterial genomes. To investigate co-transcription, RNA was extracted (see Section 2.7, Chapter 2) from wild type *C. glutamicum*, then converted to cDNA. The RT-PCR primers for amplification of the cDNA were designed to bind in the middle of each gene as shown in Figure 3.3B. Following PCR amplification, a strong band of 0.9kb was detected, which was the expected size (Figure 3.3A, lane 2), indicating co-transcription of *NCgl2760* and *NCgl2761*. In this experiment, gDNA from *C. glutamicum* served as the positive control (lane 4), whereas the negative control (lane 3) was void of random hexamers. The lack of a PCR product in lane 3 ruled out the possibility of genomic DNA contamination of the RNA sample.

To determine whether the two genes are co-transcribed in mycobacteria as well, RNA extraction was performed in an identical manner (see section 2.7, Chapter 2), however, when compared to *M. smegmatis*, the method of RT-PCR is very different. The likely orthologs of *NCgl2760* and *NCgl2761* in this organism are *MSMEG_0317* and *MSMEG_0315* (Chapter 1, Figure 1.15), respectively. Primers (*MSMEG_0317-F* and *MSMEG_0315-R*) were designed to bind near the middle of the *MSMEG_0317* and *MSMEG_0315* genes, respectively. Being orthologs, the result would show whether these genes were co-transcribed in a second species and suggest it was generally true of these two genera of the Corynebacterineae suborder. A clear RT-PCR band of ~0.8 kb was detected, once again indicating co-transcription of the two genes (Figure 3.4). Here, the negative control lanes were lane 3 with no RNA, as well as lanes 1 and 5 with no reverse transcriptase.

Evidently, co-transcription of both genes in both *C. glutamicum* and *M. smegmatis* occurs, suggesting that they belong to a single operon and may have some sort of functional association.

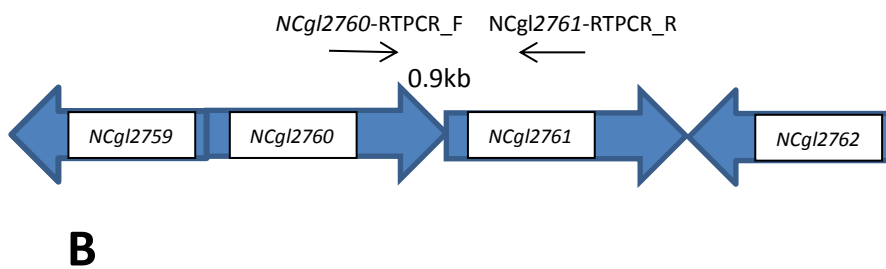
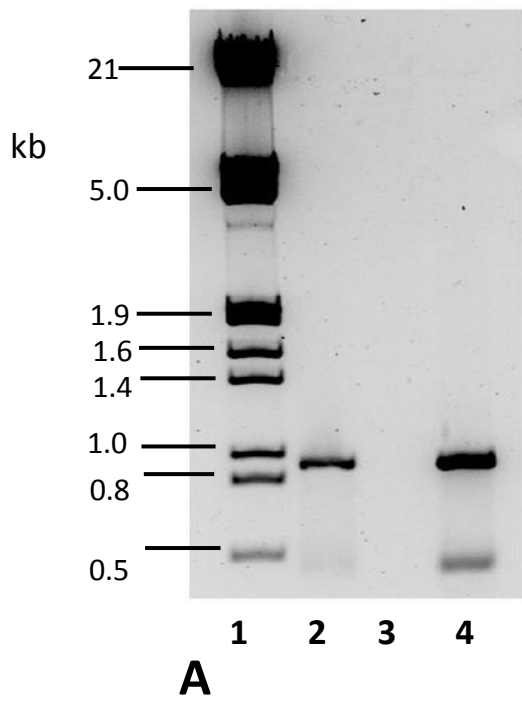


Figure 3.3

Figure 3.3 Evidence of co-transcription of *NCgl2761* and *NCgl2760*. **A)** RNA was prepared from *C. glutamicum* and incubated with reverse transcriptase (RT) in the presence of random hexamers or in their absence (as a negative control). The samples were subjected to a PCR using primers NCgl2760-RTPCR_F and NCgl2761-RTPCR_R to detect the presence of cDNA that spans both genes. Purified *C. glutamicum* genomic DNA (gDNA) PCR amplified using the same primer pair was used as a positive control. Lane 1, λ HindIII/EcoRI Marker; Lane 2, RNA + RT + random hexamers; Lane 3, RNA + RT only; Lane 4, gDNA control. **B)** Schema of co-transcription of *NCgl2761* and *NCgl2760*. Binding sites and orientations of the two RT-PCR primers are indicated by thin horizontal arrows.

Although no -RT control was included in this experiment, it was believed that a sample lacking random hexamers was sufficient as a negative control as the RT cannot function without them

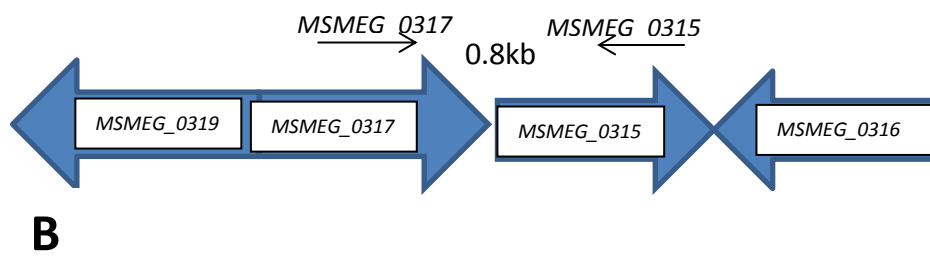
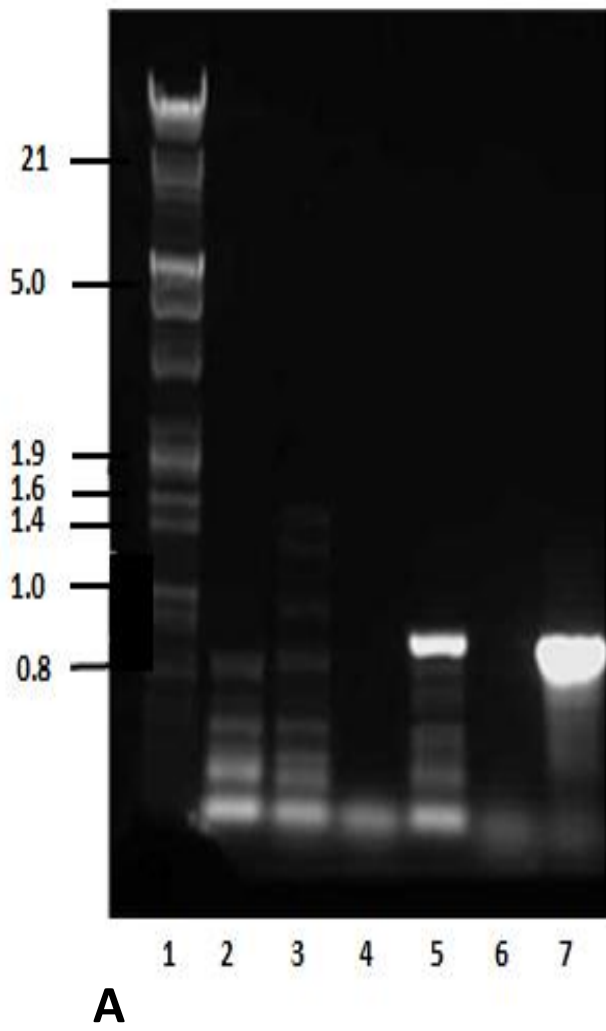


Figure 3.4

Figure 3.4. Evidence of co-transcription of *MSMEG_0315* and *MSMEG_0317*. **A)** RNA was prepared from *MSMEG_0315* and incubated with reverse transcriptase (RT) or in its absence (as a negative control). The samples were subjected to a PCR using primers *MSMEG_0317_F* and *MSMEG_0315_R* to detect the presence of cDNA which spans both genes. Purified *MSMEG_0315* genomic DNA, PCR amplified using the same primer pair, was used as a positive control. λ *HindIII/EcoRI* Marker (lane 1), 100ng RNA – RT (lane 2), 100ng RNA + RT (lane 3), no RNA (lane 4), 250ng RNA + RT (lane 5), 250ng RNA – RT (lane 6), gDNA control (lane 7). The inverted grey scale of this figure relative to Fig 3.3A is due to the experiments and image processing being performed at different times.

B) Schema of co-transcription of *MSMEG_0315* and *MSMEG_0317*. Binding sites and orientations of the two RT-PCR primers are indicated by thin horizontal lines.

3.2.4 Generation of an *NCgl2761* mutant

Studies on the *C. glutamicum* *NCgl2761* gene involved first creating a deletion mutant to allow detailed analyses of bacteria that no longer had the protein encoded by this gene. This required construction of a knockout plasmid containing a disrupted copy of *NCgl2761* and neighbouring DNA to be used for allelic replacement of *NCgl2761* in the *C. glutamicum* chromosome by homologous recombination (Figure 3.5). *C. glutamicum* genomic DNA was used as the template in all PCR reactions. The deletion construct was produced by first amplifying the left and right flanking regions of the gene by PCR using Proofstart DNA polymerase (Qiagen) according to the manufacturer's instructions. The left flanking region, ~1kb in size, was amplified by the primers *NCgl2761-left_F* and *NCgl2761-left_R* (see Appendix 3 for primer details) and cloned into the *XmaI/BamHI* sites of pUC19. A right flanking fragment of ~0.8kb in size was amplified using primers *NCgl2761-right_F* and *NCgl2761-right_R* then cloned into the *BamHI/XbaI* sites of pUC19. The *BamHI* site in the right flanking region occurs naturally in the *NCgl2761* gene whereas the *BamHI* site in the left flanking region was introduced by incorporation into the *NCgl2761-left_R* primer. DNA was cloned (see Section 2.5.3, Chapter 2) into pUC19, carrying an ampicillin resistance gene and LacZ blue/ white selection, before transformation (see Section 2.5.4, Chapter 2) into chemically competent *E.coli* DH5 α cells (see Section 2.3.1, Chapter 2). They were spread onto LB agar containing the chemical X-gal (5-bromo-4-chloro-3-indolyl-B-D-galactopyranoside) to select clones containing an insertion and left overnight to grow at 37°C. Individual clones were then incubated overnight, before isolating the plasmids. To check for the presence of correct inserts in the plasmids, a digest was performed followed by gel electrophoresis to visualize 2 bands corresponding to the insert and pUC19 vector backbone. Sequencing confirmed construct identity (Micromon Facility, Monash University). The pUC19 primers were used as they gave a longer sequencing read than the PCR primers.

Left and right flanking regions were purified, and the insert DNA digested from the plasmid (Figure 3.5). *Bam*HI and *Xba*I were used for the right and left flanking regions (while *Bam*HI and *Xma*I were used for the left region). NEB buffer 4 and 10xBSA (Bovine Serum Albumin) were added for digestion. The left and right fragments were ligated across the *Bam*HI site to create one combined fragment which was cloned into pUC19 then transformed into *E. coli* and cultured on LB solid media containing ampicillin. Next subcloning of the deletion cassette into, a suicide plasmid for *C. glutamicum*, encoding kanamycin-resistance and sucrose toxicity, using *Xma*I and *Xba*I restriction enzyme sites was performed.

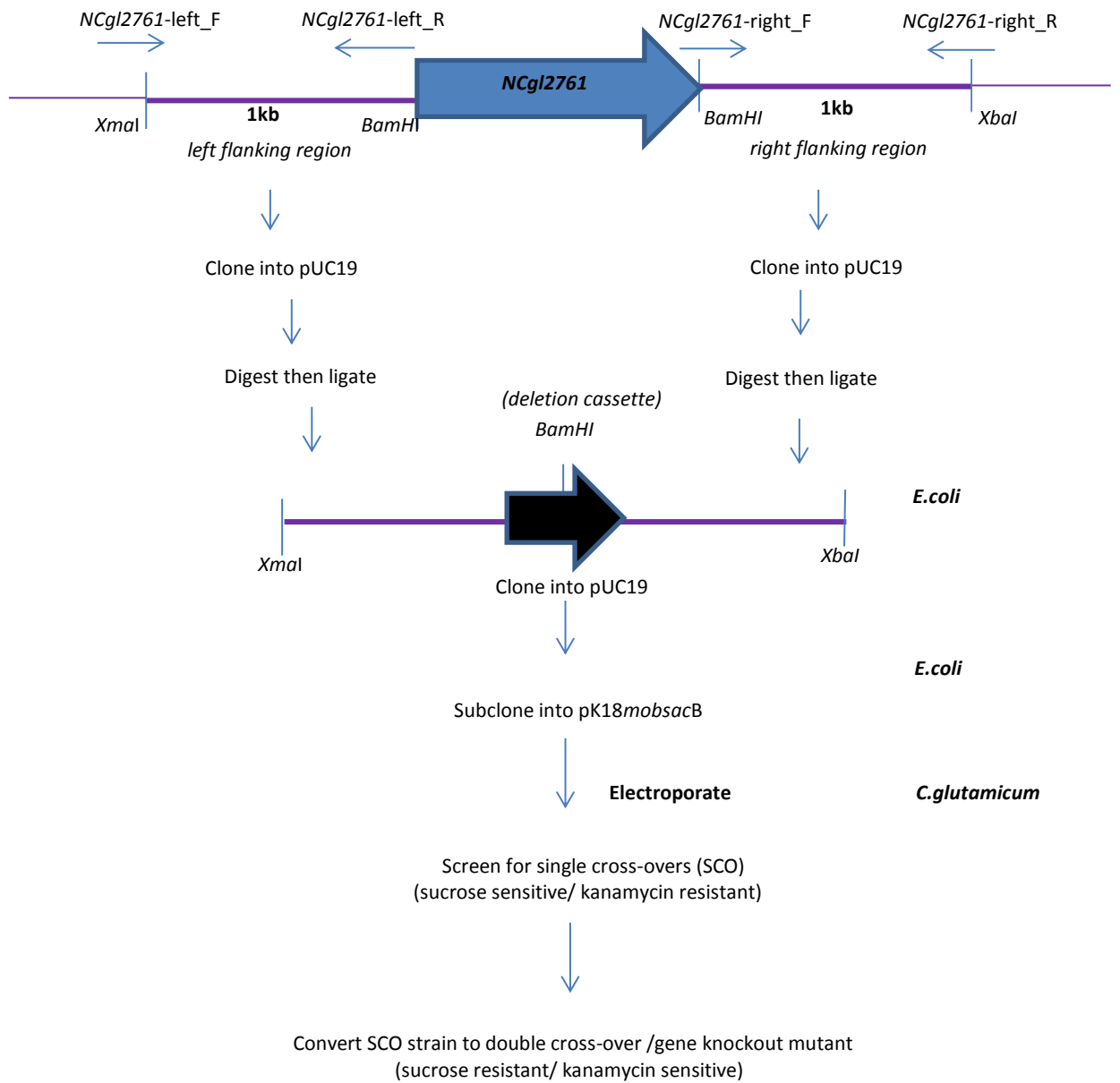


Figure 3.5

Figure 3.5. Cloning and recombination strategy to create a *C. glutamicum* $\Delta NCgl2761$ mutant. The left and right regions flanking *NCgl2761* were PCR amplified and cloned into pUC19. These two fragments were then joined together and subcloned into pK18*mobsacB*. The plasmid was then electroporated into *C. glutamicum* and kanamycin-resistant, sucrose-sensitive colonies (potential single crossovers; (SCO)) were selected. A second recombination step followed to produce colonies which were sucrose resistant and kanamycin sensitive. These potential double crossover strains (*i.e.* gene knockouts) were then analysed by PCR and Southern blot hybridization to determine whether the gene had been deleted.

The plasmid containing the deletion cassette was then electroporated into *C. glutamicum* ATCC 13032 electrocompetent cells (189) (see Section 2.3.2, Chapter 2). Kanamycin resistant transformants, representing potential single crossovers, were selected on BHI solid media. Single crossovers are resistant to kanamycin, but sensitive to sucrose due to the presence of the *sacB* gene. Potential single crossovers were cultured overnight in 10 ml liquid BHI media then spread on BHI plates containing 10% (w/v) sucrose to select for double homologous recombination events (knock-outs). After 2 -3 days, potential knockouts seen on the sucrose plates were cross-patched on BHI solid media containing kanamycin. Those colonies that were sucrose-resistant and kanamycin sensitive were screened for gene deletion by PCR, as they could either be wild-type revertents or gene knockout mutants depending on where the second crossover event occurred.

3.2.5 Identification of potential *NCgl2761* deletion mutants by PCR

Initial screening of potential knock-outs was done by PCR with candidate clones then confirmed by Southern blot hybridization. The forward primer of the left fragment of *NCgl2761* (NCgl2761-left_F) (see Appendix 3 for primer sequences) and the reverse primer of the right fragment of *NCgl2761* (NCgl2761-right_R), were used to amplify the sequence across the deletion cassette (Figure 3.6). PCR was performed using crude lysates prepared by homogenising colonies grown on BHI solid media as the templates. The PCR reactions were analysed on a 1% (w/v) agarose gel to screen for potential gene knockout strains. The mutants were expected to give product sizes of approximately 0.56kb whereas wild type revertents should give products of 1.7kb. Four clones with the expected profiles for mutants were identified (Figure 3.6), and the clones run in lanes 9, 10 and lane 11 were selected for Southern blot hybridization analysis to confirm deletion of the *NCgl2761* gene.

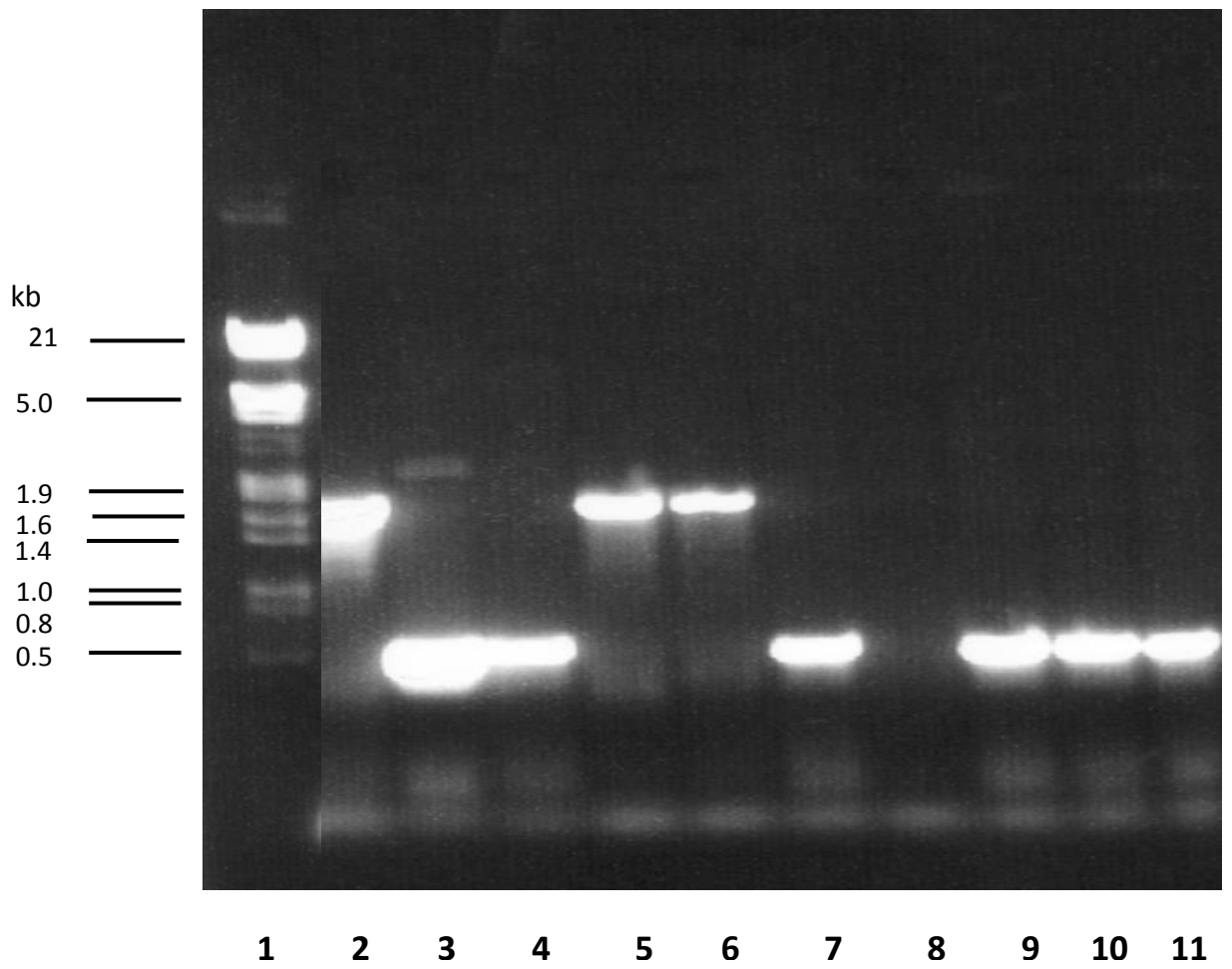


Figure 3.6

Figure 3.6 Identification of potential *NCgl2761* mutants via PCR followed by visualization on 1% agarose gel stained with GelRed™ nucleic acid dye. Wild type *C. glutamicum* genomic DNA (lane 2), single cross-over strain DNA (lane 3, 4), potential $\Delta NCgl2761$ mutants (lanes 7, 9, 10, 11) and likely wild type revertants (lanes 5, 6). The clone shown in lane 8 did not give a product. The λ HindIII/EcoRI size markers (lane 1) are shown in kilobases (kb).

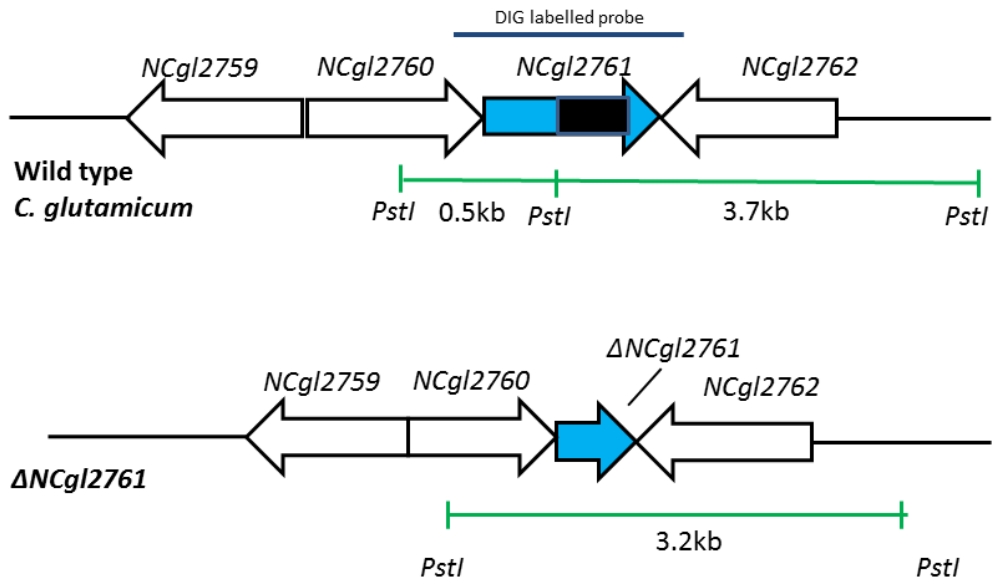
3.2.6 Confirmation of an *NCgl2761* mutant by Southern blot hybridization

Having identified several potential mutants by PCR, the next step was to confirm these by Southern blot hybridization which was performed on the samples running in lanes 7, 9, 10 and 11, figure 3.6. Genomic DNA was extracted then digested first with *Pst*I (Figure 3.7). When digesting with *Pst*I, two fragments in the wild type *C. glutamicum* strain, of 0.5kb and 3.7kb, hybridized to the probe (Figure 3.7B), as predicted (Figure 3.7A). The probe consisted of the gene (*NCgl2761*) and some flanking sequences synthesized by using primers NCgl2761-comp_L and NCgl-2761-comp_R (See Appendix 3) in a PCR reaction using wild type *C. glutamicum* DNA as the template.

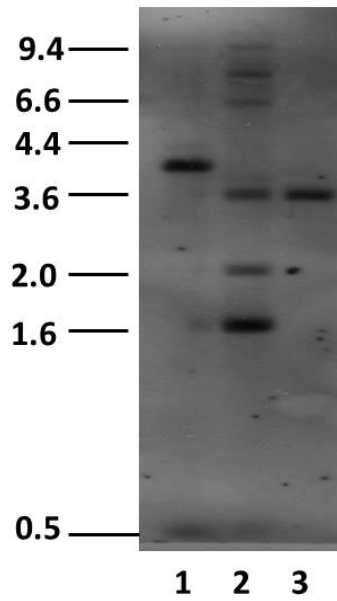
Two fragments hybridized because a *Pst*I site is located in the *NCgl2761* gene (Figure 3.7A). In the single crossover strain, several fragments were observed to hybridize due to integration of the entire suicide plasmid into the chromosome at the *NCgl2761* gene. Loss of the 3.7 kb band suggested that integration of the plasmid occurred to the right of the internal *Pst*I site of *NCgl2761*. In a knockout strain, loss of the *Pst*I site within the deleted portion of *NCgl2761* was expected to result in a 3.2 kb band hybridizing to the probe (Figure 3.7A) and this fragment was observed on the Southern blot (Figure 3.7B, lane 3). This finding suggested that the putative Δ *NCgl2761* mutant shown in lane 7 of Figure 3.6 was indeed a knockout and that deletion of the *NCgl2761* gene had been successful.

To obtain additional evidence that the *NCgl2761* mutant had been generated, the Southern hybridization experiment was repeated using an alternative restriction enzyme, *Xho*I (Figure 3.8). In this instance, the probe was expected to hybridize to a 3.8 kb fragment in the wild type strain and to a 2.82 kb fragment in the mutant. Once again, the Δ *NCgl2761* mutant in lane 7 of Figure 3.6 gave the expected profile, confirming it as a knockout mutant. Collectively, the PCR data and Southern hybridization experiments with two different restriction enzymes indicated that disruption of the

NCg/2761 gene had been accomplished. This mutant strain was designated Δ *NCg/2761* and was used for the remaining experiments described in this chapter.



A



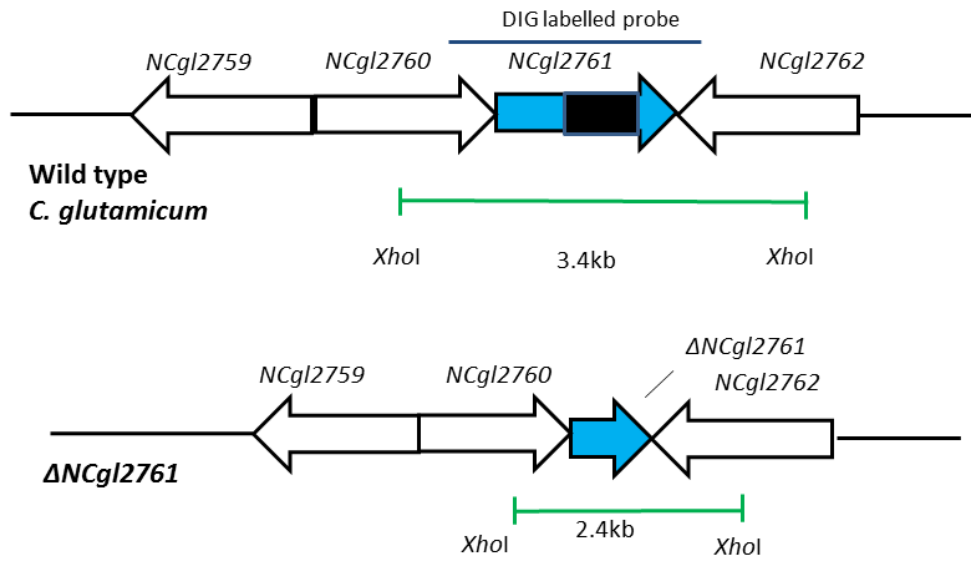
B

Figure 3.7

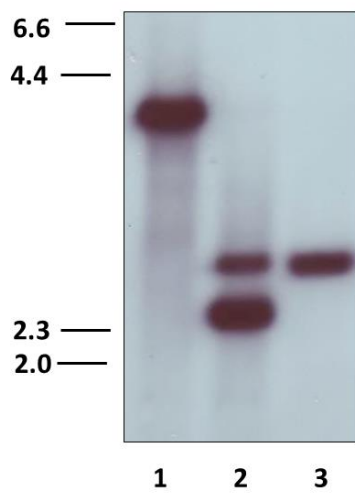
Figure 3.7 Confirmed disruption of *NCgl2761* by Southern Blot hybridization using *Pst*I

A) Schematic demonstrating the wild type *C. glutamicum* (top) and *NCgl2761* deletion (Δ *NCgl2761*, below) profiles expected following *Pst*I digestion and Southern blot hybridization. The sequence corresponding to the DIG-labelled hybridization probe is indicated. The sequence that was deleted to produce the mutant, Δ *NCgl2761*, is indicated by the black rectangle and the residual gene sequence remaining after the deletion event is shown by a grey arrow. Open arrows represent flanking genes.

B) Southern blot hybridization demonstrating disruption of *NCgl2761*. Genomic DNA was isolated from all strains, digested with *Pst*I, subjected to agarose gel electrophoresis following by a Southern hybridization. Lane 1, wild type *C. glutamicum* genomic DNA; Lane 2, *C. glutamicum* single cross-over strain genomic DNA; Lane 3, *C. glutamicum* Δ *NCgl2761* genomic DNA. Sizes and positions of the λ *Hind*III digoxigenin-labelled molecular weight markers are indicated in kb.



A



B

Figure 3.8

Figure 3.8 Confirmed disruption of *NCgl2761* by Southern Blot hybridization using *XhoI*.

A) Schematic demonstrating the wild type *C. glutamicum* (top) and *NCgl2761* deletion ($\Delta NCgl2761$, below) profiles expected following *XhoI* digestion and Southern blot hybridization. The sequence corresponding to the DIG-labelled hybridization probe is indicated. The sequence that was deleted to produce the mutant, $\Delta NCgl2761$, is indicated by the black box and the truncated gene remaining after the deletion event is shown by a grey arrow. Open arrows represent flanking genes.

B) Southern blot hybridization demonstrating disruption of *NCgl2761*. Genomic DNA was isolated from all strains, digested with *XhoI*, subjected to agarose gel electrophoresis following by a Southern hybridization. Lane 1, wild type *C. glutamicum* genomic DNA; Lane 2, *C. glutamicum* single cross-over strain genomic DNA; Lane 3, *C. glutamicum* $\Delta NCgl2761$ genomic DNA. Sizes and positions of the λ HindIII digoxigenin-labelled molecular weight markers are indicated in kb.

3.2.7 Complementation of the *C. glutamicum* Δ NCgl2761 mutant

Before commencing analyses of the new mutant including cell wall analysis, a complementation strain and a control strain were produced to confirm that any changes including cell wall defects that were detected in the mutant were due to disruption of the *NCgl2761* gene and not the result of unexpected changes in other genes. To complement the mutant, the entire 1.7kb *NCgl2761* gene plus 203bp of upstream sequence was PCR amplified using forward primer NCgl2761-comp_F and reverse primer NCgl2761-comp_R (See Appendix 3 for primer details) each containing an *Xma*I restriction site. The *Xma*I-digested product was inserted into the unique *Pvu*II site of plasmid pSM22, which carries a *Corynebacterium* origin of replication *repA* and a kanamycin resistance gene *aphA3* (190), creating pSM22:*NCgl2761*. This complementation plasmid and the empty pSM22 vector were electroporated separately into the *C. glutamicum* Δ NCgl2761 mutant and transformants selected on BHI agar plates supplemented with kanamycin. These two strains, along with the original mutant and a wild-type *C. glutamicum* control, were analysed in parallel in all subsequent experiments.

3.2.8 *Corynebacterium glutamicum* $\Delta NCg12761$ mutant has a growth phenotype

As *C. glutamicum* mutants with cell wall defects often have growth defects, particularly when orthologs of essential *M. tuberculosis* genes are disrupted (140), a growth curve was produced for the $\Delta NCg12761$ mutant and control strains. Our previous studies on three other genes within this locus resulted in knockout mutants that had a characteristic “lag” in the early to mid-log phase of growth (46) (and unpublished results). More specifically, the wild type strain has been found to reach log phase ~4 hours earlier than the three mutants. However, once in log phase all four strains grow at a similar rate. To determine whether the $NCg12761$ mutant shares this growth phenomenon with the other mutants, its growth characteristics in liquid media were investigated.

The four strains: wild type, mutant, empty vector control and complemented strain, were grown in triplicate and optical densities OD(600nm) of each culture were measured hourly. As illustrated in Figure 3.9, the *C. glutamicum* $\Delta NCg12761$ mutant and empty vector control strains had a lag in growth compared to the wild-type and complementation strains. This growth phenotype was consistent with that observed for the other mutants, as described above, and the effect was reversed by complementation with $NCg12761$, suggesting that it was due solely to the disruption of the gene. The difference manifested primarily as a lag in growth during the early log phase OD(600nm) = 1-3. This same growth difference was seen when the strains were grown on solid BHI growth media. The mutant and empty vector control strains formed smaller colonies than the other two strains when grown under identical conditions (data not shown).

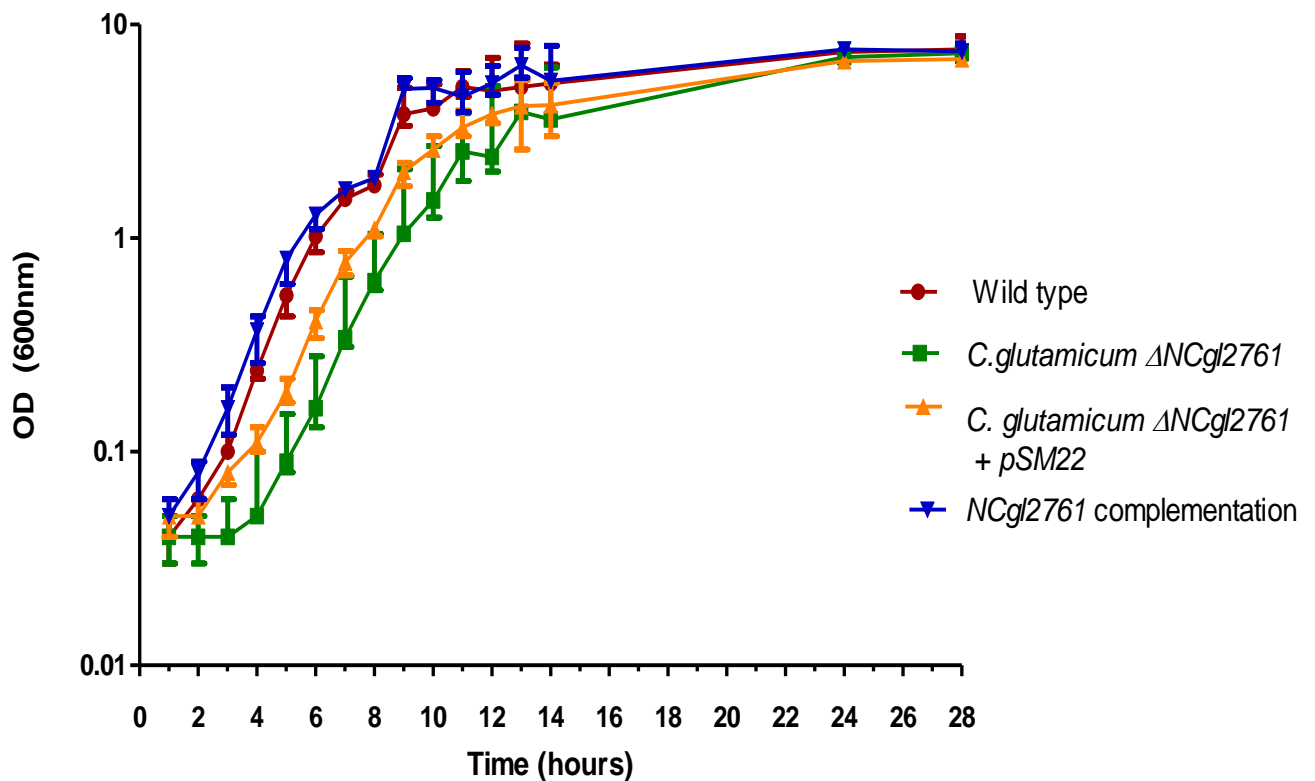


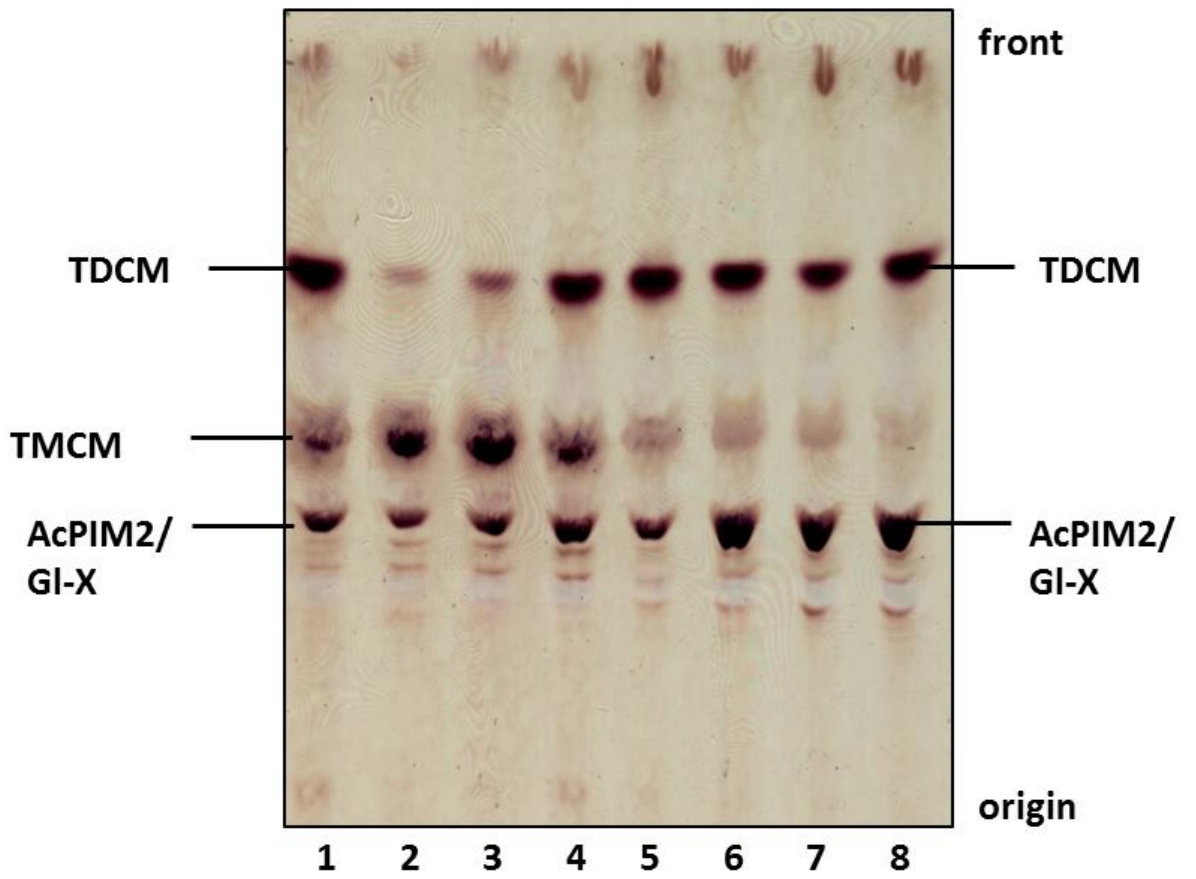
Figure 3.9 Deletion of the *NCgl2761* gene causes a lag in growth compared to wild type *C. glutamicum* which is abolished by genetic complementation. A BHI starter culture was produced overnight at 37°C then a small amount used to inoculate a 100ml BHI culture of each of the four strains. Each strain was cultured in triplicate and OD(600nm) measurements taken hourly. The mean values of the three cultures were plotted along with the standard error of the mean (SEM) using a log₁₀ scale. Mid-log phase was estimated to be ~4-10 hours post inoculation while stationary phase was ~14-30 hours. When performing the Wilcoxon signed rank test between the growth of the wild type and mutant strains, P<0.0001. This suggested that the growth lag of the mutant is statistically significant

3.2.9 Glycolipid analysis of a *Corynebacterium glutamicum* Δ NCgl2761 mutant.

The presence of a growth phenotype in the Δ NCgl2761 mutant might be indicative of a cell wall defect resulting from the absence of NCgl2761. To investigate the hypothesis that NCgl2761 has a role in cell wall synthesis, free glycolipids were extracted (see Section 2.8.2, Chapter 2) and analysed (Figure 3.10). The material was very rich in PIMs, TCMs and TDCMs because it consists of membranes previously broken down mechanically and chemically. These free glycolipids were analysed on a silica-coated aluminium backed HPTLC sheet (Figure 3.10A and B) developed using a solvent system of chloroform: methanol: 13M NH₃: 1M ammonium acetate: water (180: 140: 9: 9: 23 v/v/v/v/v). In extracts of cells harvested at the mid-log phase of growth, there was a significant accumulation of TCM in the *C. glutamicum* Δ NCgl2761 mutant and mutant plus empty vector strain relative to the wild-type control (Figure 3.10A, lanes 1-4). In addition, the amount of TDCM was significantly reduced when compared to that of the *C. glutamicum* wild type and the complementation strain. The marked accumulation of TCM was no longer evident in the stationary phase where the relative amount of TDCM among all four strains was similar (Figure 3.10A, lanes 5-8). As described earlier, this phenotype resembles that seen in *C. glutamicum* Δ NCgl2759, Δ NCgl2762 and Δ NCgl2764 mutants, suggesting a functional relationship between all of the encoded proteins. No clear differences were observed between the PIMs or phospholipids cardiolipin and phosphatidylglycerol when comparing wild-type and the NCgl2761 mutant, suggesting that the pathways forming these components are unaffected by loss of NCgl2761.

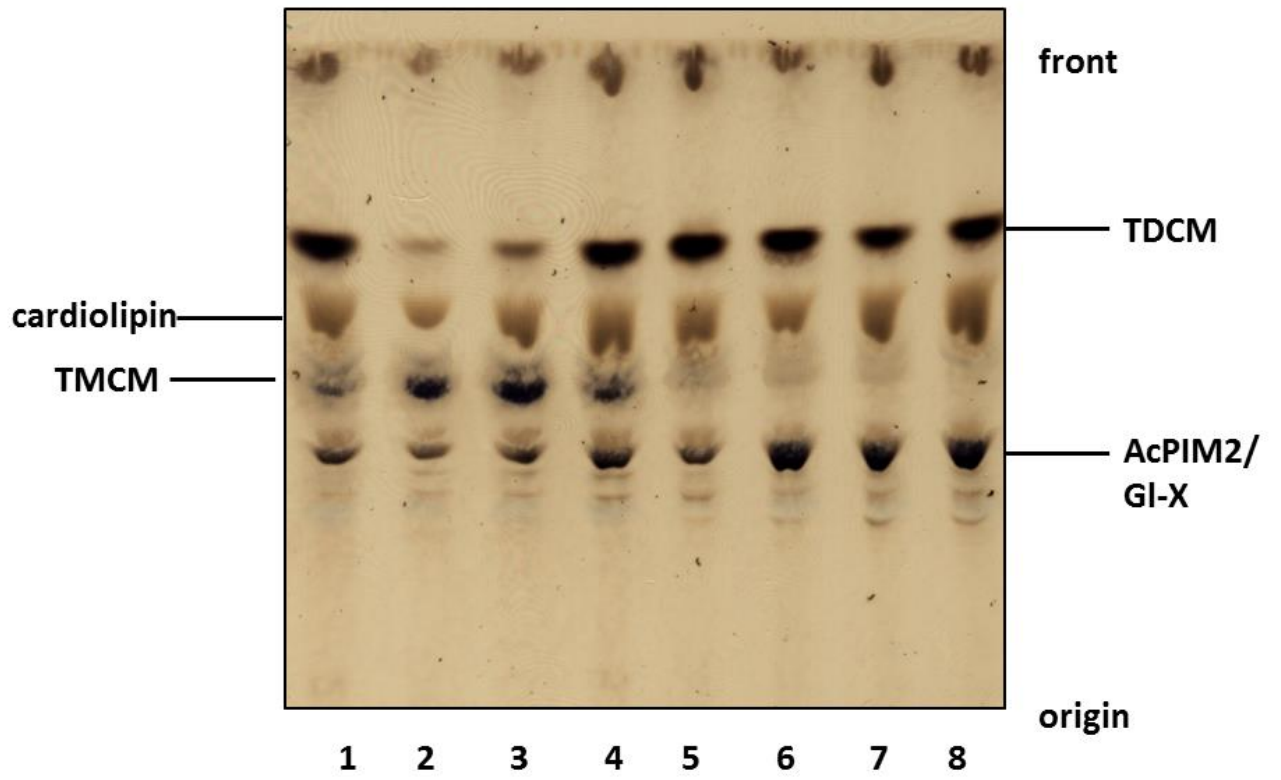
Thus the phenotype of the NCgl2761 mutant appears to be very similar to that of the other three knockout mutants of genes nearby. One possible explanation for this common phenotype is that transport of TCM across the cell membrane is occurring at a slower rate in the knockout mutants, resulting in an altered glycolipid profile that is particularly apparent when examined in the early- to

mid-log phase of the growth cycle. This idea of a reduced rate of transport rather than a block is supported by the apparent restoration of the glycolipid profile of the mutant once it reaches stationary phase.



A

Figure 3.10



B

Figure 3.10

Figure 3.10. Glycolipid analysis of a $\Delta NCgI2761$ mutant. **A)** HPTLC was used to resolve *C. glutamicum* total lipids purified from wild type *C. glutamicum* (lanes 1, 5), $\Delta NCgI2761$ mutant (lanes 2, 6) empty vector control (lanes 3, 7) and $\Delta NCgI2761$ complementation strains (lanes 4, 8). Lanes 1-5 indicate bands in the mid-log growth stage, while lanes 5-8 represent stationary phase. The glycolipids were visualised by orcinol/ H_2SO_4 staining and baking at $100^\circ C$. The positions of trehalose monocorynomycolate (TMCM), trehalose dicorynomycolate (TDCM), an acylated phosphatidylinositol dimannoside (AcPIM2) and $Man\alpha 1-4GlcA\alpha 1-3$ diacylglycerol (GI-X) are indicated, the latter two glycolipids appearing as a doublet in this solvent system. **B)** The same HPTLC was charred at $160^\circ C$ in order to visualise the phospholipids ie. cardiolipin and phosphatidylglycerol (PG) which co-migrate.

3.2.10 Lack of NCgl2761 affects transport of TMCMs across the cell membrane

The accumulation of TMCM and concomitant loss of TDCM in the mutant *C. glutamicum* is consistent with a defect affecting TMCM transport across the inner membrane, as previously described for an $\Delta NCgl2759$ mutant (46). To investigate the defect in more detail, differential solvent extraction was used to determine then compare the subcellular locations of TMCM and TDCM in the mutant and wild type strains.

After individual sequential extractions, (Figure 3.11A), 1-butanol extraction removes only the surface lipids, such as TDCM and the pool of TMCM that has been transported across the inner membrane, but not the inner cell membrane components such as cardiolipin (46). Following butanol biphasic extraction of both mutant and wild type strains, the glycolipid localisation differed significantly. While in the butanol fraction of the wild type *C. glutamicum* both TMCM and TDCM can be seen, in the mutant neither of these mycolates was evident. These profiles were very similar to those observed for a $\Delta NCgl2759$ mutant (46) which has a very similar phenotype to the $\Delta NCgl2761$ mutant presented here.

These findings (Figure 3.12) suggest that TMCM is inaccessible to the butanol, and therefore not exposed outside of the inner membrane in the $\Delta NCgl2761$ mutant. In addition, the lack of TDCM in any of the extracts from the mutant is consistent with Figure 3.10, which showed a dramatic reduction in TDCM synthesis in early-log phase in the mutant strain. In this lane whole cells were extracted directly by chloroform/methanol. In both of these lanes, mycolates are evident in the wild type while only TMCMs can be seen in *C. glutamicum* $\Delta NCgl2761$. An additional feature of this autoradiograph is the accumulation of TMCM in the $\Delta NCgl2761$ mutant similar to that seen on

HPTLC visualised with orcinol. In summary, the distribution of TMCM is consistent with a defect in TMCM transport across the cell membrane in the mutant strain.

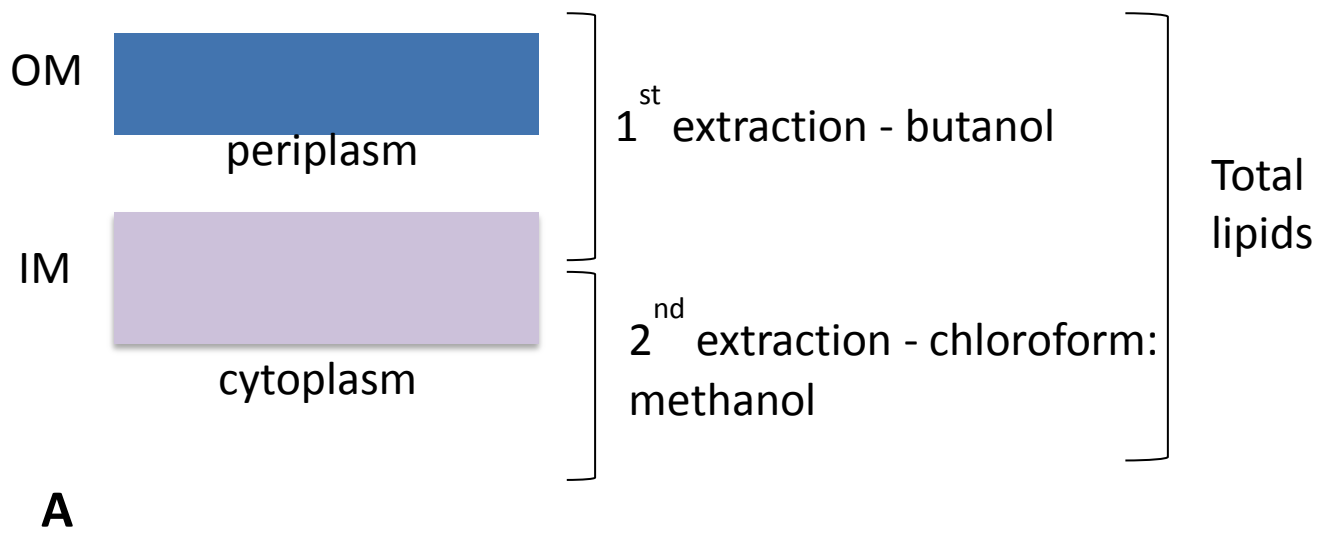
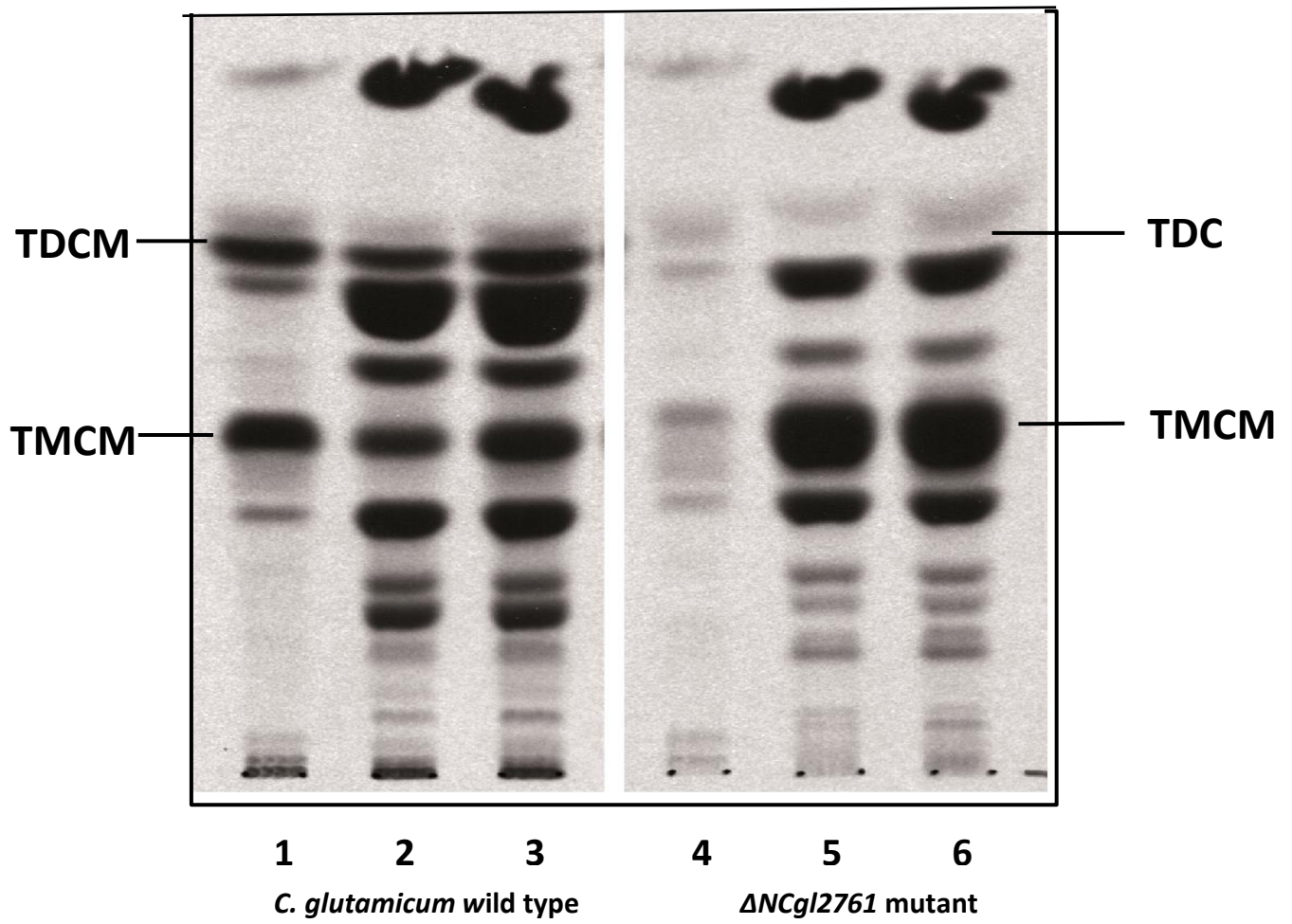


Figure 3.11



B

Figure 3.11

Figure 3.11 A) Sequential extraction of cell wall components. Butanol extracts the surface layers of the bacterial cell wall, whereas chloroform/methanol extracts deeper structures. When radioactively-labelled, components represented on each respective layer can be visualised.

B) Distribution of TMCM and TDCM in the cell wall of a $\Delta NCgl2761$ mutant. ¹⁴C-acetate was incorporated into *C. glutamicum* wild type (lanes 1-3) and $\Delta NCgl2761$ mutant (lanes 4-6). After quenching, pellets were divided and either subjected to butanol, chloroform/methanol or total lipid extraction. Lipids were then resolved by HTPLC using a solvent system of chloroform: methanol: 13M NH₃: 1M ammonium acetate: water, 180: 140: 9: 9: 23 (v/v/v/v/v) followed by X-ray film exposure. Lanes 1, 4 show the 1-butanol fractions and lanes 2, 5 show the chloroform/methanol fractions. Lanes 3, 6 show the total lipid fractions.

3.2.11 Analysis of lipomannans/ lipoarabinomannans from an $\Delta NCgl2761$ mutant

Having identified a defect in a transport step of the mycolic acid biosynthesis pathway in the $\Delta NCgl2761$ mutant, the next step was to determine whether the major cell wall lipoglycans of *C. glutamicum* had also been affected.

The residual cell pellet remaining after extraction of PIMs, trehalose mycolates and other free lipids was subjected to ethanol reflux and octyl-Sepharose column™ purification to analyse the LM/LAM content. After two freeze-drying steps, LM and LAM were solubilized in 30% 1-propanol. Next, they were separated on a TRIS-glycine SDS-PAGE gel along with Invitrogen Benchmark pre-stained molecular weight markers. These polar glycolipids were visualized after staining with a Pierce® silver stain. On SDS PAGE gels the *C. glutamicum* LM and LAM species migrate to a similar position as the 15kDa and 25kDa protein markers, respectively. There was no clear difference between the glycolipids in any of the four strains (Figure 3.12). There is good separation between LM and LAM so both can be clearly visualized. Also, in contrast to the trehalose corynomycolates, they appear to be identical in both the mid-logarithmic and stationary growth phases. Overall, it was concluded that, in contrast to the mycolic acid biosynthetic pathway, the LM/LAM pathway remained unaffected by the loss of NCgl2761.

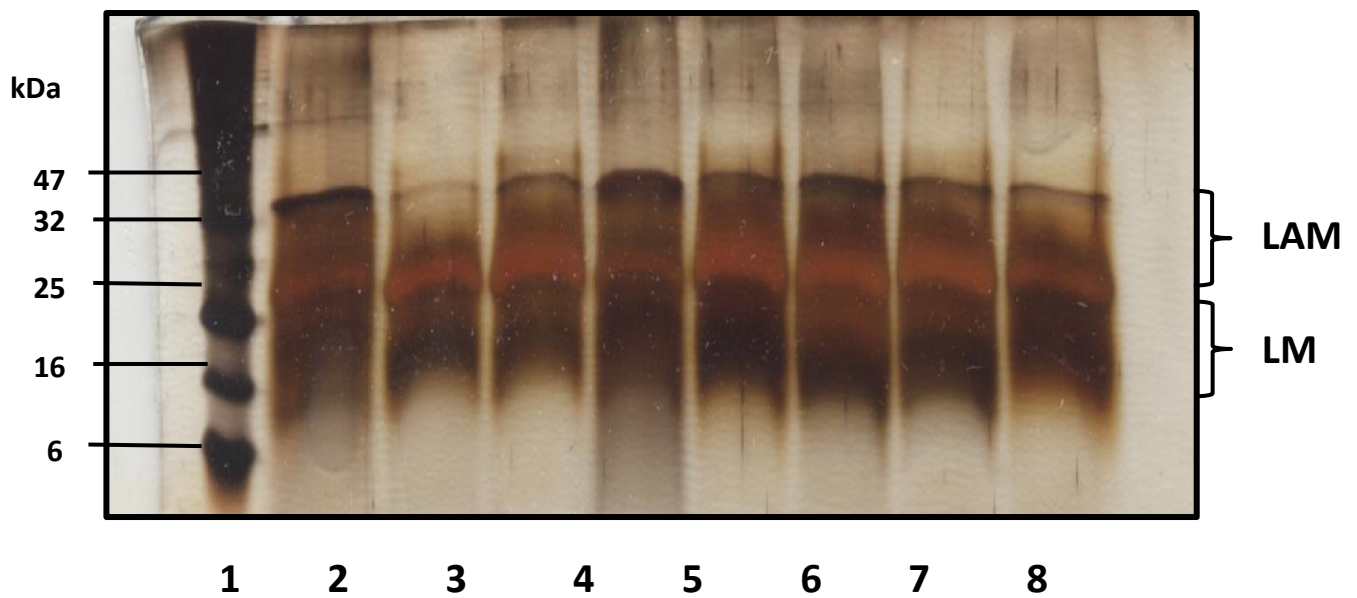


Figure 3.12. SDS-PAGE analysis of lipomannans and lipoarabinomannans from a $\Delta NCgl2761$ mutant. The glycolipids were isolated from mid-logarithmic (lanes 2-5) and stationary (lanes 6-9) phase cultures. Lane 1, Benchmark® pre-stained protein ladder (Life Technologies); lanes 2 and 6, wild type *C. glutamicum*; lanes 3 and 7, $\Delta NCgl2761$ mutant; lanes 4 and 8, $\Delta NCgl2761$ mutant containing empty pSM22 vector; lanes 5 and 9, complemented $\Delta NCgl2761$

3.3 Discussion

Like many cell wall biosynthesis pathways, synthesis of (coryno)mycolates is a carefully controlled, sequential and step-wise process beginning within the cell cytoplasm and terminating with their deposition in the cell wall. Consequently, they need to pass through the cell membrane but, until recently, how this occurs and the carrier that is used remained unknown. It is now believed that mycolic acids are transferred through the plasma membrane as TMM in Mycobacteria (191) and as TMCM, the equivalent molecule in Corynebacteria. In Mycobacteria, a recently described protein **m**ycobacterial **m**embrane **p**rotein **l**arge (MmpL3) (86, 87, 192) appears to transport TMM across the inner membrane. A study by Grzegorzewicz *et al.* (85) showed that a urea-based inhibitor designated AU1235 targeted MmpL3 in *M. tuberculosis* to block TMM transport, matching the phenotype described in this chapter for the Δ NCgl2761 mutant. A decrease in levels of TMM and AG-linked mycolic acids was noted, as well as an accumulation of TMM within the inner membrane, when treating *M. tuberculosis* with the inhibitor. Interestingly, the *C. glutamicum* ortholog of MmpL3, NCgl2769, is encoded by a gene located just four genes away from the genetic locus described in this thesis.

Recent studies in our laboratory have suggested that an acetylated form of TMCM is the transported species in Corynebacteria (46). Whether a similar species is transported in Mycobacteria is not known, although the TmaT acetyltransferase that forms AcTMCM, NCgl2759, is well conserved in all Mycobacteria, designated Rv0228 in *M. tuberculosis* H37Rv. Corynebacteria seem to express two MmpL3 orthologues, NCgl2769 and NCgl0228 (89), which may be functionally redundant. When both are knocked out in a single strain, this results in total ablation of TMCM, TDCM and AG-linked corynomycolic acids (89). In *C. glutamicum* NCgl0228 and NCgl2769 are hypothesised to shuttle

AcTMCM from the cytoplasmic to the periplasmic surface of the cell membrane, after which it is deacetylated and reacts with a second TMCM, forming TDCM, or is esterified to arabinogalactan (46). However, there appears to be still much to learn about the regulation of this important step in mycolic acid biosynthesis. Whether other proteins are involved in this process in addition to NCgl27659 (TmaT) and the transporter(s) is also currently unknown. The results presented in this chapter suggest that additional proteins are involved and that the transport process is far more complicated than previously thought.

The data presented here suggest that there is also involvement of the gene product of *NCgl2761* in the transport of (coryno)mycolic acid intermediates. By HPTLC, in the mid-logarithmic phase of growth, an accumulation of TMCM in the $\Delta NCgl2761$ mutant and the empty vector control can be seen (Figure 3.10A & B) suggesting a block in, or reduced rate of, TMCM transport. Concomitantly, there is a dramatic reduction in TDCM levels in these two strains in the mid-log phase that normalises in the stationary phase. This finding suggests a reduced rate of TMCM turnover rather than a block in the process, as TDCMs are formed eventually. NCgl2761 evidently plays a role in the conversion of TMCM to TDCM, however the protein does not appear to have any features suggesting that it is directly involved in any enzymatic step, and the mycolyltransferases that convert TMCM to TDCM are known and well characterised (93, 193). Rather, its multi-membrane structure is more suggestive of a channel or transport protein. *C. glutamium* $\Delta NCgl2761$ is very slow to synthesise TDCM. So, it seems that TMCM cannot traverse the cell membrane at the normal rate to develop into TDCM and arabinogalactan-linked mycolic acids in a $\Delta NCgl2761$ mutant. In addition, labelling experiments show that there is a lack of surface exposed, butanol-accessible TMCM in the mutant (Figure 3.11) further supporting a role for NCgl2761 in TMCM transport across the plasma membrane.

The amount of LM and LAM produced by all four strains appears to be comparable, with the characteristic homogenous smear on each silver-stained SDS-PAGE gel looking similar (allowing for small differences in the amounts of material loaded). If there are any differences in LM/LAM in the mutant, they are subtle and not detectable using this approach. This finding supports the view that any transport process mediated by *NCgl2761* does not extend to the mannosylated glycolipids of *C. glutamicum*.

Collectively, all of the data presented in this chapter support a hypothesis that *NCgl2761* performs an important function at or around the (Ac)TMCM transport step (indicated by an arrow in Figure 3.13). Combining this with our previous findings that *NCgl2759* (TmaT), *NCgl2762* and *NCgl2764* mutants also have a defect in the transport step, it is concluded that TMCM transport and its regulation are complex processes involving additional steps that remain to be fully understood. However, a bank of mutant strains now exists that which will be a useful resource to further investigate these reactions.

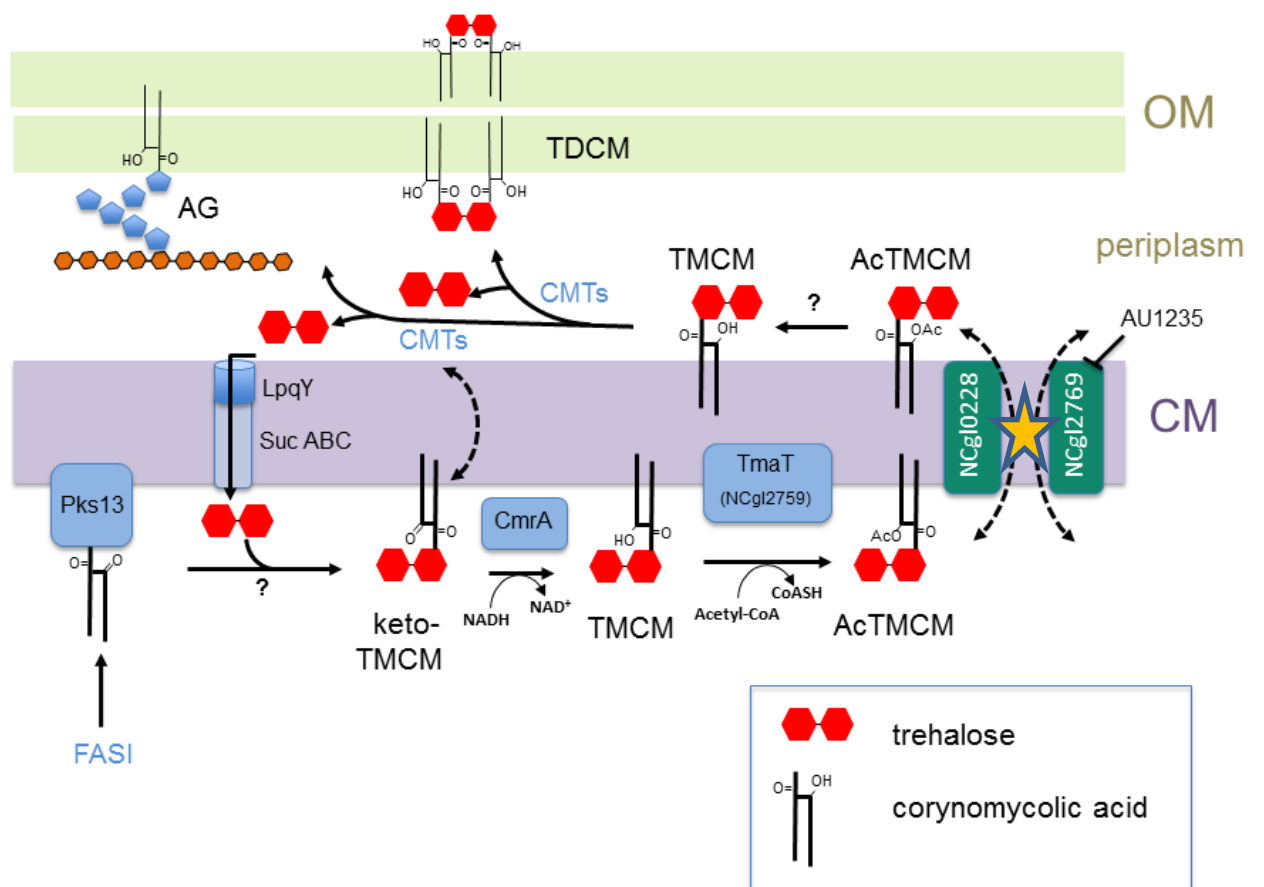


Figure 3.13

Fig 3.13 Proposed mycolic acid transport pathway in corynebacteria. The pathway begins with the fatty acid synthase cycles in the cytoplasm which ultimately produce TCMs in the inner leaflet of the plasma membrane which are then flipped to the outer leaflet by the redundant transporters NCgl2769/NCgl0228. Once in the periplasm, a series of corynomycolyltransferases (CMTs) process TCMs to TDCMs or transfer the corynomycolates to the arabinogalactan (AG) layer. The orange arrow indicates the point within the pathway where NCgl2761 is most likely to act, based on the phenotypic characterisation of a Δ NCgl2761 mutant described in this chapter and the sequence properties of the encoded protein (Adapted from Yamaryo-Botte *et al.*(46)).

The findings presented in this chapter strongly suggest a role for NCgl2761 in corynomycolate transport. The presence of orthologs in *M. tuberculosis* (Rv0226c) and other Mycobacteria and Corynebacteria (Figure 3.2) suggest that its function is conserved across the entire Corynebacterineae suborder, although the amino acid sequence of the *C. glutamicum* protein seems to have diverged from its mycobacterial counterparts. Since the protein is predicted to contain multiple transmembrane domains (Figure 3.1) and is clearly membrane-embedded, it could function on the cytoplasmic surface of the inner cell membrane to process reaction intermediates or within the membrane as part of an AcTMCM shuttling mechanism. Alternatively, rather than having a direct role it could just serve as a membrane anchor for a protein complex essential for TMCM transport, with the significant periplasmic loop near the C-terminus (Figure 3.1) being a possible interaction point. While the data presented here strongly suggest a role in some aspect of corynomycolate transport, determining the precise function of NCgl2761 (Rv0226c) in Corynebacterineae cell wall biosynthesis requires further study.

Chapter 4

Characterisation of a New Lipoarabinomannan Biosynthesis Protein in

Corynebacterium glutamicum

4.1 Rationale and Objectives

4.1.1 Introduction

Despite improving statistics in recent years, TB remains a global health emergency. In addition to the high annual death rate, one third of the world's population is now infected with *M. tuberculosis*. The incidence of multi-drug resistant (MDR), extensively-drug resistant (XDR) and more recently, totally-drug resistant (TDR) TB, continues to rise and so beckons rapid development and discovery of new and effective treatments and/or vaccines (WHO report 2015).

Several drugs target the mycobacterial cell wall, a key factor in bacterial survival. Of particular interest for future drug development are the lipoglycans, LMs and LAMs, for which the inflammatory and immunological roles are probably better understood than the biosynthetic pathways that form them. The focus of study in this thesis is a genetic locus encoding NCgl2759, an acyltransferase (46); **NCgl2761, a membrane protein described in Chapter 3**; NCgl2762, a putative glycosyltransferase; and NCgl2764, a methyltransferase. As the four genes in this region of the genome studied to date all encode proteins with similar functions in mycolic acid biosynthesis and transport, an investigation of the remaining gene, *NCgl2760*, should not only complete the study of the entire locus, but also provide insights into the role of the homologous gene in *M. tuberculosis*, *Rv0227c*. Since *Rv0227c* is

defined as an essential gene in the human pathogen, its protein product is a potential drug target and worthy of study.

4.1.2. Aims

The aim of work described in this chapter was to determine whether NCgl2760 does indeed play a role in mycobacterial cell wall biosynthesis, as suggested by the position of its gene adjacent to others in the described locus which encodes *NCgl2759 - NCgl2764*. Its location led to the hypothesis that it has a function similar to those of the other four genes, *i.e.* a role in transporting mycolic acids across the plasma membrane. To investigate this hypothesis, a gene deletion mutant was produced and subjected to a rigorous phenotypic analysis, particularly focussing on the mycolic acid components of the cell wall.

4.2 Results

4.2.1 Protter prediction of protein topology

Rv0227c is encoded by an essential gene in *M. tuberculosis*. It is conserved across mycobacterial and corynebacterial genera. The gene is 1266bp in length and encodes a protein of 421 residues. These residues are expected to encode a protein 45.5kDa in size. The Protter prediction (wlab.ethz.ch/protter) of Rv0227 (Figure 4.1A) indicates the presence of one transmembrane helix and 6 periplasmic loops. Extensive database searching revealed no significant similarity to proteins of known function and no motifs suggesting function.

The protein structure of NCgl2760 (Figure 4.1B), the orthologue of Rv0227 in corynebacteria, was analysed to search not only for similarities, but also for differences between the two orthologues. Rv0227 has 6 extracytoplasmic loops (Figure 4.1A), whereas NCgl2760 (Figure 4.1B) has only 4 loops. Rv0227 has an additional intracytoplasmic loop which is absent in NCgl2760. Both have one predicted transmembrane helix. Unfortunately, the Hidden Markov Model (HMM) predicts that Rv0227 has 2 transmembrane helices, so although there is some overall predicted structural similarities there are also differences which is perhaps to be expected from algorithms based on different assumptions.

Figure 4.1 Outer cell membrane topology according to the Protter prediction. A) *M. tuberculosis* Rv0227 and B) *C. glutamicum* NCgl2760. The additional intracytoplasmic loop, 2 additional extracytoplasmic loops as well as a longer signal sequence appear to be the main differences between the two putative orthologs. Both proteins have just one transmembrane helix.

4.2.2. Bioinformatic analysis

The alignment of proteins from four organisms in the bacterial suborder Corynebacterineae was done, *i.e.* *Mycobacterium tuberculosis* H37Rv (*Rv0227c*); *Mycobacterium leprae* (*ML2581*); *Mycobacterium smegmatis* mc² 155 (*MSMEG_0317*); and *Corynebacterium glutamicum* ATCC 13032 (*NCgl2760*) (Figure 4.2) in order to determine similarities and likely orthologs. The percentage similarity and identity between *Rv0227c* and *NCgl2760* was found to be 24.9% and 16.4%, respectively. Due to their sequence similarity (Figure 4.2) and syntenic arrangement (Figure 1.15), *NCgl2760* was considered to be the best match for *Rv0227*.

```

NCg12760      -----MKRSATVLLIAGVLFLLIFAFVTPPPYVTGQARTIPKDLDLTLVSESPQGFVRTEH
M.SMEG_0317  MNRAVALRIAACGLLGLGAALLIAALLLTYTKGKIAKIPLDIDTSLVSDGTATAFDPDS
Rv0227       -----MLRFAACGAIGLGAALLIAALLLSTYTTTSRIAIEIPLDIDATLISDGTGTALDSAS
ML2581       VNRAVILRFTACGIIGLGAFLIAALLLATYTTSSRITKIPLDIDATLVSENGTALDSSS
              :: :*   :  * . : ** * : : * . . . :   ** * : * : * : .

NCg12760      IVTAPTE-----KVDEIATHVDQTV--TDVQG--KTVAEISDDVVL
M.SMEG_0317  LVAERFKIDRDVPVALQQQMSVEAPSNADVVTFQVGTTLRRTDRQQDAGLLALVDTVMT
Rv0227       LATEHIVVNQDVPLVSQQQVTVES PANADVVTLQVGS SLRRTDKQKDSGLLLAIVDTVTL
ML2581       LSSEHIVVNQNVPLVSQQQITVES PANVDVVTFQVGV SIRRTDKQKDTGLLLAVVDTVTL
              : :                               : . * : : * : :   ** *   : : * * . :

NCg12760      -----IGHSRYPVIKPTATISGSPADSSNVVREGLHYFFPANTLRNSYPYDIDL
M.SMEG_0317  NRNTAEAVSSENNPGGAVQKPRADIEDEKPPNTNIALPHEGLTYRFPFDTEKKTYPFFDPIA
Rv0227       NRKTAMAVSDDHTTGAVQKPRGLNDENPPTAIPLRHDGLSYRFPFHTEKKTYPYFDPIA
ML2581       NRKTAMAVSDDHTTGGSIQKPRGFTDENPPTAIPLRHDGLSYRFPFHTEKKTYPYFDPIA
              .           : ** . . . *           : : ** * ** . * : : * : * :

NCg12760      GEDSPVDYVSREG----NTYTFYQHLRYVPLDD-----
M.SMEG_0317  QKAFDANYDGEEDVNGLT TYRFVQNVGYDADGKLADPIKYS SLYEDDADASVTARAEVWG
Rv0227       QKAFDANYEGEEDVNGLT TYRFTQNVGYTPEGKLVAPLKYP SLYAGDEGDGKVTTSAMWG
ML2581       QKTFDVNYQNQEDINGLT TYRFTQNVGYDADGKLVAPIT YPSLYASDEGDGKITTTAAIWG
              :   . : *   . *           . ** * * . : *           .

NCg12760      -----SHTYSVERTLKVDRFSGIIVAKDEAMTFHGPDGDDTVEFTY-----T
M.SMEG_0317  VPGEPDESITMDRFYAASRTFWVDPVSGTIVKSEEHG YQYYAREALKPEVTYVDFKVTN
Rv0227       LPGDPNEQITMTRYAAQRTFWVDPVSGTIVKETERANHY FARDPLKPEVTFADYQVTST
ML2581       LSGDPSEQITMTRYAAQRTFWVDPVSGTIVKETEHNHY FARDTLKPEVTLADYKVTST
              : * : . . ** : ** . ** ** . *           :           . * . *           .

NCg12760      ADTLKLLQDHA-HDIDQRLSWAKGFDFFSKFLGSL LLAIGVFLTGI FKRQQLMSTV NKLK
M.SMEG_0317  EESVESQVAAASDERDRALWTRILPITFTALGLVSLV GGAVLGSFALRTESTLIDPGLD
Rv0227       EETVESQVNAARDERDRALWSRVLPITFTAAGLVALVGGGLFASFSLRTEGALMAASGD
ML2581       EETIESQVNSARDERDRALWSRVLPITFTAVGLITLLSGGFLASFSLRTESALTESGLD
              : : : :           * . : * :           * : : : :           .   ** * * * . : . : * :

NCg12760      S-----
M.SMEG_0317  TADHGFFDTQGI--QVPGA EAKTEKLP AQRPTDLPPDRPI-----
Rv0227       RDDH-DYRRGGFEEPVPGA EAEETEKLPTQRPDFPR--EP SGPDPRLGSAQPPPPDAGH
ML2581       RANRDAFGHCRTEEPVPGA EAEETEKLPTQRPELRD--SS ILSVSAHRRRSSESSPPNSGP

NCg12760      -----
M.SMEG_0317  -----
Rv0227       PDPGPPERR-
ML2581       ADPGHPERG*

```

Figure 4.2. Protein sequence alignment of *M. tuberculosis* Rv0227c and putative orthologues in *C. glutamicum* (NCg12760), *M. smegmatis* (MSMEG_0317) and *M. leprae* (ML2581). Residues indicated by “*” are completely conserved among the sequences; those indicated by “.” or “:” are similar. Alignment was created using Clustal Omega. The two predicted transmembrane domains of Rv0227 presented in Figure 4.1A are indicated in bold and numbered

4.2.3 Generation of a *NCgl2760* mutant

The aim of work described in this chapter was to determine whether NCgl2760 has a role in cell wall biosynthesis and, if so, identify the biosynthetic pathway and the step where it functions. To investigate the function of NCgl2760, its gene was deleted in *C. glutamicum* strain 13032.

Studies on the *C. glutamicum* *NCgl2761* gene involved first creating a deletion mutant to allow detailed cell wall analyses of bacteria that no longer had the protein encoded by this gene. This required construction of a knockout plasmid containing a deleted copy of *NCgl2760* and neighbouring DNA to be used for allelic replacement of *NCgl2760* in the *C. glutamicum* chromosome by homologous recombination (Figure 4.3).

C. glutamicum genomic DNA was used as the template in all PCR reactions. The deletion construct was created (Figure 4.3) by first amplifying the left and right flanking regions of the gene by PCR using Hotstar HiFidelity DNA Polymerase (Qiagen) according to the manufacturer's instructions in *E. coli* DH5 α cells. The left flanking region, ~1kb in size, was amplified by the primers NCgl2760-left_F and NCgl2760-left_R (see Appendix 4 for primer details) and cloned into the *Sma*I/*Bam*HI sites of pUC19. NCgl2760-right_F and NCgl2760-right_R were cloned into the *Bam*HI/*Xba*I sites to amplify a right flanking fragment ~0.8kb in size. DNA was cloned into pUC19 containing ampicillin resistance and LacZ blue/ white selection before transformation (see Section 2.5.3, Chapter 2) into prepared, chemically competent *E. coli* DH α cells (see Section 2.3.1, Chapter 2). They were streaked onto LB-solid media (see Appendix 2 for media formulations) containing the chemical galactopyranoside to select clones containing the deletion and left overnight to grow at 37°C. Individual clones were then incubated overnight in 10ml LB media (see Appendix 2 for media formulations), before isolating the plasmids using the High Pure Plasmid Isolation Kit (Roche). To check for the presence of inserts in the

plasmids, a quick 1-hour digest and electrophoresis gel was run to visualize 2 bands representative of the DNA insert and puc19 vector. Sequencing confirmed construct identity (Micromon Facility, Monash University). The pUC19 primers (see Appendix 3 for primer sequences) were used as they gave a longer read than the pcr primers.

Left and right flanking regions were purified, and the insert DNA digested from the plasmid. *Bam*HI and *Xba*I were used for the right and left flanking regions (while *Bam*HI and *Sma*I were used for the left region). NEB buffer 4 and 10xBSA (Bovine Serum Albumin) were added for digestion. The left and right fragments were ligated across the *Bam*HI site to create one combined fragment using 1µl T4 ligase (Roche), 10µl of DNA insert, 2µl of 10xLB and 2µl of pUC19 in a 20µl reaction. So, the combined fragment was cloned into pUC19, transformed into *E. coli* and cultured on LB solid media containing ampicillin. Next subcloning of the deletion cassette into pK18*mobsacB*, a suicide plasmid for *C. glutamicum*, encoding kanamycin-resistance and sucrose toxicity, using *Xma*I and *Xba*I restriction enzyme sites was performed.

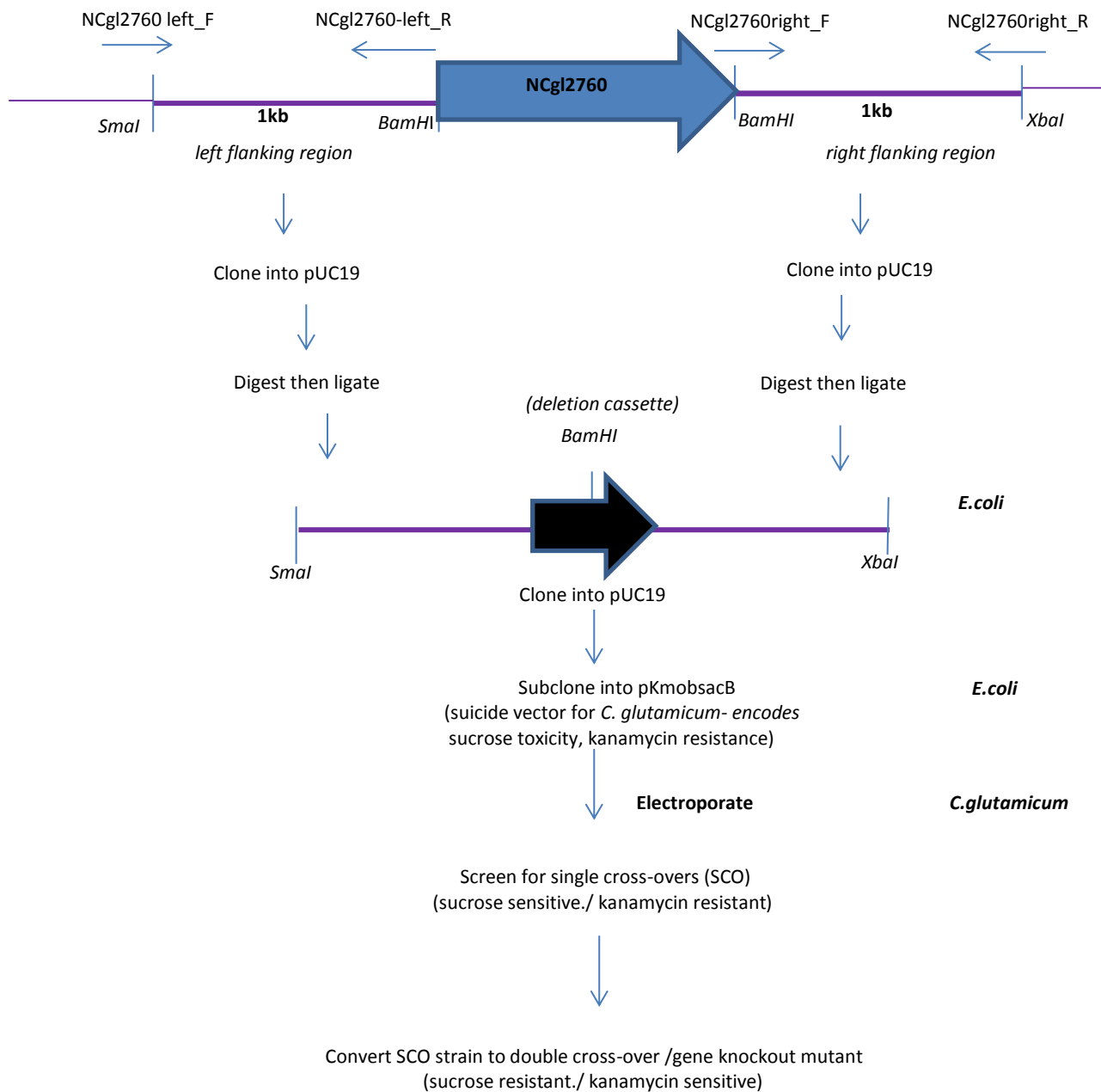


Figure 4.3

Figure 4.3. Cloning and recombination strategy to create a *C. glutamicum* $\Delta NCgl2760$ mutant. The left and right regions flanking *NCgl2760* were PCR amplified and cloned into pUC19. These two fragments were then joined together and subcloned into pK18*mobsacB*, a suicide vector for *C. glutamicum*. The plasmid was electroporated into *C. glutamicum* and kanamycin resistant colonies (potential single crossovers; SCO) were selected. A second recombination step followed to produce colonies which were sucrose resistant and kanamycin sensitive. These potential double crossover strains (*i.e.* gene knockouts) were analysed further by PCR and Southern blot hybridization to determine whether the gene had been deleted.

The plasmid containing the deletion cassette was then electroporated into *C. glutamicum* ATCC 13032 electrocompetent cells (see Section 2.5.5, Chapter 2) prepared as described in Chapter 2, Section 2.3.2. Kanamycin resistant transformants, representing potential single crossovers, were cultured on BHI solid media containing kanamycin. Single crossovers are resistant to kanamycin, but sensitive to sucrose. All potential single crossovers were cultured overnight in 10ml liquid BHI media then spread on BHI culture plates containing 10% (w/v) sucrose to select for double homologous recombination events (knock-outs). After 2 -3 days, potential knockouts seen on the sucrose plates were cross-patched on BHI solid media containing kanamycin. Those colonies that were sucrose-resistant and kanamycin sensitive were tested for gene deletion by PCR. Those appearing positive could either be wild-type revertents or gene knockout mutants where the expected band sizes were 0.7kb or 0.3kb respectively. Strains with the expected PCR profile for a knockout mutant (Figure 4.4) were then analysed further by Southern blot hybridization.

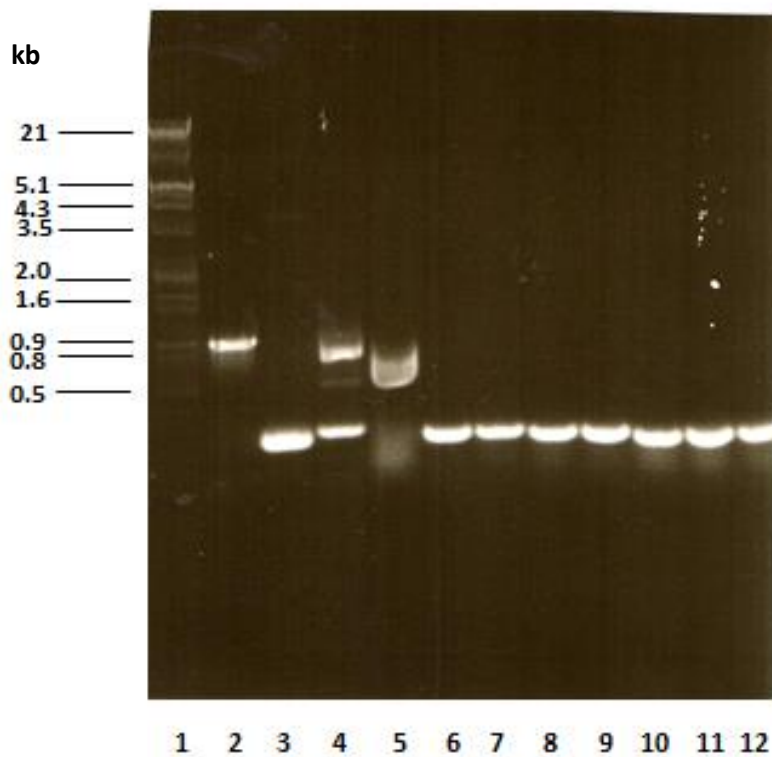


Figure 4.4 PCR profiles of seven putative $\Delta NCgl2760$ mutants compared to that of wild type. Those confirmed SCO which were cultured as individual clones on BHI solid media containing kanamycin, were cultured overnight then spread in serial dilutions on sucrose media. A λ HindIII/EcoRI nucleic acid marker (lane 1) indicated that of the eleven colonies shown, seven had PCR profiles consistent with a double cross-over (DCO) (lanes 6-12) and were selected for confirmation by Southern blot hybridization, while lane 5 showed a revertent. The *C. glutamicum* wild type (lane 2), plasmid DNA (lane 3) and single cross-over (SCO) (lane 4) serve as controls.

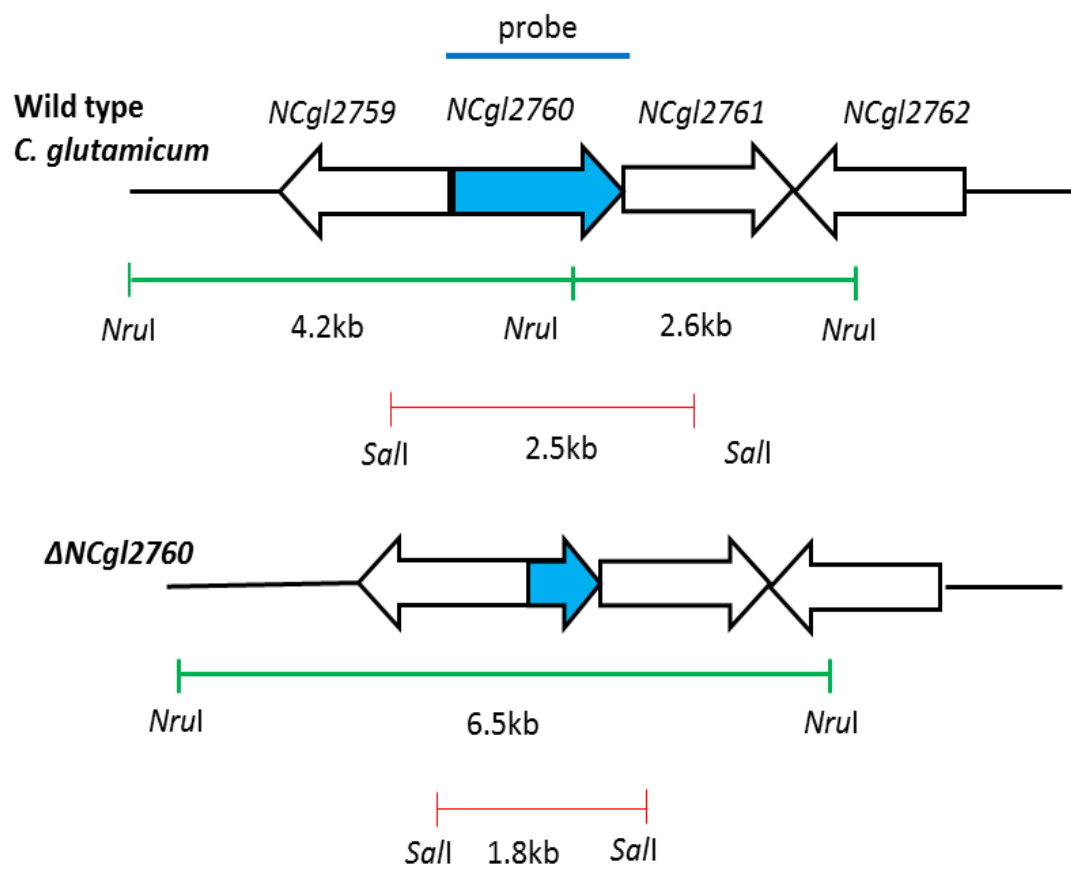
4.2.4. Southern blot hybridization confirms deletion of *NCgl2760*

Kanamycin-sensitive, sucrose-resistant clones derived from the single crossover strain could either be wild type revertants or gene knockout mutants, depending on the position of the second recombination event that ejected the plasmid from the chromosome. PCR analysis indicated seven potential knockout mutants but Southern blot hybridization was needed to confirm deletion of *NCgl2760*.

Genomic DNA of samples shown in lanes 6-9, figure 4.4 was digested separately with *NruI* and *SalI*. A probe was derived from the wild type *C. glutamicum* in lane 2, Figure 4.4. It was gel purified, of which 13µl was boiled for 10 minutes, then left on ice for 5 minutes. Components from a DIG DNA labelling kit (Roche) were combined to add to the DNA. i.e. 2µl hexonucleotide mix, 2µl DIG dNTP labelling mix, 2µl H₂O and 1µl Klenow enzyme was set up on ice. The mix was added to the DNA, then centrifuged briefly before incubating overnight at 37°C. Thereafter, 2 µl of 0.2M EDTA was added. The probe hybridized to two fragments in the wild type genomic DNA digested with *NruI*. They were 4.3 kb and 2.6 kb in size (Figure 4.5B). These sizes are very close to the expected sizes of 4250 bp and 2556 bp, based on analysis of the genome of *C. glutamicum* (Figure 4.5A). One *NruI* site is within the deleted sequence. Therefore, only one fragment would be seen in the mutant. This fragment was estimated to be 6.5 kb, very close to the predicted size of 6456 bp.

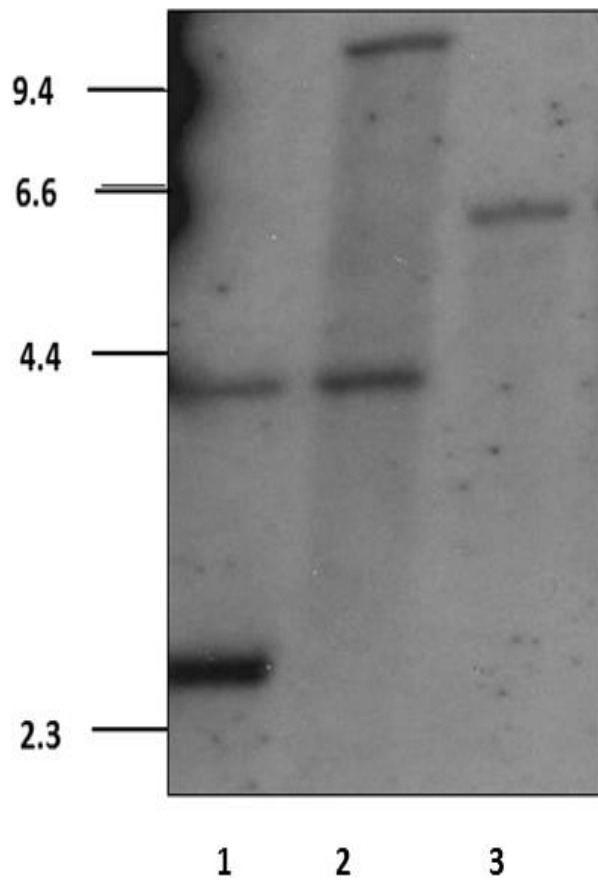
These findings strongly suggested that the gene had indeed been deleted in this strain. To obtain further confirmation, the Southern blot hybridization was repeated using the enzyme *SalI* (Figure 4.5C). With this enzyme, the wild type strain released one hybridizing band of 2.5kb (expected size was 2548bp) (Figure 4.5A), and in the potential knockout strain the probe hybridized to a fragment precisely 1800bp in size. Collectively the PCR and Southern hybridizations, performed using two

different enzymes, showed that deletion of the *NCgl2760* gene had been successful. This mutant strain was designated $\Delta NCgl2760$.

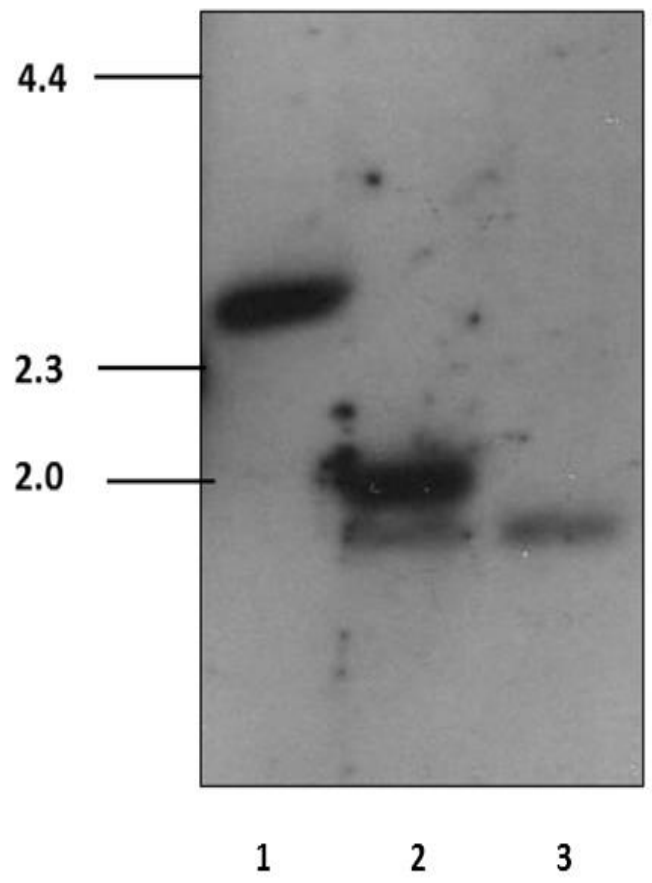


A

Figure 4.5



B



C

Figure 4.5

Figure 4.5. Confirmed disruption of *NCgl2760* by Southern blot hybridization.

A) Schematic demonstrating the wild type *C. glutamicum* (top) and *NCgl2760* deletion ($\Delta NCgl2760$, below) profiles expected following *Nru*I and *Sal*I digestion and Southern blot hybridization. The thick horizontal line indicates the hybridization probe. The sequence that was deleted in the knock-out, $\Delta NCgl2760$, is indicated by the black rectangle. Open arrows represent flanking genes.

B) Southern blot hybridization demonstrating disruption of *NCgl2760* using *Nru*I. (1) wild type *C. glutamicum* genomic DNA, (2) *C. glutamicum* single cross-over genomic DNA, (3) *C. glutamicum* $\Delta NCgl2760$ genomic DNA. Positions and sizes of λ HindIII digoxigenin-labelled molecular markers are shown in kb.

C) Southern blot hybridization demonstrating disruption of *NCgl2760* using *Sal*I. (1) wild type *C. glutamicum* genomic DNA, (2) *C. glutamicum* single cross-over genomic DNA, (3) *C. glutamicum* $\Delta NCgl2760$ genomic DNA. Positions and sizes of λ HindIII digoxigenin-labelled molecular markers are shown in kb.

4.2.5. Complementation of the $\Delta NCgl2760$ mutant

To confirm that any phenotype detected in the $\Delta NCgl2760$ mutant was solely due to disruption of the *NCgl2760* gene, a plasmid-encoded copy of the gene was introduced into the mutant. This complementation plasmid was created by PCR amplifying the entire 1051 bp gene plus 180 bp of upstream sequence using primers NCgl2760-comp_F and NCgl2760-comp_R, and cloning this fragment into the unique *PvuII* site of shuttle plasmid pSM22 (190), creating pSM22:*NCgl2760*. This plasmid and an empty pSM22 vector control were electroporated separately into the $\Delta NCgl2760$ mutant and transformants selected on kanamycin plates. The complementation strain and empty vector control strain were included in all subsequent experiments.

4.2.6. Deletion of the *NCgl2760* gene does not affect growth of *C. glutamicum*

On solid media it was observed that the wild-type, mutant, complementation and empty vector control strains grew at a similar rate, forming equal-sized colonies. To determine whether the strains also grew at the same rate in liquid culture, growth curves were performed in BHI medium at 30°C (Figure 4.6).

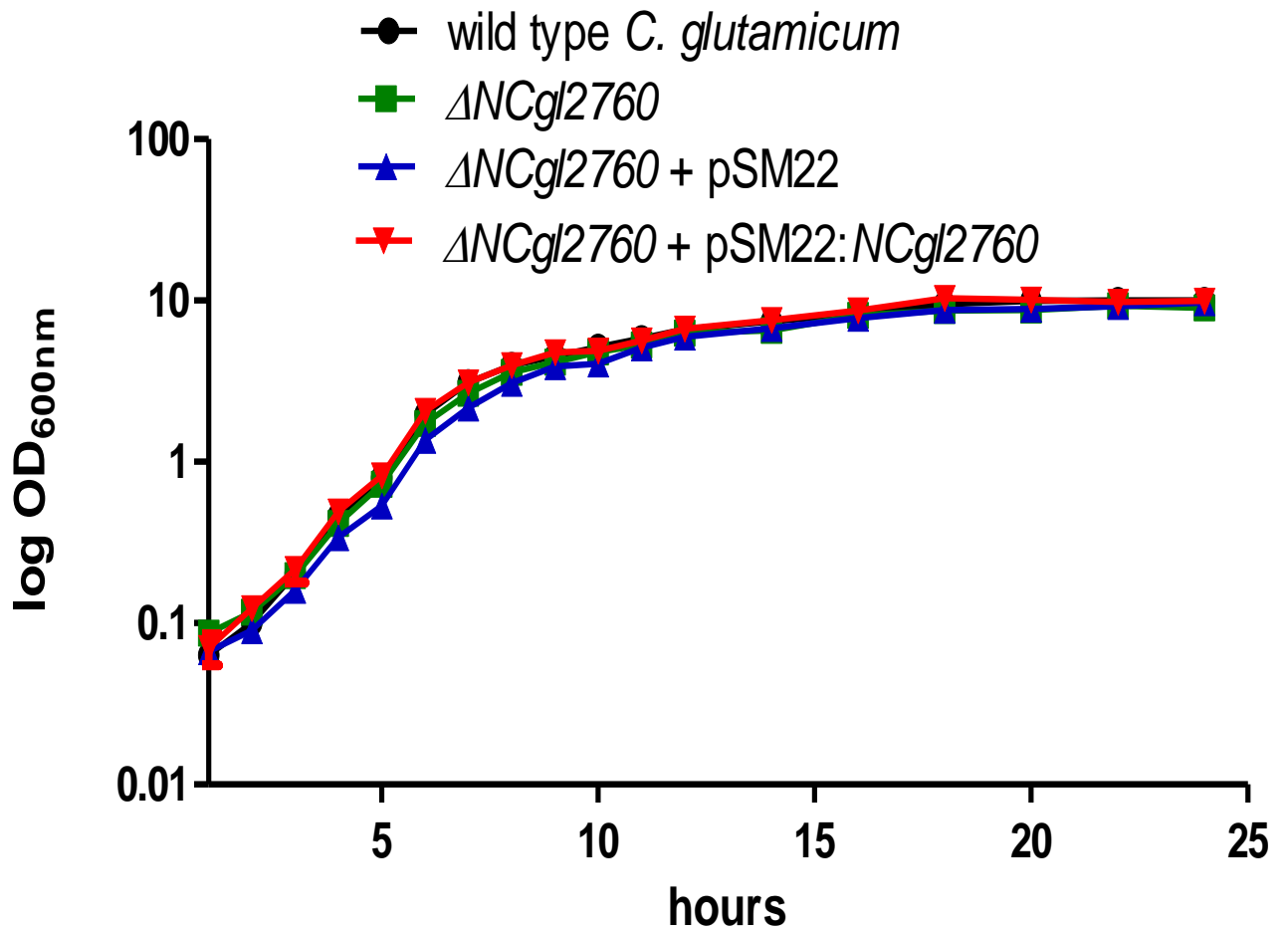


Figure 4.6. Growth characteristics of the wild type *C. glutamicum*, $\Delta NCgl2760$ mutant, $\Delta NCgl2760 + pSM22$, and $\Delta NCgl2760 + pSM22:NCgl2760$. Growth curves were performed in liquid BHI medium. OD_{600} measurements were taken from triplicate cultures and illustrated here as the mean and standard error of the mean of optical density (in \log_{10} scale).

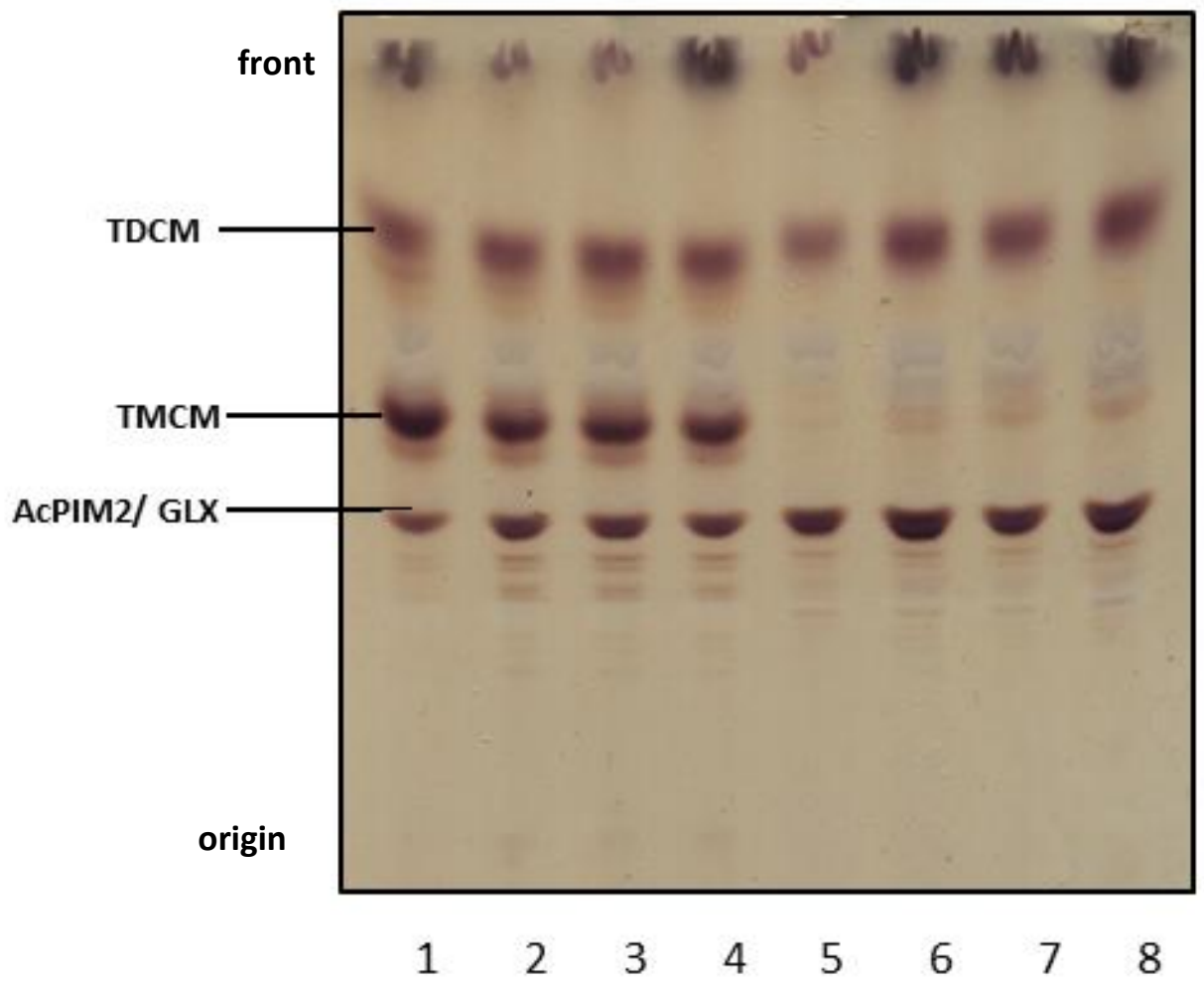
There appears to be no significant difference in growth rate between the wild type and other three strains under these growth conditions. The experiments were performed in triplicate and, again, no differences in growth rate were observed. This lack of a growth defect is inconsistent with the phenotypes of deletion mutants of *NCgl2759* (46), *NCgl2762* and *NCgl2764* (unpublished results), located adjacent to *NCgl2760*. This discrepancy suggested that *NCgl2760* might have a different role to other genes in the locus, which have been shown to encode proteins with roles in mycolic acid transport. To investigate the nature of the cell wall defect, if present, a comprehensive analysis of cell wall glycolipids was performed for the $\Delta NCgl2760$ mutant and control strains.

4.2.7. HPTLC analysis of glycolipids reveals no phenotype for a $\Delta NCgl2760$ mutant

At an OD(600nm)=1 and OD(600nm)=10, which were defined as representing log and stationary phases, respectively, samples were taken from the bacterial liquid cultures and centrifuged to obtain cell pellets weighing 0.3 - 0.4g. Extraction of the total lipids was done by three repeated steps of chloroform:methanol addition to the cell culture pellets followed by 6 hours shaking at room temperature. After each extraction and centrifugation, the supernatants were pooled and dried under a N₂ gas stream (see section 2.8.2, Chapter 2). Butanol biphasic partitioning using water-saturated 1-butanol was then performed on the extracts to purify the total lipids, including glycolipids. These were then separated by high performance thin layer chromatography (HPTLC) followed by orcinol staining to reveal the glycolipids (see section 2.10, Chapter 2) (Figure 4.7).

An aliquot (1-2 μ l) of the 1-butanol phase containing total lipids was loaded on a 10 cm silica gel 60 aluminium-backed HPTLC plate (Merck) and developed in solvent system A (chloroform:methanol:1 M ammonium acetate:13 M ammonia:water, 180:140:9:9:23, (v/v) or solvent system B (chloroform:methanol:1 M ammonium acetate:13 M ammonia:water, 180:140:9:9:2.3, (v/v) (Figure

4.7) Solvent B allows greater separation of the more polar glycolipids, particularly GI-X and AcPIM2, which co-migrate in solvent A. The migration and abundance of the TMCMs and TDCMs in all 4 strains were the same, thus no obvious phenotype relating to total lipid synthesis was detected in these analyses of the $\Delta NCgl2760$ mutant. This result was surprising given that deletion of other genes in this locus resulted in significant accumulation of TMCM at the expense of TDCM synthesis (46) and unpublished results, and figure 3.10, Chapter 3, indicating that NCgl2760 might have a different function to the other encoded proteins. AcPIM2, GLX and other more polar PIM species appeared unaltered in the mutant, indicating that the early reactions of the PIM pathway were also unaffected by the loss of NCgl2760.



A

Figure 4.7

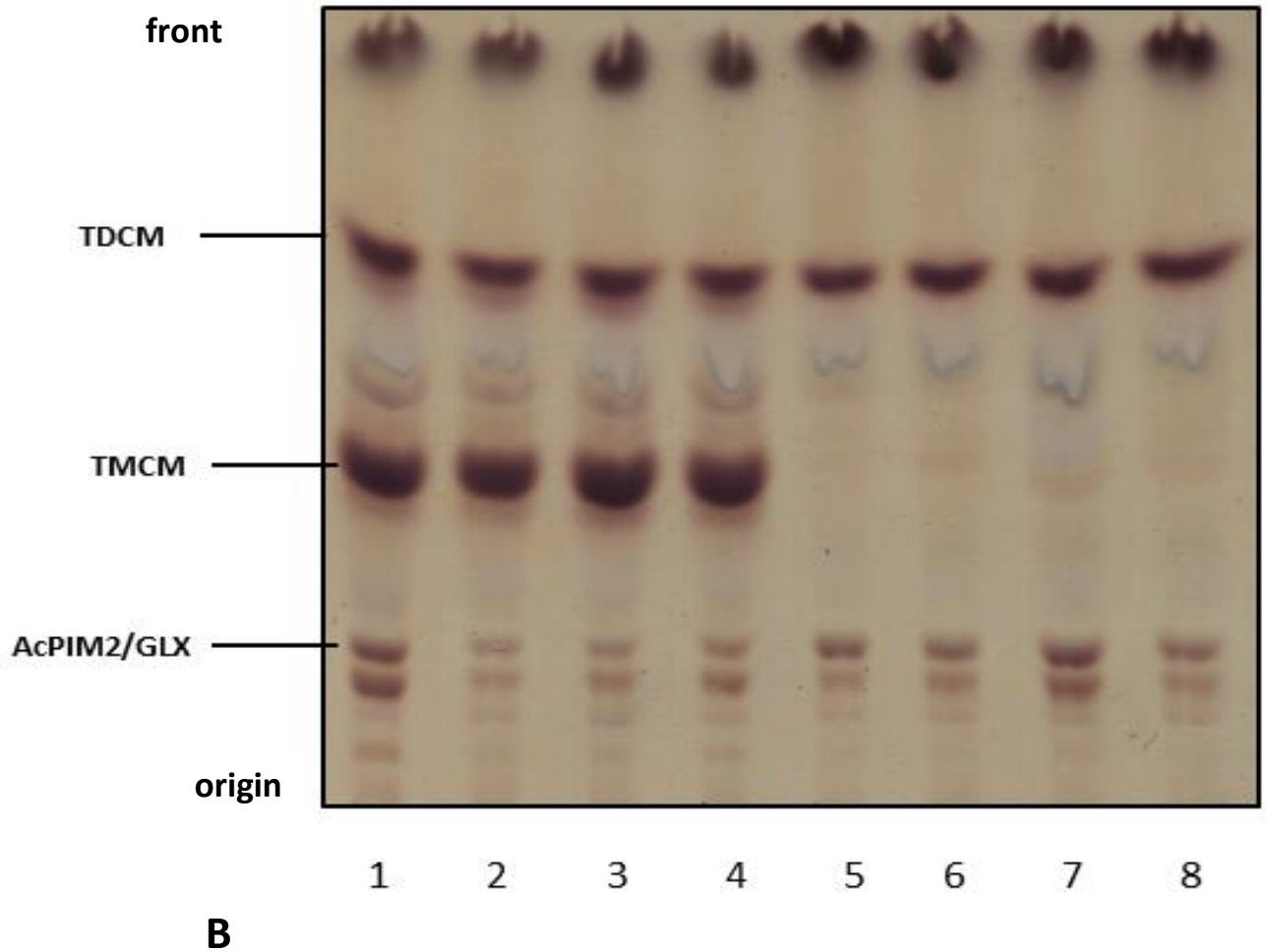


Figure 4.7. Glycolipid analysis of a $\Delta NCgl2760$ mutant. Free glycolipids of *C. glutamicum* WT (lanes 1 and 5), $\Delta NCgl2760$ mutant (lanes 2 and 6), vector control strain $\Delta NCgl2760 + pSM22$ (lanes 3 and 7), and complementation strain $\Delta NCgl2760 + pSM22:NCgl2760$ (lanes 4 and 8) were extracted in the mid-log (lanes 1-4) and stationary (lanes 5-8) growth phases. They were resolved by HPTLC and visualized by orcinol/ H_2SO_4 staining. Panel A = solvent system A; Panel B = Solvent System B.

4.2.8. Characterization of lipoglycans from a $\Delta NCgI2760$ mutant

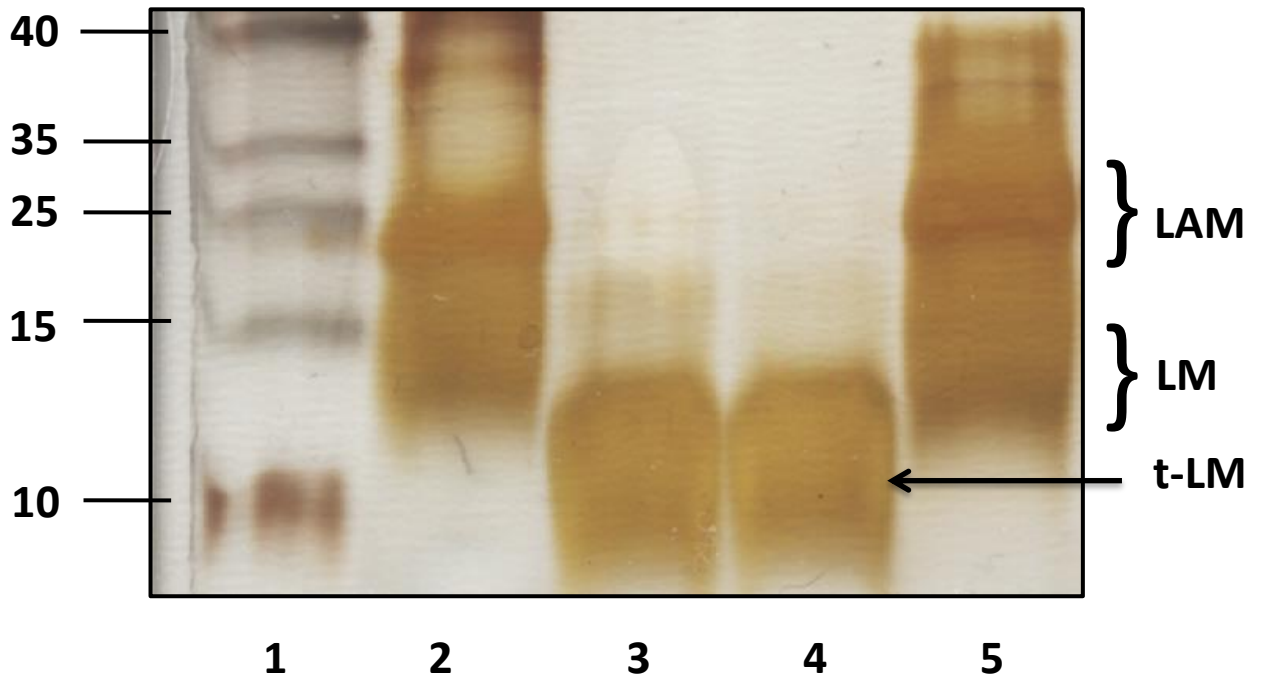
Since the trehalose mycolates and early PIM species appeared normal in the $\Delta NCgI2760$ mutant, the cell wall analysis was extended to include the more polar cell wall glycolipids. Delipidated cell pellets from the analysis described above were subjected to ethanol refluxing to isolate the lipopolysaccharides LM and LAM. This freeze-dried material was re-suspended in 30% 1-propanol and electrophoresed on a 15% SDS-polyacrylamide gel (SDS-PAGE) followed by silver staining (see Section 2.11, Chapter 2). Extracts of the WT *C. glutamicum*, $\Delta NCgI2760$ mutant, empty vector control ($\Delta NCgI2760$ + pSM22), and complementation strain ($\Delta NCgI2760$ + pSM22:*NCgI2760*) were run in adjacent lanes (Figure 4.8 A and B). The diffuse nature of bands in SDS-PAGE gels is due to heterogeneity in size, acylation and branching pattern of *C. glutamicum* LM and LAM.

This analysis revealed a striking phenotype in the $\Delta NCgI2760$ mutant. A faster migrating lipoglycan was observed in the $\Delta NCgI2760$ mutant and empty vector control ($\Delta NCgI2760$ + pSM22) strains relative to the WT and complementation strains. This novel species migrated further than the 15 kDa protein marker which usually co-migrates with *C. glutamicum* LM, suggesting it to be a truncated form of LM. To clearly distinguish it from the other lipoglycans, this new species was designated t-LM. The lipoglycan analysis also revealed a lack of mature LM and LAM in the $\Delta NCgI2760$ mutant, suggesting that the LM and LAM pathways were blocked at the new t-LM intermediate. LM and LAM synthesis were restored in the complementation strain, and t-LM was not observed, suggesting that the blockage in the biosynthetic pathway was removed by re-introduction of the *NCgI2760* gene in the $\Delta NCgI2760$ mutant. This finding strongly suggests that the lack of *NCgI2760* in the mutant is solely responsible for the accumulation of t-LM and lack of LM and LAM in this strain.

This phenotype was unexpected since disruption of other genes in the locus failed to affect any steps of the LM or LAM pathways. To confirm the phenotype, two more independent $\Delta NCgl2760$ mutants were made (data not shown) using the same strategy described earlier and subjected to the same cell wall analyses as the original mutant. The lipoglycan profiles for the two new mutants were found to be identical to those of the original mutant, and one of these is shown in Figure 4.7B (Lane 3). Introduction of the complementation plasmid pSM22:*NCgl2760* into each of the new mutants (Figure 4.8A and B, lane 5) restored their lipoglycan profiles once again while empty pSM22 did not (Figure 4.8A and B, lane 4). Therefore, this analysis of independent mutants confirmed the LM/LAM phenotype that results from disruption of the *NCgl2760* gene.

These findings suggest that *NCgl2760* is involved in the LM/LAM pathway, specifically, at a mannosylation step that extends t-LM to form LM, and before arabinosylation of LM to produce LAM. Based on its migration on the SDS-PAGE gel, t-LM is likely to have fewer mannose molecules than LM, since mannose forms the bulk of these molecules. More in-depth and specific studies, such as GC-MS and MALDI-TOF, were needed in order to confidently enumerate the number of mannose molecules and estimate the molecular structure of t-LM.

A



B

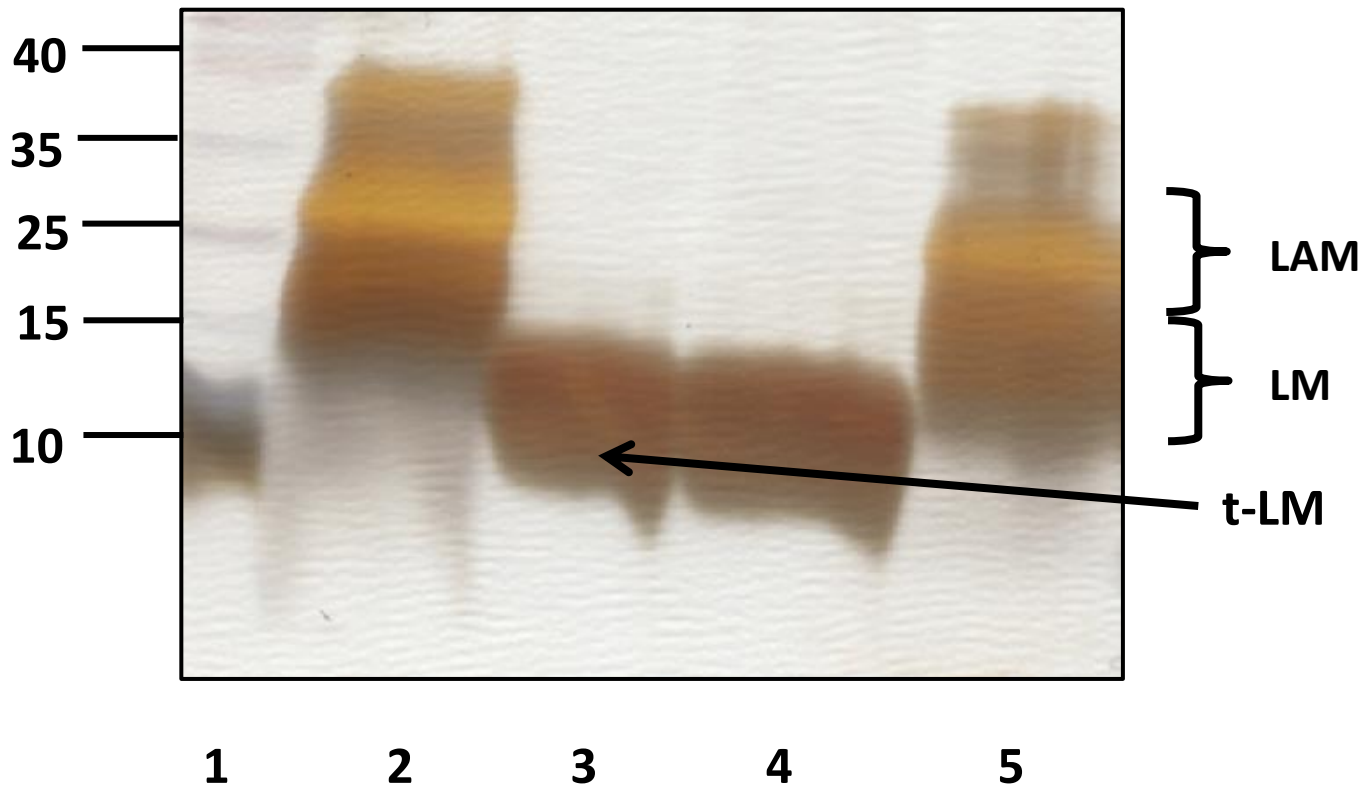


Figure 4.8

Figure 4.8. Lipoglycan profiles of wild type *C. glutamicum*, $\Delta NCgl2760$, $\Delta NCgl2760$ + pSM22 and $\Delta NCgl2760$ + pSM22:*NCgl2760*. Lipoglycans were extracted from two independently generated mutants (designated **A** and **B**), each of which had been complemented with pSM22:*NCgl2760* and also transformed with an empty pSM22 plasmid as a control. SDS-PAGE gels of lipoglycans from mutant A and mutant B strains are shown here (panels A and B, respectively). Wild type *C. glutamicum* (Lane 2), $\Delta NCgl2760$ (Lane 3), $\Delta NCgl2760$ + pSM22 (Lane 4) and $\Delta NCgl2760$ + pSM22:*NCgl2760* (Lane 5) were harvested in the log phase of growth and LM/LAM was extracted by ethanol reflux from delipidated cell pellets. Lipoglycans were analysed on a 15% SDS-polyacrylamide gel and visualised by Pierce® silver stain. Sizes of the Benchmark (Invitrogen) protein molecular weight markers (lane 1) are indicated in kilodaltons.

4.2.9 Complementation of the $\Delta NCgl2760$ mutant with *Rv0227*

Since all three independent $\Delta NCgl2760$ mutants were successfully complemented by a plasmid-encoded copy of the *NCgl2760* gene, the next step was to attempt to complement the mutant with the *Rv0227* gene from *M. tuberculosis*. This was performed to determine whether the likely mycobacterial ortholog could functionally replace the *C. glutamicum NCgl2760* gene. The primers Rv0227TB_F and Rv0227TB_R (See Appendix 3 for primer details) were used to PCR amplify *Rv0227* from *M. tuberculosis* H37Rv genomic DNA including 193bp of upstream sequence that might include the promoter. This product was then cloned into pSM22 at the unique *Pvu*II site, to create the plasmid pSM22:*Rv0227*. A positive clone was sequenced to confirm cloning of an error-free *Rv0227* gene, then electroporated into electrocompetent $\Delta NCgl2760$ cells. (Section 2.5.5, Chapter 2) A single kanamycin-resistant colony was picked for further analysis.

To determine whether introduction of the *Rv0227* gene was affecting growth, and to confirm the lack of any growth defect in the original $\Delta NCgl2760$ strain, growth curves were repeated for all the strains, this time including the new strain, $\Delta NCgl2760 + pSM22:Rv0227$. As before, single colonies were inoculated into BHI broths, grown overnight at 30°C, then diluted in 100ml of fresh broth and OD(600nm) measurements taken over a ten hour period. All 5 strains showed a similar growth pattern, *i.e.* no significant initial lag or reduced growth rate in log phase (Figure 4.9). In these growth curve experiments, a slight lag in all strains was observed relative to the wild-type control, but this was not considered to be significant and all reached stationary phase at a similar time. Having confirmed a similar growth rate in all strains, they were then analysed for cell wall LM/LAM content as described earlier.

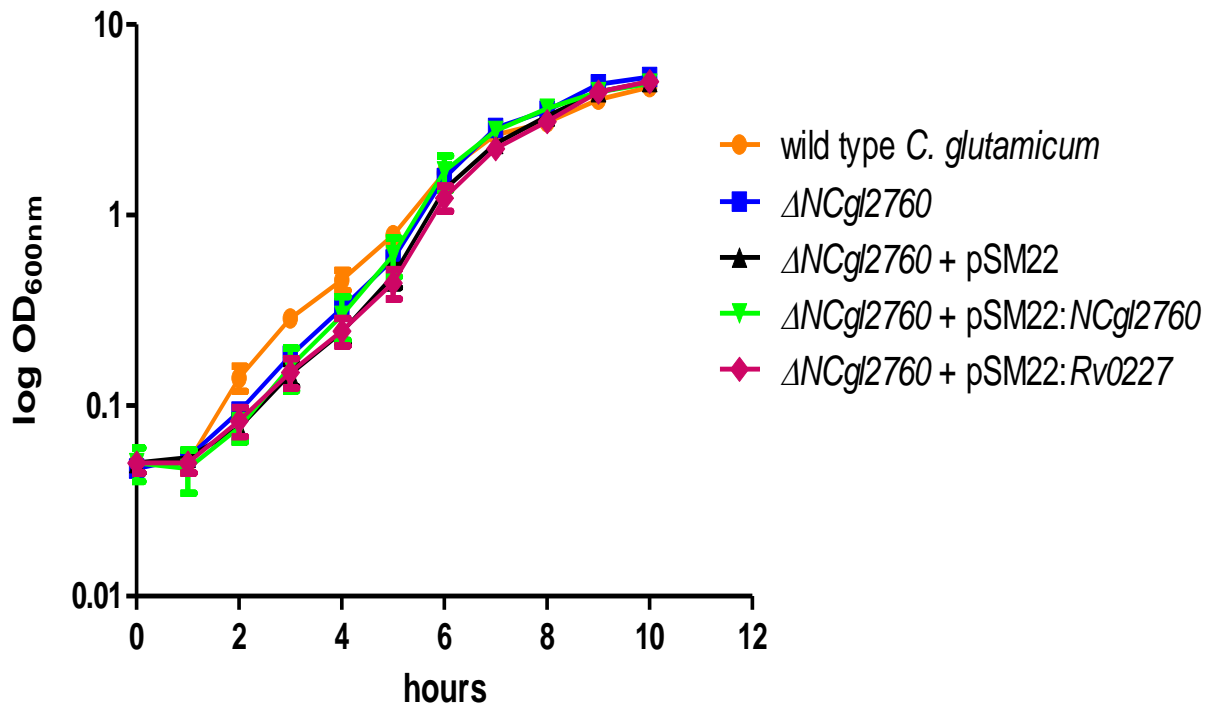


Figure 4.9. Growth characteristics of wild type *C. glutamicum*, $\Delta NCgl2760$, $\Delta NCgl2760 + pSM22$, and $\Delta NCgl2760 + pSM22:NCgl2760$ strains. Growth is shown as the mean and standard error of the mean of OD (in log₁₀ scale). It was measured hourly in BHI cultures *i.e.* 5 samples taken every hour across all cultures. All strains showed similar growth characteristics under the conditions tested.

4.2.10 LM/LAM profile when complementing $\Delta NCgl2760$ with *Rv0227*

LM and LAM were extracted from all strains as described earlier and analysed on 15% SDS-PAGE gels (Figure 4.10). The $\Delta NCgl2760$ mutant containing pSM22:*Rv0227* showed an unaltered profile relative to the original $\Delta NCgl2760$ mutant; t-LM was present and mature LM and LAM were absent. This finding indicated that the pSM22-encoded *Rv0227* gene was unable to complement the $\Delta NCgl2760$ mutant and restore LM/LAM synthesis.

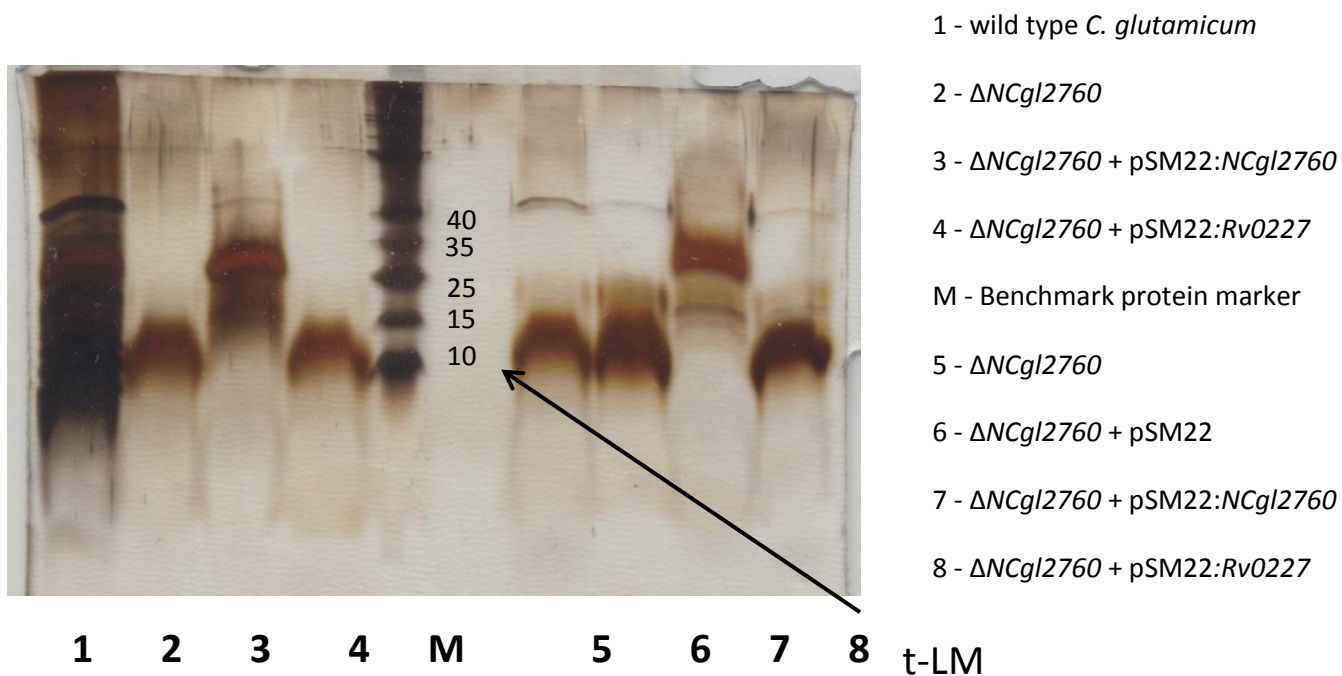


Figure 4.10. LM/LAM profiles when complementing $\Delta NCgl2760$ with both *NCgl2760* and *Rv0227*

Cells were harvested in the log phase of growth and LM/LAM was extracted by ethanol reflux from delipidated cell pellets. Lipoglycans were analysed on a 15% SDS-PAGE gel and visualised by Pierce™ silver stain. The first four lanes represent the mid-log stage of growth, while lanes 5-8 reflect data from the stationary phase. OD Sizes of the Benchmark (Invitrogen) protein molecular weight markers (lane M) are indicated in kilodaltons.

4.2.11 Complementation of $\Delta NCgl2760$ with *Rv0227* fused to the *NCgl2760* upstream sequence

The lack of complementation of the $\Delta NCgl2760$ strain with *Rv0227* from *M. tuberculosis* could be due to several factors. As shown in the protein sequence alignment (Figure 4.2), *C. glutamicum* NCgl2760 and its *M. tuberculosis* ortholog only display 24.9% similarity and 16.4% identity, so one possible explanation for the lack of complementation is that they do not share sufficient similarity for one to substitute for the other. Another possible explanation is that *Rv0227* was not being expressed in the $\Delta NCgl2760$ mutant due to lack of a promoter that is active in *C. glutamicum*. The successful complementation of $\Delta NCgl2760$ with pSM22:*NCgl2760* suggested that the upstream sequence included in that construct was promoting *NCgl2760* expression, so this upstream sequence was fused to the *Rv0227* gene via a splice overlap extension (SOE) PCR.

The SOE approach employed here is shown in Figure 4.11. A 0.4kb section of *NCgl2760* upstream sequence was PCR amplified using primers NCgl2760_upstream-L and NCgl2760_upstream-R. (See Appendix 3 for primer details) In a separate reaction, the 1.3kb *Rv0227* gene was amplified using primers Rv0227_downstream-L and Rv0227_downstream-R. (Figure 4.12). The 5' ends of primers NCgl2760_upstream-L and Rv0227_downstream-R were designed to contain complementary sequences that allowed the two PCR products to anneal when mixed together. Finally, the mixed products were used as templates in a PCR reaction with primers NCgl2760_upstream-R and Rv0227_downstream-L, which produced a fusion product of 1.7 kb. Primers NCgl2760_upstream-R and Rv0227_downstream-L contained a restriction site for the enzyme *PvuII*, allowing the final product to be cloned into the unique *PvuII* site of pSM22. A sequence verified pSM22 plasmid containing the SOE product was designated pSM22:**Rv0227*, the asterisk denoting the fact that the upstream sequence of *NCgl2760* had been fused to *Rv0227*.

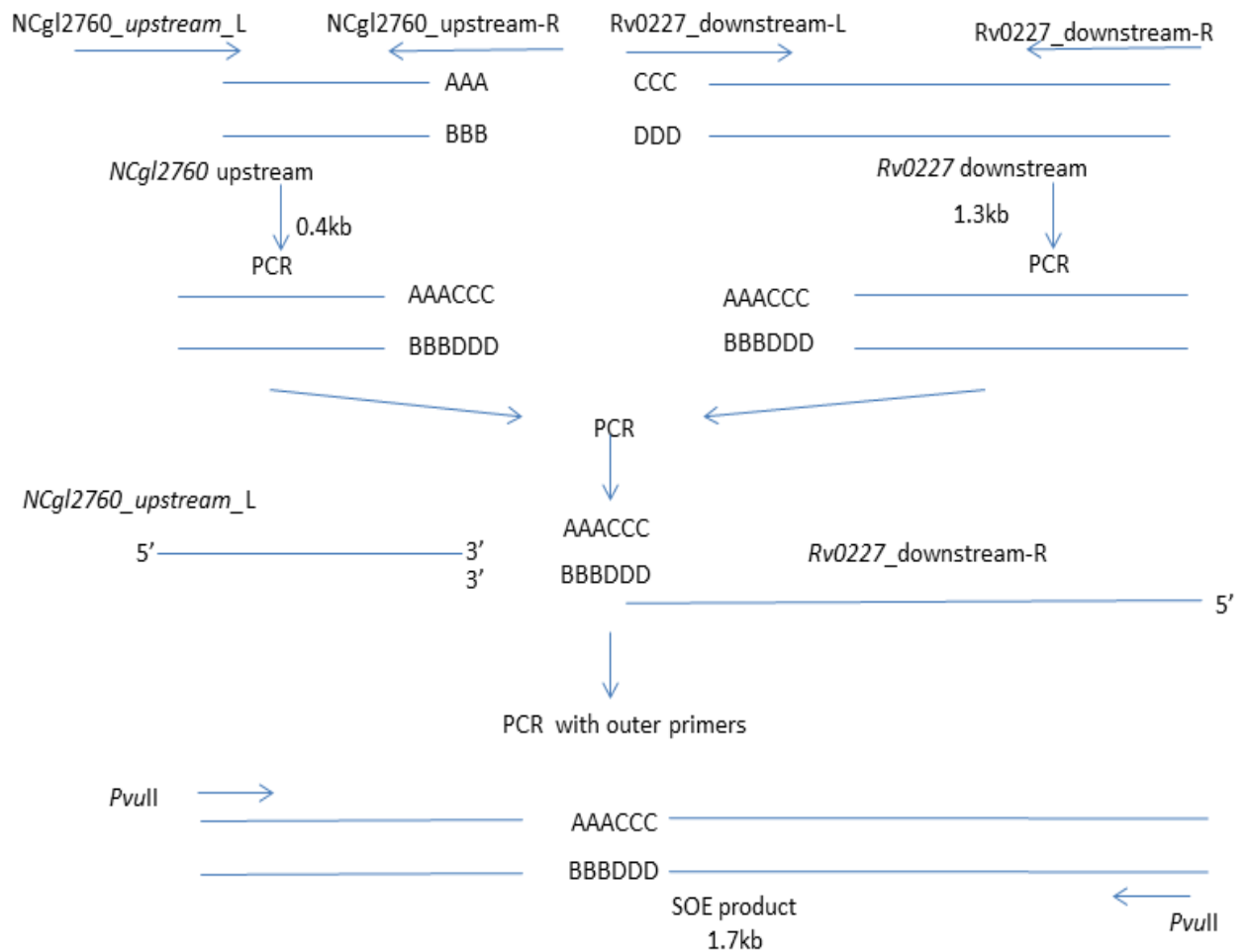


Figure 4.11 Fusion of *Rv0227* to the upstream sequence from *NCgI2760* using SOE PCR. Each fragment was PCR amplified using primers indicated by horizontal arrows. Next, the fragments were mixed and PCR amplified once again to fuse *Rv0227* to the *NCgI2760* upstream sequence. The final product was then cloned into pSM22 using *PvuII*.

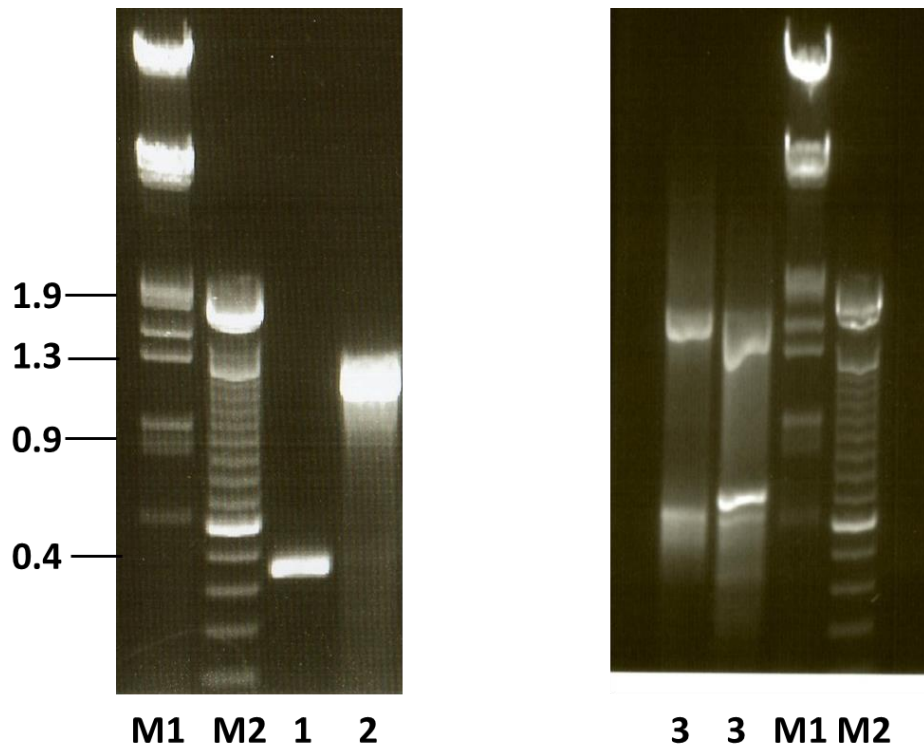


Figure 4.12 A and B. DNA profiles of A) the two individual PCR products, and B) fusion PCR products of the SOE reaction. The λ HindIII/EcoRI markers are in lane M1 while a 100bp ladder is shown in lane M2. Panel A) indicates the larger Rv0227=1.3kb (lane 2) and the shorter NCgl2760=0.4kb (lane 1) products. Panel B) shows the SOE fusion product (lane 3).

Plasmid pSM22:*Rv0227* was electroporated into Δ *NCgl2760* electrocompetent cells and the mixture plated onto BHI plates containing kanamycin. A single colony was then cultured, LM/LAM extracted and analysed as described earlier. As shown in Figure 4.13, the fusion product also failed to complement the Δ *NCgl2760* mutant and restore LM/LAM synthesis. Since the upstream sequence was the same as the sequence present in the complementing pSM22:*NCgl2760* plasmid, the lack of complementation suggested that *Rv0227* could not functionally replace *NCgl2760*, most likely due to the sequence differences noted in Figure 4.2.

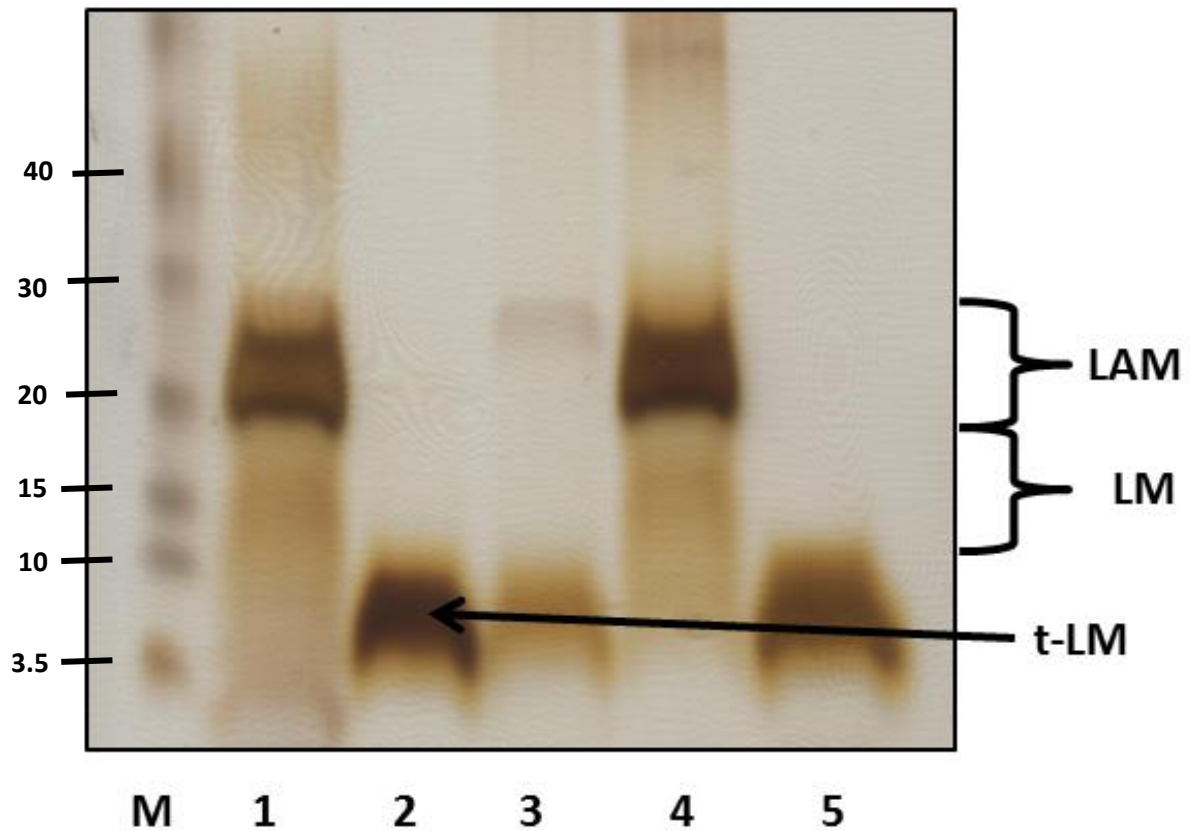


Figure 4.13. SDS-PAGE analysis of LM/LAM from the $\Delta NCgl2760$ mutant containing plasmid pSM22:*Rv0227.

Wild type *C. glutamicum* (lane 1) was compared to four other strains including $\Delta NCgl2760$ (lane 2), $\Delta NCgl2760$ + pSM22 (lane 3), $\Delta NCgl2760$ + pSM22:NCgl2760 (lane 4) and $\Delta NCgl2760$ + pSM22:*Rv0227 (lane 5). The sizes of the Novex® Prestained protein marker are shown in kilodaltons (lane M).

4.2.12 DIONEX high pH anion-exchange chromatography reveals characteristic oligosaccharides

Having constructed the mutant and identified a truncated LM/LAM, it was necessary to determine its components. LM and LAM were studied by DIONEX high pH anion -exchange chromatography (HPAEC) after first determining the glycolipid sugar head by base hydrolysis. This was done using NH₄ solubilisation followed by biphasic partition over butanol (see protocol in Chapter 2, Section 2.8.2.1) and aqueous HF dephosphorylation of the glycoconjugates. After neutralization, the solution was desalted before being ready for analysis on the Dionex machine. LM/LAM isolated from the bacterial strains were separated on HPAEC (Figure 4.14) using a NaOAc and NaOH gradient to release negatively charged ions over time. There appear to be oligosaccharides and monosaccharides in the LM/LAM fraction from the $\Delta NCgl2760$ mutant not evident in the wild type *C. glutamicum* strain.

In Figure 4.14, the Dionex reading shows the wild type *C. glutamicum* LM/LAM fraction as the grey line while the mutant $\Delta NCgl2760$ is shown in violet. As the solute passes through the Dionex columns (one filled with NAOAc and the other with NaOH), they are separated by electric charges, and their structures read onto a film as shown. The x-axis reflects time (minutes) and the y-axis is a random measure of response (nanocurrent). The conventional appearance of both variables i.e. the monosaccharide and oligosaccharide graph is somewhat erratic and is followed by the oligosaccharide region of the graph which normally smooths out. Yet, as shown in figure 4.14, there exists a noticeable difference between the detail of the wild type *C. glutamicum* and $\Delta NCgl2760$ mutant. The mutant $\Delta NCgl2760$ reading demonstrates fewer peaks, but those are taller than those of the wild type. This could reflect the less complex structure of the glycoconjugate in the

$\Delta NCg12760$ mutant. i.e. less mannose molecules. It would suggest that NCg12760 plays a role early in the LM/LAM pathway.

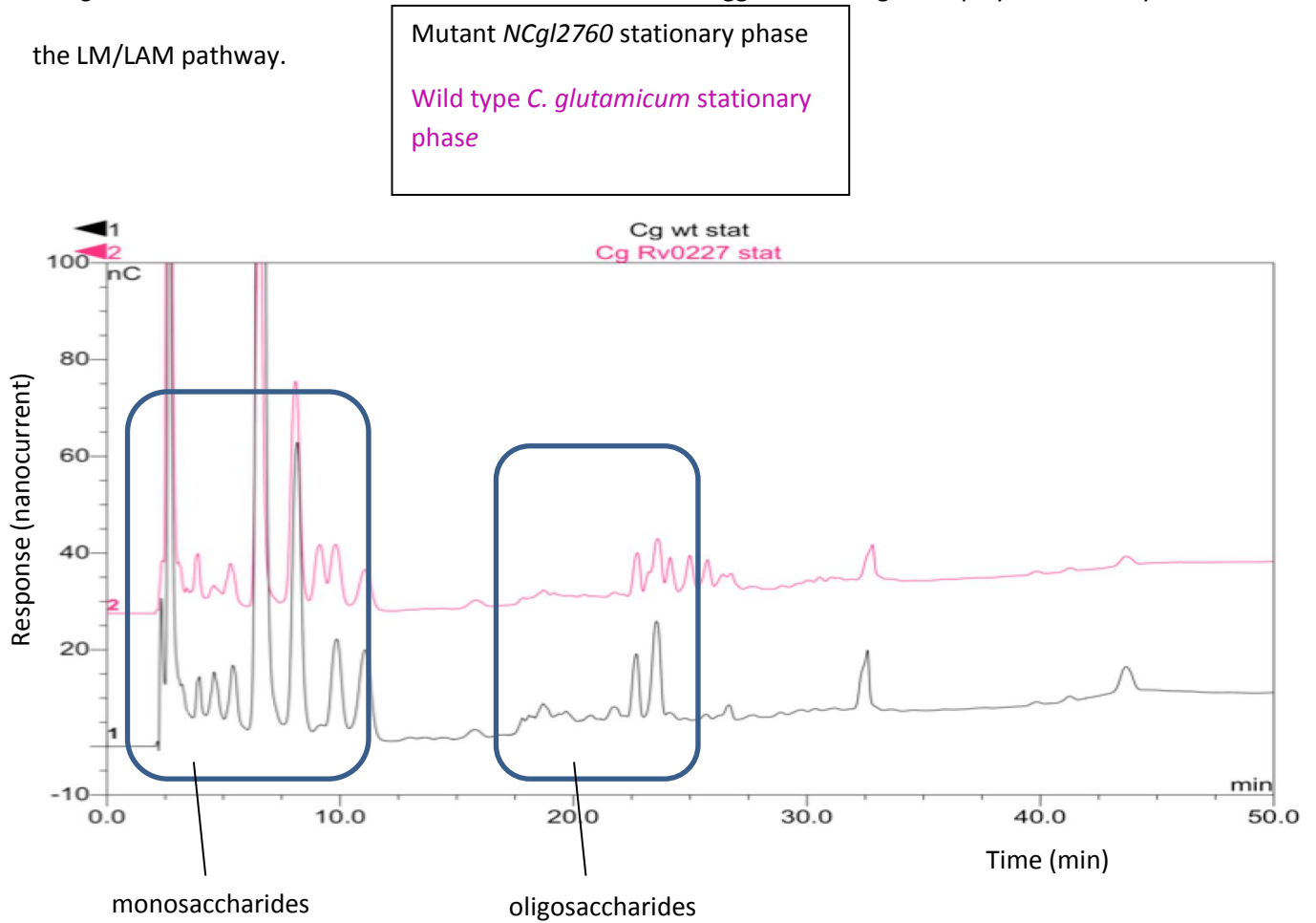


Figure 4.14. HPAEC of HF-treated LM/LAM fraction. Samples extracted from cells in stationary phase were used for analyses. Phosphates were cleaved by hydrogen fluoride, then analysed on a Dionex. Different sized oligosaccharides are evident in the $\Delta NCg12760$ mutant (from Dr F Sernee and Dr J Ralton, Bio21, Melbourne University).

4.2.13. GC-MS analysis of extracted LM/LAM samples

Analyses thus far have suggested that the LM/LAM component of the *NCgl2760* mutant differ from that of the wild type *C. glutamicum*. The oligosaccharides are different in ways that need further analysis to be understood. So gas chromatography - mass spectroscopy was utilized. It is able to detect molecular fractions within specific strains.

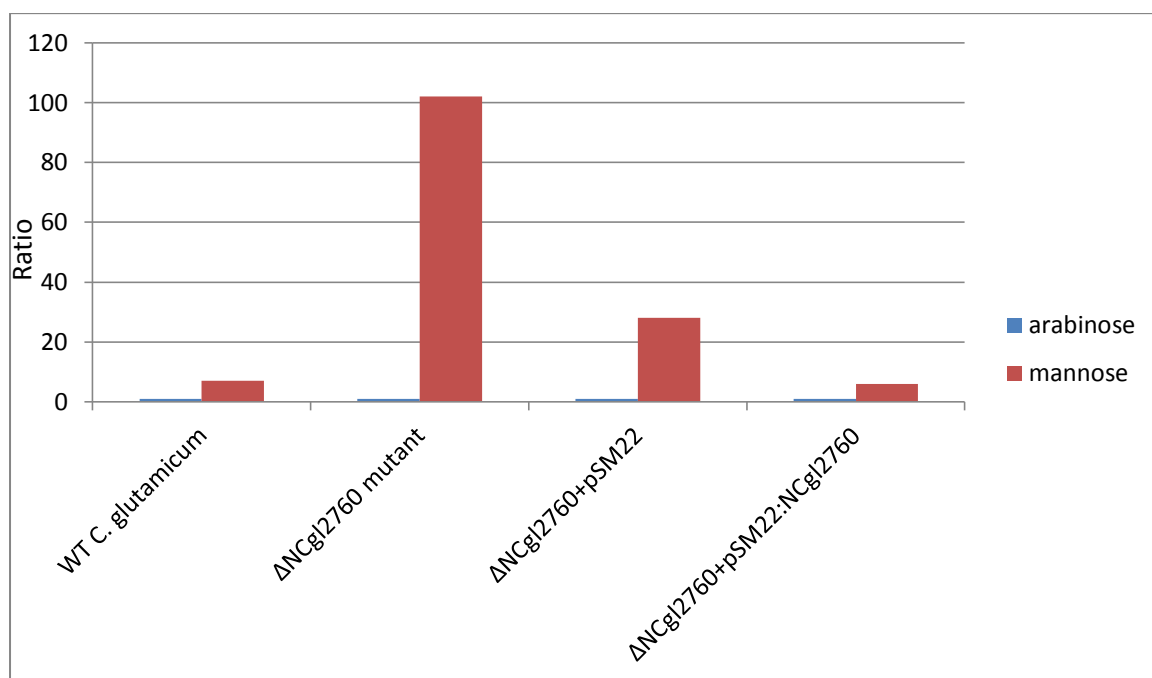


Figure 4.15. Ratio of mannose:arabinose in LM/LAM fractions isolated in LM/LAM fractions isolated from wild type *C. glutamicum*, Δ NCgl2760 mutant, Δ NCgl2760 + pSM22, and Δ NCgl2760 + pSM22:NCgl2760. The ratio of arabinose to mannose helps identify how far along the synthetic pathway the glycoconjugate structure is situated.

As shown in Figure 4.15, the ratio of arabinose:mannose in the LM/LAM fractions from wild type and $\Delta NCgl2760 + pSM22:NCgl2760$ was approximately equal (ie 1:7 and 1:6, respectively). The ratio in the $\Delta NCgl2760$ mutant was 1:102 while that of the $\Delta NCgl2760 + pSM22$ strain was 1:28. The high ratio in the mutant and $\Delta NCgl2760 + pSM22$ strains suggests a very low level of, or total lack of, LM/LAM arabinosylation. The charts would most likely be more similar in measurement with greater experimental repetition. Less or no arabinose in extracts from these two strains is consistent with the truncated nature of the LM observed by SDS-PAGE (Figure 4.8). Therefore, this intermediate appears to be a precursor of LM that is so heavily truncated that it is not a substrate for arabinosyltransferases that act later in the pathway to arabinosylate LM and form LAM.

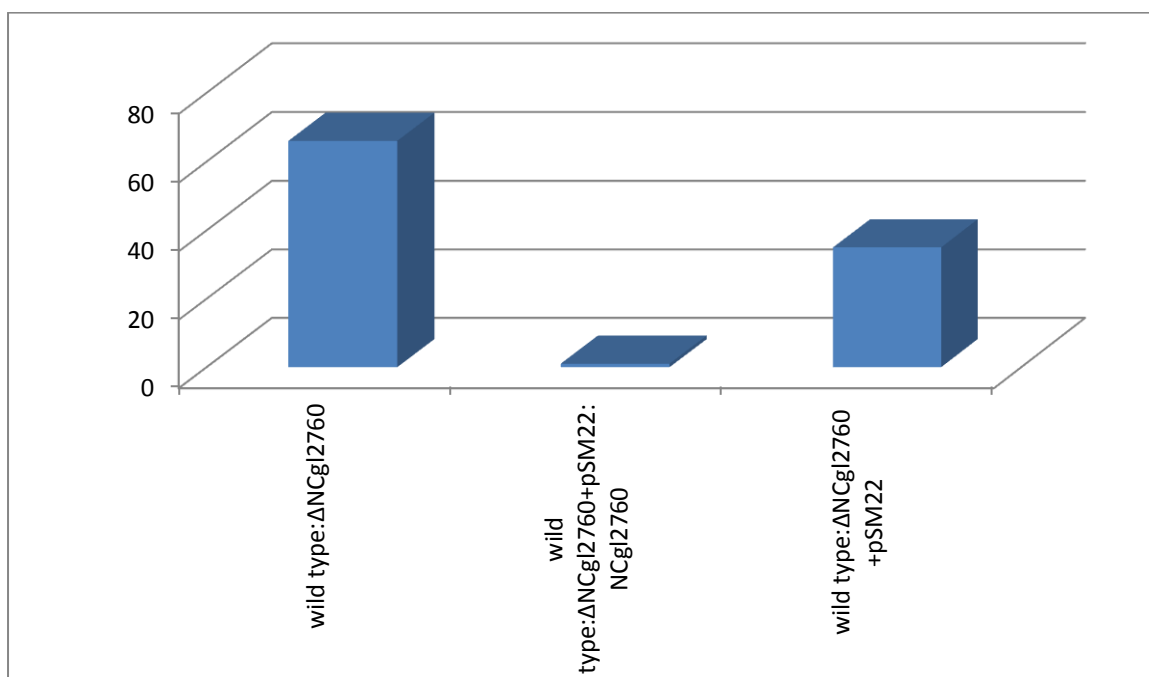


Figure 4.16 Ratio of arabinose between LM/LAM fractions of wild-type *C. glutamicum* and the $\Delta NCgl2760$ mutant strains. The absolute amount of arabinose in the wild type is equal to that of the $\Delta NCgl2760 + pSM22:NCgl2760$ strain, but the relative amount of arabinose is very much greater in the wild type than knockout lines

The absolute amount of arabinose in LM/LAM from wild type *C. glutamicum* was compared to that of the other three strains and represented as a ratio in Figure 4.16. The mutant $\Delta NCgl2760$ and $\Delta NCgl2760 + pSM22$ had a ratio very much greater than one as their arabinose content was less than that of the wild type. The wild type *C. glutamicum* and $\Delta NCgl2760 + pSM22:NCgl2760$ have a ratio equal to one *i.e.* wild type *C. glutamicum* and $\Delta NCgl2760 + pSM22:NCgl2760$ have an equal arabinose level.

The lipoglycan component of the cell wall extract was analysed (Figures 4.15 and 4.16). When calculated, the number of arabinose molecules per mannose molecule was less in the $\Delta NCgl2760$ mutant and $\Delta NCgl2760 + pSM22$, than in the wild type *C. glutamicum* and $\Delta NCgl2760 + pSM22:NCgl2760$ strains. During synthesis of the cell wall, arabinosylation occurs well after the mannose chain has been formed. Thus, it is evident that $\Delta NCgl2760$ occurs near the arabinose branchpoint. This conclusion is confirmed by the faster migration of the t-LM on SDS-PAGE gels compared to wild-type LM/LAM (Figure 4.8). The size of this species is smaller than that of the wild type, probably due to an absence of arabinosylation and reduced degree of mannosylation as well.

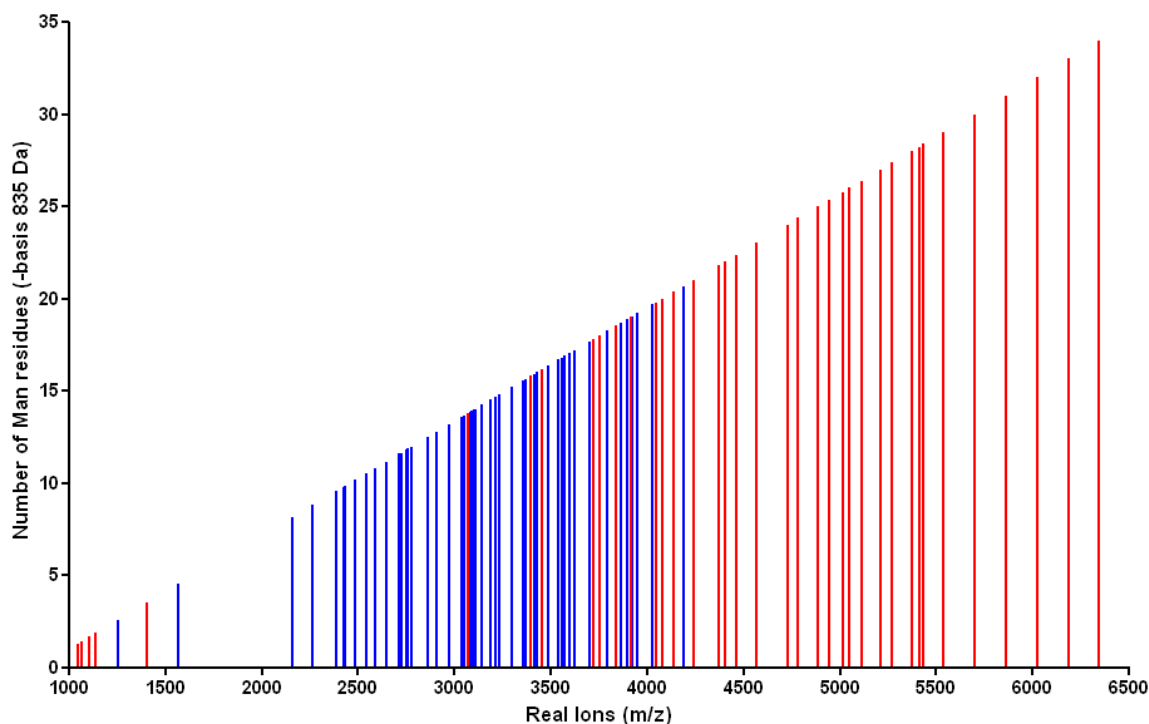


Figure 4.17. Size, distribution and number of mannose residues of different LM/LAM molecules of wild type *C. glutamicum* (red) and mutant $\Delta NCgl2760$ (blue). The measurement was done during direct infusion ESI QTOF in negative ionization mode.

Each peak/ion in figure 4.17 (wild type *C. glutamicum* (red); mutant $\Delta NCgl2760$ (blue)) represents either the molecular ion of intact mannose molecules (heterogeneity) or fragment ions of steady state mannose molecules (homogeneity). Fragmentation of these residues could have happened during ESI-QTOF but this is unlikely. So the peaks probably represent a heterogenous distribution of LAMs. The peaks of the wild type *C. glutamicum* and the mutant $\Delta NCgl2760$ indicate a clear difference in the number of mannose residues. The largest lipoglycan species in the wild type *C. glutamicum* has 36 mannose residues, whereas the biggest mutant has just 21 residues (Figure 4.17).

Therefore, the LM in the mutant *ΔNCgl2760* is much shorter than the wild type. Neither arabinose nor side-chains were detected confirming that t-LM most likely is situated within the earlier LM stage of the lipoglycan - synthesis pathway.

4.3 Discussion

A genetic locus comprising *NCgl2759*, *NCgl2760*, *NCgl2761*, *NCgl2762*, *NCgl2764* is proposed to be involved in cell wall synthesis. Deleting three of these genes individually had resulted in mutant strains sharing a common phenotype: a dramatically reduced rate of conversion of TMCM to TDCM due to a defect in TMCM transport across the membrane (46) and unpublished results. As described in Chapter 3, a deletion mutant of *NCgl2761* also had this phenotype, suggesting that all four protein products are involved in the same step of (coryno)mycolic acid transport. To complete the genetic analysis of this locus the remaining gene, *NCgl2760*, was deleted to produce a new mutant for cell wall analysis, as described in this chapter.

The *NCgl2760* gene was deleted using a two-step recombination approach as described. Briefly, sequences flanking the gene were ligated to produce a suicide vector construct for introduction into *C. glutamicum* to replace the wild-type chromosomal copy of the gene with a deleted copy. PCR screening followed by Southern hybridization confirmed that allelic replacement had been successful resulting in an *NCgl2760* mutant. The strain was complemented by introducing a cloned copy of *NCgl2760* and complementation was also attempted using the best match for the gene in *M. tuberculosis*, *Rv0227*.

Surprisingly, analysis of the *NCgl2760* mutant revealed that the protein functioned differently to those encoded by the other four genes in the locus. The new mutant differed from the others in two primary ways. First, it had no growth defect. The $\Delta NCgl2760$, and $\Delta NCgl2760$ + pSM22 strains grew at the same rate as the wild type *C. glutamicum* and $\Delta NCgl2760$ + pSM22:*NCgl2760* strains when monitored overnight in triplicate cultures of BHI media. All strains were also visually compared on solid agar and formed similar sized colonies with no obvious morphological changes. Absence of a

growth defect is rather unusual for a cell wall mutant in our experience. However, a faster migrating lipoglycan species which was identified in the mutant and named t-LM, might be able to function as a direct substitute for LM and LAM, thus stabilising the cell wall and allowing normal growth. Second, analysis of free lipids, including TMCMs and TDCMs, revealed a lack of variation between the wild type *C. glutamicum*, $\Delta NCgl2760$, $\Delta NCgl2760 + pSM22$ and $\Delta NCgl2760 + pSM22:NCgl2760$ strains. No differences were observed in either the log or stationary phases of growth. While a clear accumulation of TMCM was seen during the log phase of growth in the $\Delta NCgl2761$ mutant compared to wild type *C. glutamicum* (Chapter 3), no such accumulation was detected in the new mutant.

SDS-PAGE analysis of the lipoglycans showed a distinct phenotype in the *NCgl2760* mutant. LM/LAM isolated from cultures of wild-type, mutant and complemented mutant in both the log and stationary phases was run on a 15% SDS-PAGE gel to reveal a faster migrating species in the $\Delta NCgl2760$ and $\Delta NCgl2760 + pSM22$ strains that we designated t-LM (truncated LM). While the exact structure of t-LM is not yet known, the increased gel migration likely indicates a shorter sugar backbone similar to that described by Fukuda *et al.*(125). Studies of the function of MSMEG_4247 in *M. smegmatis* (the ortholog of Rv2181 from *M. tuberculosis*) led to their hypothesis that less activity in this branch-forming mannosyltransferase results in premature termination of elongation in the mannose backbone in turn leading to smaller LM/LAMs. *eg.* the truncated species identified may have no mannose side-branching. This may be confirmed by GC-MS. However the gene under investigation in this chapter shares no sequence similarity to Rv2181, has no glycosyltransferase motifs and is not the homologue of that gene in *C. glutamicum*.

GC-MS investigations of the LM/LAM lipoglycan fraction have shed light on the ultrastructure of the t-LM. The low ratio of arabinose content (Figure 4.16) between wild type *C. glutamicum* and $\Delta NCgl2760$ + pSM22:NCgl2760 and the $\Delta NCgl2760$ and $\Delta NCgl2760$ + pSM22 strains suggests that the pathway is restored in the complementation strain. The difference is so great, it implies a total absence of arabinose in t-LM suggesting that the biosynthetic pathway is blocked before the arabinosylation steps. Additional investigations reflect these respective similarities: the wild type *C. glutamicum* and $\Delta NCgl2760$ + pSM22: NCgl2760 are approximately equivalent, thereby approximating a ratio of one (Figure 4.16). These data are in agreement with the faster migrating, smaller molecule seen on SDS-PAGE gel designated t-LM in this study.

Gram-positive bacteria frequently have glycosylated diacylglycerols functioning as precursors or anchors for hyperglycosylated variants such as lipomannans. ManGlcAGroAc₂ is the first time a mannosylated description of glucuronosyl diacylglycerol has been made in Corynebacterineae (139). Although this truncated species appears even smaller than the LM of wild-type *C. glutamicum*, so it likely represents a precursor of LM-A and/or LM-B. Minimal data exists relating to *Mycobacteria*, except for diglycosyl diacylglycerol (194).

As it appears that an aberrant LM/LAM profile has no effect on growth rate, it may be that overall cell wall integrity is not grossly compromised suggesting that the truncated species observed in the mutant can substitute to a first approximation for mature LM/LAM. Indeed, HPTLC analysis of the PIMs, TMCM and TDCM showed no further change in the mutant, confirming that other cell wall components have not been affected. The study by Sena *et al.*(195) comparing MSMEG_4247 with WT showed similar levels of PIMs, phospholipids, TDM and glycopeptidolipids, with no clear morphological changes nor sensitivity to malachite green, SDS and crystal violet suggesting a lack of

any adverse effects on membrane structure and permeability as a result of replacing LM/LAM with a truncated LM.

A search of the literature revealed that an *mptA* mutant showed a remarkably similar phenotype to the one described here for the *NCgl2760* mutant (135). Disruption of *mptA* in *C. glutamicum* (*NCgl2093*) did not cause any growth defect and resulted in formation of a truncated LM that migrated similarly to the t-LM described in this chapter. Further analysis revealed that MptA is a PPM-dependent mannosyltransferase that elongates the main chain of LM following the initial elongation by MptB (196) and initial insertion of mannose side chains by Rv2181 (138). The striking similarity between the *mptA* and *NCgl2760* mutants raises the possibility that both are blocked at the same step in LM elongation. Whereas *NCgl2760* has no motifs that suggest its function, it may act by assisting the MptA mannosyltransferase to elongate LM intermediates, as described in more detail below. Such a role would explain the common phenotype observed in the two mutants. The apparent similarity between the two mutant phenotypes has allowed the position of *NCgl2760* within the LM/LAM biosynthetic pathway to be estimated (Figure 4.18).

To gain further insights into the possible function of *NCgl2760* and its likely orthologs Rv0227c and MSMEG_0317, we have searched for the closest homologues using the Protein Homology/analogy Recognition Engine (PHYRE; v0.2; Kelley and Sternberg, 2009). Analysis of the Rv0227c sequence by PHYRE2 (P. Crellin, personal communication) resulted in a model for 108 residues (from amino acid 126 to 266, 37% coverage) based on the lipoprotein LprF from *M. tuberculosis* (PDB accession number 4QA8; Kim et al, 2014). The homology model generated, based on the C-terminal region of Lprf, was assigned with >95% confidence. Considering that Rv0227c is predicted to be composed primarily of parallel beta sheets strands with one alpha helix at the C-terminal end, it is expected

that Rv0227c will have a similar fold to LprF and possibly a similar function. A similar search was performed for NCgl2760. Analysis of the sequence by PHYRE2 resulted in a model for 93 residues (from amino acid 92 to 185, 45% coverage) based again on the lipoprotein LprF from *M. tuberculosis*. In this case, the homology model generated, again based on the C-terminal region of Lprf, was assigned with 62.5% confidence.

The apparent structural similarities between NCgl2760/Rv0227 and LprF suggest that these proteins share common features and perform related functions. While the precise function of LprF is unknown, a homologous lipoprotein, LprG, is well studied. Both lipoproteins have a central hydrophobic cavity that binds glycolipids. Indeed, analysis of the crystallised LprF revealed the presence of an *E. coli* lipid (1,2-glycero-diacyl (C12:0/C15:1)-3-phospho-*myo*-inositol di-(L- β -D-heptose) in the hydrophobic pocket (197). Since *E. coli* contains only trace amounts of phosphatidylinositol (PI), this binding appeared to be highly specific, suggesting that LprF binds a PI-based lipid in its native host as well. This raises the possibility that NCgl2760/Rv0227 also binds a PI-based lipid, consistent with the phenotype of the NCgl2760 mutant in which synthesis of LM/LAM (both PI-based lipids) is blocked.

While little is known about LprF beyond its crystal structure, the closely related LprG has been well characterized. LprG expressed in *M. tuberculosis* binds to lipoglycans, particularly LAM, and a *lprG* null mutant has reduced levels of LAM on its surface resulting in a reduced capacity to inhibit phagosome-lysosome fusion (198). Authors of this work have suggested that LprG promotes LAM transfer from the plasma membrane to the cell envelope, essential to the pathogenesis of *M. tuberculosis* since surface-exposed LAM promotes *M. tuberculosis* survival in macrophages.

Based on the predicted structural similarities between NCgl2760/Rv0227 and the lipid binding proteins LprF and LprG, and the phenotypes of the *NCgl2760* mutant (presented here) and *lprG* mutant (198), it is proposed that NCgl2760/Rv0227 function as LM binding proteins. While the precise role is unclear, their capacity to bind LM intermediates appears essential for LM elongation, since the *NCgl2760* mutant was blocked at the t-LM step and failed to produce full-length LM or LAM. A likely substrate for binding is the t-LM intermediate itself. The apparently common phenotype of a *NCgl2760* mutant and a *mptA* mutant (135) also suggests that t-LM binding by NCgl2760 is essential for MptA-based elongation of t-LM. NCgl2760 may release t-LM from the membrane in a way that allows MptA to process it, although it is unclear why MptA would require NCgl2760 for this purpose since other PPM-dependent mannosyltransferases appear to process PIM/LM intermediates without the assistance of other proteins. One possibility is that MptA functions at the outer membrane and NCgl2760 is needed to bind then transfer t-LM from the inner membrane to interact with MptA. If this hypothesis is correct, it would lead to a significant revision of the current LM/LAM pathway.

An alternative scenario is that NCgl2760 binds the mannose donor PPM and donates this to MptA. Again, why MptA would require such a protein is unclear. However, this scenario would explain why *Rv0227* was unable to complement the *NCgl2760* mutant since PPMs from *Mycobacteria* and *Corynebacteria* are different in chain length and structure (112, 199) and *Rv0227* may not recognize the C₅₅ *C. glutamicum* PPM. Determination of the crystal structure of NCgl2760 and/or *Rv0227* and identification of the lipid(s) bound by these proteins should begin to answer some of these key questions about the role of NCgl2760/Rv0227 in the LM/LAM biosynthetic pathway.

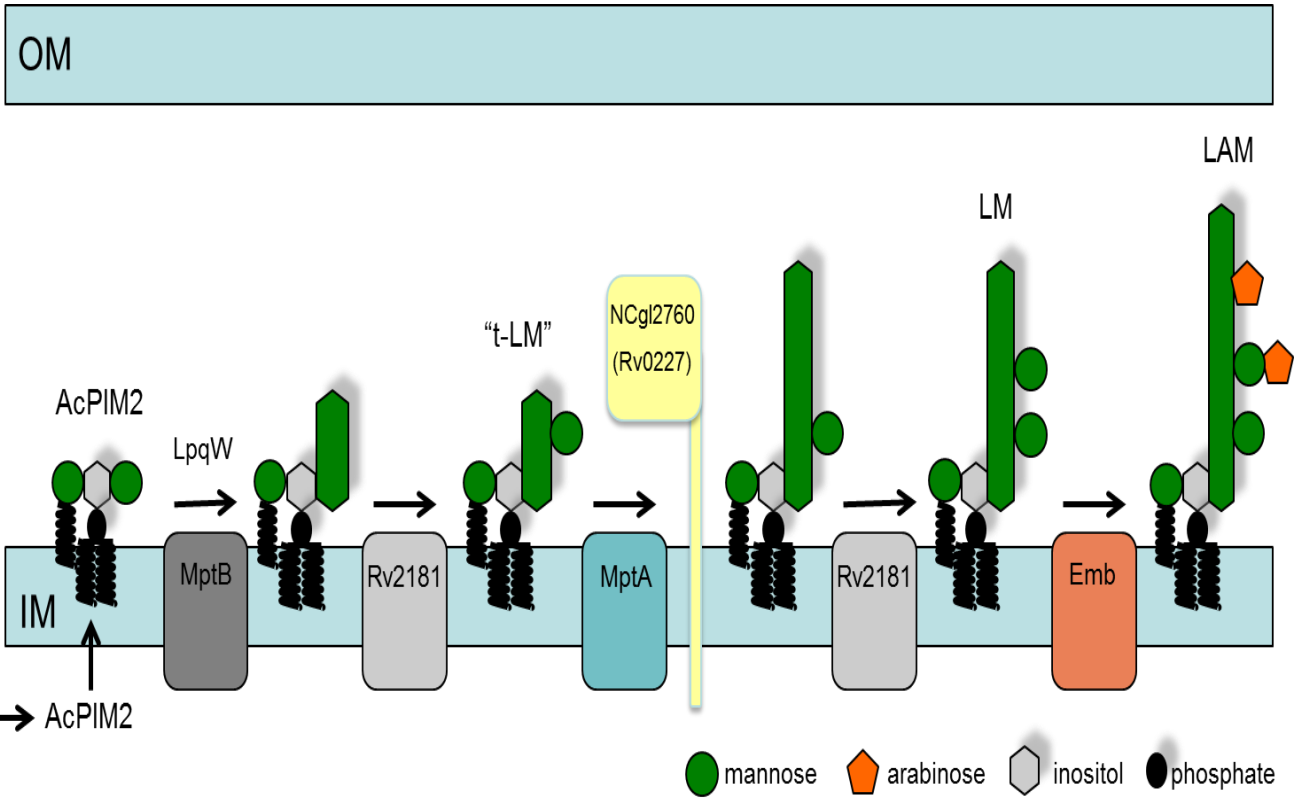


Figure 4.18

Figure 4.18. Proposed site of action of NCgl2760 in the *C. glutamicum* LM/LAM biosynthetic pathway. PIMs are formed on the cytoplasmic side of the inner membrane then transported to the periplasmic side. Here, a series of PPM-dependent membrane bound mannosyltransferases process AcPIM2 to form LMs. MptB and MptA elongate the main α 1-6 linked mannan chain while Rv2181 adds α 1-2 linked mannose side-branches following MptB and MptA elongation (Mishra, 2007; Mishra 2008). Finally, membrane arabinosyltransferases convert the LMs to LAMs. Based on the apparent similarity between the NCgl2760 mutant described in this chapter and the previously characterised *mptA* mutant (Mishra et al ref), membrane-anchored NCgl2760 (yellow) is postulated to act at the MptA step of LM elongation. OM, outer membrane; IM, inner membrane.

Chapter 5

Final Discussion

Current anti-tubercular medication regimes utilize 1st and 2nd line antibiotics to kill *M. tuberculosis* that have been in clinical use for many years. Not surprisingly therefore, there are now significant levels of resistance to these agents present in mycobacteria strains worldwide. Novel treatments targeting mycobacterial survival and metabolism that would kill the Mycobacterium, or affect its ability to cause disease, need to be developed as alternative therapies. They could be targeted at a small core number of metabolic processes such as DNA/ RNA synthesis, cell wall synthesis and processes (200), and energy metabolic pathways. However some of these are likely to use enzymatic machinery shared with the host, whereas others such as cell wall synthesis are likely to be unique to the pathogen. Whatever strategy for drug design is utilized, the relevant underlying target pathway(s) needs to be understood and the characterisation of unknown steps, within pathways of cell wall biosynthesis in this instance, was the focus of the research presented in this thesis.

In an attempt to understand such processes, the functions of proteins encoded by **two** previously unstudied genes, *NCgl2760* and *NCgl2761*, were investigated in this project. These were selected for analysis since they form part of a very interesting locus of genes in *C. glutamicum* comprising *NCgl2764*, *NCgl2762*, *NCgl2761*, *NCgl2760*, and *NCgl2759*, with likely orthologs named *Rv0224*, *Rv0225*, *Rv0226*, *Rv0227*, and *Rv0228*, respectively, in *M. tuberculosis*. Previous studies suggested that *NCgl2764*, *2762* and *2759* are required for the efficient transport of corynomycolic acids, in the form of trehalose monocorynomycolates (TMCM), across the plasma membrane. Indeed, the most well studied member of the locus, *NCgl2759*, was shown to be an acetyltransferase that produced acetyl-TMCM (AcTMCM), the optimal substrate for transport (46). This enzyme was designated TmaT. The other two proteins are also required for AcTMCM synthesis and transport, and their

precise functions are currently being investigated through the analysis of deletion mutants. A similar strategy involving gene deletion studies was employed here for the remaining two genes of the locus, *NCgl2760* and *NCgl2761*. Whereas *NCgl2761* was found to have a role in corynomycolate transport like other members of the locus, analysis of a *NCgl2670* mutant revealed normal TMCM transport and a block in an unrelated cell wall biosynthesis pathway that produces the major cell wall lipoglycans LM and LAM. This discovery was unexpected. Therefore it appears that while this new locus is involved in cell wall synthesis, it is not restricted to just one biosynthetic pathway as previously thought. In addition, RT-PCR studies showed that *NCgl2760* and *NCgl2671* are co-transcribed, despite their protein products functioning in two different cell wall pathways. This finding raises the possibility of links between two pathways previously considered to be independent and unrelated. This might be due to a need to co-ordinate synthesis of mycolic acids and LAMs in dividing bacteria. If so, it may be that these two enzymes catalyse key regulatory steps in their corresponding synthetic pathways. Further studies in which the promoter for these two genes is altered to be up and downregulated may lead to interesting cell wall mutants.

Although the results of this study suggest that *NCgl2760* and *NCgl2761* function in two pathways of cell wall synthesis, their precise functions within the pathways remain unknown. These proteins, all being encoded by the same genetic locus, could form complexes with one another. *NCgl2761* and *NCgl2759*, the two integral membrane proteins of the group, might serve to anchor such a complex within the cell membrane thus placing it in the necessary position to perform its function (201). Each protein may be an essential part of such a complex, with loss of any one component leading to the collapse of the entire structure. Such a scenario would explain why so many of these mutants share a common phenotype. For example, *NCgl2761*, with its 10 transmembrane helices, may act as the anchor of the putative complex and/or stabilise *NCgl2759* (TmaT) allowing it to perform its function as the TMCM acetyltransferase. Other key membrane proteins such as MmpLs (mycobacterial

membrane protein large) and CmpLs (corynebacterial membrane protein large) may also act as scaffolds on the cell membrane for localisation of biosynthetic pathways facilitating metabolite transport.

The putative scaffold could be an ideal environment for the biosynthetic pathway forming TMCM and TDCM which involves a progressive synthesis from the inner cytoplasmic leaflet to the outer leaflet and periplasm. This is enabled by the MmpL3 transporter in Mycobacteria, and the NCgl0228 and NCgl2769 transporters in Corynebacteria. This transport appears to be regulated by acetylation of TMCM by NCgl2759, or TMCM mycolyl acetyltransferase (TmaT) (46). Our current working model predicts that AcTMCM is transported to the outer membrane where it is deacetylated by an unknown enzyme, then is either linked to arabinogalactan or converted to TDCM by a series of mycolyltransferases.

NCgl2759 (TmaT), NCgl2762 and NCgl2764 have all been shown to have roles in mycolic acid synthesis. The first is an acyltransferase with nine transmembrane domains, NCgl2762 is predicted to be a cytoplasmic glycosyltransferase, and NCgl2764 is also a cytoplasmic protein but has the characteristics of a methyltransferase. This project has found NCgl2761, a membrane protein, to also be involved in corynomycolic acid synthesis. Loss of any of these proteins delays transition of TMCM to TDCM in the mid-log phase and causes a delayed growth rate. NCgl2761 appears to be involved in transporting AcTMCM across the plasma membrane. Already, NCgl0228 and NCgl2769 have been found to be the transporters responsible for this reaction, suggesting that the other proteins have roles related to, but separate from, the transport step itself, eg. the formation of the optimal transport substrate AcTMCM.. Since the synthetic drug AU1235 inhibits mycobacteria by blocking

TMCM transport, the ortholog of NCgl2761 in *M. tuberculosis*, Rv0226, could also be considered a potential drug target for this devastating human pathogen if it is involved in the same process.

In complete contrast to the findings described for NCgl2761, this study has revealed a role for NCgl2760 in lipoglycan synthesis in *C. glutamicum*. Although its precise function is not yet known, the mutant strain produced in this study has a very clear blockage in the LM/LAM pathway at a step upstream of the formation of LM-A and LM-B. NCgl2760 has no motifs indicating its function but does have a signal sequence and one likely transmembrane domain, strongly suggesting that it is membrane-anchored with the bulk of the protein located in the periplasm. This location fits well with the known steps of LM biosynthesis that involve periplasmic mannosyltransferases such as MptA and MptB that rely on the periplasmic lipid-linked mannose donor, PPM, for activity (135, 196). One possibility is that NCgl2760 is required for the optimal activity of one or more of these mannosyltransferases, either by acting as a chaperone for the enzyme or by assisting the mannosyltransferase to access either its glycolipid substrate or the mannose donor PPM. Intriguingly, an *mptA* mutant of *C. glutamicum* produces a truncated LM (135) of ~10 kDa that migrates similarly on SDS-PAGE gels to the truncated LM shown to accumulate here in the *NCgl2760* mutant, raising the possibility that NCgl2760 is needed for MptA activity. This possibility is currently being investigated in our laboratory by the production of a *C. glutamicum mptA* mutant for direct comparison to the *NCgl2760* mutant described here.

Structural modelling of NCgl2760 and its mycobacterial orthologs has revealed similarities with the lipid binding lipoproteins LprF and LprG, the latter of which binds LAM and has been proposed to shuttle these lipoglycans from the inner membrane to the cell surface in *M. tuberculosis* (198). This raises the possibility that NCgl2760 also binds a glycolipid, with t-LM and PPM being the most likely

candidates. NCgl2760 binding of either of these lipids may be necessary for subsequent elongation of t-LM by MptA using PPM as the source of mannose. Experiments aimed at determining the crystal structure of this protein are currently underway, along with the identification of any bound lipid, to provide further insights into the role of NCgl2760.

Since LM and LAM are considered to be the Corynebacterineae equivalent of lipopolysaccharide (LPS) in gram-negative bacteria, it is tempting to speculate that NCgl2760 may have a similar role to a component of the LPS biosynthetic pathway of other bacteria. In function, the LPS controls permeability, including antibiotic resistance, as well as serving as a virulence factor by activating the innate immune system upon host infection (202). Thus, LM/LAM and the LPS are notably alike with both being situated on the outer cell surface and serving as immunogens. As it progresses through the stages of development, LPS passes from one Lpt protein to the next and finally reaches the outer-membrane-attached complex LptD-LptE (203, 204). So in a similar manner NCgl2760 may anchor an equivalent complex of proteins involved in transferring LM to the outer membrane, analogous to the LptC lipoprotein. This scenario would suggest that MptA is located in the outer membrane and requires NCgl2760 and other proteins to bind then shuttle its substrate(s) across to the outer membrane for elongation.

In this study, a phenotype involving production of a highly truncated LM has been described in Corynebacteria via deletion of the *NCgl2760* gene. Previous studies in our and other laboratories have shown that, while essential *M. tuberculosis* cell wall biosynthesis genes can be disrupted in *C. glutamicum* to give viable mutants (46, 84), these mutants usually have significant growth defects. The lack of such a defect described here for the NCgl2760 mutant raises the possibility that the equivalent gene in a Mycobacterium species might be non-essential. It would be of great significance

if a knockout mutant of the equivalent gene could be produced in a Mycobacterium, for example, *MSMEG_0317* in *M. smegmatis*. This might be possible if the truncated LM was able to substitute for mature LM and LAM within the cell wall, as seems to be the case in the *C. glutamicum* NCgl2760 mutant which grows normally despite lacking LM-A, LM-B and LAM. Efforts to produce such a *M. smegmatis* mutant are currently underway. If they are successful it raises the question as to whether this protein may not be a useful drug target. Certainly, it would not be a conventional bacteriocidal agent but it may be bacteriostatic or may lead to decreased disease in the host as the immunogenic and immune evading LAM molecules would be absent in their mature forms.

In order to identify the complexes proposed here between the respective protein products, protein-protein interactions between all proteins encoded by the locus could be investigated. It will be particularly interesting to investigate a NCgl2760-NCgl2761 interaction since the RT-PCR studies indicated co-transcription. As part of this study, bacterial two-hybrid experiments were commenced by cloning the various genes into pKT25 and pUT18 vectors (205). While initial results indicated a positive interaction between NCgl2761 and NCgl2760, the plasmids were unstable and the results were not reproducible. These studies could not be followed up more thoroughly as time did not permit. In parallel, Blue Native PAGE electrophoresis could also be performed to try and identify complexes. To date, analysis of biosynthetic and metabolic pathways has been the method of investigating the functions of NCgl2760 and NCgl2761. Although neither protein shares significant similarity with known proteins, determination of crystal structures could reveal structural matches that are not apparent at the amino acid level to provide clues regarding protein function which in turn will give a clearer, more precise idea of protein function. While crystallisation of NCgl2761 is unlikely to be successful due to its extremely hydrophobic nature, the expression, purification and crystallisation of the periplasmic domain of NCgl2760 is currently underway.

In summary, the studies described in this thesis have revealed two new cell wall biosynthesis proteins in *C. glutamicum*, NCgl2760 and NCgl2761, which, despite being encoded by adjacent genes, function in two pathways previously thought to be independent of one another. Moreover, the findings are novel as RT-PCR suggests that their genes are co-transcribed, creating an unusual (if not unique?) relationship between the mycolic acid and glycolipid biosynthetic pathways. Since the equivalent genes in *M. tuberculosis* are both reported to be essential for growth of the human pathogen, their protein products could be considered targets for future drug development.

References

1. Stackebrandt E. Towards a strategy to enhance access to microbial diversity. *Int J Syst Evol Microbiol.* 2011 Mar;61(Pt 3):479-81.
2. Wendisch VF. Microbial production of amino acids and derived chemicals: synthetic biology approaches to strain development. *Curr Opin Biotechnol.* 2014 Dec;30:51-8.
3. Salgame P, Geadas C, Collins L, Jones-Lopez E, Ellner JJ. Latent tuberculosis infection--Revisiting and revising concepts. *Tuberculosis (Edinb).* 2015 Jul;95(4):373-84.
4. Wejse C, Gustafson P, Nielsen J, Gomes VF, Aaby P, Andersen PL, et al. TBscore: Signs and symptoms from tuberculosis patients in a low-resource setting have predictive value and may be used to assess clinical course. *Scand J Infect Dis.* 2008;40(2):111-20.
5. Feleke Y, Abdulkadir J, Aderaye G. Prevalence and clinical features of tuberculosis in Ethiopian diabetic patients. *East Afr Med J.* 1999 Jul;76(7):361-4.
6. Munoz L, Stagg HR, Abubakar I. Diagnosis and Management of Latent Tuberculosis Infection. *Cold Spring Harb Perspect Med.* 2015 Jun 8.
7. Assari R, Ziaee V, Ahmadinejad Z, Vasei M, Moradinejad MH. Caseous granuloma: tuberculosis or chronic recurrent multifocal osteomyelitis? *Iran J Pediatr.* 2014 Dec;24(6):770-4.
8. Salgame P. MMPs in tuberculosis: granuloma creators and tissue destroyers. *J Clin Invest.* 2011 May;121(5):1686-8.
9. Algood HM, Lin PL, Flynn JL. Tumor necrosis factor and chemokine interactions in the formation and maintenance of granulomas in tuberculosis. *Clin Infect Dis.* 2005 Aug 1;41 Suppl 3:S189-93.
10. Organization WH. *A Manual for Medical Students* 2003.
11. Facchini L, Venturini E, Galli L, Martino M, Chiappini E. Vitamin D and tuberculosis: a review on a hot topic. *J Chemother.* 2015 Jun;27(3):128-38.

12. Velayati AA, Masjedi MR, Farnia P, Tabarsi P, Ghanavi J, Ziazarifi AH, et al. Emergence of new forms of totally drug-resistant tuberculosis bacilli: super extensively drug-resistant tuberculosis or totally drug-resistant strains in iran. *Chest*. 2009 Aug;136(2):420-5.
13. Organization WH. "Totally Drug Resistant" tuberculosis: a WHO consultation on the diagnostic definition and treatment options 2012.
14. Kamath S, Vaccaro SA, Rea TH, Ochoa MT. Recognizing and managing the immunologic reactions in leprosy. *J Am Acad Dermatol*. 2014 Oct;71(4):795-803.
15. Portaels F, Chemlal K, Elsen P, Johnson PD, Hayman JA, Hibble J, et al. *Mycobacterium ulcerans* in wild animals. *Rev Sci Tech*. 2001 Apr;20(1):252-64.
16. Stinear TP, Mve-Obiang A, Small PL, Frigui W, Pryor MJ, Brosch R, et al. Giant plasmid-encoded polyketide synthases produce the macrolide toxin of *Mycobacterium ulcerans*. *Proc Natl Acad Sci U S A*. 2004 Feb 3;101(5):1345-9.
17. Horsburgh CR, Jr. *Mycobacterium avium* complex infection in the acquired immunodeficiency syndrome. *N Engl J Med*. 1991 May 9;324(19):1332-8.
18. Horsburgh CR, Jr., Gettings J, Alexander LN, Lennox JL. Disseminated *Mycobacterium avium* complex disease among patients infected with human immunodeficiency virus, 1985-2000. *Clin Infect Dis*. 2001 Dec 1;33(11):1938-43.
19. Fowler J, Mahlen SD. Localized cutaneous infections in immunocompetent individuals due to rapidly growing mycobacteria. *Arch Pathol Lab Med*. 2014 Aug;138(8):1106-9.
20. Kaur P, Ghosh A, Krishnamurthy RV, Bhattacharjee DG, Achar V, Datta S, et al. A high-throughput cardinality screen for mycobacterium tuberculosis. *PLoS One*. 2015;10(2):e0117577.
21. Funke G, von Graevenitz A, Clarridge JE, 3rd, Bernard KA. Clinical microbiology of coryneform bacteria. *Clin Microbiol Rev*. 1997 Jan;10(1):125-59.
22. Peel MM, Palmer GG, Stacpoole AM, Kerr TG. Human lymphadenitis due to *Corynebacterium pseudotuberculosis*: report of ten cases from Australia and review. *Clin Infect Dis*. 1997 Feb;24(2):185-91.

23. Join-Lambert OF, Ouache M, Canioni D, Beretti JL, Blanche S, Berche P, et al. *Corynebacterium pseudotuberculosis* necrotizing lymphadenitis in a twelve-year-old patient. *Pediatr Infect Dis J*. 2006 Sep;25(9):848-51.
24. Zahoor A, Lindner SN, Wendisch VF. Metabolic engineering of *Corynebacterium glutamicum* aimed at alternative carbon sources and new products. *Comput Struct Biotechnol J*. 2012;3:e201210004.
25. Dauendorffer JN, Guillemin I, Aubry A, Truffot-Pernot C, Sougakoff W, Jarlier V, et al. Identification of mycobacterial species by PCR sequencing of quinolone resistance-determining regions of DNA gyrase genes. *J Clin Microbiol*. 2003 Mar;41(3):1311-5.
26. Glickman MS, Jacobs WR, Jr. Microbial pathogenesis of *Mycobacterium tuberculosis*: dawn of a discipline. *Cell*. 2001 Feb 23;104(4):477-85.
27. Daffe M, Brennan PJ, McNeil M. Predominant structural features of the cell wall arabinogalactan of *Mycobacterium tuberculosis* as revealed through characterization of oligoglycosyl alditol fragments by gas chromatography/mass spectrometry and by ¹H and ¹³C NMR analyses. *J Biol Chem*. 1990 Apr 25;265(12):6734-43.
28. Dover LG, Cerdeno-Tarraga AM, Pallen MJ, Parkhill J, Besra GS. Comparative cell wall core biosynthesis in the mycolated pathogens, *Mycobacterium tuberculosis* and *Corynebacterium diphtheriae*. *FEMS Microbiol Rev*. 2004 May;28(2):225-50.
29. Hoffmann C, Leis A, Niederweis M, Plitzko JM, Engelhardt H. Disclosure of the mycobacterial outer membrane: cryo-electron tomography and vitreous sections reveal the lipid bilayer structure. *Proc Natl Acad Sci U S A*. 2008 Mar 11;105(10):3963-7.
30. Brennan PJ, Nikaido H. The envelope of mycobacteria. *Annu Rev Biochem*. 1995;64:29-63.
31. Imai T, Kageyama Y, Tobar J. *Mycobacterium smegmatis* malate dehydrogenase: activation of the lipid-depleted enzyme by anionic phospholipids and phosphatidylethanolamine. *Biochim Biophys Acta*. 1995 Jan 19;1246(2):189-96.

32. Crick DC, Mahapatra S, Brennan PJ. Biosynthesis of the arabinogalactan-peptidoglycan complex of *Mycobacterium tuberculosis*. *Glycobiology*. 2001 Sep;11(9):107R-18R.
33. McNeil M, Daffe M, Brennan PJ. Evidence for the nature of the link between the arabinogalactan and peptidoglycan of mycobacterial cell walls. *J Biol Chem*. 1990 Oct 25;265(30):18200-6.
34. Minnikin DE, Minnikin SM, Goodfellow M, Stanford JL. The mycolic acids of *Mycobacterium chelonae*. *J Gen Microbiol*. 1982 Apr;128(4):817-22.
35. Takayama K, Wang C, Besra GS. Pathway to synthesis and processing of mycolic acids in *Mycobacterium tuberculosis*. *Clin Microbiol Rev*. 2005 Jan;18(1):81-101.
36. Brennan PJ. Structure, function, and biogenesis of the cell wall of *Mycobacterium tuberculosis*. *Tuberculosis (Edinb)*. 2003;83(1-3):91-7.
37. Venisse A, Riviere M, Vercauteren J, Puzo G. Structural analysis of the mannan region of lipoarabinomannan from *Mycobacterium bovis* BCG. Heterogeneity in phosphorylation state. *J Biol Chem*. 1995 Jun 23;270(25):15012-21.
38. Vercellone A, Nigou J, Puzo G. Relationships between the structure and the roles of lipoarabinomannans and related glycoconjugates in tuberculosis pathogenesis. *Front Biosci*. 1998 Aug 6;3:e149-63.
39. Besra GS, Morehouse CB, Rittner CM, Waechter CJ, Brennan PJ. Biosynthesis of mycobacterial lipoarabinomannan. *J Biol Chem*. 1997 Jul 18;272(29):18460-6.
40. Morita YS, Patterson JH, Billman-Jacobe H, McConville MJ. Biosynthesis of mycobacterial phosphatidylinositol mannosides. *Biochem J*. 2004 Mar 1;378(Pt 2):589-97.
41. Chatterjee D, Hunter SW, McNeil M, Brennan PJ. Lipoarabinomannan. Multiglycosylated form of the mycobacterial mannosylphosphatidylinositols. *J Biol Chem*. 1992 Mar 25;267(9):6228-33.
42. Kremer L, Gurcha SS, Bifani P, Hitchen PG, Baulard A, Morris HR, et al. Characterization of a putative alpha-mannosyltransferase involved in phosphatidylinositol trimannoside biosynthesis in *Mycobacterium tuberculosis*. *Biochem J*. 2002 May 1;363(Pt 3):437-47.

43. Daffe M, Etienne G. The capsule of *Mycobacterium tuberculosis* and its implications for pathogenicity. *Tuber Lung Dis.* 1999;79(3):153-69.
44. Bansal-Mutalik R, Nikaido H. Mycobacterial outer membrane is a lipid bilayer and the inner membrane is unusually rich in diacyl phosphatidylinositol dimannosides. *Proc Natl Acad Sci U S A.* 2014 Apr 1;111(13):4958-63.
45. Daffe M, Draper P. The envelope layers of mycobacteria with reference to their pathogenicity. *Adv Microb Physiol.* 1998;39:131-203.
46. Yamaro-Botte Y, Rainczuk AK, Lea-Smith DJ, Brammananth R, van der Peet PL, Meikle P, et al. Acetylation of trehalose mycolates is required for efficient MmpL-mediated membrane transport in *Corynebacterineae*. *ACS Chem Biol.* 2015 Mar 20;10(3):734-46.
47. Schroeder EK, de Souza N, Santos DS, Blanchard JS, Basso LA. Drugs that inhibit mycolic acid biosynthesis in *Mycobacterium tuberculosis*. *Curr Pharm Biotechnol.* 2002 Sep;3(3):197-225.
48. Adam A, Petit JF, Wietzerbin-Falszpan J, Sinay P, Thomas DW, Lederer E. *FEBS Lett.* 1969 Jul;4(2):87-92.
49. Favrot L, Ronning DR. Targeting the mycobacterial envelope for tuberculosis drug development. *Expert Rev Anti Infect Ther.* 2012 Sep;10(9):1023-36.
50. Bhamidi S, Scherman MS, Rithner CD, Prenni JE, Chatterjee D, Khoo KH, et al. The identification and location of succinyl residues and the characterization of the interior arabinan region allow for a model of the complete primary structure of *Mycobacterium tuberculosis* mycolyl arabinogalactan. *J Biol Chem.* 2008 May 9;283(19):12992-3000.
51. Lee RE, Li W, Chatterjee D. Rapid structural characterization of the arabinogalactan and lipoarabinomannan in live mycobacterial cells using 2D and 3D HR-MAS NMR: structural changes in the arabinan due to ethambutol treatment and gene mutation are observed. *Glycobiology.* 2005 Feb;15(2):139-51.
52. Besra GS, Khoo KH, McNeil MR, Dell A, Morris HR, Brennan PJ. A new interpretation of the structure of the mycolyl-arabinogalactan complex of *Mycobacterium tuberculosis* as revealed

through characterization of oligoglycosylalditol fragments by fast-atom bombardment mass spectrometry and ¹H nuclear magnetic resonance spectroscopy. *Biochemistry (Mosc)*. 1995 Apr 4;34(13):4257-66.

53. Alderwick LJ, Birch HL, Mishra AK, Eggeling L, Besra GS. Structure, function and biosynthesis of the *Mycobacterium tuberculosis* cell wall: arabinogalactan and lipoarabinomannan assembly with a view to discovering new drug targets. *Biochem Soc Trans*. 2007 Nov;35(Pt 5):1325-8.

54. Minnikin DE, Kremer L, Dover LG, Besra GS. The methyl-branched fortifications of *Mycobacterium tuberculosis*. *Chem Biol*. 2002 May;9(5):545-53.

55. Alderwick LJ, Radmacher E, Seidel M, Gande R, Hitchen PG, Morris HR, et al. Deletion of Cg-emb in corynebacteriaceae leads to a novel truncated cell wall arabinogalactan, whereas inactivation of Cg-ubiA results in an arabinan-deficient mutant with a cell wall galactan core. *J Biol Chem*. 2005 Sep 16;280(37):32362-71.

56. Skovierova H, Larrouy-Maumus G, Zhang J, Kaur D, Barilone N, Kordulakova J, et al. AftD, a novel essential arabinofuranosyltransferase from mycobacteria. *Glycobiology*. 2009 Nov;19(11):1235-47.

57. Mikusova K, Slayden RA, Besra GS, Brennan PJ. Biogenesis of the mycobacterial cell wall and the site of action of ethambutol. *Antimicrob Agents Chemother*. 1995 Nov;39(11):2484-9.

58. Alderwick LJ, Seidel M, Sahm H, Besra GS, Eggeling L. Identification of a novel arabinofuranosyltransferase (AftA) involved in cell wall arabinan biosynthesis in *Mycobacterium tuberculosis*. *J Biol Chem*. 2006 Jun 9;281(23):15653-61.

59. Seidel M, Alderwick LJ, Birch HL, Sahm H, Eggeling L, Besra GS. Identification of a novel arabinofuranosyltransferase AftB involved in a terminal step of cell wall arabinan biosynthesis in *Corynebacteriaceae*, such as *Corynebacterium glutamicum* and *Mycobacterium tuberculosis*. *J Biol Chem*. 2007 May 18;282(20):14729-40.

60. Birch HL, Alderwick LJ, Appelmelk BJ, Maaskant J, Bhatt A, Singh A, et al. A truncated lipoglycan from mycobacteria with altered immunological properties. *Proc Natl Acad Sci U S A*. 2010 Feb 9;107(6):2634-9.
61. Radmacher E, Stansen KC, Besra GS, Alderwick LJ, Maughan WN, Hollweg G, et al. Ethambutol, a cell wall inhibitor of *Mycobacterium tuberculosis*, elicits L-glutamate efflux of *Corynebacterium glutamicum*. *Microbiology*. 2005 May;151(Pt 5):1359-68.
62. Escuyer VE, Lety MA, Torrelles JB, Khoo KH, Tang JB, Rithner CD, et al. The role of the embA and embB gene products in the biosynthesis of the terminal hexaarabinofuranosyl motif of *Mycobacterium smegmatis* arabinogalactan. *J Biol Chem*. 2001 Dec 28;276(52):48854-62.
63. Zhang N, Torrelles JB, McNeil MR, Escuyer VE, Khoo KH, Brennan PJ, et al. The Emb proteins of mycobacteria direct arabinosylation of lipoarabinomannan and arabinogalactan via an N-terminal recognition region and a C-terminal synthetic region. *Mol Microbiol*. 2003 Oct;50(1):69-76.
64. Alahari A, Trivelli X, Guerardel Y, Dover LG, Besra GS, Sacchetti JC, et al. Thiacetazone, an antitubercular drug that inhibits cyclopropanation of cell wall mycolic acids in mycobacteria. *PLoS One*. 2007;2(12):e1343.
65. Jackson M, Raynaud C, Laneelle MA, Guilhot C, Laurent-Winter C, Ensergueix D, et al. Inactivation of the antigen 85C gene profoundly affects the mycolate content and alters the permeability of the *Mycobacterium tuberculosis* cell envelope. *Mol Microbiol*. 1999 Mar;31(5):1573-87.
66. Huc E, Meniche X, Benz R, Bayan N, Ghazi A, Tropis M, et al. O-mycoloylated proteins from *Corynebacterium*: an unprecedented post-translational modification in bacteria. *J Biol Chem*. 2010 Jul 16;285(29):21908-12.
67. Tropis M, Meniche X, Wolf A, Gebhardt H, Strelkov S, Chami M, et al. The crucial role of trehalose and structurally related oligosaccharides in the biosynthesis and transfer of mycolic acids in *Corynebacterineae*. *J Biol Chem*. 2005 Jul 15;280(28):26573-85.

68. Barry CE, 3rd, Lee RE, Mdluli K, Sampson AE, Schroeder BG, Slayden RA, et al. Mycolic acids: structure, biosynthesis and physiological functions. *Prog Lipid Res.* 1998 Jul-Aug;37(2-3):143-79.
69. Goude R, Parish T. The genetics of cell wall biosynthesis in *Mycobacterium tuberculosis*. *Future Microbiol.* 2008 Jun;3(3):299-313.
70. Barkan D, Hedhli D, Yan HG, Huygen K, Glickman MS. *Mycobacterium tuberculosis* lacking all mycolic acid cyclopropanation is viable but highly attenuated and hyperinflammatory in mice. *Infect Immun.* 2012 Jun;80(6):1958-68.
71. Glickman MS. The *mmaA2* gene of *Mycobacterium tuberculosis* encodes the distal cyclopropane synthase of the alpha-mycolic acid. *J Biol Chem.* 2003 Mar 7;278(10):7844-9.
72. Glickman MS, Cahill SM, Jacobs WR, Jr. The *Mycobacterium tuberculosis cmaA2* gene encodes a mycolic acid trans-cyclopropane synthetase. *J Biol Chem.* 2001 Jan 19;276(3):2228-33.
73. Behr MA, Schroeder BG, Brinkman JN, Slayden RA, Barry CE, 3rd. A point mutation in the *mma3* gene is responsible for impaired methoxymycolic acid production in *Mycobacterium bovis* BCG strains obtained after 1927. *J Bacteriol.* 2000 Jun;182(12):3394-9.
74. Dubnau E, Chan J, Raynaud C, Mohan VP, Laneelle MA, Yu K, et al. Oxygenated mycolic acids are necessary for virulence of *Mycobacterium tuberculosis* in mice. *Mol Microbiol.* 2000 May;36(3):630-7.
75. Julian E, Roldan M, Sanchez-Chardi A, Astola O, Agusti G, Luquin M. Microscopic cords, a virulence-related characteristic of *Mycobacterium tuberculosis*, are also present in nonpathogenic mycobacteria. *J Bacteriol.* 2010 Apr;192(7):1751-60.
76. Nakao H, Matsunaga I, Morita D, Aboshi T, Harada T, Nakagawa Y, et al. Mycolyltransferase from *Mycobacterium leprae* excludes mycolate-containing glycolipid substrates. *J Biochem.* 2009 Nov;146(5):659-65.
77. Crellin PK. Metabolism of Plasma Membrane Lipids in Mycobacteria and Corynebacteria. In: Baez RV, editor. *Lipid Metabolism: Intech Open Minds*; 2013. p. 472.

78. Choi KH, Kremer L, Besra GS, Rock CO. Identification and substrate specificity of beta - ketoacyl (acyl carrier protein) synthase III (mtFabH) from *Mycobacterium tuberculosis*. *J Biol Chem*. 2000 Sep 8;275(36):28201-7.
79. Banerjee A, Dubnau E, Quemard A, Balasubramanian V, Um KS, Wilson T, et al. inhA, a gene encoding a target for isoniazid and ethionamide in *Mycobacterium tuberculosis*. *Science*. 1994 Jan 14;263(5144):227-30.
80. Takayama K, Qureshi N. Isolation and characterization of the monounsaturated long chain fatty acids of *Mycobacterium tuberculosis*. *Lipids*. 1978 Sep;13(9):575-9.
81. Portevin D, De Sousa-D'Auria C, Houssin C, Grimaldi C, Chami M, Daffe M, et al. A polyketide synthase catalyzes the last condensation step of mycolic acid biosynthesis in mycobacteria and related organisms. *Proc Natl Acad Sci U S A*. 2004 Jan 6;101(1):314-9.
82. Trivedi OA, Arora P, Sridharan V, Tickoo R, Mohanty D, Gokhale RS. Enzymic activation and transfer of fatty acids as acyl-adenylates in mycobacteria. *Nature*. 2004 Mar 25;428(6981):441-5.
83. Portevin D, de Sousa-D'Auria C, Montrozier H, Houssin C, Stella A, Laneelle MA, et al. The acyl-AMP ligase FadD32 and AccD4-containing acyl-CoA carboxylase are required for the synthesis of mycolic acids and essential for mycobacterial growth: identification of the carboxylation product and determination of the acyl-CoA carboxylase components. *J Biol Chem*. 2005 Mar 11;280(10):8862-74.
84. Lea-Smith DJ, Pyke JS, Tull D, McConville MJ, Coppel RL, Crellin PK. The reductase that catalyzes mycolic motif synthesis is required for efficient attachment of mycolic acids to arabinogalactan. *J Biol Chem*. 2007 Apr 13;282(15):11000-8.
85. Grzegorzewicz AE, Pham H, Gundi VA, Scherman MS, North EJ, Hess T, et al. Inhibition of mycolic acid transport across the *Mycobacterium tuberculosis* plasma membrane. *Nat Chem Biol*. 2012 Apr;8(4):334-41.
86. Tahlan K, Wilson R, Kastrinsky DB, Arora K, Nair V, Fischer E, et al. SQ109 targets MmpL3, a membrane transporter of trehalose monomycolate involved in mycolic acid donation to the cell wall core of *Mycobacterium tuberculosis*. *Antimicrob Agents Chemother*. 2012 Apr;56(4):1797-809.

87. La Rosa V, Poce G, Canseco JO, Buroni S, Pasca MR, Biava M, et al. MmpL3 is the cellular target of the antitubercular pyrrole derivative BM212. *Antimicrob Agents Chemother.* 2012 Jan;56(1):324-31.
88. Kamp F, Hamilton JA. How fatty acids of different chain length enter and leave cells by free diffusion. *Prostaglandins Leukot Essent Fatty Acids.* 2006 Sep;75(3):149-59.
89. Varela C, Rittmann D, Singh A, Krumbach K, Bhatt K, Eggeling L, et al. MmpL genes are associated with mycolic acid metabolism in mycobacteria and corynebacteria. *Chem Biol.* 2012 Apr 20;19(4):498-506.
90. Kacem R, De Sousa-D'Auria C, Tropis M, Chami M, Gounon P, Leblon G, et al. Importance of mycolyltransferases on the physiology of *Corynebacterium glutamicum*. *Microbiology.* 2004 Jan;150(Pt 1):73-84.
91. Belisle JT, Vissa VD, Sievert T, Takayama K, Brennan PJ, Besra GS. Role of the major antigen of *Mycobacterium tuberculosis* in cell wall biogenesis. *Science.* 1997 May 30;276(5317):1420-2.
92. Salman M, Brennan PJ, Lonsdale JT. Synthesis of mycolic acids of mycobacteria: an assessment of the cell-free system in light of the whole genome. *Biochim Biophys Acta.* 1999 Mar 25;1437(3):325-32.
93. Brand S, Niehaus K, Puhler A, Kalinowski J. Identification and functional analysis of six mycolyltransferase genes of *Corynebacterium glutamicum* ATCC 13032: the genes *cop1*, *cmt1*, and *cmt2* can replace each other in the synthesis of trehalose dicorynomycolate, a component of the mycolic acid layer of the cell envelope. *Arch Microbiol.* 2003 Jul;180(1):33-44.
94. Marchand CH, Salmeron C, Bou Raad R, Meniche X, Chami M, Masi M, et al. Biochemical disclosure of the mycolate outer membrane of *Corynebacterium glutamicum*. *J Bacteriol.* 2012 Feb;194(3):587-97.
95. Kalscheuer R, Weinrick B, Veeraraghavan U, Besra GS, Jacobs WR, Jr. Trehalose-recycling ABC transporter LpqY-SugA-SugB-SugC is essential for virulence of *Mycobacterium tuberculosis*. *Proc Natl Acad Sci U S A.* 2010 Dec 14;107(50):21761-6.

96. Doz E, Rose S, Court N, Front S, Vasseur V, Charron S, et al. Mycobacterial phosphatidylinositol mannosides negatively regulate host Toll-like receptor 4, MyD88-dependent proinflammatory cytokines, and TRIF-dependent co-stimulatory molecule expression. *J Biol Chem.* 2009 Aug 28;284(35):23187-96.
97. Rhoades ER, Archambault AS, Greendyke R, Hsu FF, Streeter C, Byrd TF. Mycobacterium abscessus Glycopeptidolipids mask underlying cell wall phosphatidyl-myo-inositol mannosides blocking induction of human macrophage TNF-alpha by preventing interaction with TLR2. *J Immunol.* 2009 Aug 1;183(3):1997-2007.
98. Fischer K, Scotet E, Niemeyer M, Koebernick H, Zerrahn J, Maillet S, et al. Mycobacterial phosphatidylinositol mannoside is a natural antigen for CD1d-restricted T cells. *Proc Natl Acad Sci U S A.* 2004 Jul 20;101(29):10685-90.
99. Driessen NN, Ummels R, Maaskant JJ, Gurcha SS, Besra GS, Ainge GD, et al. Role of phosphatidylinositol mannosides in the interaction between mycobacteria and DC-SIGN. *Infect Immun.* 2009 Oct;77(10):4538-47.
100. Guerin ME, Schaeffer F, Chaffotte A, Gest P, Giganti D, Kordulakova J, et al. Substrate-induced conformational changes in the essential peripheral membrane-associated mannosyltransferase PimA from mycobacteria: implications for catalysis. *J Biol Chem.* 2009 Aug 7;284(32):21613-25.
101. Hunter SW, Brennan PJ. Evidence for the presence of a phosphatidylinositol anchor on the lipoarabinomannan and lipomannan of *Mycobacterium tuberculosis*. *J Biol Chem.* 1990 Jun 5;265(16):9272-9.
102. Pitarque S, Larrouy-Maumus G, Payre B, Jackson M, Puzo G, Nigou J. The immunomodulatory lipoglycans, lipoarabinomannan and lipomannan, are exposed at the mycobacterial cell surface. *Tuberculosis (Edinb).* 2008 Nov;88(6):560-5.
103. Chatterjee D, Khoo KH. Mycobacterial lipoarabinomannan: an extraordinary lipoheteroglycan with profound physiological effects. *Glycobiology.* 1998 Feb;8(2):113-20.

104. Gilleron M, Ronet C, Mempel M, Monsarrat B, Gachelin G, Puzo G. Acylation state of the phosphatidylinositol mannosides from *Mycobacterium bovis* bacillus Calmette Guerin and ability to induce granuloma and recruit natural killer T cells. *J Biol Chem*. 2001 Sep 14;276(37):34896-904.
105. Khoo KH, Douglas E, Azadi P, Inamine JM, Besra GS, Mikusova K, et al. Truncated structural variants of lipoarabinomannan in ethambutol drug-resistant strains of *Mycobacterium smegmatis*. Inhibition of arabinan biosynthesis by ethambutol. *J Biol Chem*. 1996 Nov 8;271(45):28682-90.
106. Lemassu A, Daffe M. Structural features of the exocellular polysaccharides of *Mycobacterium tuberculosis*. *Biochem J*. 1994 Jan 15;297 (Pt 2):351-7.
107. Kremer L, Douglas JD, Baulard AR, Morehouse C, Guy MR, Alland D, et al. Thiolactomycin and related analogues as novel anti-mycobacterial agents targeting KasA and KasB condensing enzymes in *Mycobacterium tuberculosis*. *J Biol Chem*. 2000 Jun 2;275(22):16857-64.
108. Sibley LD, Adams LB, Krahenbuhl JL. Inhibition of interferon-gamma-mediated activation in mouse macrophages treated with lipoarabinomannan. *Clin Exp Immunol*. 1990 Apr;80(1):141-8.
109. Lee YC, Ballou CE. Complete structures of the glycopospholipids of mycobacteria. *Biochemistry (Mosc)*. 1965 Jul;4(7):1395-404.
110. Kovacevic S, Anderson D, Morita YS, Patterson J, Haites R, McMillan BN, et al. Identification of a novel protein with a role in lipoarabinomannan biosynthesis in mycobacteria. *J Biol Chem*. 2006 Apr 7;281(14):9011-7.
111. Morita YS, Sena CB, Waller RF, Kurokawa K, Sernee MF, Nakatani F, et al. PimE is a polyprenol-phosphate-mannose-dependent mannosyltransferase that transfers the fifth mannose of phosphatidylinositol mannoside in mycobacteria. *J Biol Chem*. 2006 Sep 1;281(35):25143-55.
112. Gibson KJ, Eggeling L, Maughan WN, Krumbach K, Gurucha SS, Nigou J, et al. Disruption of Cg-Ppm1, a polyprenyl monophosphomannose synthase, and the generation of lipoglycan-less mutants in *Corynebacterium glutamicum*. *J Biol Chem*. 2003 Oct 17;278(42):40842-50.

113. Liu D, Crellin P, Chalmers R. Cyclic changes in the affinity of protein-DNA interactions drive the progression and regulate the outcome of the Tn10 transposition reaction. *Nucleic Acids Res.* 2005;33(6):1982-92.
114. Morita YS, Velasquez R, Taig E, Waller RF, Patterson JH, Tull D, et al. Compartmentalization of lipid biosynthesis in mycobacteria. *J Biol Chem.* 2005 Jun 3;280(22):21645-52.
115. Liu J, Mushegian A. Three monophyletic superfamilies account for the majority of the known glycosyltransferases. *Protein Sci.* 2003 Jul;12(7):1418-31.
116. Kordulakova J, Gilleron M, Mikusova K, Puzo G, Brennan PJ, Gicquel B, et al. Definition of the first mannosylation step in phosphatidylinositol mannoside synthesis. PimA is essential for growth of mycobacteria. *J Biol Chem.* 2002 Aug 30;277(35):31335-44.
117. Mishra AK, Batt S, Krumbach K, Eggeling L, Besra GS. Characterization of the *Corynebacterium glutamicum* Δ pimB' Δ tamgtA double deletion mutant and the role of *Mycobacterium tuberculosis* orthologues Rv2188c and Rv0557 in glycolipid biosynthesis. *J Bacteriol.* 2009 Jul;191(13):4465-72.
118. Lea-Smith DJ, Martin KL, Pyke JS, Tull D, McConville MJ, Coppel RL, et al. Analysis of a new mannosyltransferase required for the synthesis of phosphatidylinositol mannosides and lipoarabinomannan reveals two lipomannan pools in corynebacterineae. *J Biol Chem.* 2008 Mar 14;283(11):6773-82.
119. Bifani PJ, Mathema B, Liu Z, Moghazeh SL, Shopsin B, Tempalski B, et al. Identification of a W variant outbreak of *Mycobacterium tuberculosis* via population-based molecular epidemiology. *JAMA.* 1999 Dec 22-29;282(24):2321-7.
120. Fratti RA, Chua J, Vergne I, Deretic V. *Mycobacterium tuberculosis* glycosylated phosphatidylinositol causes phagosome maturation arrest. *Proc Natl Acad Sci U S A.* 2003 Apr 29;100(9):5437-42.
121. Nigou J, Gilleron M, Puzo G. Lipoarabinomannans: from structure to biosynthesis. *Biochimie.* 2003 Jan-Feb;85(1-2):153-66.

122. Adams LB, Fukutomi Y, Krahenbuhl JL. Regulation of murine macrophage effector functions by lipoarabinomannan from mycobacterial strains with different degrees of virulence. *Infect Immun*. 1993 Oct;61(10):4173-81.
123. Schlesinger LS, Hull SR, Kaufman TM. Binding of the terminal mannosyl units of lipoarabinomannan from a virulent strain of *Mycobacterium tuberculosis* to human macrophages. *J Immunol*. 1994 Apr 15;152(8):4070-9.
124. Berman JS, Blumenthal RL, Kornfeld H, Cook JA, Cruikshank WW, Vermeulen MW, et al. Chemotactic activity of mycobacterial lipoarabinomannans for human blood T lymphocytes in vitro. *J Immunol*. 1996 May 15;156(10):3828-35.
125. Fukuda T, Matsumura T, Ato M, Hamasaki M, Nishiuchi Y, Murakami Y, et al. Critical roles for lipomannan and lipoarabinomannan in cell wall integrity of mycobacteria and pathogenesis of tuberculosis. *MBio*. 2013;4(1):e00472-12.
126. Dinadayala P, Kaur D, Berg S, Amin AG, Vissa VD, Chatterjee D, et al. Genetic basis for the synthesis of the immunomodulatory mannose caps of lipoarabinomannan in *Mycobacterium tuberculosis*. *J Biol Chem*. 2006 Jul 21;281(29):20027-35.
127. Khoo KH, Tang JB, Chatterjee D. Variation in mannose-capped terminal arabinan motifs of lipoarabinomannans from clinical isolates of *Mycobacterium tuberculosis* and *Mycobacterium avium* complex. *J Biol Chem*. 2001 Feb 9;276(6):3863-71.
128. Guerardel Y, Maes E, Briken V, Chirat F, Leroy Y, Locht C, et al. Lipomannan and lipoarabinomannan from a clinical isolate of *Mycobacterium kansasii*: novel structural features and apoptosis-inducing properties. *J Biol Chem*. 2003 Sep 19;278(38):36637-51.
129. Nigou J, Gilleron M, Cahuzac B, Bounery JD, Herold M, Thurnher M, et al. The phosphatidyl-myo-inositol anchor of the lipoarabinomannans from *Mycobacterium bovis* bacillus Calmette Guerin. Heterogeneity, structure, and role in the regulation of cytokine secretion. *J Biol Chem*. 1997 Sep 12;272(37):23094-103.

130. Chatterjee D, Bozic CM, McNeil M, Brennan PJ. Structural features of the arabinan component of the lipoarabinomannan of *Mycobacterium tuberculosis*. *J Biol Chem*. 1991 May 25;266(15):9652-60.
131. McNeil MR, Brennan PJ. Structure, function and biogenesis of the cell envelope of mycobacteria in relation to bacterial physiology, pathogenesis and drug resistance; some thoughts and possibilities arising from recent structural information. *Res Microbiol*. 1991 May;142(4):451-63.
132. Rastogi N. Recent observations concerning structure and function relationships in the mycobacterial cell envelope: elaboration of a model in terms of mycobacterial pathogenicity, virulence and drug-resistance. *Res Microbiol*. 1991 May;142(4):464-76.
133. Tatituri RV, Alderwick LJ, Mishra AK, Nigou J, Gilleron M, Krumbach K, et al. Structural characterization of a partially arabinosylated lipoarabinomannan variant isolated from a *Corynebacterium glutamicum* ubiA mutant. *Microbiology*. 2007 Aug;153(Pt 8):2621-9.
134. Raetz CR, Whitfield C. Lipopolysaccharide endotoxins. *Annu Rev Biochem*. 2002;71:635-700.
135. Mishra AK, Alderwick LJ, Rittmann D, Tatituri RV, Nigou J, Gilleron M, et al. Identification of an alpha(1-->6) mannopyranosyltransferase (MptA), involved in *Corynebacterium glutamicum* lipomanann biosynthesis, and identification of its orthologue in *Mycobacterium tuberculosis*. *Mol Microbiol*. 2007 Sep;65(6):1503-17.
136. Berg S, Starbuck J, Torrelles JB, Vissa VD, Crick DC, Chatterjee D, et al. Roles of conserved proline and glycosyltransferase motifs of EmbC in biosynthesis of lipoarabinomannan. *J Biol Chem*. 2005 Feb 18;280(7):5651-63.
137. Appelmek BJ, den Dunnen J, Driessen NN, Ummels R, Pak M, Nigou J, et al. The mannose cap of mycobacterial lipoarabinomannan does not dominate the *Mycobacterium*-host interaction. *Cell Microbiol*. 2008 Apr;10(4):930-44.
138. Kaur D, Berg S, Dinadayala P, Gicquel B, Chatterjee D, McNeil MR, et al. Biosynthesis of mycobacterial lipoarabinomannan: role of a branching mannosyltransferase. *Proc Natl Acad Sci U S A*. 2006 Sep 12;103(37):13664-9.

139. Tatituri RV, Illarionov PA, Dover LG, Nigou J, Gilleron M, Hitchen P, et al. Inactivation of *Corynebacterium glutamicum* NCgl0452 and the role of MgtA in the biosynthesis of a novel mannosylated glycolipid involved in lipomannan biosynthesis. *J Biol Chem*. 2007 Feb 16;282(7):4561-72.
140. Rainczuk AK, Yamaryo-Botte Y, Brammananth R, Stinear TP, Seemann T, Coppel RL, et al. The lipoprotein LpqW is essential for the mannosylation of periplasmic glycolipids in *Corynebacteria*. *J Biol Chem*. 2012 Dec 14;287(51):42726-38.
141. Mishra AK, Klein C, Gurcha SS, Alderwick LJ, Babu P, Hitchen PG, et al. Structural characterization and functional properties of a novel lipomannan variant isolated from a *Corynebacterium glutamicum* pimB¹ mutant. *Antonie Van Leeuwenhoek*. 2008 Aug;94(2):277-87.
142. Astarie-Dequeker C, Le Guyader L, Malaga W, Seaphanh FK, Chalut C, Lopez A, et al. Phthiocerol dimycocerosates of *M. tuberculosis* participate in macrophage invasion by inducing changes in the organization of plasma membrane lipids. *PLoS Pathog*. 2009 Feb;5(2):e1000289.
143. Daffe M, Laneelle MA. Distribution of phthiocerol diester, phenolic mycosides and related compounds in mycobacteria. *J Gen Microbiol*. 1988 Jul;134(7):2049-55.
144. Azad AK, Sirakova TD, Fernandes ND, Kolattukudy PE. Gene knockout reveals a novel gene cluster for the synthesis of a class of cell wall lipids unique to pathogenic mycobacteria. *J Biol Chem*. 1997 Jul 4;272(27):16741-5.
145. Camacho LR, Ensergueix D, Perez E, Gicquel B, Guilhot C. Identification of a virulence gene cluster of *Mycobacterium tuberculosis* by signature-tagged transposon mutagenesis. *Mol Microbiol*. 1999 Oct;34(2):257-67.
146. Moody DB, Ulrichs T, Muhlecker W, Young DC, Gurcha SS, Grant E, et al. CD1c-mediated T-cell recognition of isoprenoid glycolipids in *Mycobacterium tuberculosis* infection. *Nature*. 2000 Apr 20;404(6780):884-8.

147. Hunter RL, Olsen MR, Jagannath C, Actor JK. Multiple roles of cord factor in the pathogenesis of primary, secondary, and cavitary tuberculosis, including a revised description of the pathology of secondary disease. *Ann Clin Lab Sci.* 2006 Autumn;36(4):371-86.
148. Armstrong JA, Hart PD. Phagosome-lysosome interactions in cultured macrophages infected with virulent tubercle bacilli. Reversal of the usual nonfusion pattern and observations on bacterial survival. *J Exp Med.* 1975 Jul 1;142(1):1-16.
149. Wurmser AE, Gary JD, Emr SD. Phosphoinositide 3-kinases and their FYVE domain-containing effectors as regulators of vacuolar/lysosomal membrane trafficking pathways. *J Biol Chem.* 1999 Apr 2;274(14):9129-32.
150. Ferrari G, Langen H, Naito M, Pieters J. A coat protein on phagosomes involved in the intracellular survival of mycobacteria. *Cell.* 1999 May 14;97(4):435-47.
151. Via LE, Deretic D, Ulmer RJ, Hibler NS, Huber LA, Deretic V. Arrest of mycobacterial phagosome maturation is caused by a block in vesicle fusion between stages controlled by rab5 and rab7. *J Biol Chem.* 1997 May 16;272(20):13326-31.
152. Fratti RA, Backer JM, Gruenberg J, Corvera S, Deretic V. Role of phosphatidylinositol 3-kinase and Rab5 effectors in phagosomal biogenesis and mycobacterial phagosome maturation arrest. *J Cell Biol.* 2001 Aug 6;154(3):631-44.
153. Venisse A, Berjeaud JM, Chaurand P, Gilleron M, Puzo G. Structural features of lipoarabinomannan from *Mycobacterium bovis* BCG. Determination of molecular mass by laser desorption mass spectrometry. *J Biol Chem.* 1993 Jun 15;268(17):12401-11.
154. Ernst JD. Macrophage receptors for *Mycobacterium tuberculosis*. *Infect Immun.* 1998 Apr;66(4):1277-81.
155. Tailieux L, Schwartz O, Herrmann JL, Pivert E, Jackson M, Amara A, et al. DC-SIGN is the major *Mycobacterium tuberculosis* receptor on human dendritic cells. *J Exp Med.* 2003 Jan 6;197(1):121-7.

156. Maeda N, Nigou J, Herrmann JL, Jackson M, Amara A, Lagrange PH, et al. The cell surface receptor DC-SIGN discriminates between Mycobacterium species through selective recognition of the mannose caps on lipoarabinomannan. *J Biol Chem*. 2003 Feb 21;278(8):5513-6.
157. Jaconi ME, Lew DP, Carpentier JL, Magnusson KE, Sjogren M, Stendahl O. Cytosolic free calcium elevation mediates the phagosome-lysosome fusion during phagocytosis in human neutrophils. *J Cell Biol*. 1990 May;110(5):1555-64.
158. Rojas M, Garcia LF, Nigou J, Puzo G, Olivier M. Mannosylated lipoarabinomannan antagonizes Mycobacterium tuberculosis-induced macrophage apoptosis by altering Ca²⁺-dependent cell signaling. *J Infect Dis*. 2000 Jul;182(1):240-51.
159. Yonekawa A, Saijo S, Hoshino Y, Miyake Y, Ishikawa E, Suzukawa M, et al. Dectin-2 is a direct receptor for mannose-capped lipoarabinomannan of mycobacteria. *Immunity*. 2014 Sep 18;41(3):402-13.
160. Ishikawa E, Ishikawa T, Morita YS, Toyonaga K, Yamada H, Takeuchi O, et al. Direct recognition of the mycobacterial glycolipid, trehalose dimycolate, by C-type lectin Mincle. *J Exp Med*. 2009 Dec 21;206(13):2879-88.
161. Apostolou I, Takahama Y, Belmont C, Kawano T, Huerre M, Marchal G, et al. Murine natural killer T(NKT) cells [correction of natural killer cells] contribute to the granulomatous reaction caused by mycobacterial cell walls. *Proc Natl Acad Sci U S A*. 1999 Apr 27;96(9):5141-6.
162. Guerardel Y, Maes E, Ellass E, Leroy Y, Timmerman P, Besra GS, et al. Structural study of lipomannan and lipoarabinomannan from Mycobacterium chelonae. Presence of unusual components with alpha 1,3-mannopyranose side chains. *J Biol Chem*. 2002 Aug 23;277(34):30635-48.
163. Shui W, Petzold CJ, Redding A, Liu J, Pitcher A, Sheu L, et al. Organelle membrane proteomics reveals differential influence of mycobacterial lipoglycans on macrophage phagosome maturation and autophagosome accumulation. *J Proteome Res*. 2011 Jan 7;10(1):339-48.

164. Chan J, Fan XD, Hunter SW, Brennan PJ, Bloom BR. Lipoarabinomannan, a possible virulence factor involved in persistence of *Mycobacterium tuberculosis* within macrophages. *Infect Immun*. 1991 May;59(5):1755-61.
165. Nigou J, Zelle-Rieser C, Gilleron M, Thurnher M, Puzo G. Mannosylated lipoarabinomannans inhibit IL-12 production by human dendritic cells: evidence for a negative signal delivered through the mannose receptor. *J Immunol*. 2001 Jun 15;166(12):7477-85.
166. Geijtenbeek TB, Van Vliet SJ, Koppel EA, Sanchez-Hernandez M, Vandenbroucke-Grauls CM, Appelmek B, et al. Mycobacteria target DC-SIGN to suppress dendritic cell function. *J Exp Med*. 2003 Jan 6;197(1):7-17.
167. Koppel EA, van Gisbergen KP, Geijtenbeek TB, van Kooyk Y. Distinct functions of DC-SIGN and its homologues L-SIGN (DC-SIGNR) and mSIGNR1 in pathogen recognition and immune regulation. *Cell Microbiol*. 2005 Feb;7(2):157-65.
168. Dao DN, Kremer L, Guerardel Y, Molano A, Jacobs WR, Jr., Porcelli SA, et al. Mycobacterium tuberculosis lipomannan induces apoptosis and interleukin-12 production in macrophages. *Infect Immun*. 2004 Apr;72(4):2067-74.
169. Camacho LR, Constant P, Raynaud C, Laneelle MA, Triccas JA, Gicquel B, et al. Analysis of the phthiocerol dimycocerosate locus of *Mycobacterium tuberculosis*. Evidence that this lipid is involved in the cell wall permeability barrier. *J Biol Chem*. 2001 Jun 8;276(23):19845-54.
170. Rousseau C, Winter N, Pivert E, Bordat Y, Neyrolles O, Ave P, et al. Production of phthiocerol dimycocerosates protects *Mycobacterium tuberculosis* from the cidal activity of reactive nitrogen intermediates produced by macrophages and modulates the early immune response to infection. *Cell Microbiol*. 2004 Mar;6(3):277-87.
171. Lienhardt C, Raviglione M, Spigelman M, Hafner R, Jaramillo E, Hoelscher M, et al. New drugs for the treatment of tuberculosis: needs, challenges, promise, and prospects for the future. *J Infect Dis*. 2012 May 15;205 Suppl 2:S241-9.

172. Belanger AE, Besra GS, Ford ME, Mikusova K, Belisle JT, Brennan PJ, et al. The embAB genes of *Mycobacterium avium* encode an arabinosyl transferase involved in cell wall arabinan biosynthesis that is the target for the antimycobacterial drug ethambutol. *Proc Natl Acad Sci U S A*. 1996 Oct 15;93(21):11919-24.
173. Brennan PJ, Crick DC. The cell-wall core of *Mycobacterium tuberculosis* in the context of drug discovery. *Curr Top Med Chem*. 2007;7(5):475-88.
174. Barnes PF, Chatterjee D, Abrams JS, Lu S, Wang E, Yamamura M, et al. Cytokine production induced by *Mycobacterium tuberculosis* lipoarabinomannan. Relationship to chemical structure. *J Immunol*. 1992 Jul 15;149(2):541-7.
175. Amin AG, Goude R, Shi L, Zhang J, Chatterjee D, Parish T. EmbA is an essential arabinosyltransferase in *Mycobacterium tuberculosis*. *Microbiology*. 2008 Jan;154(Pt 1):240-8.
176. Alsteens D, Verbelen C, Dague E, Raze D, Baulard AR, Dufrene YF. Organization of the mycobacterial cell wall: a nanoscale view. *Pflugers Arch*. 2008 Apr;456(1):117-25.
177. Zhang Y, Post-Martens K, Denkin S. New drug candidates and therapeutic targets for tuberculosis therapy. *Drug Discov Today*. 2006 Jan;11(1-2):21-7.
178. Freundlich JS, Wang F, Vilcheze C, Gulten G, Langley R, Schiehser GA, et al. Triclosan derivatives: towards potent inhibitors of drug-sensitive and drug-resistant *Mycobacterium tuberculosis*. *ChemMedChem*. 2009 Feb;4(2):241-8.
179. Matviiuk T, Mori G, Lherbet C, Rodriguez F, Pasca MR, Gorichko M, et al. Synthesis of 3-heteryl substituted pyrrolidine-2,5-diones via catalytic Michael reaction and evaluation of their inhibitory activity against InhA and *Mycobacterium tuberculosis*. *Eur J Med Chem*. 2014 Jan;71:46-52.
180. Scorpio A, Lindholm-Levy P, Heifets L, Gilman R, Siddiqi S, Cynamon M, et al. Characterization of pncA mutations in pyrazinamide-resistant *Mycobacterium tuberculosis*. *Antimicrob Agents Chemother*. 1997 Mar;41(3):540-3.

181. Saguy M, Gillet R, Skorski P, Hermann-Le Denmat S, Felden B. Ribosomal protein S1 influences trans-translation in vitro and in vivo. *Nucleic Acids Res.* 2007;35(7):2368-76.
182. Telenti A, Imboden P, Marchesi F, Lowrie D, Cole S, Colston MJ, et al. Detection of rifampicin-resistance mutations in *Mycobacterium tuberculosis*. *Lancet.* 1993 Mar 13;341(8846):647-50.
183. Riccardi G, Pasca MR. Trends in discovery of new drugs for tuberculosis therapy. *J Antibiot (Tokyo).* 2014 Sep;67(9):655-9.
184. Eggeling L, Krumbach K, Sahm H. L-glutamate efflux with *Corynebacterium glutamicum*: why is penicillin treatment or Tween addition doing the same? *J Mol Microbiol Biotechnol.* 2001 Jan;3(1):67-8.
185. Puech V, Chami M, Lemassu A, Laneelle MA, Schiffler B, Gounon P, et al. Structure of the cell envelope of corynebacteria: importance of the non-covalently bound lipids in the formation of the cell wall permeability barrier and fracture plane. *Microbiology.* 2001 May;147(Pt 5):1365-82.
186. Kalinowski J, Bathe B, Bartels D, Bischoff N, Bott M, Burkovski A, et al. The complete *Corynebacterium glutamicum* ATCC 13032 genome sequence and its impact on the production of L-aspartate-derived amino acids and vitamins. *J Biotechnol.* 2003 Sep 4;104(1-3):5-25.
187. Nigou J, Dover LG, Besra GS. Purification and biochemical characterization of *Mycobacterium tuberculosis* SuhB, an inositol monophosphatase involved in inositol biosynthesis. *Biochemistry (Mosc).* 2002 Apr 2;41(13):4392-8.
188. Nataraj V, Varela C, Javid A, Singh A, Besra GS, Bhatt A. Mycolic acids: deciphering and targeting the Achilles' heel of the tubercle bacillus. *Mol Microbiol.* 2015 Jul 2.
189. van der Rest ME, Lange C, Molenaar D. A heat shock following electroporation induces highly efficient transformation of *Corynebacterium glutamicum* with xenogeneic plasmid DNA. *Appl Microbiol Biotechnol.* 1999 Oct;52(4):541-5.
190. McKean S, Davies J, Moore R. Identification of macrophage induced genes of *Corynebacterium pseudotuberculosis* by differential fluorescence induction. *Microbes Infect.* 2005 Oct;7(13):1352-63.

191. North EJ, Jackson M, Lee RE. New approaches to target the mycolic acid biosynthesis pathway for the development of tuberculosis therapeutics. *Curr Pharm Des.* 2014;20(27):4357-78.
192. Remuinan MJ, Perez-Herran E, Rullas J, Alemparte C, Martinez-Hoyos M, Dow DJ, et al. Tetrahydropyrazolo[1,5-a]pyrimidine-3-carboxamide and N-benzyl-6',7'-dihydrospiro[piperidine-4,4'-thieno[3,2-c]pyran] analogues with bactericidal efficacy against *Mycobacterium tuberculosis* targeting MmpL3. *PLoS One.* 2013;8(4):e60933.
193. Matsunaga I, Naka T, Talekar RS, McConnell MJ, Katoh K, Nakao H, et al. Mycolyltransferase-mediated glycolipid exchange in *Mycobacteria*. *J Biol Chem.* 2008 Oct 24;283(43):28835-41.
194. Hunter SW, McNeil MR, Brennan PJ. Diglycosyl diacylglycerol of *Mycobacterium tuberculosis*. *J Bacteriol.* 1986 Nov;168(2):917-22.
195. Sena CB, Fukuda T, Miyanagi K, Matsumoto S, Kobayashi K, Murakami Y, et al. Controlled expression of branch-forming mannosyltransferase is critical for mycobacterial lipoarabinomannan biosynthesis. *J Biol Chem.* 2010 Apr 30;285(18):13326-36.
196. Mishra AK, Alderwick LJ, Rittmann D, Wang C, Bhatt A, Jacobs WR, Jr., et al. Identification of a novel $\alpha(1\rightarrow6)$ mannopyranosyltransferase MptB from *Corynebacterium glutamicum* by deletion of a conserved gene, NCgl1505, affords a lipomannan- and lipoarabinomannan-deficient mutant. *Mol Microbiol.* 2008 Jun;68(6):1595-613.
197. Kim JS, Jiao L, Oh JI, Ha NC, Kim YH. Crystal structure and functional implications of LprF from *Mycobacterium tuberculosis* and *M. bovis*. *Acta Crystallogr D Biol Crystallogr.* 2014 Oct;70(Pt 10):2619-30.
198. Shukla S, Richardson ET, Athman JJ, Shi L, Wearsch PA, McDonald D, et al. *Mycobacterium tuberculosis* lipoprotein LprG binds lipoarabinomannan and determines its cell envelope localization to control phagolysosomal fusion. *PLoS Pathog.* 2014 Oct;10(10):e1004471.
199. Gurcha SS, Baulard AR, Kremer L, Loch C, Moody DB, Muhlecker W, et al. Ppm1, a novel polyprenol monophosphomannose synthase from *Mycobacterium tuberculosis*. *Biochem J.* 2002 Jul 15;365(Pt 2):441-50.

200. Boshoff HI, Manjunatha UH. The impact of genomics on discovering drugs against infectious diseases. *Microbes Infect.* 2006 May;8(6):1654-61.
201. Deshayes C, Bach H, Euphrasie D, Attarian R, Coureuil M, Sougakoff W, et al. MmpS4 promotes glycopeptidolipids biosynthesis and export in *Mycobacterium smegmatis*. *Mol Microbiol.* 2010 Nov;78(4):989-1003.
202. Qiao S, Luo Q, Zhao Y, Zhang XC, Huang Y. Structural basis for lipopolysaccharide insertion in the bacterial outer membrane. *Nature.* 2014 Jul 3;511(7507):108-11.
203. Bos MP, Tefsen B, Geurtsen J, Tommassen J. Identification of an outer membrane protein required for the transport of lipopolysaccharide to the bacterial cell surface. *Proc Natl Acad Sci U S A.* 2004 Jun 22;101(25):9417-22.
204. Wu T, McCandlish AC, Gronenberg LS, Chng SS, Silhavy TJ, Kahne D. Identification of a protein complex that assembles lipopolysaccharide in the outer membrane of *Escherichia coli*. *Proc Natl Acad Sci U S A.* 2006 Aug 1;103(31):11754-9.
205. Jankute M. Elucidation of a protein-protein interaction network involved in *Corynebacterium glutamicum* cell wall biosynthesis as determined by bacterial two-hybrid analysis. *Glycoconj J* [serial on the Internet]. 2014.

Appendix 1

Bacterial Strains

Escherichia coli strains

strain	genotype	source
DH5α	<i>supE44 ΔlacU169(Ø80lacΔZM15)hsdR17 recA1 gyrA96 thi-1 relA1</i>	Stratagene
XL1-Blue MRF'	<i>Δ(mcrA)183 Δ(mcrCB-hsdSMR-mrr)173 endA1 supE44 thi-1 recA1 gyrA96 relA1 lac [F'proAB lac^qZ ΔM15 Tn10 (Tet^R)]</i>	Stratagene

Table A.1 *Escherichia coli* strains used in this project.

The *E. coli* DH5α and Xli-Blue MRF' strains were used as hosts for all plasmids described in this project.

Corynebacteria glutamicum strain

Corynebacterium glutamicum 13032™ acquired from the ATCC in 2011.

Deposited as *Micrococcus glutamicus* genome sequencing strain. Transformation host. Produces glutamic acid (glutamate). Patent may not be used to infringe the patent aims.

Appendix 2

Bacteriological Media Formulations

Antibiotic Supplements

Kanamycin 20 µg/ml

Ampicillin 100 µg/ml

Streptomycin 20 µg/ml

Luria-Bertani (LB) Broth

1% (w/v) bacto-tryptone

0.5% (w/v) yeast extract

1% (w/v) NaCl

Sterilise by autoclaving for 20 minutes at 121°C.

Luria-Bertani (LB) Agar

1% (w/v) bacto-tryptone

0. (w/v) yeast extract

1% (w/v) NaCl

1.5% (w/v) bacteriological agar

Sterilise by autoclaving for 20 minutes at 121°C.

Brain Heart Infusion (BHI) Broth

37%: (w/v) BHI (Oxoid®) media

Sterilise by autoclaving for 15 minutes at 121°C.

Brain Heart Infusion (BHI) Agar

37%: (w/v) BHI (Oxoid®) media

2% (w/v) bacteriological agar.

Sterilise by autoclaving for 15 minutes at 121°C.

Difco Middlebrook-7H9 Broth (BD™)

Per litre: Resuspend 4.7g of Middlebrook 7H9 (Difco Laboratories) in 900ml of distilled water containing 2 ml of glycerol

Sterilise by autoclaving for 20 minutes at 121°C. When cooled to ~45°C, add 100ml sterile modified DC Enrichment media.

Middlebrook 7H10 Agar

Per litre: Resuspend 19g of Middlebrook 7H10 (Difco Laboratories) in 900ml of distilled water containing 5 ml of glycerol.

Sterilise by autoclaving for 20 minutes at 121°C. When cooled to ~45°C, add with 100ml sterile modified DC Enrichment media.

Modified DC Enrichment

2% (w/v) glucose

0.85% (w/v) NaCl

Sterilise by autoclaving for 10 minutes at 121°C.

SOB Media

2% (w/v) tryptone

0.5% (w/v) yeast extract

10 mM NaCl

2.5 mM KCl

Add 1 ml sterile 25% (w/v) glucose + 1 ml of 1M MgCl₂+MgSO₄ just before use.

Appendix 3

Oligonucleotide Primers

The table below includes the sequences of each of the oligonucleotide primers used in this study

<u>Primer Name</u>	<u>Sequence</u>
NCgl2760-comp_F	5' TCG GAT ATC GCG AGT ACT GCA CCG 3'
NCgl2760-comp_R	5' TCG GAT ATC GGG TCG GGG TCA TAA GGA TTT AAC TCC 3'
NCgl2761-comp_F	5' TCG CCC GGG TAT ACT GCG GAT ACG TTG AAG CTT CTG C 3'
NCgl2761-comp_R	5' TCGCCCGGGA ACTACAAGTGGGAC 3'
NCgl2760-left_F	5' GTCACCCGGGTAAATAAAGGCAACC 3'
NCgl2760-left_R	5' GATAGGATCCCAATAATGAGGACCG 3'
NCgl2760-right_F	5' TAG CGG ATC CAA TTT TCA AGC GCG GCC AGC TGA TGA GC 3'
NCgl2760-right_R	5' GAT ATC TAG ATT TTC ACC CCG GCG G 3'
NCgl2761-left_F	5' ATC CCC GGG TTT GGA ATG CAA CGT GG 3'
NCgl2761-left_R	5' ATC GGA TCC CAC AGT CGT CCA TGC C 3'
NCgl2761-right_F	5' ATG GGA TCC CGG TTG TCG 3'
NCgl2761-right_R	5' TAC TCT AGA CGT GCC GCT GCA CAC 3'
Rv0227TB_F	5' TGA CAG CTG ACG GGT TTT GCC TCG CTT GG 3'
Rv0227TB_R	5' CCT CAG CTG AAC AGC AGC ACC AAG ACC AGC 3'
msmeg 0317_F	5' GCA GGA AAC CGC GGG TGC CG 3'
msmeg 0315_R	5' CCG CCG TCG AGC ACC GAT GAG G 3'
NCgl2760-RTPCR_F	5' CGT ATT GGG TGA GGA TTC C 3'
NCgl2761-RTPCR_R	5' AAC TCG CCA CGC CCG TGA C 3'
NCgl2760 upstream L	5' CCT CAG CTG AGG CCG TCT GGC CAG TAG 3'
NCgl2760 upstream R	5' GAA CCG CAA CAT AAA AAC AGC CCA CAC CTT TC 3'
Rv0227 downstream L	5' TGG GCT GTT TTT ATG TTG CGG TTC GCC GCG 3'
Rv0227 downstream R	5' CCT CAG CTG TTA GCG CCG CTC GGG CGG 3'
pUC_F	5' GTT GTA AAA CGA CGG CCA GT 3'
pUC_R	5' AGC GGA TAA CAA TTT CAC ACA CAG GA 3'